THE NONUNIFORM MAGNETOHYDRODYNAMIC NATURE OF THE SOLAR ATMOSPHERE

Andrew De Ville

A Thesis Submitted for the Degree of PhD
at the
University of St Andrews

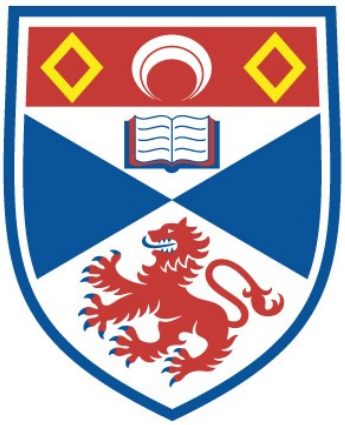

1991

The Nonuniform Magnetohydrodynamic Nature Of The Solar Atmosphere.

Andrew de Ville

Thesis Submitted For The Degree Of Doctor Of Philosophy Of The University Of St. Andrews.

Abstract

The nonuniform structure observed in the solar atmosphere, and in particular the corona, is thought to arise due to the interaction between the magnetic field and plasma. Using a linear theory, the nature of these interactions is investigated, and it is shown how coronal structure may be modelled in a simple way by extended standing disturbances. The effect of inertial forces in considered in both a cartesian and cylindrical geometries, and a first correction due to gravity is calculated. The restrictions of a linear theory may be overcome by finding exact solutions. Solutions are presented which may model plasma flows in closed, partially open and open magnetic fieldline structures. A new method for finding particular classes of exact steady solutions in an gravitationally stratified, isothermal atmosphere is presented, along with some examples of possible solutions.

Declaration

I . . hereby certify that this thesis has been composed by myself, that it is a record of my own work, and that it has not been accepted in partial or complete fulfilment of any other degree of professional qualification.

Signed Date ٢٨١٨١٩٥

Certificate

I hereby certify that the candidate has fulfilled the conditions of the Resolution and Regulations appropriate to the Degree of Ph.D.

Signature of Supervisor ... Date 7.1.8.90

Postgraduate Career

I was admitted to the Faculty of Science of thr University of St. Andrews under Ordinance General No 12 on 10/10/87 and as a candidate for the degree of Ph.D on 10/10/88.

Signed Date 2/1/8/90

Copyright

Acknowledgements

It gives me great pleasure to thank my supervisor, Professor E.R. Priest for all his help and encouragement over the past three years, and for suggesting a profitable topic for research. I would also like to express my sincere gratitude to Dr H. Allen for the numerous occasions she has given help and advice on computing. Finally, this acknowledgement would not be complete without thanking Alan Miles and Rekha Jain for stimulating discussions on waves!

Contents

Chapter One : Introduction

This thesis is concerned with the solution of the steady magnetohydrodynamic (MHD) equations, with the particular aim of modeling the interaction between the magnetic field and plasma. Our motivation for this study is drawn largely from a desire to understand how the nonuniform structure of the solar corona arises. Some of the solutions presented are applied to other regions of the solar atmosphere, noticebly the photosphere, and in particular, to plasma flows above sunspots. We now present a brief resume of the type of structure observed in the solar atmosphere.

(1.1) The Solar Atmosphere

It is usual to subdivide the solar atmosphere into broadly three regions, the photosphere, the chromosphere, and the outer region known as the corona. We shall focus our attention on the corona, which extends from the top of the transition region into interplanatary space.

Observations using coronagraph and X-ray telescopes reveal the corona to be highly structured and continually changing and evolving in a complex way. The structure we see is thought to arise from the interaction between the coronal plasma and magnetic field. In this thesis, it is our intention to present simple models to illustrate how such interactions could form the type of magnetic structures which are observed, using the MHD approximation of a plasma.

There is a great variety of structure in the corona, the nature of which depends upon the magnetic field topology. This may be either 'open' or 'closed', though some structures have elements of both. In the former category we have coronal holes, in the latter loops and arcades. Often a region of closed magnetic field has an open, overlying magnetic field, such as in a coronal streamer.

Coronal streamers are radial-like structures which extend from heights of 0.5R (R= 1 solar radii) to 1R up to as much as 10R above the solar surface. The density is enhanced by a factor 3 to 10 times that of the surrounding corona ($n \sim 10^{14}$ m^{-3}). Helmet streamers are found above quiescent prominences, and active region streamers, not surprisingly, above active regions. A streamer consists of a base of closed fieldlines, forming a magnetic arcade, with an overlying 'blade' of open fieldlines. From the end it bears the appearance of a helmet, from the side it looks like a fan. Bohlin (1969) found the lifetime of a high-latitude streamer to be 4.5-5.5 solar rotations.

Plumes are ray-like structures, and are found at the poles, particularly at sunspot minimum.They exist for about 15 hours defore disappearing.

Coronal holes are regions of the corona with open, diverging magnetic field, and appear as dark regions on soft X-ray photographs. The density is lower than the background corona (by about a factor of 3), and the temperature is also thought to to lower ($1.4\text{-}1.6 \times 10^6$ K compared with 2×10^6K in other parts of the corona).They have a lifetime of approximately six solar rotations, though some have lasted 10 or more rotations. Coronal holes grow and then decay at a rate of about $(1.5 \pm 0.5) \times 10^4$ $km^2 s^{-1}$ (Bohlin,1973), though curiously they appear to show little or no differential rotation over their lifetime, but behave as a rigid body (Bohlin,1977). At the boundary of coronal holes, one finds closed magnetic field structure in the form of arcades of coronal loops.

Since coronal holes are regions of open magnetic field it is natural to suspect that these regions will be closely associated with the solar wind. The correlation of high-speed streamers with low density regions, such as coronal holes, has been known for some time (Wilcox 1968, Hundhausen 1972) and identification of coronal holes with open field regions was first made by Altschuler et al (1972).

In the inner corona, we find regions where the magnetic fields are closed, forming loops or arcades. Regions of closed structure are denser than open regions, and radiate more strongly. The time-scale of a loop system can be up to

several days, an individual loop lasting for about 6 hours (Pneuman and Orrall, 1986). Flows of plasma have been observed in such structures (eg Bruzek and Durrant ,1977) : for example, siphon flow may be driven by pressure differences between endpoints of the loop.

The above brief description serves to illustrate the variety and complexity of the structure that exists. To the above list we could add prominences, coronal mass ejections and X-ray bright points, though we shall not be concerned with these in this work.

(1.2) Modelling The Corona

There have been many theoretical investigations of the solar corona and these have been of several types. Numerical experiments have been used to model the interaction between the plasma and the magnetic field (eg Steinolfson 1982, 1984, Wu et al ,1983) and has the advantage that other important physics, such as realistic energy equations can be included. However, like physical experiments, they are complicated to interpret in detail and so it is difficult to form an understanding of the essential physics of the observed effects.

On the other side of the spectrum, some have neglected the plasma behaviour altogether, and regard the magnetic field as potential or force-free. Alternatively, one can assume the the magnetic field is rigid and study the plasma behaviour. Early steps in understanding the MHD of the corona adopting the latter philosophy were taken by Pneuman (1966,1972), Pneuman and Kopp (1971) and Kopp and Holzer (1976). In the latter two papers, one-dimensional models in a spherical geometry were used to model helmet streamers and coronal holes, respectively. In a new development Priest (1988) showed how the interaction between the magnetic field and the plasma could be modelled as extended standing disturbances, using a two-dimensional linear theory. This simple theory illustrated the rich variety of ways in which the coronal plasma and magnetic field

could affect each other in producing observed structure. In chapters 2-4 we extend the basic model produced by Priest.

The nonlinear nature of the the MHD equations is the major obstacle to analytical progress in producing models that incorporate the interaction between the magnetic field and plasma. However Tsinganos (1982,1983) has developed a systematic method of generating two-dimensional exact solutions to the MHD equations. Low and Tsinganos (1986) have used this approach to find 'wind-like' solutions. We discuss this method in more detail in chapters 5 and 6, where we present a new class of exact solutions.

(1.3) Equations of Magnetohydrodynamics

Magnetohydrodynamics (MHD) is the simplest model that idealises a plasma in terms of its fluid-like properties. In so doing, many potentially important features are neglected, noticeably, quantum, electromagnetic, relativistic and kinetic effects. Thus, it is proper to speak of MHD as modeling a plasma, rather than being a fundamental theory. For detailed microscopic studies of plasma behaviour, one must resort to a more sophisticated kinetic theory, but for many macroscopic studies MHD proves to be adequate. Indeed, despite its limitations, MHD has proved to be an invaluable tool for the theoretical investigation of plasma behaviour in the solar atmosphere. In this thesis we take the MHD equations as the starting point for our discussion.

We now state, for reference, the MHD equations. The magnetic induction **B** is taken to satisty the divergence-free, or solenoidal condition

$$\nabla.\underline{B} = 0. \qquad (1.1)$$

Equation (1.1) implies that there are no magnetic monopoles. Henceforth, we will refer loosely to **B** as the magnetic field, a usage which has become common in the literature. We supplement equation (1.1) by the simplified Maxwell equations

$$\nabla \mathbf{x} \mathbf{B} = \mu \mathbf{j}\,, \qquad (1.2)$$

$$\nabla \times \mathbf{E} = -\frac{\partial \mathbf{B}}{\partial t}\ , \tag{1.3}$$

and Ohm's law

$$\mathbf{j} = \sigma (\mathbf{E} + \mathbf{v} \times \mathbf{B})\ , \tag{1.4}$$

from which we may derive the induction equation

$$\frac{\partial \mathbf{B}}{\partial t} = \nabla \times (\mathbf{v} \times \mathbf{B}) + \eta \nabla^2 \mathbf{B}\ . \tag{1.5}$$

In the above **j** is the electric current, **E** the electric field, **v** the plasma velocity, μ the magnetic permeability, σ the electrical conductivity, and $\eta = (\sigma\mu)^{-1}$, the magnetic diffusivity. In equation (1.2) the displacement current has been neglected under the assumption that the characteristic speed u of the plasma is such that $u << c$, where c is the speed of light. In summary, we take equations (1.1) and (1.5) to describe the magnetic field behaviour in MHD.

The plasma motion is governed by the equations of mass continuity, momentum and energy. When ρ is the plasma density, and **v** is the plasma velocity, the mass continuity equation can be written as

$$\frac{\partial \rho}{\partial t} + \nabla \cdot (\rho \mathbf{v}) = 0\ ; \tag{1.6}$$

the equation of motion as

$$\rho \left\{ \frac{\partial \mathbf{v}}{\partial t} + (\mathbf{v} \cdot \nabla)\mathbf{v} \right\} = -\nabla p + \mu^{-1} (\nabla \times \mathbf{B}) \times \mathbf{B} + \mathbf{F}\ ; \tag{1.7}$$

and the energy equation

$$\frac{\rho^{\gamma}}{\gamma - 1} \left\{ \frac{\partial}{\partial t} \left(\frac{p}{\rho^{\gamma}} \right) + \mathbf{v} \cdot \nabla \left(\frac{p}{\rho^{\gamma}} \right) \right\} = -\ L\ , \tag{1.8}$$

where p is the plasma pressure.

In equation (1.7), **F** may represent gravitational, viscous, and rotational forces. In this thesis we will on occasion take **F** to be a gravitational force of the form

$$\mathbf{F} = \rho g(x_1)\mathbf{e}_1 , \qquad (1.9)$$

where $\mathbf{e}_1$ is a unit vector in the x_1-direction.

The term L on the right-hand side of equation (1.8) is the energy loss function, and may be written as

$$L = L_r - j^2/\sigma - H - \nabla.(\kappa \nabla T) ,$$

where κ is the thermal conduction tensor, T is the temperature, L_r radiation loss, j^2/σ Ohmic heating, and H represents all other heating sources. The special case L=0, considers the plasma that is thermally isolated from its surroundings. For the remainder of this thesis, we take this assumption to hold.

In assuming that the plasma is modelled by equations (1.6)-(1.8) we suppose that the Debye length λ_D, the cyclotron radius r_c and the mean-free path λ are small compared with the characteristic length scale l of the plasma. Along with the condition u<<c, these constitute the major assumptions behind the MHD approximation.

Returning to equation (1.5), we note that it may be rewritten in the dimensionless form

$$\frac{\partial \mathbf{B}^*}{\partial t} = \nabla \mathbf{x} (\mathbf{v}^* \mathbf{x} \mathbf{B}^*) + \frac{1}{R_m} \nabla^2 \mathbf{B}^* ,$$

where $R_m = lv_0/\eta$ is the magnetic Reynolds number (l, v_0 being characteristic length and velocity scales of the plasma).

In the limit $R_m << 1$, called the diffusive limit, the magnetic field diffuses over a time scale $t_d = l^2/\eta$.

Alternatively, for $R_m >> 1$, the plasma is perfectly conducting, and equation (1.5) simplifies to

$$\frac{\partial \mathbf{B}}{\partial t} = \nabla \mathbf{x}(\mathbf{v} \mathbf{x} \mathbf{B}). \qquad (1.10)$$

This limit of MHD is called ideal MHD, and we take this to hold for the purpose of our subsequent discussion. This is reasonable for the solar corona where $R_m \sim 10^{12}$. Following from the ideal limit, the 'frozen-in flux' theorem of Alfven holds; namely 'In a perfectly conducting plasma, fieldlines behave as if they move with the plasma.'

To simplify the mathematical structure of the MHD equations further, we make the assumption that all timescales are much larger than the Alfven travel time. This is not an unreasonable assumption when modelling the corona, (at least to first order) where structures evolve fairly slowly (ranging from hours to months). Thus, all time-dependent terms are neglected and we have the following set of steady equations;

$$\nabla . \mathbf{B} = 0 , \tag{1.11}$$

$$\nabla . (\rho \mathbf{v}) = 0 , \tag{1.12}$$

$$\nabla \times (\mathbf{v} \times \mathbf{B}) = \mathbf{0} , \tag{1.13}$$

$$\rho(\mathbf{v}.\nabla)\,\mathbf{v} = -\nabla p + \mu^{-1}(\nabla \times \mathbf{B})\times\mathbf{B} + \mathbf{F} , \tag{1.14}$$

$$\mathbf{v}.\nabla (p/\rho^{\gamma}) = 0 . \tag{1.15}$$

The non-linear nature of equations (1.11)-(1.15) presents theorists with a formidable challenge. In order to make analytical progress we adopt the linear approximation to these equations for chapters 2-4.

Consider the steady background state with magnetic field $\mathbf{B}_0$, velocity $\mathbf{v}_0$, density ρ_0, and plasma pressure p_0. We take the body force $\mathbf{F}$ to be a gravitational term, written

$$\mathbf{F} = -\rho \nabla V,$$

for some gravitational potential V. Let us perturb this background state, taking departures going as

$$\mathbf{B} = \mathbf{B}_0 + \varepsilon \mathbf{B}_1,$$

$$\mathbf{v} = \mathbf{v}_0 + \varepsilon \mathbf{v}_1 ,$$

$$\rho = \rho_0 + \varepsilon \rho_1 ,$$

$$p = p_0 + \varepsilon p_1,$$

where $\varepsilon<<1$, and expanding equations (1.11)-(1.15) in powers of the small parameter ε. To O(1) the equations become

$$\nabla \cdot \mathbf{B}_0 = 0 , \tag{1.17}$$

$$\rho_0 \nabla \cdot \mathbf{v}_0 + \mathbf{v}_0 \cdot \nabla \rho_0 = 0, \tag{1.18}$$

$$\nabla \times (\mathbf{v}_0 \times \mathbf{B}_0) = \mathbf{0}, \tag{1.19}$$

$$\rho_0 (\mathbf{v}_0 \cdot \nabla) \mathbf{v}_0 = - \nabla p_0 - \frac{1}{2\mu} \nabla B_0^2 + \frac{1}{\mu} (\mathbf{B}_0 \cdot \nabla) \mathbf{B}_0 - \rho_0 \nabla V , \tag{1.20}$$

$$\mathbf{v}_0 \cdot \nabla (p_0 \rho_0^{-\gamma}) = 0 . \tag{1.21}$$

To next order $O(\varepsilon)$, the equations become

$$\nabla \cdot \mathbf{B}_1 = 0 , \tag{1.22}$$

$$\rho_0 \nabla \cdot \mathbf{v}_1 + \rho_1 \nabla \cdot \mathbf{v}_0 + \mathbf{v}_0 \cdot \nabla \rho_1 + \mathbf{v}_1 \cdot \nabla \rho_0 = 0, \tag{1.23}$$

$$\nabla \times (\mathbf{v}_0 \times \mathbf{B}_1) + \nabla \times (\mathbf{v}_1 \times \mathbf{B}_1) = 0 , \tag{1.24}$$

$$\rho_0 (\mathbf{v}_0 \cdot \nabla) \mathbf{v}_1 + \rho_0 (\mathbf{v}_1 \cdot \nabla) \mathbf{v}_0 + \rho_1 (\mathbf{v}_0 \cdot \nabla) \mathbf{v}_0 = - \nabla p_1 - \mu^{-1} \nabla (\mathbf{B}_0 \cdot \mathbf{B}_1)$$
$$\mu^{-1} (\mathbf{B}_0 \cdot \nabla) \mathbf{B}_1 + \mu^{-1} (\mathbf{B}_1 \cdot \nabla) \mathbf{B}_0 - \rho_1 \nabla V , \tag{1.25}$$

$$\mathbf{v}_0 \cdot \nabla (\rho_0^{-\gamma} (p_1 - c_s^2 \rho_1)) + \mathbf{v}_1 \cdot \nabla (p_0 \rho_0^{-\gamma}) = 0 , \tag{1.26}$$

where $c_s^2 = \gamma p_0 / \rho_0$ is the adiabatic sound speed. Equations (1.22)-(1.26) form the basis of the subsequent discussion in chapters 2-4.

(1.4) Outline of Thesis

An outline of the main body of the thesis is now given. The material presented divides naturally into two parts, the first dealing with linear theory, the latter treating exact solutions of the two-dimensional MHD equations.

Part 1 consists of chapters 2 to 4 where a generalisation of the work of Priest (1988) for modelling the solar corona as extended standing disturbances is given.

In chapter 2, inertial effects are included in the model of Priest, who considered only small plasma flows. This analysis is performed in a cartesian geometry, with a two-dimensional spatial dependence. Chapter 3 extends this work to a cylindrical geometry for both axisymmetric and nonaxisymmetric

perturbations. Returning to a cartesian geometry in chapter 4, the effect of gravity is included, and a first gravitational correction is calculated to illustrate its effect. The material presented in these chapters forms the basis of the papers (de Ville and Priest 1989a,b ,1990a).

Part 2 is comprised of chapters 5 to 7 and deals with exact solutions to the steady MHD equations. In chapter 5 a derivation is given of the reduction of the MHD equations to a single equation in an orthogonal coordinate system, following the work of Tsinganos (1981). A class of exact solutions in a cartesian geometry is then presented, which may model plasma flows in arcades, including siphon flow. A similar class of exact solutions in a cylindrical geometry is presented in chapter 6. These may provide a model for Evershed flow in sunspot, and flows in partially open magnetic fields.

Finally, in chapter 7 a method is presented for finding particular classes of exact solutions which have flows across magnetic field lines, due to a constant electric field in the ignorable coordinate direction.

In chapter 8, a brief summary of the conclusions of the research is given, along with some suggestions for future work.

Part 1

Chapter 2 : Inertial Effects

(2.1) Introduction

The nonuniform nature of the two-dimensional magnetohydrodynamic interactions which produce observed coronal structures has been modelled by Priest (1988, hereafter Paper 1) as extended standing disturbances. Working in a semi-infinite rectangular region, a uniform plasma flow with an embedded magnetic field was considered. The plasma flow was assumed to be much less than the Alfven speed, thus neglecting the effect of inertial forces. Four possible types of interaction arise, namely,**a fast-mode compression, a fast-mode expansion, a slow-mode compression, and a slow-mode expansion.** As plasma moves along a magnetic fieldline, a **fast-mode** occurs if magnetic and plasma pressures are in phase. Otherwise, we have a **slow-mode**. A **compression** occurs when the plasma pressure increases, whereas an **expansion** occurs when it decreases. For example, a **fast-mode expansion** occurs when both plasma and magnetic pressures decrease.

In this chapter the restriction on the magnitude of the plasma flow is relaxed and so a more general governing equation is obtained (section 2.2). Symmetric solutions are developed in section 2.3, and the properties of their fundamental modes are discussed in section 2.4. In particular, the dependence of the solutions upon the parameters which characterise the uniform background state, and the perturbed state is investigated. For some values of the uniform background flow (v_0), the solutions for the perturbed quantities become oscillatory in both spatial variables. These solutions are determined in section 2.5. By altering the boundary conditions, solutions may be found which allow magnetic flux to escape across the side boundaries of the region under consideration (section 2.6). A simple expression for the width of a coronal hole is suggested. The final two sections address more general considerations. In section 2.7 it is illustrated how

nonseparable solutions to the governing equation may be found, and finally in section 2.8 the relationship between the standing disturbances presented here and MHD waves in a uniform media is indicated.

(2.2) Basic Equations

We consider steady, adiabatic MHD disturbances in two dimensions, described by the standard MHD equations, in the absence of gravity, given by (1.11)-(1.15). The plasma velocity and magnetic field are taken to be

$$\mathbf{v}(x,z) = v_x\hat{\mathbf{x}} + v_y\hat{\mathbf{y}} + v_z\hat{\mathbf{z}}\,; \quad \mathbf{B}(x,z) = B_x\hat{\mathbf{x}} + B_y\hat{\mathbf{y}} + B_z\hat{\mathbf{z}}\,,$$

respectively.

Suppose now that we consider a steady state with uniform flow ($v_0\hat{\mathbf{z}}$), magnetic field ($B_0\hat{\mathbf{z}}$), pressure p_0, and density ρ_0. This uniform flow and field will model a locally uniform corona. In order to understand nonuniform coronal structures, it seems natural to perturb the uniform state and discover what deviations are possible. In practice such perturbations may be a result of waves propagating through the corona in response to motions at the coronal base. In order to perturb the uniform state, set

$$\mathbf{v} = \mathbf{v}_0+\varepsilon\mathbf{v}_1\,,\ \mathbf{B}=\mathbf{B}_0+\varepsilon\mathbf{B}_1,\ p=p_0+\varepsilon p_1\,,\ \rho=\rho_0+\varepsilon\rho_1\,, \tag{2.1}$$

here $\varepsilon<<1$ is a perturbation parameter. Substitute equations (2.1) into equations (1.11)-(1.15) and linearise by neglecting squares and products of quantities $\mathbf{v}_1$, $\mathbf{B}_1$, p_1, ρ_1 which are assumed to be of order v_0,B_0, $B_0^2(2\mu)^{-1}$, ρ_0 respectively. Alternatively, substitute the particular background state chosen here into the general linearised equations (1.21)-(1.26), neglecting gravity for simplicity.

The x-component of the equation of motion, (1.25) becomes

$$\rho_0 v_0 \frac{\partial v_{1x}}{\partial z} = -\frac{\partial p_1}{\partial x} - \frac{B_0}{\mu}\frac{\partial B_{1z}}{\partial x} + \frac{B_0}{\mu}\frac{\partial B_{1x}}{\partial z}\,, \tag{2.2}$$

while the z-component yields

$$\rho_0 v_0 \frac{\partial v_{1z}}{\partial z} = -\frac{\partial p_1}{\partial z}\,. \tag{2.3}$$

Observe that equation (2.2) has terms due to the plasma pressure and the magnetic field, and so the interaction between the two may be incorporated in a simple way. Under the assumption of a sub-Alfvenic background flow with $v_0 << B_0/(\mu\rho_0)^{1/2}$, Priest (Paper 1) neglected the inertial terms on the left-hand side of equations (2.2) and (2.3). This has the immediate consequence that the perturbed plasma pressure is a function of x alone, from equation (2.3). In this analysis no restrictions are placed on v_0, and the terms on the left-hand side are kept, allowing us to examine inertial effects.

Integrating the y-component of the the induction equation (1.24) we obtain

$$v_{1x} = \frac{E_1}{B_0} + \frac{v_0}{B_0} B_{1x} , \qquad (2.4)$$

where E_1 is a constant electric field associated with sideways motion along the x-direction. For simplicity we henceforth set $E_1 \equiv 0$, implying that the plasma flow is along the magnetic fieldlines.

The mass continuity equation (1.23) reduces to

$$v_0 \frac{\partial \rho_1}{\partial z} + \rho_0 \left\{ \frac{\partial v_{1x}}{\partial x} + \frac{\partial v_{1z}}{\partial z} \right\} = 0 , \qquad (2.5)$$

and the adiabatic energy equation (1.26) becomes

$$\frac{\partial}{\partial z} \left\{ \frac{p_1}{p_0} - \frac{\gamma \rho_1}{\rho_0} \right\} = 0 . \qquad (2.6)$$

Integrating equation (2.6) with respect to z one obtains

$$p_1 = c_s^2 \rho_1 + f_1(x) ,$$

where $c_s^2 = \gamma p_0/\rho_0$ is the isothermal sound speed and $f_1(x)$ can, for example, be determined from the values of p_1 and ρ_1 at $z=0$ or $z \to \infty$. For simplicity, we shall set this function to zero, so that

$$p_1 = c_s^2 \rho_1 . \qquad (2.7)$$

The solenoidal condition (1.22) is satisfied by the flux function A_1, defined by

$$B_{1x} = \frac{\partial A_1}{\partial z} , \quad B_{1z} = - \frac{\partial A_1}{\partial x} . \qquad (2.8)$$

The set of equations (2.2)-(2.7) can now be reduced to a single partial differential equation in A_1.

Eliminate p_1 from equations (2.2) and (2.3) using equation (2.7), to give

$$\rho_0 v_0 \frac{\partial v_{1x}}{\partial z} = - c_s^2 \frac{\partial \rho_1}{\partial x} - \frac{B_0}{\mu} \frac{\partial B_{1z}}{\partial x} + \frac{B_0}{\mu} \frac{\partial B_{1x}}{\partial z} \quad ; \tag{2.9}$$

$$\rho_0 v_0 \frac{\partial v_{1z}}{\partial z} = - c_s^2 \frac{\partial \rho_1}{\partial z} . \tag{2.10}$$

Equation (2.10) implies that

$$\rho_0 v_0 v_{1z} + c_s^2 \rho_1 = F(x) ,$$

or

$$\rho_1 = \frac{F(x)}{c_s^2} - \frac{\rho_0 v_0}{c_s^2} v_{1z} . \tag{2.11}$$

Using equation (2.11), eliminate ρ_1 from equation (2.5), to give

$$\frac{\partial v_{1z}}{\partial z} = - \frac{1}{1-M^2} \frac{\partial v_{1x}}{\partial x} , \tag{2.12}$$

where $M=v_0/c_s$ is the Mach number.

Differentiating equation (2.9) with respect to z, and using equations (2.11) and (2.12), one obtains

$$\rho_0 v_0 \frac{\partial^2 v_{1x}}{\partial z^2} = - \frac{\rho_0 v_0}{1-M^2} \frac{\partial^2 v_{1x}}{\partial x^2} - \frac{B_0}{\mu} \frac{\partial^2 B_{1z}}{\partial x \partial z} + \frac{B_0}{\mu} \frac{\partial^2 B_{1x}}{\partial z^2} = 0 , \tag{2.13}$$

which, after employing equation (2.4), becomes

$$- \frac{M_A^2}{1-M^2} \frac{\partial^2 B_{1x}}{\partial x^2} - \frac{\partial^2 B_{1z}}{\partial x \partial z} + (1-M_A^2) \frac{\partial^2 B_{1x}}{\partial z^2} = 0 ,$$

where $M_A = v_0/v_A$ is the Alfven Mach number, and $v_A = B_0(\mu\rho_0)^{-1/2}$ is the Alfven speed. Using equations (2.8), one finally obtains

$$\frac{\partial}{\partial z} \left[\left(\frac{1-M_T^2}{1-M^2} \right) \frac{\partial^2 A_1}{\partial x^2} + (1-M_A^2) \frac{\partial^2 A_1}{\partial z^2} \right] = 0 ,$$

where $M_T = v_0/c_T$ is the cusp Mach number, with

$$c_T^2 = \frac{c_s^2 v_A^2}{c_s^2 + v_A^2} ,$$

the square of the cusp speed. The governing equation may then be rewritten in the form

$$\frac{\partial}{\partial z} \left[\frac{\partial^2 A_1}{\partial z^2} + \alpha^2 \frac{\partial^2 A_1}{\partial x^2} \right] = 0 , \tag{2.13}$$

where

$$\alpha^2 = \frac{1-M_T^2}{(1-M^2)(1-M_A^2)} .$$

Integrating equation (2.13) with respect to z, and rescaling the variables, gives Poisson's equation, and hence several standard techniques may be employed to find solutions for A_1. In this chapter only separable solutions of equation (2.13) will be considered in detail. Note that in the limit $v_0 << v_A$, considered by Priest (Paper 1), the constant α becomes unity. It is also of interest to note the presence of the cusp speed c_T, which arises as a result of the interaction between the magnetic field and plasma in a compressible medium.

It may also be noted that the y-components of the velocity and magnetic field become uncoupled, as they only appear in the y-component of the equation of motion (1.25) and the x-component of the induction equation (1.24), namely;

$$\rho_0 v_0 \frac{\partial v_{1y}}{\partial z} = \frac{\partial B_{1y}}{\partial z} ,$$

and

$$v_{1y} = \frac{v_0}{B_0} B_{1y} ,$$

which give

$$(1-M_A^2)\frac{\partial B_{1y}}{\partial z} = 0 .$$

Thus, when $M_A^2=1$, B_{1y} and v_{1y} are arbitary functions of x and z. When $M_A^2 \neq 1$, $B_{1y}$and v_{1y} are functions of x alone, that is,

$$B_{1y} = f_2(x) , \quad v_{1y} = \frac{v_0}{B_0} f_2(x).$$

These are purely Alfvenic disturbances in the y-direction. For the remainder of the chapter our attention will focus on the x and z-components of the velocity and the magnetic field.

(2.3) Symmetric Solutions

Seeking separable solutions to equation (2.13) of the form

$$A_1 = X(x)Z(z),$$

one obtains the ordinary differential equations

$$\frac{d^2X}{dx^2} + c^2 X = 0 , \tag{2.14}$$

and

$$\frac{d^2Z}{dz^2} - c^2\alpha^2 Z = b , \tag{2.15}$$

where b is a constant and c^2 is the separation constant.

Solutions to equations (2.14) and (2.15) are sought following Paper 1 in a region $-L \le x \le L$, $z \ge 0$ for B_{1z} symmetric about x=0, with the following boundary conditions satisfied (Figure 2.1) ;

$$B_{1z} \equiv -\frac{\partial A_1}{\partial x} = B_0 f(x) \text{ on } z = 0 , \tag{2.16}$$

$$B_{1x} \equiv \frac{\partial A_1}{\partial z} \to 0 \text{ as } z \to \infty , \tag{2.17}$$

$$B_{1x} \equiv \frac{\partial A_1}{\partial z} = 0 \text{ on } x = 0 , \tag{2.18}$$

$$\frac{\partial B_{1z}}{\partial x} \equiv -\frac{\partial^2 A_1}{\partial x^2} = 0 \text{ on } x = L . \tag{2.19}$$

The form f(x) of the normal magnetic field is imposed at the base of the corona (equation (2.16)), while equation (2.17) implies that the fieldlines become vertical at large distances. Symmetry on the axis x=0 is ensured by equation (2.18), and equation (2.19) represents a free-floating boundary condition, allowing B_{1z} to attain whatever value the solution determines along x=L. In view of equation (2.15) it is equivalent to imposing $B_{1x} = 0$.

Imposition of the boundary conditions (2.17)-(2.19) implies that the separation constant c is $n\pi/L$ for n=1,2,3,.., and the solution of equation (2.13) is

$$A_1 = \sum_{n=1}^{\infty} - \frac{a_n B_0 L}{n\pi} \sin\left(\frac{n\pi x}{L}\right)\left[b_n + \exp\left(-\frac{n\pi\alpha z}{L}\right)\right] . \tag{2.20}$$

From equations (2.8) the magnetic field components can be determined to be

$$B_{1x} = \sum_{n=1}^{\infty} a_n B_0 \alpha \sin\left(\frac{n\pi x}{L}\right)\exp\left(-\frac{n\pi\alpha z}{L}\right), \tag{2.21}$$

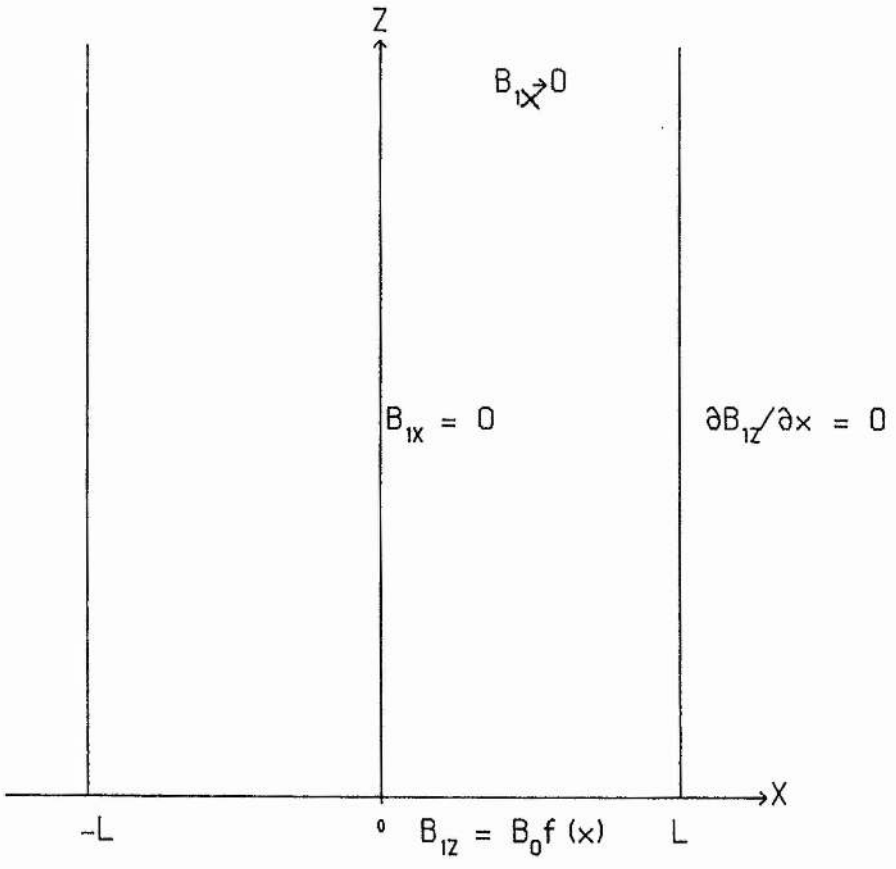

Figure 2.1: Boundary conditions for solutions with the perturbed longitudinal magnetic field B_{1z} symmetric in x about x=0.

$$B_{1z} = \sum_{n=1}^{\infty} a_n B_0 \cos\left(\frac{n\pi x}{L}\right)\left\{b_n + \exp\left(-\frac{n\pi\alpha z}{L}\right)\right\}. \qquad (2.22)$$

It can be seen that , as with the case of the slow flow, B_{1z} does not in general approach zero as $z \to \infty$, unless $b_n = 0$ for all n.

The boundary condition (2.16) implies that

$$f(x) = \sum_{n=1}^{\infty} a_n (b_n + 1)\cos\left(\frac{n\pi x}{L}\right),$$

from which we deduce that

$$\frac{1}{2} a_n (b_n + 1) = \frac{1}{L}\int_0^L f(x)\cos\left(\frac{n\pi x}{L}\right)dx \equiv I_{n1} . \qquad (2.23)$$

Also,equation (2.4) gives

$$v_{1x} = \sum_{n=1}^{\infty} v_0 \alpha a_n \sin\left(\frac{n\pi x}{L}\right)\exp\left(-\frac{n\pi\alpha z}{L}\right), \qquad (2.24)$$

and so from equation (2.2) we obtain

$$p_1 = p_e - \frac{B_0^2}{\mu}\sum_{n=1}^{\infty} a_n \cos\left(\frac{n\pi x}{L}\right)\left\{b_n + \frac{M_A^2}{1-M^2}\exp\left(-\frac{n\pi\alpha z}{L}\right)\right\}. \qquad (2.25)$$

It may be noted at this point that p_1 is now a function of both x and z, whereas for the slow flow (Paper 1), p_1 depended only on x. This implies that the isobars will now be curved rather than being straight lines. From equation (2.25), one can deduce that at the base of the corona (z=0)

$$\frac{1}{2} a_n \left\{b_n + \frac{M_A^2}{1-M^2}\right\} = -\frac{1}{L}\int_0^L \frac{\mu p_1(x,0)}{B_0^2}\cos\left(\frac{n\pi x}{L}\right)dx \equiv I_{n2} , \qquad (2.26)$$

and

$$p_e = \int_0^L p_1(x,0)dx .$$

Equations (2.23) and (2.26) may then be solved to give

$$a_n = 2\left\{\frac{1-M^2}{1-M_T^2}\right\}(I_{n1} - I_{n2}) , \qquad (2.27a)$$

and

$$b_n = \frac{1}{(I_{n1} - I_{n2})} \left\{ I_{n2} - \frac{M_A^2}{1-M^2} I_{n1} \right\}. \qquad (2.27b)$$

Once the functions f and $p_1(x,0)$ are prescibed, the resulting MHD response (equations (2.21),(2.22),(2.24) and (2.25)) of the overlying corona can be deduced, the constants a_n and b_n being determined from equations (2.27a) and (2.27b).

Finally, assuming that the perturbed normal component of velocity v_{1z} is zero at z=0, eqation (2.12) may be integrated to give

$$v_{1z} = - \sum_{n=1}^{\infty} \frac{a_n v_0}{1-M^2} \cos\left(\frac{n\pi x}{L}\right) \left\{ 1 - \exp\left(- \frac{n\pi\alpha z}{L}\right) \right\}. \qquad (2.28)$$

In the limit $v_0 << c_s, v_A$, equations (2.20)-(2.28) reduce to the corresponding symmetric solutions in Paper 1, since

$$\alpha^2 = 1 \, , \frac{M_A^2}{1-M^2} \approx 0 \, .$$

The major difference between the results obtained here compared with those obtained by Priest is the inclusion of the constant α, different from unity, and the dependence of p_1 on both x and z. The inclusion of α will cause the behaviour of the solutions to vary as the value of v_0 changes, and this is investigated in the following section.

(2.4) Fundamental Mode Solutions

To discover the basic physics of the MHD interactions studied here, it is necessary to consider only the fundamental mode (n=1). The first-order perturbation quantities may be written as

$$B_{1x} = a_1 B_0 \alpha \sin\left(\frac{\pi x}{L}\right) \exp\left(- \frac{\alpha\pi z}{L}\right), \qquad (2.29)$$

$$B_{1z} = a_1 B_0 \cos\left(\frac{\pi x}{L}\right) \left\{ b_1 + \exp\left(- \frac{\alpha\pi z}{L}\right) \right\} , \qquad (2.30)$$

$$p_1 = - \frac{B_0^2}{\mu} a_1 \cos\left(\frac{\pi x}{L}\right) \left\{ b_1 + \frac{M_A^2}{1-M^2} \exp\left(- \frac{\alpha\pi z}{L}\right) \right\} , \qquad (2.31)$$

$$v_{1x} = a_1 v_0 \alpha \sin\left(\frac{\pi x}{L}\right) \exp\left(-\frac{\alpha \pi z}{L}\right), \tag{2.32}$$

$$v_{1z} = -\frac{a_1 v_0}{1-M^2} \cos\left(\frac{\pi x}{L}\right)\left\{1 - \exp\left(-\frac{\alpha \pi z}{L}\right)\right\}, \tag{2.33}$$

where

$$a_1 B_0 = \frac{B_{10}}{b_1+1},$$

$$b_1 = -\frac{\left\{p_{10} + \frac{B_0^2 f(0) M_A^2}{\mu \quad 1-M^2}\right\}}{\left\{p_{10} + \frac{B_0^2 f(0)}{\mu}\right\}},$$

and by definition

$$B_{10} = B_{1z}(0,0) = B_0 f(0), \tag{2.34a}$$

$$p_{10} = p_1(0,0), \tag{2.34b}$$

$$\beta_{10} = \frac{\mu p_{10}}{B_0 B_{10}}. \tag{2.34c}$$

The effect of altering the form of the normal magnetic field $B_0 f(x)$ and the plasma pressure at the coronal base will be expressed in changes in the perturbation parameters B_{10} and β_{10}. Also, since we wish to consider the effect of altering v_0 and p_0 in the uniform state, it is advantageous to express the unperturbed quantities in terms of M_A and β,where

$$M_A = \frac{v_0}{v_A}, \quad \beta = \frac{2\mu p_0}{B_0^2}.$$

With these changes in the parameters, we may rewrite equations (2.31) and (2.33) as

$$p_1 = -\frac{B_0^2}{\mu} a_1 \cos\left(\frac{\pi x}{L}\right)\left\{b_1 + \left[\frac{M_A^2}{1-2M_A^2/(\gamma\beta)}\right]\exp\left(-\frac{\alpha \pi z}{L}\right)\right\}, \tag{2.35}$$

$$v_{1z} = -\frac{a_1 v_0}{1-2M_A^2/(\gamma\beta)} \cos\left(\frac{\pi x}{L}\right)\left\{1 - \exp\left(-\frac{\alpha \pi z}{L}\right)\right\}, \tag{2.36}$$

where

$$\alpha^2 = \frac{1-M_T^2}{(1-M^2)(1-M_A^2)} = \frac{1-[2/(\gamma\beta)+1]M_A^2}{(1-2M_A^2/(\gamma\beta))(1-M_A^2)}, \tag{2.37}$$

$$a_1 = \frac{B_{10}}{B_0}(1+\beta_{10})\left\{\frac{1-M^2}{1-M_T^2}\right\} = \frac{\mu p_{T1}}{B_0^2}\left\{\frac{1-2M_A^2/(\gamma\beta)}{1-[2/(\gamma\beta)+1]M_A^2}\right\}, \tag{2.38}$$

$$b_1 = -\frac{1}{\beta_{10}+1}\left\{\beta_{10}+\frac{M_A^2}{1-M^2}\right\} = -\frac{1}{\beta_{10}+1}\left\{\beta_{10}+\frac{M_A^2}{1-2M_A^2/(\gamma\beta)}\right\}, \tag{2.39}$$

and

$$\frac{\mu p_{T1}}{B_0^2} = \frac{B_{10}}{B_0}(1+\beta_{10}) = \frac{\mu p_{10} + B_0 B_{10}}{B_0^2}. \qquad (2.40)$$

Before investigating the properties of these solutions ,we note that the equation of the fieldlines passing through the point $(x_0,0)$ on the coronal base may be determined from

$$\frac{dx}{B_{1x}} = \frac{dz}{B_0},$$

as

$$a_1\left\{1 - \exp\left(-\frac{\alpha\pi z}{L}\right)\right\} = \log\left\{\frac{\tan\left(\frac{\pi x}{2L}\right)}{\tan\left(\frac{\pi x_0}{2L}\right)}\right\}. \qquad (2.41)$$

When $a_1>0$, the fieldlines diverge from the z-axis, and when $a_1<0$ they converge. The isobar $p_1=k$ is given by

$$z = \frac{L}{\alpha\pi}\log\left(\left(\frac{2M_A^2/(\gamma\beta)-1}{M_A^2}\right)\left(\frac{k\mu}{B_0^2 a_1}\sec\left(\frac{\pi x}{L}\right) + 1\right)\right). \qquad (2.42)$$

Observe that the isobars are no longer straight lines, as in the slow-flow case, since the plasma pressure has now a z-dependence. The tendency is for regions of high plasma pressure to broaden as z increases.

Returning to the fundamental mode solutions, it is clear that their nature depends upon the sign of α^2. For flow speeds v_0 such that $c_T<v_0<c_s$ (i.e., $[2/(\gamma\beta)+1]^{-1/2}<M_A<[2/(\gamma\beta)]^{-1/2}$) or $v_0>v_A$ (i.e., $M_A>1$), α^2 is negative (Figure 2.2), and so the z-dependent terms become oscillatory. When we are in the frame of reference of the plasma , it is only for these two intervals that energy can be propagated at speed v_0 by the disturbance. For $c_T<v_0<c_s$, the plasma and magnetic pressures are out of phase, and so the disturbance is **slow-mode**. In contrast, when $v_0>v_A$ the disturbance is **fast-mode**,since magnetic and plasma pressures are in phase.

However, note that the oscillatory nature of the z-dependence means that the boundary condition (2.17) cannot be satisfied. To find non-trivial solutions, one can replace equation (2.17) by ,for example

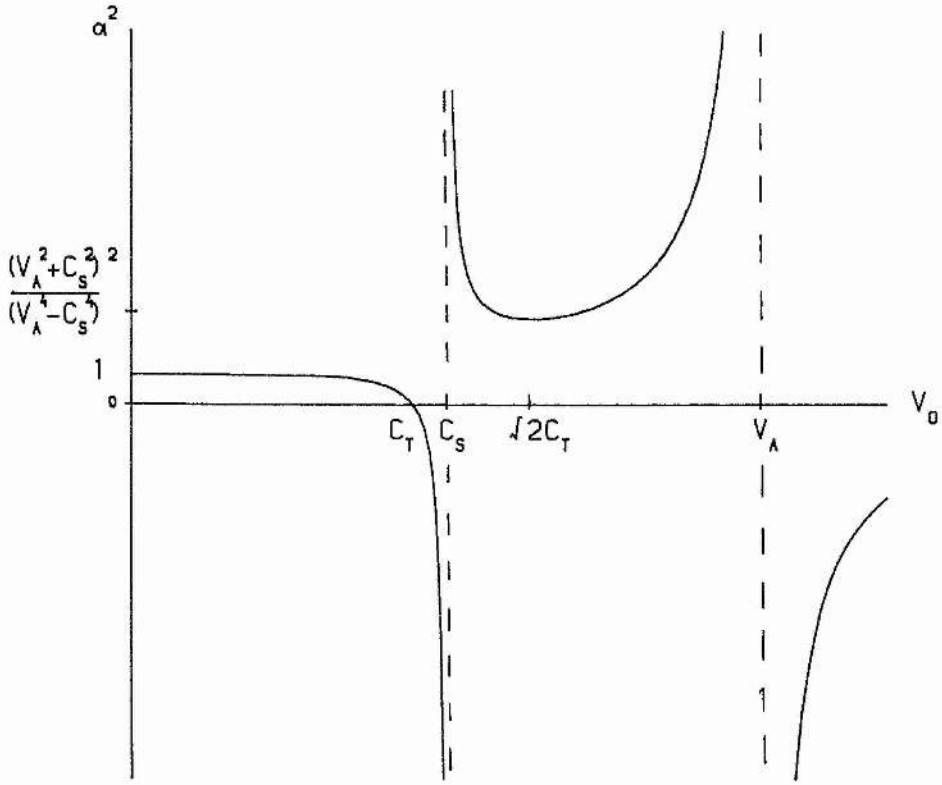

Figure 2.2: The dependence on the flow speed v_0 of

$$\alpha^2=(1-M_T^2)/((1-M^2)(1-M_A^2)).$$

$$\frac{\partial B_{1x}}{\partial z} = \frac{\partial^2 A_1}{\partial z^2} = 0 \text{ on } z=z_0 \ (z_0>0)\,, \qquad (2.43)$$

which provides an upper boundary condition. These solutions are determined in the next section.

At $v_0 = c_T$ or c_s the fundamental mode solutions break down. On returning to the linearised MHD equations, one finds no solutions of physical interest in the context of the present study.

When $v_0=v_A$, one finds that $B_{1x}$and v_{1x} are both constant, while p_1 and B_{1z} are independent of z, being proportional to the functional form of the normal component of magnetic field imposed at the base. These are Alfvenic disturbances in the direction of the uniform field and flow.

In the regions $0<v_0<c_T$ (i.e., $0<M_A<[2/(\gamma\beta)+1\}^{-1/2}$) and $c_s<v_0<v_A$ (i.e., $[2/(\gamma\beta)]^{-1/2}<M_A<1$), the z-dependence of the solutions remains exponentially decaying. These solutions will now be examined in more detail for the interval $0<v_0<c_T$.

As discovered in Paper 1, four physically distinct cases arise. When plasma near the axis x=0 rises, one can deduce from Figure 3 that

(i) $a_1>0$, $b_1<0$ gives a **fast-mode expansion** ,

(ii) $a_1<0$, $b_1>0$ gives a **fast-mode compression,**

(iii) $a_1<0$, $b_1<0$ gives a **slow-mode expansion,**

(iv) $a_1>0$,$b_1>0$ gives a **slow-mode compression.**

These are the same as for the slow flow case, though now inequalities (i)-(iv) may be related to the signs of the perturbation parameters B_{10} and β_{10}.

a) $B_{10} > 0$

From equation (2.38) it can be seen that the sign of a_1 is determined by that of $(\beta_{10}+1)$ when $0<v_0<c_T$. The critical values of β_{10} are $-M_A^2[1-2M_A^2/(\gamma\beta)]^{-1}$ and -1. Equation (2.39) determines the value of b_1.

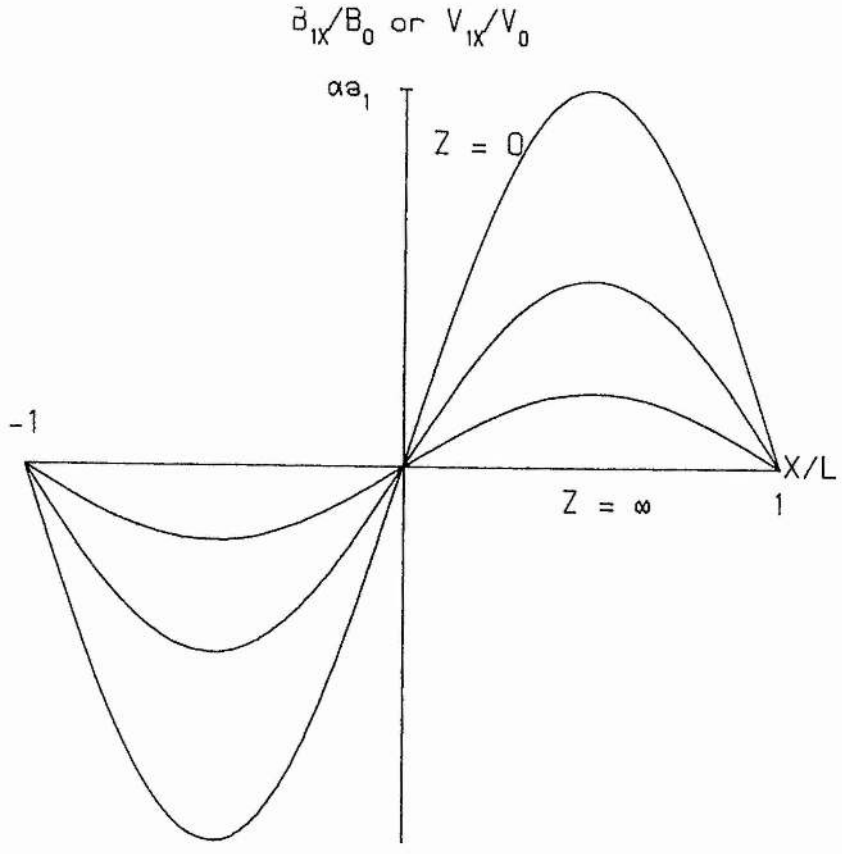

Figure 2.3a

Figure 2.3: The x-dependence of : (a) perturbed transverse magnetic field B_{1x} and v_{1x} , (b) longitudinal field B_{1z} , (c) pressure p_1, (d) longitudinal flow speed v_{1z}, for several values of z for the fundamental mode.

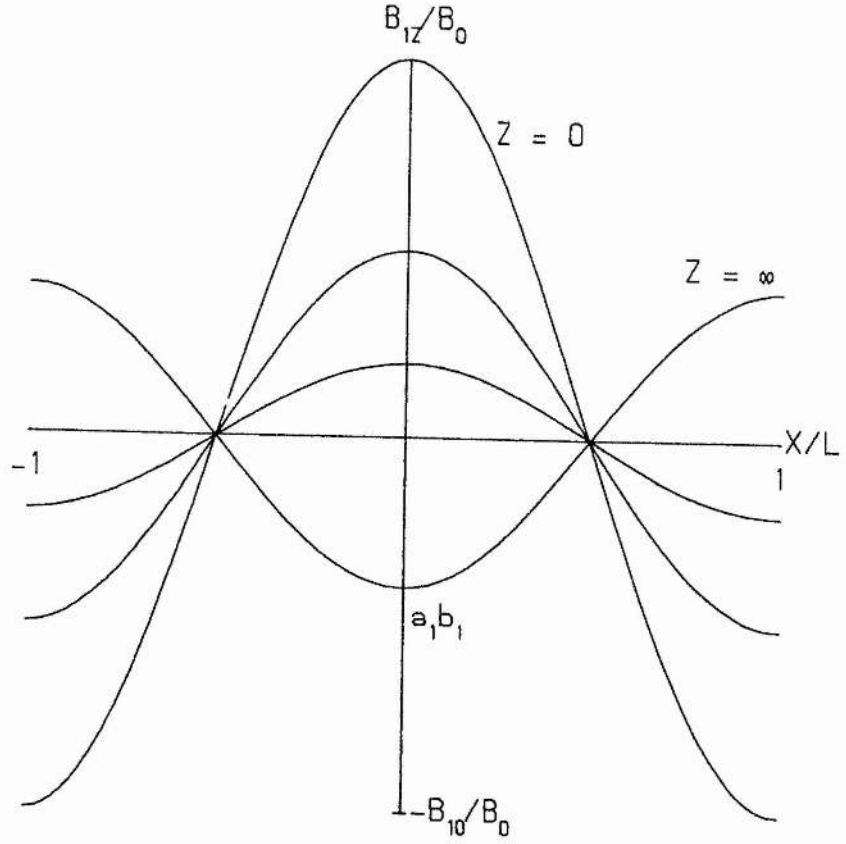

Figure 2.3b

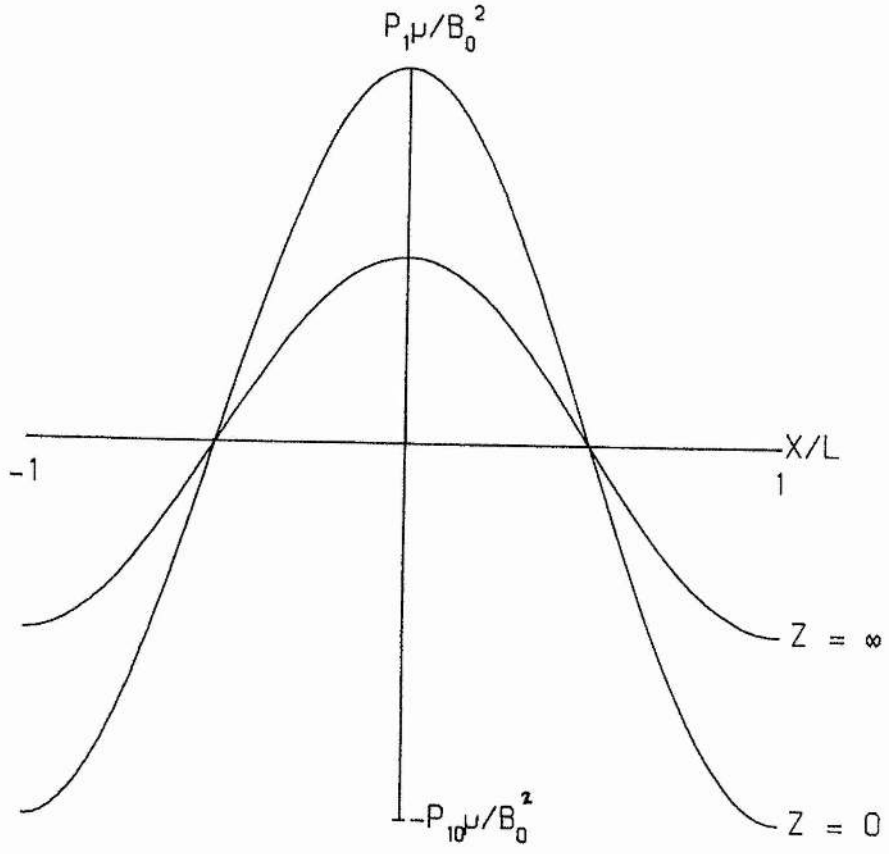

Figure 2.3c

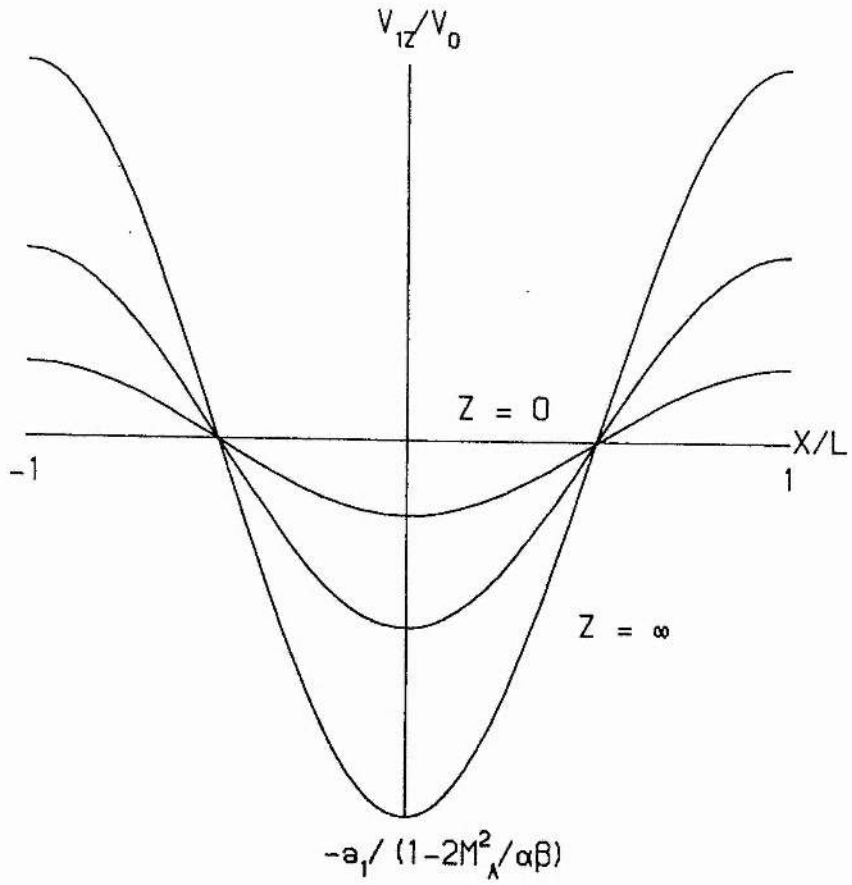

Figure 2.3d

First, when $\beta_{10}<-1$, then $a_1<0$ from equation (2.38). Also, since $\beta_{10}+M_A^2[1-2M_A^2/(\gamma\beta)]^{-1}<0$ then $b_1<0$, and the hence the disturbance is a **slow-mode expansion.**

For $-1<\beta_{10}<-M_A^2[1-2M_A^2/(\gamma\beta)]^{-1}$, $a_1>0$ and $b_1>0$ since $0<M_A^2[1-2M_A^2/(\gamma\beta)]^{-1}<1$ for $0<v_0<c_T$. Hence the disturbance is a **slow-mode compression.**

Finally, when $\beta_{10}>-M_A^2[1-2M_A^2/(\gamma\beta)]^{-1}$, one finds that $a_1>0$ and $b_1<0$, giving a **fast-mode expansion.**

b) $B_{10} < 0$

When $\beta_{10}<-1$, it can be clearly seen that $a_1>0$, and from equation (2.39) $b_1<0$, resulting in a **fast-mode expansion.**

When $-1<\beta_{10}<-M_A^2[1-2M_A^2/(\gamma\beta)]^{-1}$, $a_1<0$ and $b_1>0$ resulting in a **fast-mode compression.** Finally, when $\beta_{10}> -M_A^2[1-2M_A^2/(\gamma\beta)]^{-1/2}$, $a_1<0$ and $b_1<0$ giving **slow-mode expansion.** The above results are summarised in Table 2.1.

Observe that the expected physical behaviour depends critically upon the sign and form of the normal component of magnetic field and plasma pressure imposed at the base.

The solutions (2.29)-(2.33) are also valid when $c_s<v_0<v_A$. To determine the type of disturbance that occurs as plasma rises near the z-axis, adopt the same proceedure as before, to obtain the results shown in Table 2.2.

From Figure 2.3 note that the maximum values of B_{1x}(at z=0), B_{1z}(as $z\rightarrow\infty$), $p_1(z\rightarrow\infty)$ all depend upon the parameters M_A and β. Figure 2.4 reveals that increasing v_0, and hence M_A, in the range $0<v_0<c_T$ increases the maximum values. Likewise, increasing p_0, and hence β, has the effect of decreasing the maximum values for any given value of v_0.

To explain physically why these variations occur it is necessary to return to the equation of motion and consider the inertial term. Putting $\mathbf{v} = v\hat{\mathbf{s}}$, where $\hat{\mathbf{s}}$ is the unit vector along a streamline ,the term $(\mathbf{v}.\nabla)\mathbf{v}$ may be decomposed into

Table 2.1 : The variation of type of disturbance with B_{10} and β_{10} for $v_0<c_T$.

	$B_{10}<0$	$B_{10}>0$
$\beta_{10}>-M_A^2(1-2M_A^2/(\gamma\beta))^{-1}$	slow-mode expansion	fast-mode expansion
$-1<\beta_{10}<-M_A^2(1-2M_A^2/(\gamma\beta))^{-1}$	fast-mode compression	slow-mode compression
$\beta_{10}<-1$	fast-mode expansion	slow-mode expansion

Table 2.2 : The variation of the type of disturbance for $c_S<v_0<v_A$.

	$B_{10}<0$	$B_{10}>0$
$\beta_{10}>-M_A^2(1-2M_A^2/(\gamma\beta))^{-1}$	fast-mode expansion	slow-mode expansion
$-1<\beta_{10}<-M_A^2(1-2M_A^2/(\gamma\beta))^{-1}$	fast-mode compression	slow-mode compression
$\beta_{10}<-1$	fast-mode expansion	slow-mode expansion

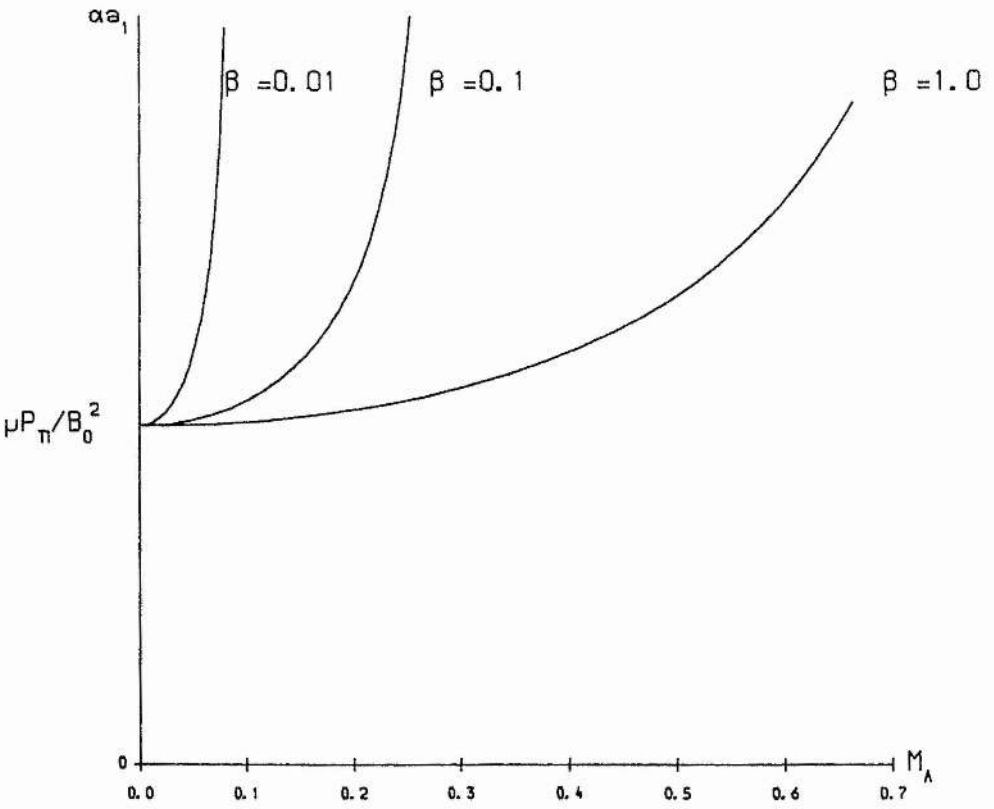

Figure 2.4a

Figure 2.4 : The v_0-dependence of the maxima of (a) B_{1x} and v_{1x} ,(b) B_{1z} and p_1, (c) v_{1z}, for several values of $\beta=2\mu p_0/B_0^2$ when $0<M_A^2<(1+2/(\gamma\beta))^{-1/2}$.

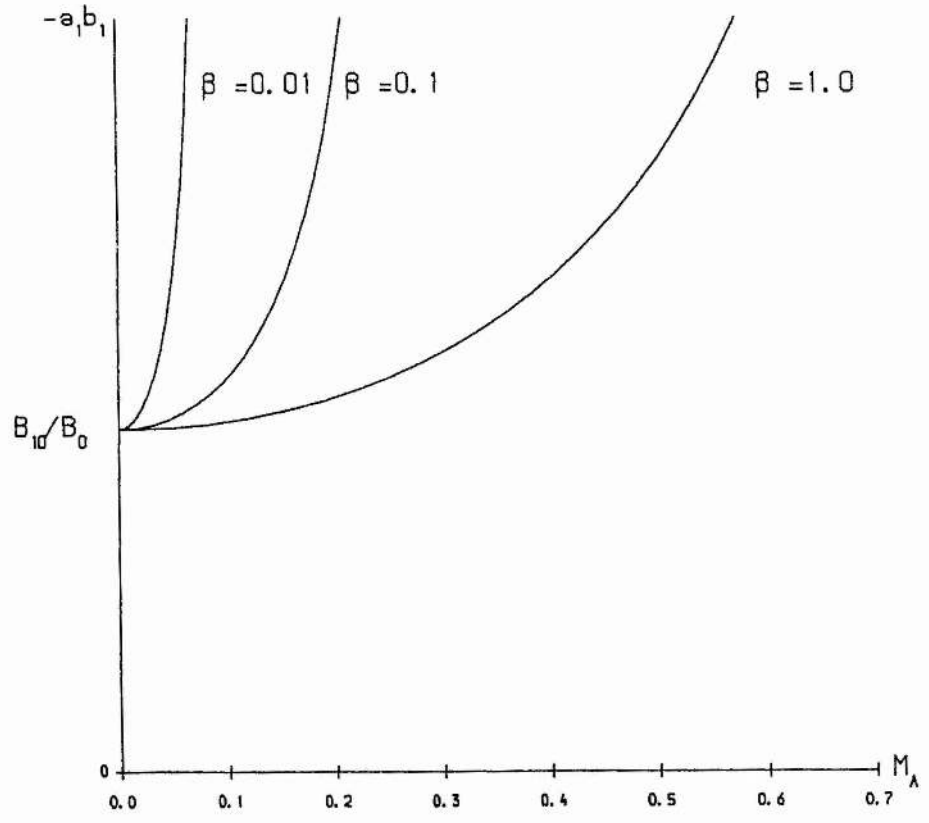

Figure 2.4b

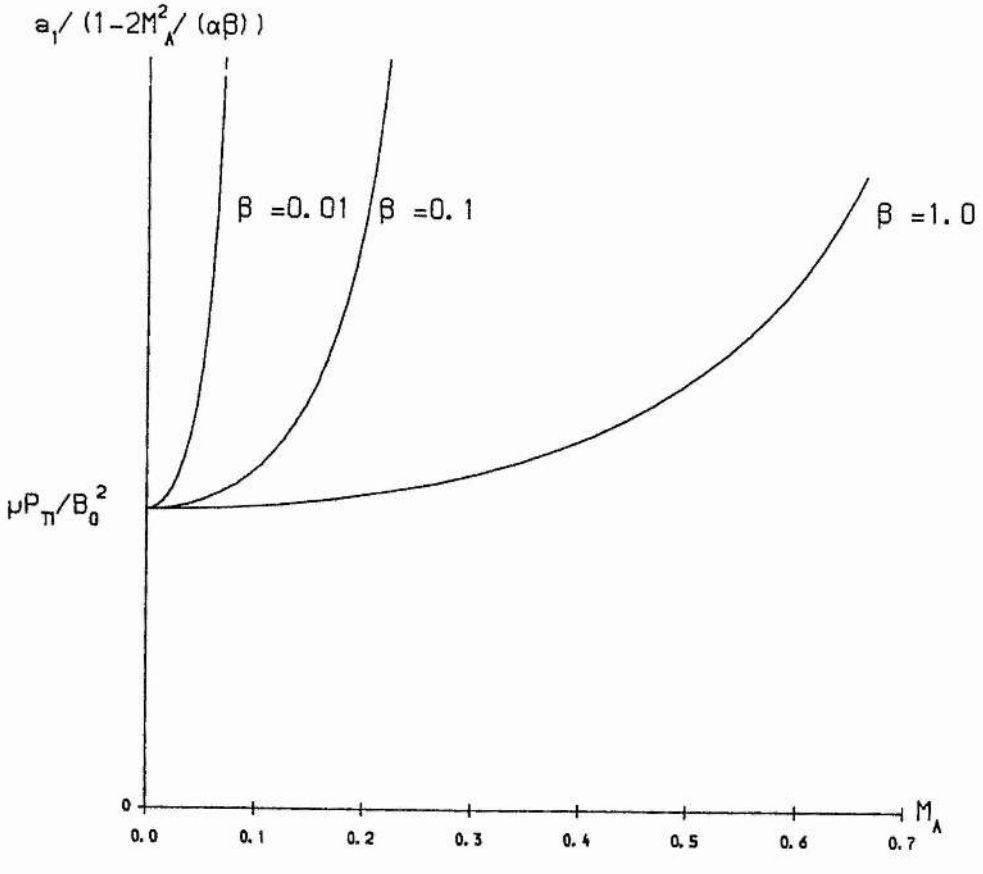

Figure 2.4c

$$v\frac{d}{ds}(v\hat{s}) = v\frac{dv}{ds}\hat{s} + v^2\frac{d\hat{s}}{ds}$$
$$= \frac{d}{ds}\left(\frac{1}{2}v^2\right)\hat{s} + \frac{v^2}{\mathcal{R}}\hat{n}, \qquad (2.44)$$

where $\hat{n}$ is the principal normal to the streamline and $\mathcal{R}$ is its radius of curvature. The second term on the right-hand side results in a centrifugal force acting on the plasma. Increasing v_0 increases the centrifugal force. To balance this, there tends to be a corresponding increase in the tension of the fieldlines which decreases their radius of curvature. This increase in the curvature of the field is consistent with the solutions here (in which the maximum of B_{1x} increases). More magnetic fieldlines become bunched in the regions of strong field, thus explaining the increase in B_{1z} at $z\rightarrow\infty$ as v_0 increases.

To explain the pressure variations, consider the case of converging fieldlines. As plasma rises, the flow velocity increases, with the streamlines becoming closer together, and so the plasma pressure falls. Increasing v_0 bunches the streamlines clser together, and so we expect an increase in the flow velocity maximum and a decrease in the plasma pressure minima. For diverging fieldlines, the opposite would occur (i.e., flow velocity minima to decrease, and plasma pressure maxima to increase).

These intuitive ideas may be verified from the equation of motion (1.25) as follows, since it may be decomposed into components along a streamline ($\hat{s}$) (the same direction as the fieldlines in this model) and perpendicular to a streamline ($\hat{n}$). This gives

$$\rho\frac{d}{ds}\left(\frac{v^2}{2}\right)\hat{s} + \rho\frac{v^2}{\mathcal{R}}\hat{n} = -\frac{dp}{ds}\hat{s} - \frac{dp}{dn}\hat{n} - \frac{d}{dn}\left(\frac{B^2}{2\mu}\right)\hat{n} + \frac{B^2}{\mu\mathcal{R}}\hat{n}, \qquad (2.45)$$

where the symbols have their usual meaning. Linearising equation (2.45), the above equation may be rewritten as

$$\gamma\frac{v_0^2}{c_s^2}\frac{d}{ds}\left(\frac{v_1}{v_0}\right)\hat{s} + \frac{2\gamma}{\mathcal{R}}\frac{v_0^2}{c_s^2}\left(\frac{v_1}{v_0}\right)\hat{n} = -\frac{d}{ds}\left(\frac{p_1}{p_0}\right)\hat{s} - \frac{d}{dn}\left(\frac{p_1}{p_0}\right)\hat{n}$$
$$+\frac{2}{\beta}\frac{d}{dn}\left(\frac{B_1}{B_0}\right)\hat{n} + \frac{1}{\beta}\left(\frac{B_1}{B_0}\right)\frac{1}{\mathcal{R}}\hat{n}.$$

In terms of the components, we have

$$\gamma \frac{v_0^2}{c_s^2} \frac{d}{ds}\left(\frac{v_1}{v_0}\right) = -\frac{d}{ds}\left(\frac{p_1}{p_0}\right), \tag{2.46}$$

and

$$\frac{2\gamma v_0^2}{c_s^2}\left(\frac{v_1}{v_0}\right) = -\frac{d}{dn}\left(\frac{p_1}{p_0}\right) + \frac{2}{\beta}\frac{d}{dn}\left(\frac{B_1}{B_0}\right) + \frac{1}{\beta \mathcal{R}}\left(\frac{B_1}{B_0}\right). \tag{2.47}$$

Now, as v_0 increases, the left-hand side of equation (2.46) increases, and so $-d(p_1/p_0)/ds$ increases. In other words, the pressure gradient $d(p_1/p_0)/ds$ decreases. Since the plasma pressure is fixed at the base (z=0), the pressure gradient may be decreased only by increasing the maximum pressure at $z \to \infty$. It then follows that the maximum flow velocity will decrease in accord with our solutions.

Turning now to variations that occur when β is altered, note that increasing β decreases the strength of the magnetic field. In the case of diverging fieldlines (Figure 2.5a), increasing β will reduce the bunching of the fieldlines in regions of strong field, i.e, the fieldlines will move toward the axis x=0.

Now increasing β (or p_0) in equation (2.46) requires a corresponding increase in the flow velocity maximum of v_{1z}. Increasing β in equation (2.46) requires an increase in the radius of curvature $\mathcal{R}$ to balance the increase in β on the right-hand side. This reduces the curvature of the fieldlines, and so they become less bunched with a smaller field strength. Since the flow velocity increases, one expects a larger pressure gradient in equation (2.47). This may be achieved by decreasing the maximum of plasma pressure at $z \to \infty$, in agreement with our solutions.

The fieldlines are given by equation (2.41) and in Figure 2.5a to demonstrate the effect of varying v_0. For $a_1>0$, $b_1>0$ the fieldlines diverge. Increasing v_0 (Figure 2.5b) bends the fieldlines more towards the boundaries $x=\pm L$. Also, increasing v_0 broadens the region of high plasma pressure near $x=\pm L$. This can be seen in equation (2.47), where an increase in v_0 may be balanced by a decrease in dp/dn, i.e, an increase in the plasma pressure. Priest (Paper 1) has suggested that these **slow-mode compressions** may appear in the corona as

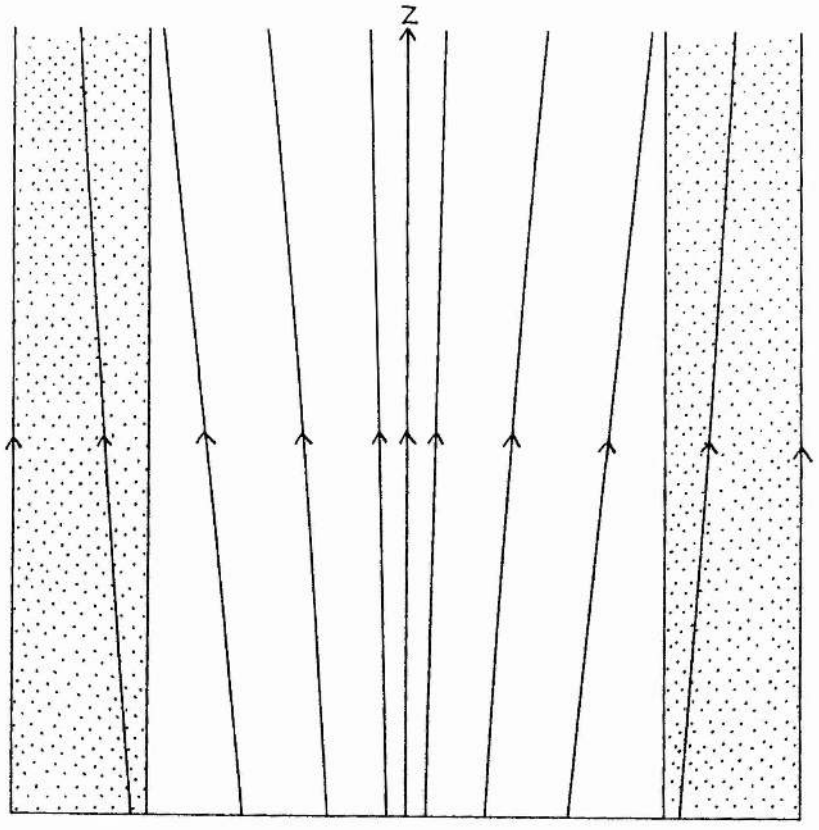

Figure 2.5a

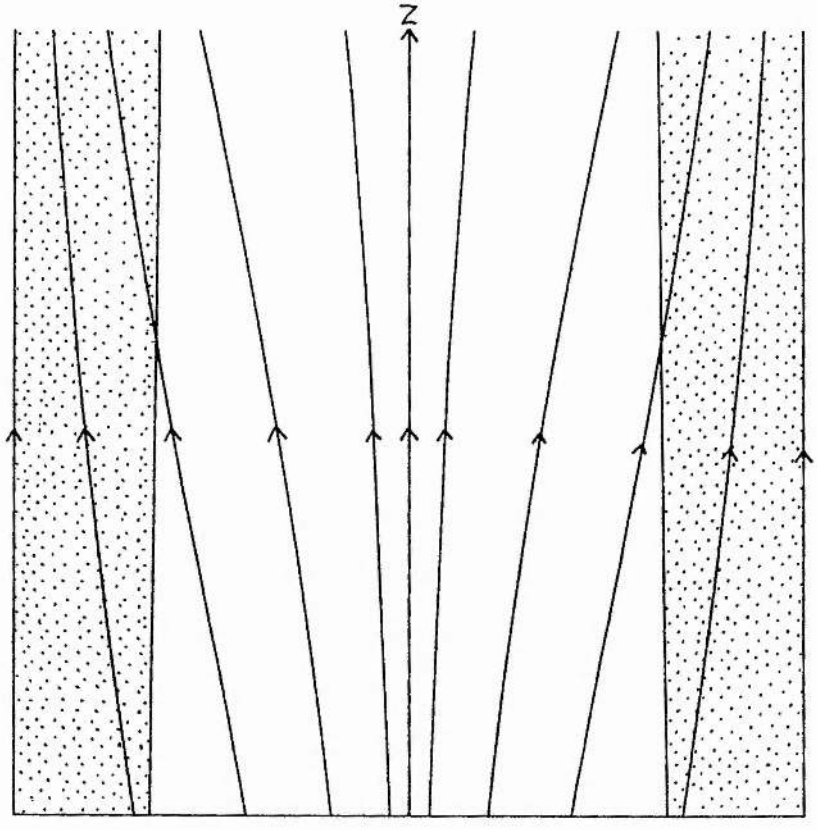

Figure 2.5b

Figure 2.5 : Holes or voids associated with slow-mode expansions for, (a) low-speed flow (M_A=0.1,β=0.5), (b)high-speed flow (M_A=0.5,β=0.5). Magnetic fieldlines are arrowed and high plasma pressure regions are shaded.

strong (i.e., diverging) coronal holes or voids of reduced plasma pressure. From this model, we suggest that the 'strength' of the coronal hole or void depends upon the flow speed v_0.

When $a_1 < 0$, $b_1 > 0$, we have an example of converging fieldlines (Figure 2.6a). Again, increasing v_0 bunches the fieldlines toward the region of stronger field near the axis x=0. The region of high plasma pressure near x=0 broadens with increasing v_0. Priest (Paper 1) has suggested that such **fast-mode compressions** may show up in the corona as strong (i.e., converging) plumes of enhanced pressure.

(2.5) Solutions With Oscillatory z-Dependence

It has been already noted that when $\alpha^2<0$ the oscillatory z-dependence fails to satisfy boundary conditions (2.17), which we can replace and so find valid solutions for (i) $c_T<v_0<c_s$ and (ii) $v_0>v_A$.

When $c_T<v_0<c_s$ equations (2.14) and (2.15) may be written as

$$\frac{d^2X}{dx^2} + c^2X=0 , \quad \frac{d^2Z}{dz^2} + \alpha^2c^2Z = b ,$$

where

$$\alpha^2 = \frac{M_T^2-1}{(M^2-1)(M_A^2-1)} .$$

On applying boundary conditions (2.43),(2.18) and (2.19), the solution of equation (2.13) is found to be

$$A_1 = \sum_{n=1}^{\infty} - \frac{a_n B_0 L}{n\pi} \sin\left(\frac{n\pi x}{L}\right)\left\{d_n \cos\left(\frac{n\pi\alpha z_0}{L}\right) + \cos\left(\frac{n\pi\alpha(z-z_0)}{L}\right)\right\} ,$$

and from equations (2.8) and (2.4) we obtain

$$B_{1x} = \sum_{n=1}^{\infty} a_n B_0 \alpha \sin\left(\frac{n\pi x}{L}\right)\sin\left(\frac{n\pi\alpha(z-z_0)}{L}\right), \qquad (2.48)$$

$$B_{1z} = \sum_{n=1}^{\infty} a_n B_0 \cos\left(\frac{n\pi x}{L}\right)\left\{d_n \cos\left(\frac{n\pi\alpha z_0}{L}\right) + \cos\left(\frac{n\pi\alpha(z-z_0)}{L}\right)\right\}, \qquad (2.49)$$

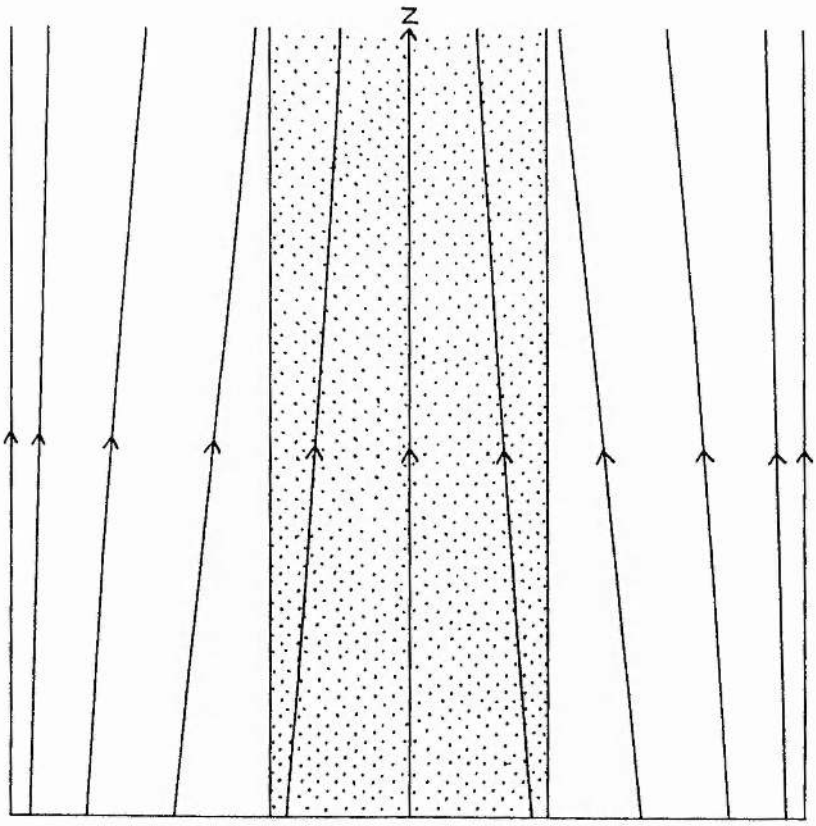

Figure 2.6a

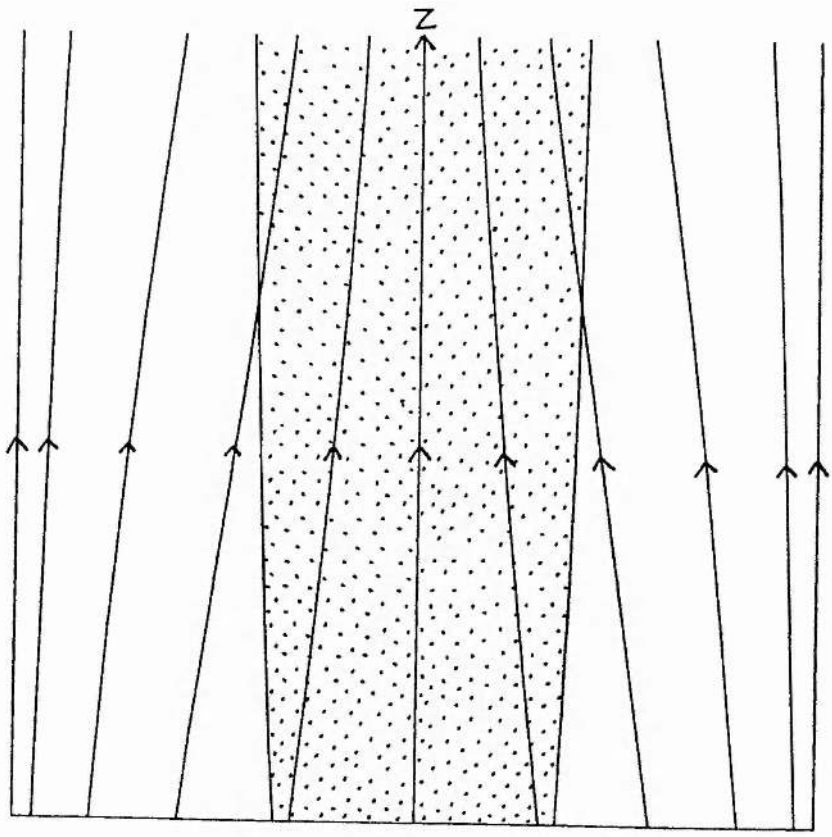

Figure 2.6b

Figure 2.6: Plumes of enhanced pressure (shaded) associated with fast-mode expansions for ,(a) low-speed flow (M_A=0.1,β=0.5) (b) high-speed flow (M_A=0.1,β=0.3).

$$v_{1x} = \sum_{n=1}^{\infty} a_n v_0 \alpha \sin\left(\frac{n\pi x}{L}\right) \sin\left(\frac{n\pi\alpha(z-z_0)}{L}\right) \qquad (2.50)$$

Substitution of equations (2.48),(2.49) and (2.50) into equation (2.2) and integrating gives

$$p_1 = -\frac{B_0^2}{\mu} \sum_{n=1}^{\infty} a_n \cos\left(\frac{n\pi x}{L}\right) \left\{ d_n \cos\left(\frac{n\pi\alpha z_0}{L}\right) + \frac{M_A^2}{1-M^2} \cos\left(\frac{n\pi\alpha(z-z_0)}{L}\right) \right\},$$

and hence from equation (2.12)

$$v_{1z} = \sum_{n=1}^{\infty} \frac{a_n v_0}{M^2-1} \cos\left(\frac{n\pi x}{L}\right) \left\{ 1 - \cos\left(\frac{n\pi\alpha(z-z_0)}{L}\right) \right\}.$$

By a similar procedure solutions when $v_0 > v_A$ may be found which are similar to those above, except that the sign of v_{1z} is reversed.

(2.6) Alternative Side Boundary Conditions

A natural development of the symmetric solutions presented earlier is to modify the boundary condition on $x=\pm L$, to allow magnetic flux to enter or leave the region $-L \le x \le L$, $z \ge 0$. This may be accomplished by replacing equation (2.19) by

$$B_{1z} = 0 \text{ on } x=\pm L\,. \qquad (2.51)$$

It is possible to find solutions for which B_{1z} is symmetric or asymmetric about $x=0$, although only the symmetric case is considered here. In particular, the magnetic flux Φ crossing the boundaries $x=\pm L$ is calculated, and the dependence upon the uniform state parameters M_A and β considered. When all the flux entering the region leaves across the boundaries $x=\pm L$, we have a coronal hole-like structure whose width is determined.

a) Symmetric Solutions

Applying the boundary conditions (2.17),(2.18) and (2.51) to the solutions of equations (2.14) and (2.15), it is easily shown that the solution to (2.13) for $-L \le x \le L$, $z \ge 0$ is

$$A_1 = \sum_{n=1}^{\infty} - \frac{a_n B_0 L}{(n-1/2)\pi} \sin\left(\frac{(n-1/2)\pi x}{L}\right)\left\{b_n + \exp\left(-\frac{(n-1/2)\pi\alpha z}{L}\right)\right\}, \qquad (2.52)$$

where α is given by equation (2.37). The resulting perturbation quantities are

$$B_{1x} = \sum_{n=1}^{\infty} a_n B_0 \alpha \sin\left(\frac{(n-1/2)\pi x}{L}\right)\exp\left(-\frac{(n-1/2)\pi\alpha z}{L}\right), \qquad (2.53)$$

$$B_{1z} = \sum_{n=1}^{\infty} a_n B_0 \cos\left(\frac{(n-1/2)\pi x}{L}\right)\left\{b_n + \exp\left(-\frac{(n-1/2)\pi\alpha z}{L}\right)\right\}, \qquad (2.54)$$

$$v_{1x} = \sum_{n=1}^{\infty} a_n v_0 \alpha \sin\left(\frac{(n-1/2)\pi x}{L}\right)\exp\left(-\frac{(n-1/2)\pi\alpha z}{L}\right), \qquad (2.55)$$

$$p_1 = -\frac{B_0^2}{\mu}\sum_{n=1}^{\infty} a_n \cos\left(\frac{(n-1/2)\pi x}{L}\right)\left\{b_n + \frac{M_A^2}{1-M^2}\exp\left(-\frac{(n-1/2)\pi\alpha z}{L}\right)\right\}, \qquad (2.56)$$

$$v_{1z} = -\sum_{n=1}^{\infty} \frac{a_n v_0}{1-M^2} \cos\left(\frac{(n-1/2)\pi x}{L}\right)\left\{1 - \exp\left(-\frac{(n-1/2)\pi\alpha z}{L}\right)\right\}. \qquad (2.57)$$

Treating the fundamental mode in the same way as the solutions discussed in section 2.4 is left for an exercise for the reader.

To determine the equation of the fieldlines of the fundamental mode, we note that

$$B_{1x} = a_1 B_0 \alpha \sin\left(\frac{\pi x}{2L}\right)\exp\left(-\frac{\pi\alpha z}{2L}\right),$$

and so the fieldlines are given by

$$\frac{dz}{dx} = \frac{B_0}{B_{1x}}$$

$$= \frac{1}{\left[a_1 \alpha \sin\left(\frac{\pi x}{2L}\right) \exp\left(-\frac{\alpha \pi z}{2L}\right)\right]} . \qquad (2.58)$$

Solving equation (2.58) for a fieldline passing through the footpoint $(x_0,0)$, we obtain

$$a_1\left\{1 - \exp\left(-\frac{\alpha \pi z}{2L}\right)\right\} = \log\left\{\frac{\tan\left(\frac{\pi x}{4L}\right)}{\tan\left(\frac{\pi x_0}{4L}\right)}\right\} . \qquad (2.59)$$

When $a_1>0$, the fieldlines diverge from the line x=0 (Figure 2.7), and the flux leaves the region $-L \le x \le L$, $z \ge 0$. However, when $a_1<0$, the fieldlines converge toward the axis x=0, and so flux enters the region. We will consider the case $a_1>0$ in a little more detail, since it may resemble a coronal hole magnetic field. In practice, the field leaving the region would probably form a closed field structure.

b) Magnetic Flux Calculations

The magnetic flux Φ_b, entering the region at the base (z=0), is given by

$$\Phi_b = \int_{-L}^{L} B_{1z}(x,0)dx$$
$$= \frac{4LB_{10}}{\pi B_0} , \qquad (2.60)$$

which depends upon the form of the normal component of the magnetic field imposed at the coronal base.

The magnetic flux Φ crossing the boundary x=L is given by

$$\Phi = \int_{0}^{\infty} B_{1x}(L,x)dz$$
$$= \frac{2L}{\pi} B_{10}(\beta_{10}+1)\left(\frac{1-M^2}{1-M_T^2}\right)$$
$$= \frac{2L}{\pi} B_{10}(\beta_{10}+1)\left(\frac{1-2M_A^2/(\gamma\beta)}{1-[2/(\gamma\beta)+1]M_A^2}\right), \qquad (2.61)$$

which depends upon both the uniform state and perturbation parameters. From Figure 2.7b, we see that increasing M_A increases the amount of flux crossing the boundary x=l, when we restrict our attention to $0<v_0<c_T$.

To explain why this occurs, we return to the equation

$$\frac{\rho v^2}{\mathcal{R}} = -\frac{dp}{dn} - \frac{d}{dn}\left(\frac{\mathbf{B}^2}{2\mu}\right) + \frac{\mathbf{B}^2}{\mu\mathcal{R}}, \tag{2.62}$$

the component of the equation of motion normal to the fieldlines. Linearising equation (2.62), we obtain the first-order equation

$$\frac{2\rho_0 \mathbf{v}_0.\mathbf{v}_1}{\mathcal{R}} = -\frac{dp_1}{dn} - \frac{d}{dn}\left(\frac{\mathbf{B}_0.\mathbf{B}_1}{\mu}\right) + \frac{2\mathbf{B}_0.\mathbf{B}_1}{\mu\mathcal{R}} . \tag{2.63}$$

The terms of equation(2.63) may be identified from left to right as the centrifugal force F_c, the plasma pressure gradient F_p, the magnetic pressure gradient F_{mp}, and the magnetic tension F_T. When the x-component of the equation of motion is considered, namely;

$$\rho_0 v_0 \frac{\partial v_{1x}}{\partial z} = -\frac{\partial p_1}{\partial x} - \frac{B_0}{\mu}\frac{\partial B_{1z}}{\partial x} + \frac{B_0}{\mu}\frac{\partial B_{1x}}{\partial z},$$

the various force terms may be calculated from the fundamental modes of the equations (2.53)-(2.57) to be

$$F_c = -\frac{\pi\gamma p_0 B_{10}}{2LB_0}(\beta_{10}+1)\frac{M^2}{1-M_A{}^2}\sin\left(\frac{\pi x}{2L}\right)\exp\left(-\frac{\pi\alpha z}{2L}\right), \tag{2.64}$$

$$F_p = -\frac{\pi B_0{}^2 a_1}{2L\mu}\sin\left(\frac{\pi x}{2L}\right)\left\{b_1+\frac{M_A{}^2}{1-M^2}\exp\left(-\frac{\pi\alpha z}{2L}\right)\right\}, \tag{2.65}$$

$$F_{mp} = \frac{\pi B_0{}^2 a_1}{2L\mu}\sin\left(\frac{\pi x}{2L}\right)\left\{b_1+\exp\left(-\frac{\pi\alpha z}{2L}\right)\right\}, \tag{2.66}$$

$$F_T = -\frac{B_0{}^2}{\mu(1-M^2)}\sin\left(\frac{\pi x}{2L}\right)\exp\left(-\frac{\pi\alpha z}{2L}\right). \tag{2.67}$$

We note that the static parts of the magnetic and plasma pressures cancel. Thus, for the remaining parts as v_0 increases in $0<v_0<c_T$,

$$F_c \sim \frac{M^2}{1-M_A{}^2}; \tag{2.68}$$

$$F_p \sim \frac{M_A{}^2}{1-M_T{}^2}; \tag{2.69}$$

and

$$F_{mp} \sim \frac{1-M^2}{1-M_T{}^2}. \tag{2.70}$$

These all increase with v_0, with F_p increasing faster than F_{mp}. To maintain horizontal force balance, F_T is required to increase, which will result in a greater curvature of the fieldlines and hence an increase in Φ. From equation (2.67), we note that there is indeed an increase in F_T with v_0.

When β is increased, we find that Φ decreases (Figure 2.7b) for any value of M_A. Increasing β is equivalent to increasing c_s or decreasing M. From equations (2.69) and (2.70) we see that F_p and F_{mp} decrease with increasing β, with F_{mp} decreasing faster. For force balance, we then require a decrease in F_c, which is observed to occur from equation (2.68). This results in a decrease in the curvature of the fieldlines and hence a decrease in Φ.

c) Case of Total Flux Loss - Coronal Holes

It is instructive to consider the case

$$|\Phi| = \Phi_b, \tag{2.71}$$

that is, when all the flux entering at the base escapes across the boundaries $x=\pm L$, which may be relevent for modelling coronal holes.The coronal hole would be taken to be the interval lying between the two innermost fieldlines. When equation (2.71) holds, one finds that

$$M_A^2 = \frac{\beta_{10}}{2\beta_{10}/(\gamma\beta)-1}. \tag{2.72}$$

Substituting equation (2.72) in equation (2.38) and (2.39) gives

$$a_1 = \frac{B_{10}}{B_0}, \; b_1 = 0. \tag{2.73}$$

A simple expression for the widths of the hole at the coronal base may be derived as follows.

Setting x=L, and allowing $z \to \infty$ in equation (2.59), we obtain an expression for the footpoint of the fieldline closest to the axis x=0, namely ,

$$x_0 = \frac{4L}{\pi} \tan^{-1}[\exp(-a_1)]. \tag{2.74}$$

By symmetry of the equation (2.54) for B_{1z}, the base width D of the coronal hole may thus be approximated by

$$\begin{aligned} D &= \frac{8L}{\pi} \tan^{-1}[\exp(-a_1)] \\ &= \frac{8L}{\pi} \tan^{-1}\left[\exp\left(-\frac{B_{10}}{B_0}\right)\right]. \end{aligned} \tag{2.75}$$

Clearly D is dependent upon the form of the magnetic field imposed at z=0, but independent of the other parameters β_{10},M_A and β.

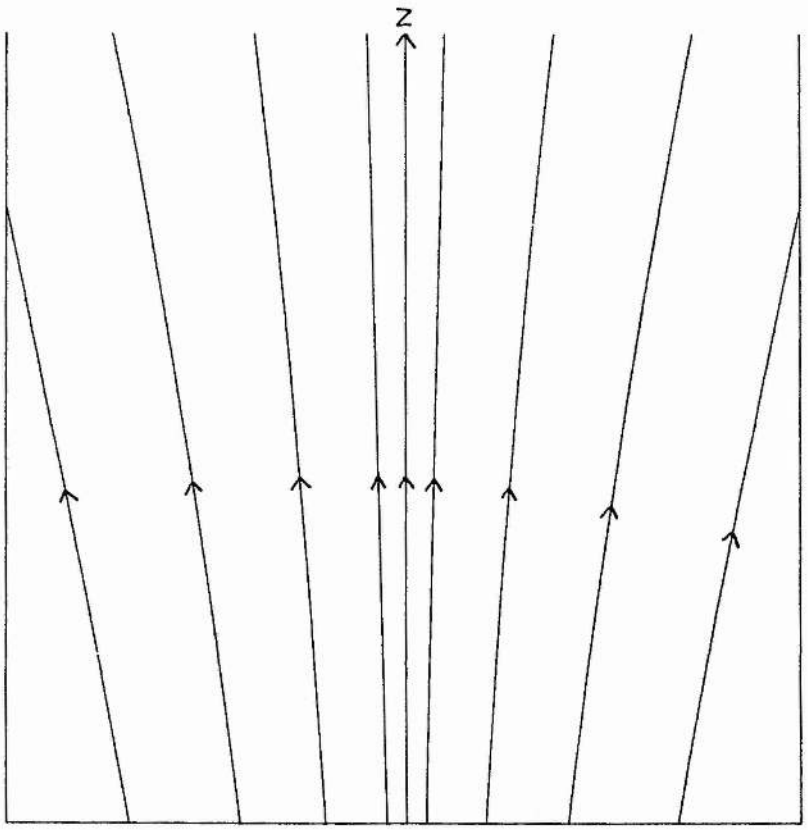

Figure 2.7(a): Diverging fieldlines with flux crossing the boundaries $x=\pm L$ with $M_A=0.01, \beta=0.3$.

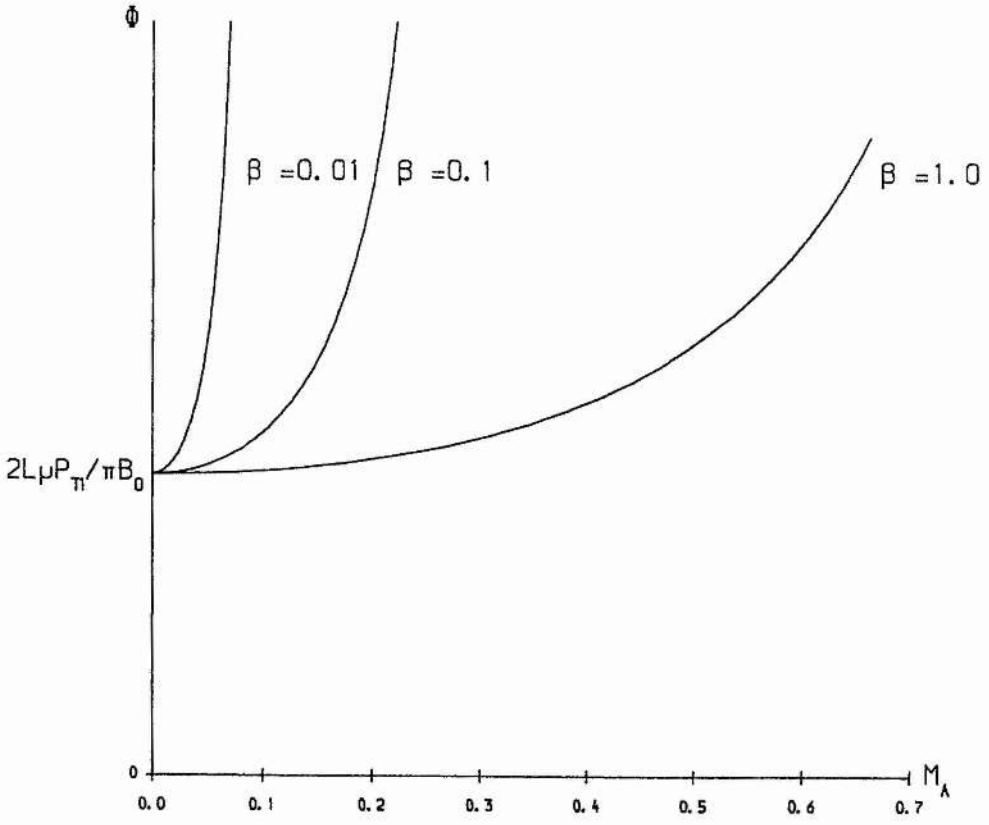

Figure 2.7(b): The M_A-dependence of magnetic flux Φ through the side boundary for several values of β when $0<M_A<(1+2/(\gamma\beta))^{-1/2}$.

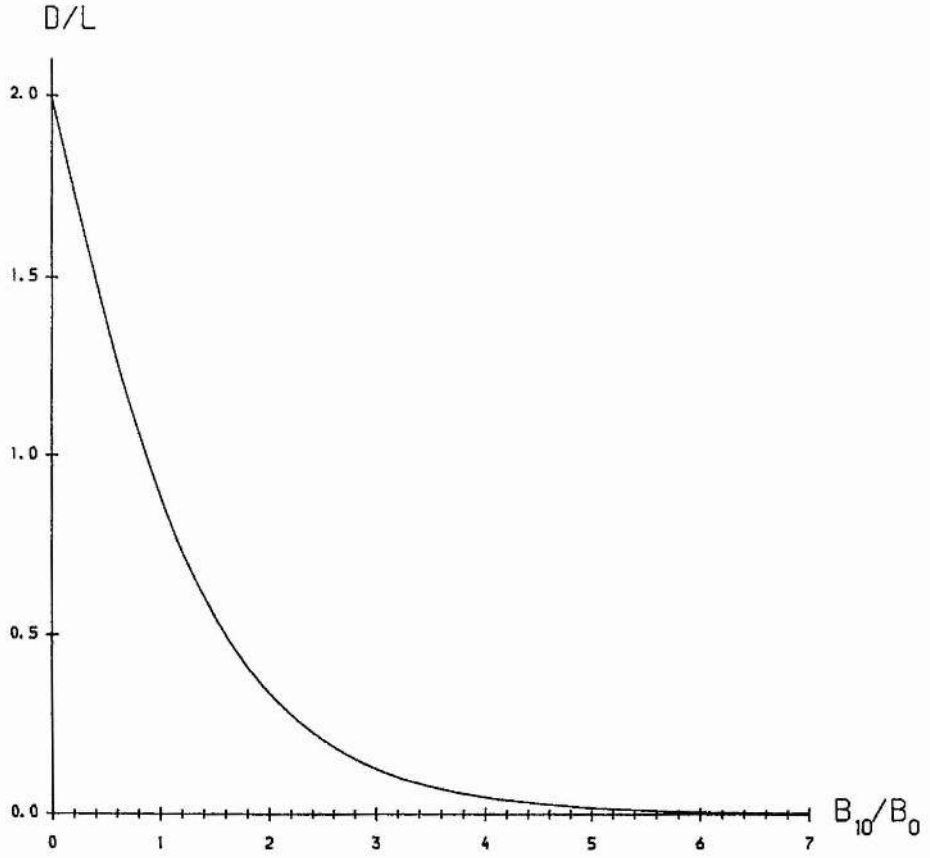

Figure 2.7(c): The dependence of the coronal hole width D/L on B_{10}/B_0, where $B_0 f(0)$ is the imposed normal magnetic field on the and $B_{1z}(x,0)=B_0 f(x)$.

As one would expect increasing B_{10} (increasing the size of the magnetic field imposed at the base) results in a decrease in the coronal hole width D (Figure 2.7c), with the maximum coronal width occurring when $B_{10}=0$.

(2.7) Nonseparable Solutions

Up to this point only separable solutions of the governing equation (2.13) have been considered. However, it is possible to employ other standard techniques to determine wider classes of solutions, which may be relevant when studying the solar corona.

First, we integrate (2.13) with respect to z to give

$$\frac{\partial^2 A_1}{\partial z^2} + \alpha^2 \frac{\partial^2 A_1}{\partial x^2} = h(x), \qquad (2.76)$$

where h is some function of x. In the special case when $v_0 << c_s, v_A$, h(x) has been identified as the plasma pressure gradient $(\mu/B_0)dp_1/dx$.

The nature of equation (2.76) depends upon the magnitude of v_0. When $0<v_0<c_T$, and $c_s<v_0<v_A$, equation (2.76) is elliptic (Poisson's equation), while in the intervals $c_T<v_0<c_s$ and $v_0>v_A$, equation (2.76) becomes hyperbolic. We shall consider the two cases separately.

a) Elliptic Case

Introducing the variables

$$\upsilon_1 = x/\alpha \ , \upsilon_2 = z \ ,$$

equation (2.76) may be written in the canonical form

$$\frac{\partial^2 A_1}{\partial \upsilon_1^2} + \frac{\partial^2 A_1}{\partial \upsilon_2^2} = h(\alpha \upsilon_1) \ . \qquad (2.77)$$

The boundary conditions (2.16)-(2.19) become

$$\frac{\partial A_1}{\partial \upsilon_1} = - \alpha B_0 f(\alpha \upsilon_1) \text{ on } \upsilon_2 = 0 \ ,$$

$$\frac{\partial A_1}{\partial \upsilon_2} \to 0 \text{ as } \upsilon_2 \to \infty \ ,$$

$$\frac{\partial A_1}{\partial \upsilon_2} = 0 \text{ on } \upsilon_1 = 0, \qquad (2.78)$$

$$\frac{\partial A_1}{\partial \upsilon_2} = 0 \text{ on } \upsilon_1 = \pm \frac{L}{\alpha},$$

in terms of the new variables. Equations (2.77) and (2.78) constitute an inhomogeneous Neumann-boundary value problem, which can be solved using Green's functions, giving a solution of the form

$$A_1 = \frac{1}{4\pi} \int_0^{\infty} \int_{-L/\alpha}^{L/\alpha} (h(\alpha\xi) + \alpha B_0 f(\alpha\xi)) G(\xi,\eta,\upsilon_1,\upsilon_2) d\xi d\eta , \qquad (2.79)$$

where G is the appropriate Green's function. Once the specific functional form of h and f are specified, it is possible to use (2.79) to determine all the remaining perturbation quantities.

b) Hyperbolic Case

Setting

$$-\gamma_1^2(v_0) = \frac{1-M_T^2}{(1-M^2)(1-M_A^2)},$$

where $c_T < v_0 < c_s$ and $v_0 > v_A$, we may transform (x,z) into the variables (ξ_1,η_1) defined by

$$\xi_1 = x + \gamma_1 z , \quad \eta_1 = x - \gamma_1 z.$$

This transformation will change equation (2.77) into the canonical form

$$\frac{\partial^2 A_1}{\partial \xi_1 \partial \eta_1} = -\frac{1}{4} h\left(\frac{1}{2}(\xi_1+\eta_1)\right).$$

Integrating this equation with respect to ξ_1 and η_1, we obtain

$$A_1 = -\frac{1}{4} \int_D d\eta_1 \int h((\xi_1+\eta_1)/2) d\xi_1 + S(\xi_1) + T(\eta_1) , \qquad (2.80)$$

where $S(\xi_1)$ and $T(\eta_1)$ are determined by the boundary conditions, and D is the domain of the solution. The boundary conditons may be recast in the form

$$\frac{\partial A_1}{\partial \xi_1} + \frac{\partial A_1}{\partial \eta_1} = B_0 f((\xi_1+\eta_1)/2) \text{ on } (\xi_1+\eta_1) = 0 ,$$

$$\frac{\partial A_1}{\partial \xi_1} - \frac{\partial A_1}{\partial \eta_1} \to 0 \text{ as } (\xi_1 - \eta_1) \to \infty,$$

$$\frac{\partial A_1}{\partial \xi_1} - \frac{\partial A_1}{\partial \eta_1} = 0 \text{ on } (\xi_1+\eta_1) = 0 ,$$

$$\frac{\partial A_1}{\partial \xi_1} - \frac{\partial A_1}{\partial \eta_1} = 0 \text{ on } (\xi_1+\eta_1) = \pm L.$$

Thus, we have illustrated that equation (2.13) has more general classes of solutions, which may be of importance in the solar corona, particularly when the form of the pressure gradient dp_1/dx is known.

(2.8) Connection With MHD Waves

Noting that

$$\frac{\partial A_1}{\partial z} = \frac{B_0}{v_0} v_{1x} ,$$

equation (2.13) may be written as

$$\frac{\partial^2 v_x}{\partial x^2} + \alpha^{-2} \frac{\partial^2 v_x}{\partial z^2} = 0 . \qquad (2.81)$$

Setting

$$v_{1x}(x,z) = \hat{v}_{1x}(x) e^{ikz},$$

and making the transformation $v_0 \rightarrow \omega/k_z$, equation (2.81) becomes

$$\frac{d^2 \hat{v}_{1x}}{dx^2} + m_0^2 \hat{v}_{1x} = 0 ,$$

where

$$m_0^2 = \frac{(k_z^2 v_A^2 - \omega^2)(k_z^2 c_s^2 - \omega^2)}{(c_s^2 + v_A^2)(k_z^2 c_s^2 - \omega^2)} .$$

This is just the usual wave equation for a uniform medium (see for example Roberts, 1986). We have obtained this result by a 'Doppler ' shift from the steady state. However, it is important to see that it is not proper to think of the solutions presented in this chapter as merely a Doppler shift of the usual wave solutions. The reason for this is related to the boundary conditions we impose. By specifying quantities at z=0, we give a reference level which does not move as the plasma flows into the region $-L \leq x \leq L$, $z \geq 0$, and hence is not Doppler shifted.

(2.9) Conclusions

In this chapter we have sought to clarify further the nature of MHD interactions which create observed structures. We have shown that the nature of the interaction depends critically upon the parameters B_{10} and β_{10} representing

the perturbed magnetic field and plasma beta at the base (equation (2.34)). By changing the form of B_{10} and β_{10}, the interaction can switch from a **slow-mode** to a **fast-mode**, and from an **expansion** to a **compression**. The uniform state parameters $M_A$and β, representing the Alfven Mach number and plasma beta of the basic state determine the strength of the interaction. For example, plumes of enhanced pressure become more enhanced by increasing M_A.

From the discussion in section 2.6 it becomes evident that there is a complex balance between centrifugal, pressure, and tension forces. The magnitude of these forces depends not only on the spatial coordinates but also upon the parameters which characterise the uniform state. It is interesting to note that such a simple example still reveals a rich complexity in the physics.

By including inertial effects, we have shown that the theory developed by Priest (Paper 1) can be extended to include all flow speeds v_0. The generalised governing equation derived in section 2.2 allows us to construct solutions which depend upon the flow speed v_0 and the plasma pressure of the uniform state. Increasing v_0, for $0<v_0<c_T$, increases the maximum values of the magnetic field strength and the flow velocity. Increasing p_0 decreases the maximum values of the magnetic field strength and flow. The curvature of the fieldlines and isobars is also a function of v_0.

Altering the side boundary conditions allows us to find solutions for which magnetic flux leaves the region of interest, which may be relevant in studying coronal holes. An expression for the width of a coronal hole and the way it varies with the parameters of the perturbed state is also obtained.

Finally,we have shown how more general classes of solutions to our governing equation may be found, and we indicated our solutions are related to MHD waves in a uniform medium.

Chapter 3 : Cylindrical Geometry

(3.1) Introduction

The analysis of the previous chapter is here extended to a cylindrical geometry, which is more realistic when modelling three-dimensional structures in the solar corona, such as plumes and coronal holes. Both axial symmetric and nonaxial symmetric magnetic fields are treated. For the axisymmetric case there are solutions with an azimuthal component of magnetic field $B_{1\phi}$. These represent Alfvenic disturbances and decouple from the magnetoacoustic disturbances that we consider in detail. The basic characteristics of the axisymmetric solutions are found to be similar to the Cartesian case considered in the previous chapter. Quantitatively, the interactions are stronger in the central region of the cylinder, weaker at the outer boundary. Pressure gradients are found to be smaller in the cylindrical case.

Solutions dependent upon all three spatial variables exhibit an asymmetry because of the angular angular dependence. They depend upon the azimuthal field imposed at the coronal base.

We now give an outline of the chapter. In section 2.3, the governing equation for both the symmetric and nonaxisymmetric cases are derived from the linearised MHD equations. Section 3.3 is devoted to the axially symmetric case where we note the qualitative similarities with the rectangular case, and point out the quantitative differences. The non-symmetric solutions are developed in section 3.4, and the properties of a particular mode is discussed.

(3.2) Derivation of Governing Equations

Consider a steady state in a cylindrical geometry (r,ϕ,z) with uniform flow $(v_0\hat{z})$, magnetic field $(B_0\hat{z})$, plasma pressure (p_0), and density (ρ_0). Linearising

the steady MHD equations about this basic state in the manner described in chapter 1 gives an equation of motion ;

$$\rho_0 v_0 \frac{\partial v_{1r}}{\partial z} = -\frac{\partial p_1}{\partial r} - \frac{B_0}{\mu}\frac{\partial B_{1z}}{\partial r} + \frac{B_0}{\mu}\frac{\partial B_{1r}}{\partial z}, \tag{3.1a}$$

$$\rho_0 v_0 \frac{\partial v_{1\phi}}{\partial z} = -\frac{1}{r}\frac{\partial p_1}{\partial \phi} - \frac{B_0}{\mu}\frac{1}{r}\frac{\partial B_{1z}}{\partial \phi} + \frac{B_0}{\mu}\frac{\partial B_{1\phi}}{\partial z}, \tag{3.1b}$$

$$\rho_0 v_0 \frac{\partial v_{1z}}{\partial z} = -\frac{\partial p_1}{\partial z}\ ; \tag{3.1c}$$

the solenoidal condition

$$\frac{1}{r}\frac{\partial}{\partial r}(rB_{1r}) + \frac{1}{r}\frac{\partial B_{1\phi}}{\partial \phi} + \frac{\partial B_{1z}}{\partial z} = 0\ ; \tag{3.2}$$

the continuity equation

$$v_0\frac{\partial \rho_1}{\partial z} + \rho_0\left[\frac{1}{r}\frac{\partial}{\partial r}(rv_{1r}) + \frac{1}{r}\frac{\partial v_{1\phi}}{\partial \phi} + \frac{\partial v_{1z}}{\partial z}\right] = 0\ ; \tag{3.3}$$

the induction equation

$$B_0\frac{\partial v_{1r}}{\partial z} - v_0\frac{\partial B_{1r}}{\partial z} = 0\ , \tag{3.4a}$$

$$B_0\frac{\partial v_{1\phi}}{\partial z} - v_0\frac{\partial B_{1\phi}}{\partial z} = 0, \tag{3.4b}$$

$$B_0\left(\frac{\partial}{\partial r}(rv_{1r}) + \frac{\partial v_{1\phi}}{\partial \phi}\right) - v_0\left(\frac{\partial}{\partial r}(rB_{1r}) + \frac{\partial B_{1\phi}}{\partial \phi}\right) = 0\ ; \tag{3.4c}$$

and finally, an adiabatic energy equation

$$p_1 = c_s^2\rho_1, \tag{3.5}$$

where $c_s = (\gamma p_0/\rho_0)^{1/2}$ is the sound speed. Again we neglect gravity in equation (3.1), for simplicity. Its effect is negligible by comparision with the pressure gradients only when the height of the region considered is much smaller than the coronal scale height, typically 100Mm . In equation (3.5) the effects of thermal conduction, radiation, and coronal heating are neglected for simplicity, and so we assume variations are adiabatic. Their neglect is valid only when the time for plasma to flow over the region of interest is much smaller than the time scales for these nonadiabatic processes.

For a three-dimensional field (i.e, a magnetic field that depends upon r,ϕ and z), equation (3.2) is identically satisfied by

$$\mathbf{B}_1 = \nabla \times (S\hat{\mathbf{z}}) + \nabla \times \nabla \times (T\hat{\mathbf{z}}), \tag{3.6}$$

where S and T are functions of r,ϕ and z. In component form, equation (3.6) becomes

$$\mathbf{B}_1 = \left(\frac{\partial^2 T}{\partial z \partial r} + \frac{1}{r}\frac{\partial S}{\partial \phi}\right)\hat{\mathbf{r}} + \left(\frac{1}{r}\frac{\partial^2 T}{\partial z \partial \phi} - \frac{\partial S}{\partial r}\right)\hat{\phi} - \left(\frac{1}{r}\frac{\partial}{\partial r}\left(r\frac{\partial T}{\partial r}\right) + \frac{1}{r^2}\frac{\partial^2 T}{\partial \phi^2}\right)\hat{\mathbf{z}}. \tag{3.7}$$

The most important point to note is that in three dimensions two functions S and T are required to describe a fieldline, compared with one function in two dimensions. Using equations (3.1c), (3.4c), (3.5) and (3.7), equation (3.3) may be written in the form

$$c_s^2 \frac{\partial \rho_1}{\partial z} = \frac{\rho_0 v_0^2}{B_0(1-M^2)} \frac{\partial}{\partial z}\left(\frac{1}{r}\frac{\partial}{\partial r}\left(r\frac{\partial T}{\partial r}\right) + \frac{1}{r^2}\frac{\partial^2 T}{\partial \phi^2}\right), \tag{3.8}$$

where $M=v_0/c_s$ is the Mach number. Substituting equation (3.4a), (3.5), (3.8), and (3.7) into equation (3.1a) we obtain

$$\frac{\partial}{\partial z}\left(\frac{\partial}{\partial z}\left(\frac{\partial^2 T}{\partial z \partial r} + \frac{1}{r}\frac{\partial S}{\partial \phi}\right) + \alpha^2 \frac{\partial}{\partial r}\left(\frac{1}{r}\frac{\partial}{\partial r}\left(r\frac{\partial T}{\partial r}\right) + \frac{1}{r^2}\frac{\partial^2 T}{\partial \phi^2}\right)\right) = 0, \tag{3.9}$$

where

$$\alpha^2 = \frac{1-M_T^2}{(1-M^2)(1-M_A^2)},$$

with M_T being the cusp Mach number, and M_A the Alfven Mach number. Similarly, from equation (3.1b) we deduce that

$$\frac{\partial}{\partial z}\left(\frac{\partial}{\partial z}\left(\frac{1}{r}\frac{\partial^2 T}{\partial r \partial \phi} - \frac{\partial S}{\partial r}\right) + \frac{\alpha^2}{r}\frac{\partial}{\partial r}\left(\frac{1}{r}\frac{\partial}{\partial r}\left(r\frac{\partial T}{\partial r}\right) + \frac{1}{r^2}\frac{\partial^2 T}{\partial \phi^2}\right)\right) = 0. \tag{3.10}$$

The properties of the constant α^2 have already been discussed in chapter 2. In this chapter we restrict attention to $\alpha^2>0$, which is more relevant to the low corona.

In the axially symmetric case, the ϕ-components of the equations decouple from the r,z-components. This allows us to set

$$A_1 = r\frac{\partial T}{\partial r}\ ;\ B_{1\phi} = -\frac{\partial S}{\partial r},$$

so that

$$\mathbf{B}_1 = \frac{1}{r}\frac{\partial A_1}{\partial z}\hat{\mathbf{r}} + B_{1\phi}\hat{\phi} - \frac{1}{r}\frac{\partial A_1}{\partial r}\hat{\mathbf{z}}, \tag{3.11}$$

and equation (3.9) becomes

$$\frac{\partial}{\partial z}\left(\frac{\partial^2 A_1}{\partial z^2} + \alpha^2 r \frac{\partial}{\partial r}\left(r\frac{\partial A_1}{\partial r}\right)\right) = 0 . \qquad (3.12)$$

The solutions of this equation will be considered in section 3.3. Observe, however, that from equations (3.1b) and (3.4b) we also have the azimuthal components (when $M_A \neq 1$)

$$B_{1\phi} = B_{1\phi}(r)$$

and

$$v_{1\phi} = v_{1\phi}(r),$$

giving purely Alfvenic disturbances in the azimuthal direction, which is analogous to what was found in the previous chapter in the cartesian geometry.

Returning to the ϕ-dependent case, the governing equation is obtained by eliminating S from equations (3.9) and (3.10), which yields, on using equation (3.7)

$$\frac{\partial}{\partial z}\left(\frac{\partial^2 B_{1z}}{\partial z^2} + \alpha^2\left(\frac{1}{r}\frac{\partial}{\partial r}\left(r\frac{\partial B_{1z}}{\partial r}\right) + \frac{1}{r^2}\frac{\partial^2 B_{1z}}{\partial \phi^2}\right)\right) = 0 . \qquad (3.13)$$

Equations (3.9) and (3.10) may be written in terms of the magnetic field components to give

$$\frac{\partial}{\partial z}\left(\frac{\partial B_{1r}}{\partial z} - \alpha^2 \frac{\partial B_{1z}}{\partial r}\right) = 0 , \qquad (3.14a)$$

and

$$\frac{\partial}{\partial z}\left(\frac{\partial B_{1\phi}}{\partial z} - \frac{\alpha^2}{r}\frac{\partial B_{1z}}{\partial \phi}\right) = 0 , \qquad (3.14b)$$

respectively. Thus, having solved equation (3.13) for B_{1z}, B_{1r} and $B_{1\phi}$ may be deduced from equations (3.14a) and (3.14b), respectively.

(3.3) Axisymmetic Solutions

(a) Derivation of Solutions

We seek solutions of equation (3.12) of the form

$$A_1 = rR(cr)Z(z),$$

and so obtain the ordinary differential equations

$$\frac{d^2Z}{dz^2} - c^2\alpha^2 Z = b\,, \tag{3.15a}$$

and Bessel's equation of first order

$$(cr)^2 \frac{d^2R(cr)}{d(cr)^2} + (cr)\frac{dR(cr)}{d(cr)} + [(cr)^2 - 1]R(cr) = 0\,, \tag{3.15b}$$

where c^2 is the separation constant, and b is a constant of integration.

We shall consider solutions to equation (3.15) in the cylindrical region $0 \le r \le L$, $z \ge 0$ for which the longitudinal component of magnetic field B_{1z} is symmetric about r=0. The following boundary conditions are imposed (Figure 3.1);

$$B_{1r} \to 0 \text{ as } z \to \infty\,, \qquad B_{1r} = 0 \text{ on } r = 0, L\,, \tag{3.16a}$$

$$B_{1z} = B_0 f(r) \text{ on } z=0. \tag{3.16b}$$

These are effectively the same as the conditions imposed in the rectangular case treated in chapter 2. Applying conditions (3.16a) to the solutions of equation (3.15a) and (3.15b) we may show that the solution to equation (3.12) is

$$A_1 = -\sum_{n=1}^{\infty} \frac{a_n B_0 L}{\mu_{1,n}} r\, J_1\left(\frac{\mu_{1,n} r}{L}\right)\left(b_n + \exp\left(-\frac{\mu_{1,n}\alpha z}{L}\right)\right),$$

where $\mu_{1,n}$ is the n'th zero of the Bessel function J_1.

From equation (3.11), the resulting components of the magnetic field are

$$B_{1r} = \sum_{n=1}^{\infty} a_n \alpha B_0 J_1\left(\frac{\mu_{1,n} r}{L}\right)\exp\left(-\frac{\mu_{1,n}\alpha z}{L}\right), \tag{3.17a}$$

$$B_{1z} = \sum_{n=1}^{\infty} a_n B_0 J_0\left(\frac{\mu_{1,n} r}{L}\right)\left(b_n + \exp\left(-\frac{\mu_{1,n}\alpha z}{L}\right)\right), \tag{3.17b}$$

and from equation (3.4a)

$$v_{1r} = \sum_{n=1}^{\infty} a_n \alpha v_0 J_1\left(\frac{\mu_{1,n} r}{L}\right)\exp\left(-\frac{\mu_{1,n}\alpha z}{L}\right). \tag{3.17c}$$

From equations (3.1a) and (3.1c), one may obtain

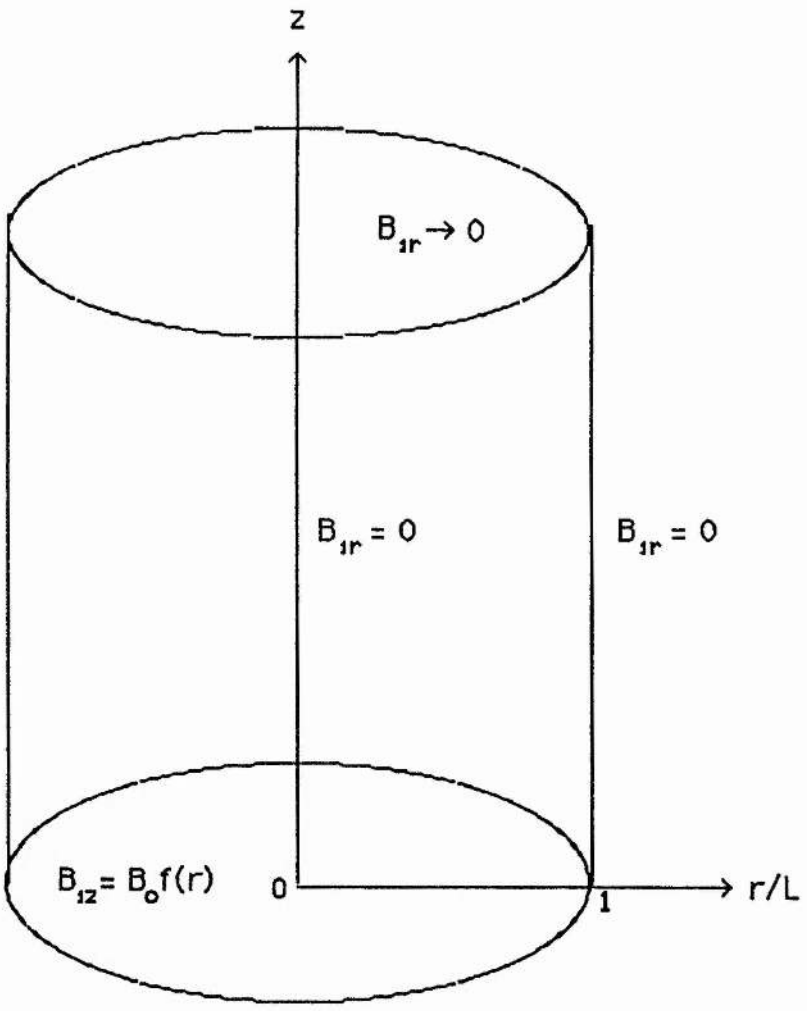

Figure 3.1: Boundary conditions for solutions with the longitudinal magnetic field B_{1z} symmetric in r about r=0.

$$p_1 = -\frac{B_0^2}{\mu}\sum_{n=1}^{\infty} a_n J_0\left(\frac{\mu_{1,n} r}{L}\right)\left(b_n + \frac{M_A^2}{1-M^2}\exp\left(-\frac{\mu_{1,n}\alpha z}{L}\right)\right), \qquad (3.17d)$$

and

$$v_{1z} = -\sum_{n=1}^{\infty}\frac{v_0 a_n}{1-M^2} J_0\left(\frac{\mu_{1,n} r}{L}\right)\left(1 - \exp\left(-\frac{\mu_{1,n}\alpha z}{L}\right)\right). \qquad (3.17e)$$

Here, we have assumed that $v_{1z}=0$ on $z=0$, in keeping with Priest (Paper 1). Note that, as with the rectangular case, $B_{1z}\to 0$ as $z\to\infty$ only if $b_n\equiv 0$. From equation (3.16b) we deduce that

$$f(r) = \sum_{n=1}^{\infty} a_n (b_n+1) J_0\left(\frac{\mu_{1,n} r}{L}\right),$$

from which one deduces that

$$a_n(b_n+1) = \frac{2}{L^4 (J_0(\mu_{1,n}))^2}\int_0^L r J_0\left(\frac{\mu_{1,n} r}{L}\right) f(r)\,dr \equiv I_{n1},$$

on using the orthogonality property of Bessel functions. Similarly from equation (3.17d) we have

$$a_n\left(b_n + \frac{M_A^2}{1-M^2}\right) = \frac{-2}{L^4 (J_0(\mu_{1,n}))^2}\int_0^L \frac{\mu p_1(r,0)}{B_0^2} r J_0\left(\frac{\mu_{1,n} r}{L}\right) dr \equiv I_{n2};$$

from which one can solve for the coefficients a_n and b_n to give

$$a_n = 2\left(\frac{1-M^2}{1-M_T^2}\right)(I_{n1} - I_{n2});$$

$$b_n = \frac{1}{I_{n1} - I_{n2}}\left(I_{n2} - \frac{M_A^2}{1-M^2}\right).$$

The above two expressions have the same v_0-dependence as the corresponding results in the rectangular case. The arguments given for the physical effects of different values of v_0 in the rectangular case still hold for the cylindrical geometry. The major quantitative difference is that Bessel functions replace trigonometrical functions in the cylindrical case.

The above the solutions may also be extended to give periodic z-dependence when $\alpha^2<0$, in the same way as was possible with the rectangular case.

(b) Fundamental Mode Solutions

To discuss in more detail the quantitative differences between the rectangular and cylindrical cases, we will consider the fundamental mode; namely,

$$B_{1r} = a_1 \alpha B_0 J_1\left(\frac{\mu_{1,1} r}{L}\right)\exp\left(-\frac{\mu_{1,1}\alpha z}{L}\right); \tag{3.18a}$$

$$B_{1z} = a_1 B_0 J_0\left(\frac{\mu_{1,1} r}{L}\right)\left(b_1+\exp\left(-\frac{\mu_{1,1}\alpha z}{L}\right)\right); \tag{3.18b}$$

$$v_{1r} = a_1 \alpha v_0 J_1\left(\frac{\mu_{1,1} r}{L}\right)\exp\left(-\frac{\mu_{1,1}\alpha z}{L}\right); \tag{3.18c}$$

$$v_{1z} = \frac{-a_1 v_0}{1-M^2} J_0\left(\frac{\mu_{1,1} r}{L}\right)\left(1-\exp\left(-\frac{\mu_{1,1}\alpha z}{L}\right)\right); \tag{3.18d}$$

$$p_1 = -\frac{B_0^2}{\mu} a_1 J_0\left(\frac{\mu_{1,1} r}{L}\right)\left(b_1+\frac{M_A^2}{1-M^2}\exp\left(-\frac{\mu_{1,1}\alpha z}{L}\right)\right); \tag{3.18e}$$

where

$$a_1 = \frac{B_{10}}{B_0}(1+\beta_{10})\left(\frac{1-M^2}{1-M_T^2}\right)$$

$$= \frac{B_{10}}{B_0}(1+\beta_{10})\left(\frac{1-2M_A^2/(\gamma\beta)}{1-[1+2/(\gamma\beta)]M_A^2}\right);$$

$$b_1 = -(1+\beta_{10})^{-1}\left(\beta_{10}+\frac{M_A^2}{1-M^2}\right)$$

$$= -(1+\beta_{10})^{-1}\left(\beta_{10}+\frac{M_A^2}{1-2M_A^2/(\gamma\beta)}\right);$$

and by definition

$$B_{10} = B_{1z}(0,0) = B_0 f(0)\ ,\ \beta_{10} = \frac{\mu p_1(0,0)}{B_0 B_{10}} = \frac{\mu p_{10}}{B_0 B_{10}}\ .$$

The equation of a fieldline with footpoint $(r_0,0)$ is obtained from

$$\frac{dr}{B_{1r}} = \frac{dz}{B_0}\ ,$$

i.e, $$\exp\left(-\frac{\mu_{1,1}\alpha z}{L}\right) = 1 - \{I(r) - I(r_0)\}\ ,$$

where

$$I(r) = \int^{r} \frac{d\zeta}{J_1\left(\frac{\mu_{1,1}\zeta}{L}\right)}\ .$$

The isobar $p_1 = k$ is given by

$$z = \frac{-L}{\alpha\mu_{1,1}} \log\left\{\left(\frac{M^2-1}{M_A{}^2}\right)\left(\frac{k\mu}{B_0{}^2 a_1 J_0\left(\frac{\mu_{1,1} r}{L}\right)} + b_1\right)\right\},$$

and from Figure (3.2), we observe that there is a tendancy for regions of high plasma pressure to broaden slightly with increasing z. The geometrical configuration of the fieldlines depends upon the sign of a_1. When $a_1<0$, they converge toward r=0, and if in addition $b_1>0$, we have a **fast-mode compression** which may show up in the corona as a plume of enhanced pressure (Figure 3.2a). Increasing the basic flow speed v_0 makes flow speed and the magnetic field converge more and broadens the high-pressure regions (Figure 3.2b).

For $a_1>0$, the fieldlines diverge from r=0. In particular, when $b_1>0$, we have a **slow-mode compression**, which may show up in the corona as a coronal hole, void or depletion (Figure 3.2c). Again, increasing v_0 makes the field and flow diverge more and lowers the plasma pressure on the z-axis (Figure 3.2d).

From a consideration of Figure 3.3a-3.3d it can be seen that the classification of the solutions determined for the rectangular case holds for the cylindrical case also. However, we note some quantitative differences between the solutions. The zeros of the quantities B_{1z}, v_{1z} and p_1 have been shifted toward the outer boundary, thus destroying the tranverse symmetry in the cylindrical case. Of more physical importance is to note that the maxima and minima of B_{1z}, v_{1z} and p_1 are no longer equal in magnitude. This will result in interactions being stronger along the axis r=0 than close to the outer boundary r=L. Plasma pressure gradients in the transverse directions are also reduced in the cylindrical case (Figure 3.4). However, it is interesting to note that the magnetic flux is still equally divided between the two regions, as in the rectangular case.

Thus, although the solutions are qualitatively the same as the rectangular case, there are noticeable quantitative differences between the two geometries.

Figure 3.2(a)

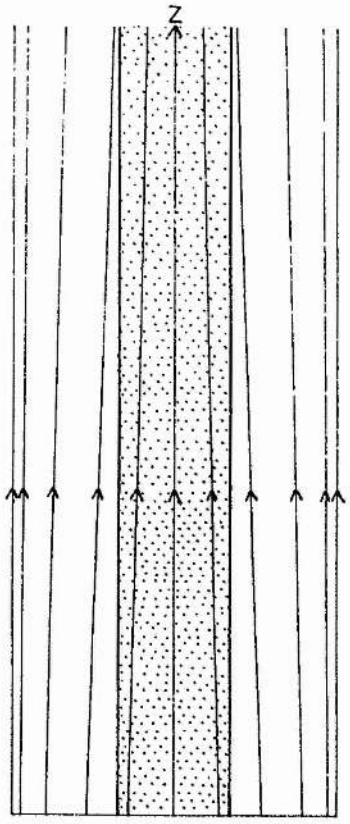

Figure 3.2(b)

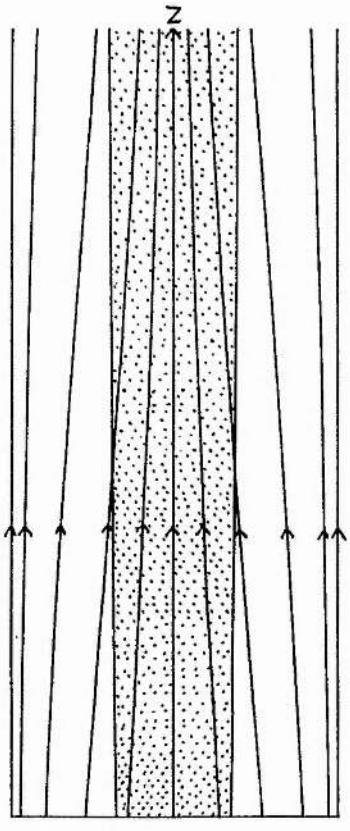

Figure 3.2(a),(b): Plumes of enhanced pressure associated with fast-mode compressions for (a) low-speed flow (M_A=0.1,β=0.5),(b) high-flow (M_A=0.3,β=0.5).

Figure 3.2c

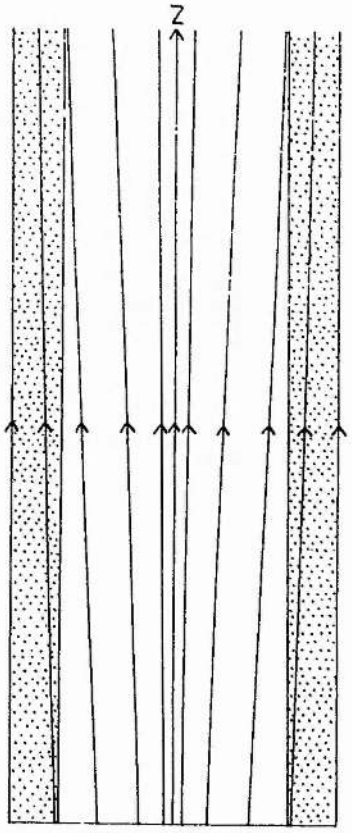

Figure 3.2d

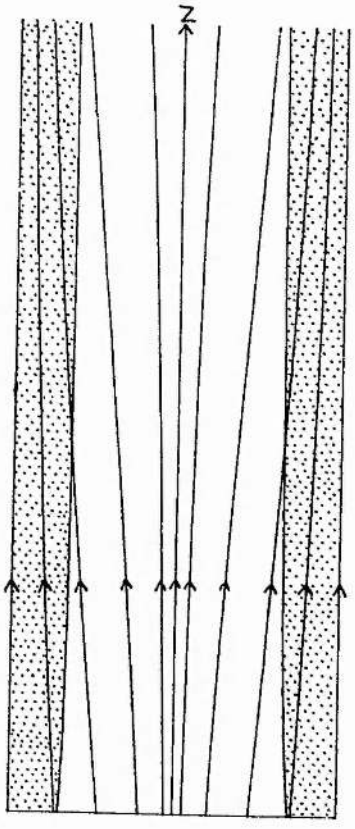

Figure 3.2(c),(d): Holes, voids or depletions associated with slow-mode compressions for (a) low-speed flow (M_A=0.1,β=0.5), (b) higher speed flow (M_A=0.3,β=0.5).

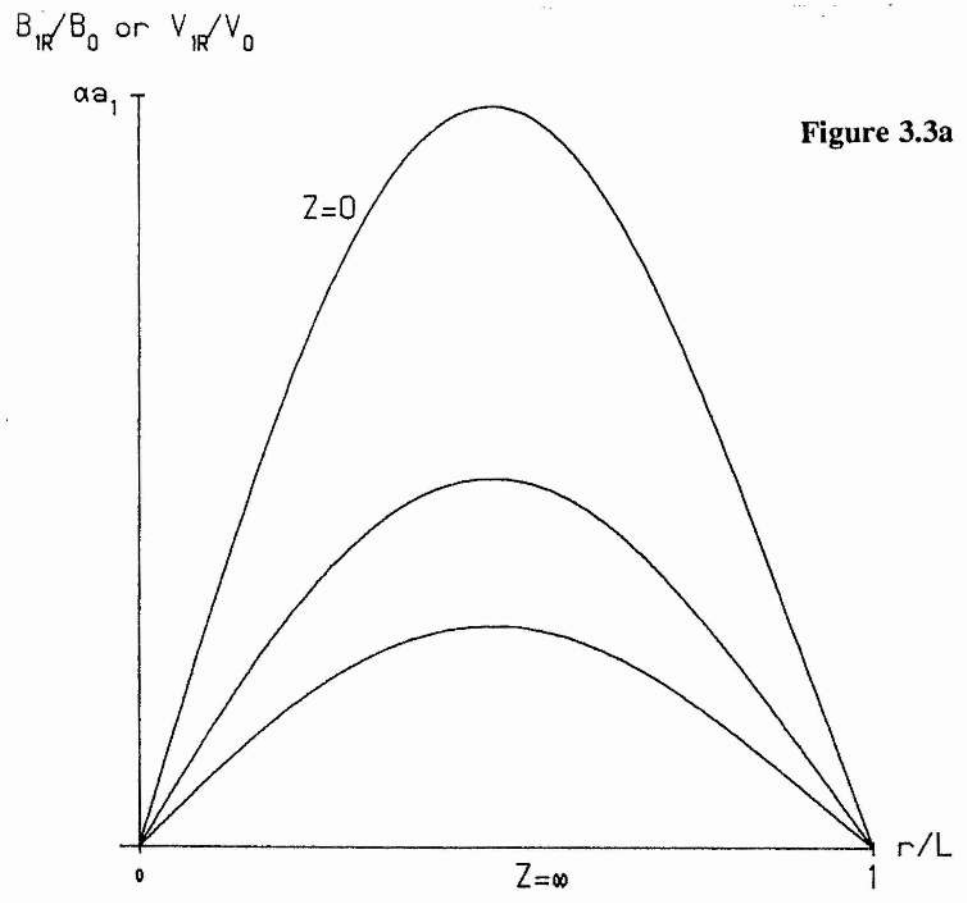

Figure 3.3a

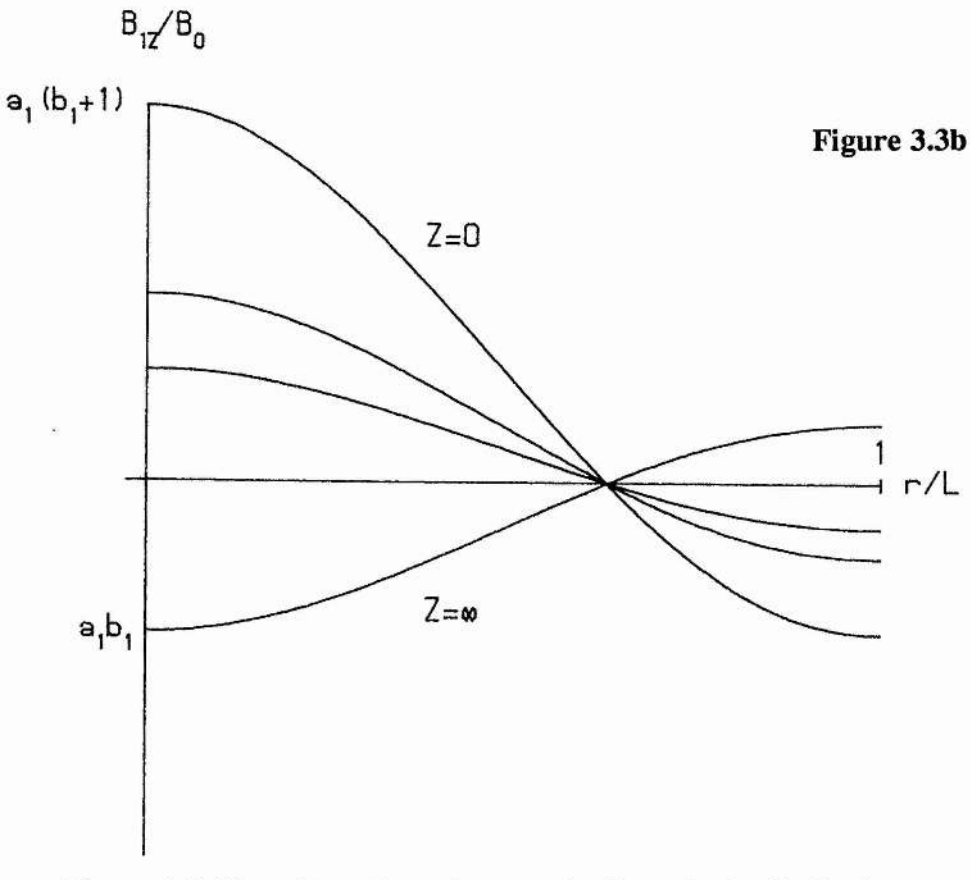

Figure 3.3b

Figure 3.3: The r-dependence (at several values of z for the fundamental axisymmetric mode) of (a) perturbed transverse magnetic field B_{1r} and flow v_{1r}, (b) longitudinal field B_{1z}, (c) plasma pressure p_1, (d) longitudinal flow speed v_{1z}.

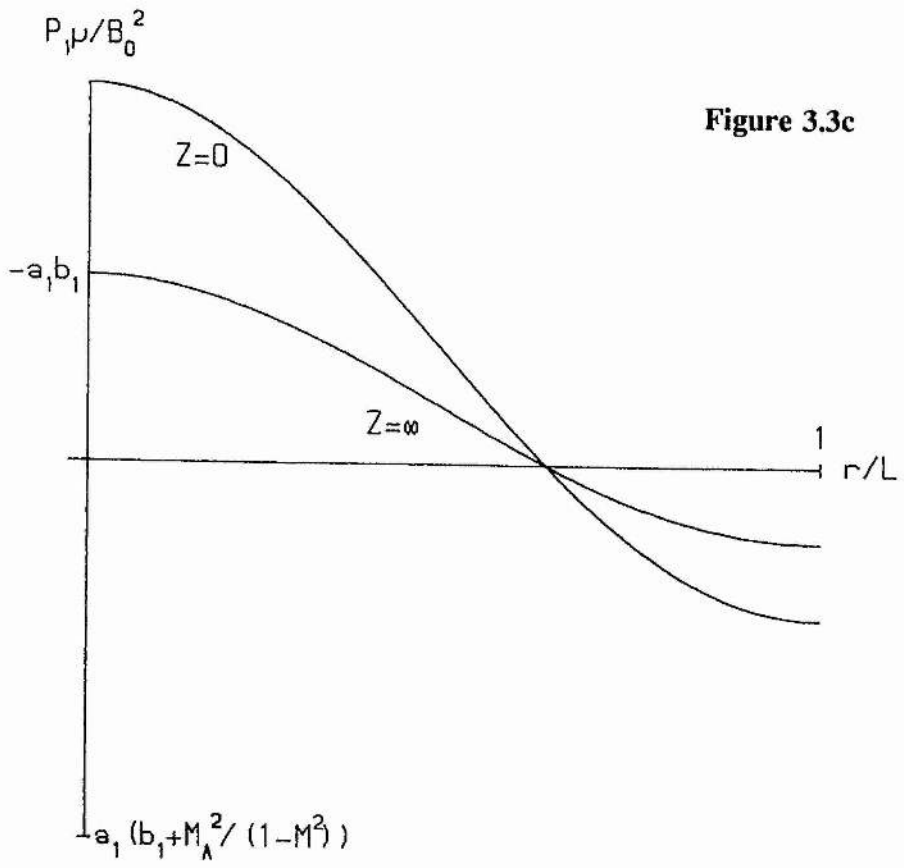

Figure 3.3c

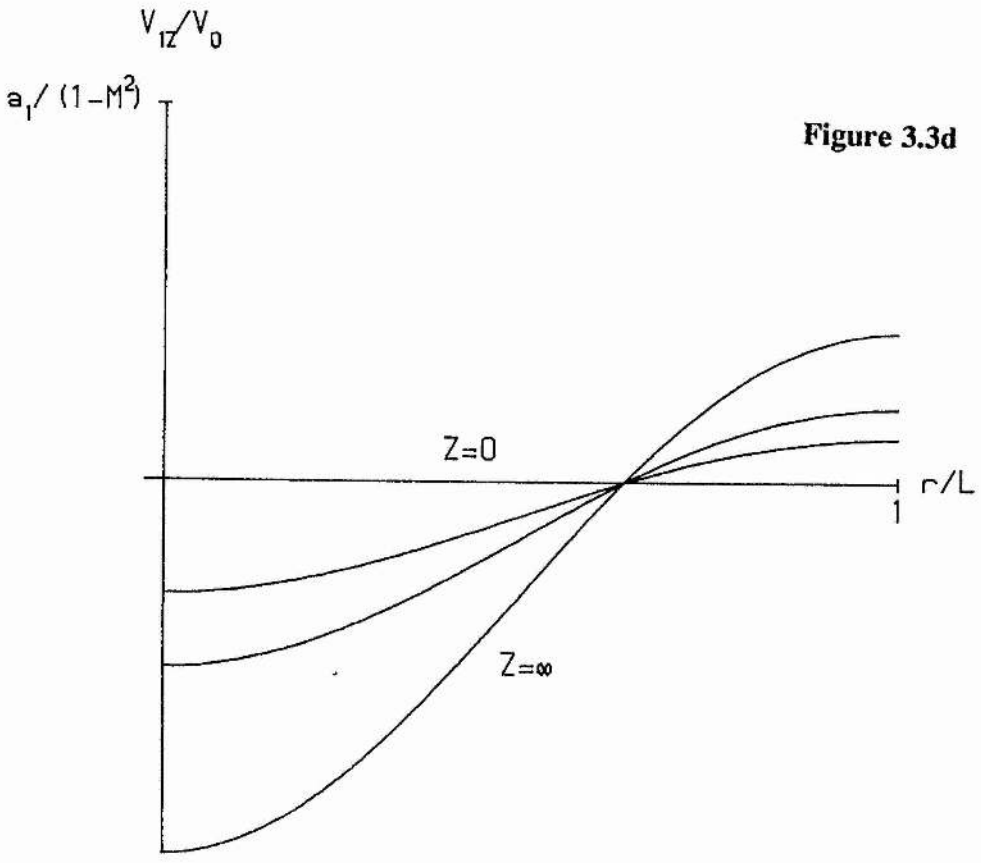

Figure 3.3d

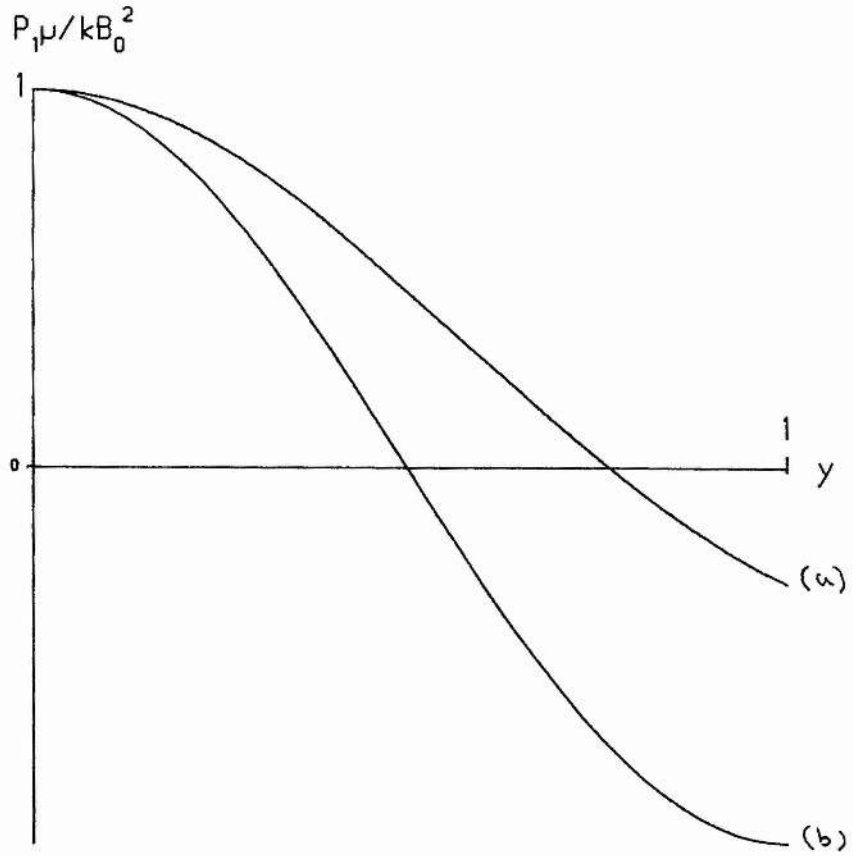

Figure 3.4: Perturbed plasma pressure at z=0 for the fundamental axisymmetric mode in (a) cylindrical geometry, (b) rectangular geometry, where y is a normalised variable ((a) y = r/L, (b) y=x/L) and $k= -a_1(b_1+M_A^2/(1-M^2))$.

(c) Boundary Condition Allowing Flux Loss

By replacing the bondary condition on r=L by $B_{1z}=0$, solutions may be constructed that allow magnetic flux to cross the outer boundary of the region $0\le r\le L$, $z\ge 0$. As noted in the previous chapter, the case where flux enters the region may be relevant to coronal holes. The resulting fundamental mode has

$$B_{1r} = a_1 \alpha B_0 J_1\left(\frac{\mu_{0,1} r}{L}\right)\exp\left(-\frac{\mu_{0,1}\alpha z}{L}\right);$$

$$B_{1z} = a_1 B_0 J_0\left(\frac{\mu_{0,1} r}{L}\right)\left(b_1+\exp\left(-\frac{\mu_{0,1}\alpha z}{L}\right)\right),$$

where $\mu_{0,1}$ is the first zero of the Bessel function J_0.

The magnetic flux Φ_b entering at the base (z=0) of the cylinder is

$$\Phi_b = \int_A B_{1z}(r,0)dA$$

$$= \frac{2\pi L^2}{\mu_{0,1}}\frac{B_{10}}{B_0} J_1(\mu_{0,1}),$$

where A is the area of the base of the cylinder. The magnetic flux Φ_s crossing the curved surface S of the cylinder at r=L is given by

$$\Phi_s = \int_S B_{1r}(L,z)dS$$

$$= \frac{2\pi L^2}{\mu_{0,1}}\frac{B_{10}}{B_0}(1+\beta)\left(\frac{1-M^2}{1-M_T^2}\right)J_1(\mu_{0,1}).$$

Again, the v_0-dependence of these results is the same as for the rectangular case, although the presence of the Bessel functions will alter the actual value of the flux.

When all the flux entering through the base leaves across the side of the cylinder $a_1=B_{10}/B_0$ and $b_1=0$. By calculating the equation of the fieldlines, with footpoint $(r_0,0)$, in the usual way, and setting r=L, $z\to\infty$, the footpoint of the innermost fieldline is found to be given by

$$I(r) - I(r_0) = \frac{B_{10}L}{B_0\mu_{0,1}},$$

where

$$I(r) = \int^{r}\frac{1}{J_1\left(\frac{\mu_{0,1}\zeta}{L}\right)}d\zeta.$$

When the hole is small $J_1 \sim x/2$ and so the area A_H of the coronal hole would be approximated by

$$A_H \sim 2\pi L^2 \exp\left(-\frac{B_{10}}{B_0}\right).$$

This depends upon the form of the imposed longitudinal field. The stronger the field the smaller the area A_H. The distance 2L may be taken as roughly the distance between two active regions, for instance.

3.4 Solution of ϕ-Dependent Equation

a) Derivation of Nonaxisymmetric Solutions

Seeking solutions to equation (3.13) of the form

$$B_{1z} = R(r)\Phi(\phi)Z(z),$$

yields the differential equations

$$\frac{d^3Z}{dz^3} - \sigma^2\alpha^2\frac{dZ}{dz} = 0, \tag{3.19a}$$

$$\frac{d^2\Phi}{d\phi^2} + \nu^2\Phi = 0, \tag{3.19b}$$

$$(\sigma r)^2\frac{d^2R(\sigma r)}{d(\sigma r)^2} + (\sigma r)\frac{dR(\sigma r)}{d(\sigma r)} + [(\sigma r)^2 - \nu^2]R(\sigma r) = 0, \tag{3.19c}$$

where ν^2 and $\sigma^2$are separation constants. We will solve equations (3.19a), (3.19b), (3.19c) subject to the boundary conditions

$$B_{1r}, B_{1\phi} \to 0 \text{ as } z \to \infty, \tag{3.20a}$$

$$B_{1r} = 0 \text{ on } r=0,L, \tag{3.20b}$$

$$B_{1\phi}(r,0,z) = B_{1\phi}(r,2\pi,z), \tag{3.20c}$$

$$B_{1z} = B_0 f(r,\phi) \text{ on } z=0, \tag{3.20d}$$

$$B_{1\phi} = B_0 g(r,\phi) \text{ on } z=0. \tag{3.20e}$$

These conditions are similar to those imposed in the axisymmetric (ϕ-independent) case. Note that we also require $B_{1\phi}$ to be (1) zero as $z \to \infty$ from equation (3.20a), and (2) periodic from equation (3.20c). The form of the longitudinal magnetic field (B_{1z}) imposed at the coronal base now depends on both the coordinates r and ϕ. In three dimensions, we generally have to impose

the form $g(r,\phi)$ of the angular component ($B_{1\phi}$) of magnetic field at the base z=0. Applying conditions (3.20a)-(3.20c), the magnetic field components may be shown to be (using equations (3.14a)-(3.14b)),

$$B_{1z} = \sum_{m=1}^{\infty}\sum_{n=0}^{\infty} B_0 a_{mn} J_n\left(\frac{\tau_{mn} r}{L}\right)(\cos n\phi - c_{mn}\sin n\phi)\exp\left(-\frac{\tau_{mn}\alpha z}{L}\right), \qquad (3.21a)$$

$$B_{1r} = -\sum_{m=1}^{\infty}\sum_{n=0}^{\infty} B_0 a_{mn}\frac{\alpha}{2}\left(J_{n-1}\left(\frac{\tau_{mn} r}{L}\right) - J_{n+1}\left(\frac{\tau_{mn} r}{L}\right)\right)(\cos n\phi - c_{mn}\sin n\phi)$$
$$\times \exp\left(-\frac{\tau_{mn}\alpha z}{L}\right), \qquad (3.21b)$$

and

$$B_{1\phi} = \sum_{m=1}^{\infty}\sum_{n=0}^{\infty} B_0 a_{mn}\alpha n L\frac{1}{\tau_{mn} r} J_n\left(\frac{\tau_{mn} r}{L}\right)(\sin n\phi + c_{mn}\cos n\phi)\exp\left(-\frac{\tau_{mn}\alpha z}{L}\right), \qquad (3.21c)$$

where τ_{mn} is the m'th root of

$$J_{n-1}(u) - J_{n+1}(u) = 0 .$$

For small values of r, equation (3.21c) may be approximated by

$$B_{1\phi} \sim \sum_{m=1}^{\infty}\sum_{n=0}^{\infty} B_0 a_{mn} n\frac{\alpha}{2}(\tau_{mn} r L^{-1})^{n-1}(\sin n\phi + c_{mn}\cos n\phi)\exp\left(-\frac{\tau_{mn}\alpha z}{L}\right),$$

which is well behaved as r approaches zero.

We might note at this stage that $B_{1z}\to 0$ as $z\to\infty$, which was not generally true for the two-dimensional case. This is due to the extra requirement here that $B_{1\phi}\to 0$ as $z\to\infty$. Putting n=0 recovers the particular axisymmetric solutions (equation (3.17)) which have b_n=0.

$$v_{1r} = -\sum_{m=1}^{\infty}\sum_{n=0}^{\infty} v_0 a_{mn}\frac{\alpha}{2}\left(J_{n-1}\left(\frac{\tau_{mn} r}{L}\right) - J_{n+1}\left(\frac{\tau_{mn} r}{L}\right)\right)(\cos n\phi - c_{mn}\sin n\phi)$$
$$\times \exp\left(-\frac{\tau_{mn}\alpha z}{L}\right), \qquad (3.22)$$

and from (3.1a) we can show that

$$p_1 = -\frac{B_0^2}{\mu}\sum_{m=1}^{\infty}\sum_{n=0}^{\infty}\frac{M_A^2}{1-M^2} a_{mn} J_n\left(\frac{\tau_{mn} r}{L}\right)(\cos n\phi - c_{mn}\sin n\phi)\exp\left(-\frac{\tau_{mn}\alpha z}{L}\right). \qquad (3.23)$$

Using boundary conditions (3.20d)-(3.20e), and the orthogonality properties of cosine and Bessel functions, it can be shown that

$$a_{mn} = \frac{2}{\pi L^4 J_n^2(\tau_{mn})} \int_0^L \int_{-\pi}^{\pi} r J_n\left(\frac{\tau_{mn} r}{L}\right) \cos n\phi f(r,\phi) dr d\phi \equiv I_{n3} ,$$

and

$$\alpha a_{mn} c_{mn} = \frac{4}{\alpha \pi n L^3 J_n^2(\tau_{mn})} \int_0^L \int_{-\pi}^{\pi} r^2 J_n\left(\frac{\tau_{mn} r}{L}\right) \cos n\phi g(r,\phi) dr d\phi \equiv I_{n4} .$$

Hence we have

$$a_{mn} = I_{n3} , c_{mn} = \frac{I_{n4}}{\alpha I_{n3}} .$$

Alternatively, we could have imposed the plasma pressure at the coronal base in place of the longitudinal magnetic field B_{1z}. However, to determine both a_{mn} and c_{mn} the angular component of $B_{1\phi}$ at z=0 must be imposed. When c_{mn}=0, then only one of p_1 or B_{1z}need to be specified. Note that in the axisymmetric case we were required to impose both B_{1z} and p_1 at the coronal base to determine the response of the overlying corona. This difference arises solely from the presence of the additional condition $B_{1\phi} \rightarrow 0$ as $z \rightarrow \infty$ in the three-dimensional case.

b) Properties of m=1,n=1 mode.

In discussing some of the properties of the solutions (3.21)-(3.23) we restricted our attention to the m=1,n=1 mode. Two cases of interest arise, namely, c_{11}=0 and $c_{11} \neq 0$ (henceforth we shall replace c_{11}, a_{11} and τ_{11} by c_1,a_1 and τ respectively).

Case 1; c_1=0 . This corresponds to the case where only one of B_{1z},p_1 are specified at the base (z=0) and we shall suppose that it is B_{1z} that is imposed. The solutions are sketched in Figures 3.5a-3.5d for several values of z. The corresponding sketches for $c_1 \neq 0$ look essentially the same with $\cos\phi$ replaced by $(\cos\phi - c_1 \sin\phi)$ in Figures 3.5a-3.5c and $\sin\phi$ by $(\sin\phi + c_1 \cos\phi)$ in Figure 3.5d.

For any fixed ϕ, we have essentially picked up the generalisation of the particular solutions that have b_n=0. The changes in the properties of the solutions which result are as follows. The maxima (or minima) of the radial component of

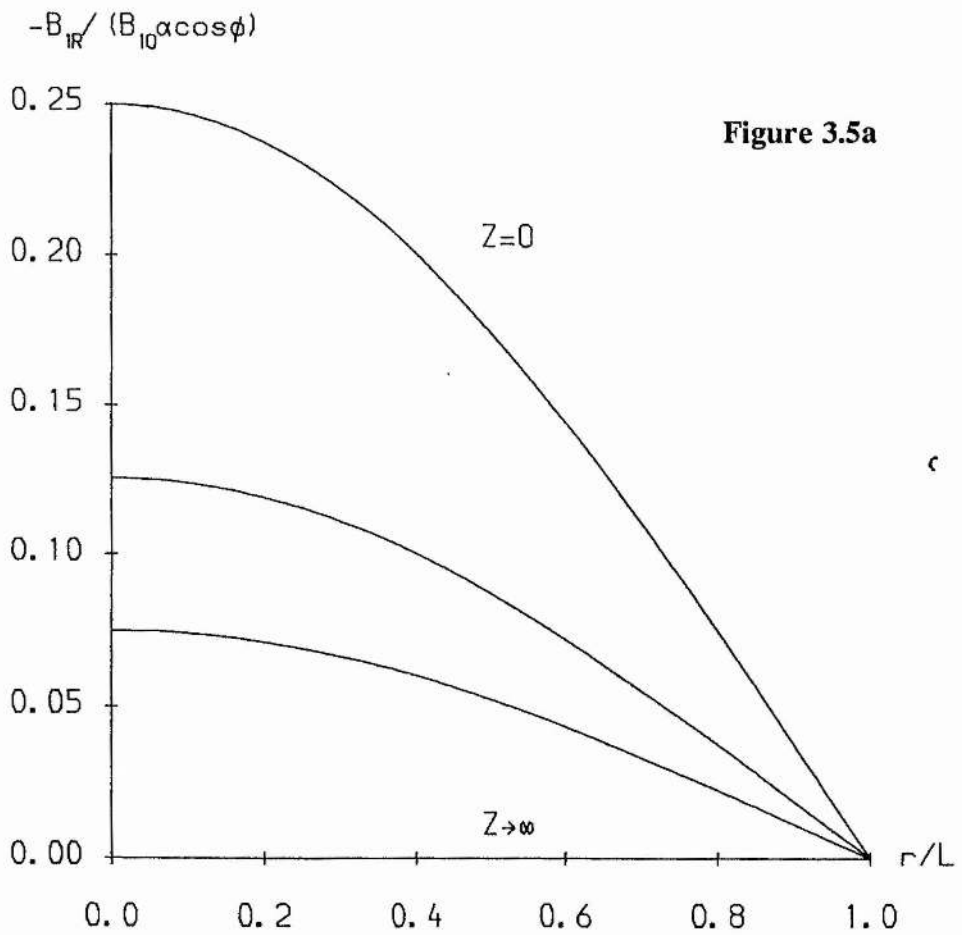

Figure 3.5a

Figure 3.5: At several values of z the r-dependence for the m=1,n=1 mode of (a) perturbed transverse magnetic field B_{1r}, (b) longitudinal field B_{1z}, (c) plasma pressure p_1, (d) angular field $B_{1\phi}$.

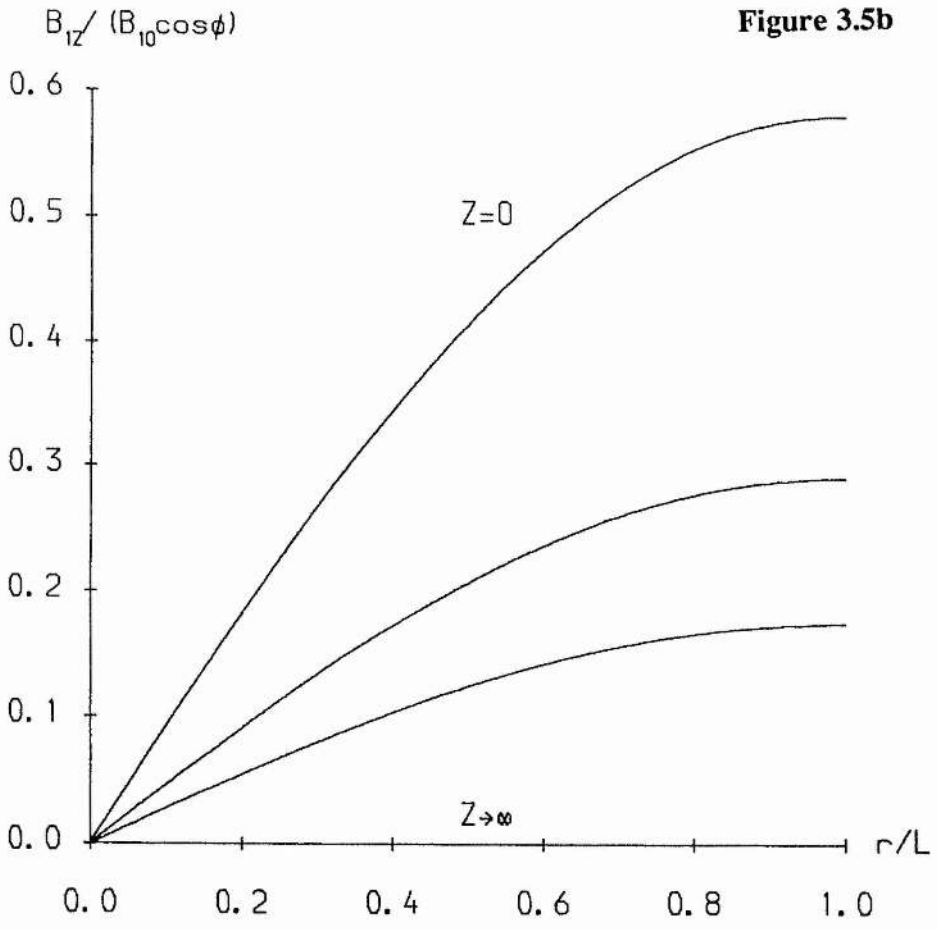

Figure 3.5b

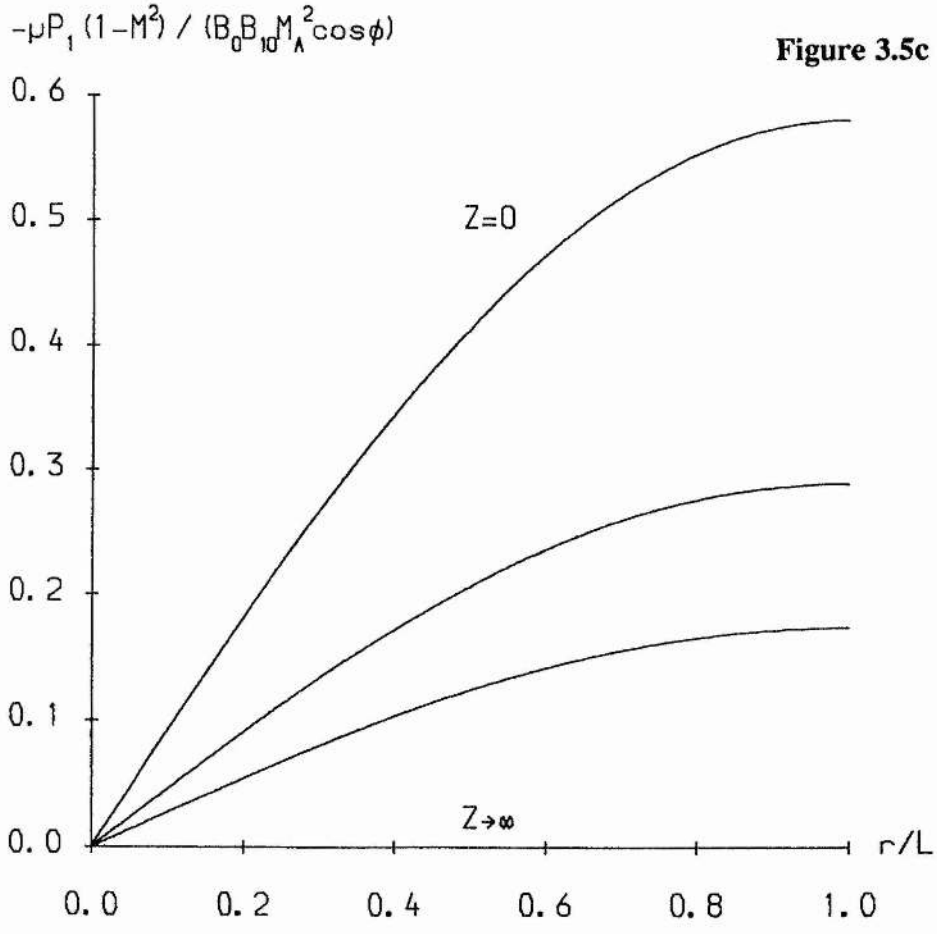

Figure 3.5c

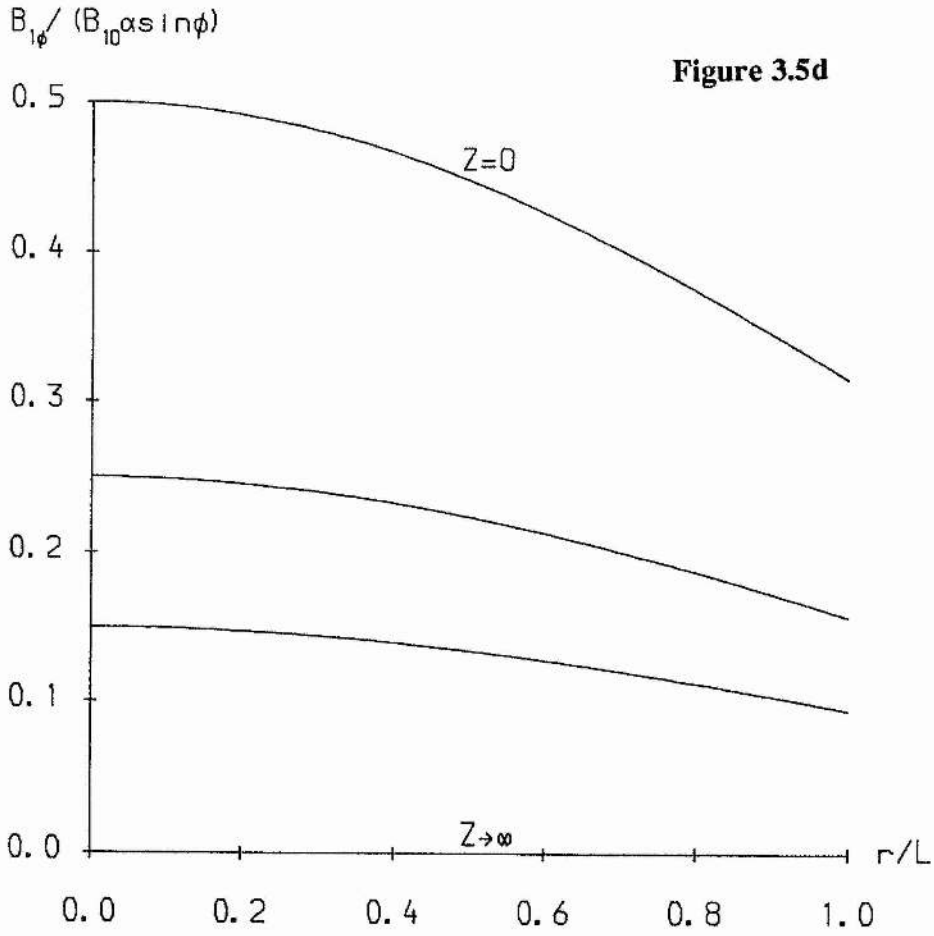

Figure 3.5d

the magnetic field B_{1r} occur on the axis r=0, whereas in the axisymmetric case they occurred in general between r=0 and the outer boundary. The maxima (or minima) of B_{1z} and p_1 now occur at the outer boundary (r/L=1) whereas before they occurred at the axis r=0. From this we deduce that the interaction will be stronger at the outer boundary, in contrast to the axisymmetric case, where the reverse was true. Note also that the sign of B_{1z},B_{1r},p_1 now depends upon $\cos\phi$, so that if ϕ is increased by π, then the signs reverse.

Also, the longitudinal component of the field B_{1z} and plasma pressure p_1 now only have a zero between r=0 and r/L=1. From this point we conclude that the nature of the MHD interaction will not change as we move from r=0 to r=L along a chosen ϕ which is contrary to what we found for the two-dimensional case.

By considering plasma rising from the base of the cylindrical region we may classify the solutions in the usual way. The classification depends upon B_{10} [=f(0)], ϕ and M. In particular, we shall consider cases where $0<v_0<c_T$ (subsonic flow) and $c_s<v_0<v_A$ (supersonic flow), in order to ensure that $\alpha^2>0$.

For $\cos\phi>0$ and $0<v_0<c_T$, a **slow-mode compression** occurs when $B_{10}>0$, and a **slow-mode expansion** for $B_{10}<0$. In the supersonic branch ($c_s<v_0<v_A$) the interactions switch to **fast-modes.** In particular, $B_{10}>0$ gives a **fast-mode expansion,** $B_{10}<0$ a **fast-mode compression.** These results are summarised in Table 3.1, along with the classification of the solutions when $\cos\phi$.

Note that going from a subsonic to a supersonic basic flow changes the interaction from a **slow-mode compression (or expansion)** to a **fast-mode expansion (or compression).**

We now consider in more detail when $c_1\neq 0$.

Case 2; $c_1\neq 0$. To determine a_1 and c_1 consider the z- and ϕ– components of the magnetic field, namely,

$$B_{1z} = B_0 a_1 J_1\left(\frac{\tau r}{L}\right)(\cos\phi - c_1\sin\phi)\exp\left(-\frac{\tau\alpha z}{L}\right), \tag{3.25a}$$

$$B_{1\phi} = B_0 a_1 \frac{L\alpha}{\tau r} J_1\left(\frac{\tau r}{L}\right)(\sin\phi + c_1\cos\phi)\exp\left(-\frac{\tau\alpha z}{L}\right). \tag{3.25b}$$

Table 3.1: The variation of the type of disturbance with B_{10},v_0 and cosϕ.

$\cos\phi > 0$		
$0 < v_0 < c_T$	$B_{10} > 0$	slow-mode compression
	$B_{10} < 0$	slow-mode expansion
$c_s < v_0 < v_A$	$B_{10} > 0$	fast-mode expansion
	$B_{10} < 0$	fast-mode compression
$\cos\phi < 0$		
$0 < v_0 < c_T$	$B_{10} > 0$	slow-mode expansion
	$B_{10} < 0$	slow-mode compression
$c_s < v_0 < v_A$	$B_{10} > 0$	fast-mode compression
	$B_{10} < 0$	fast-mode expansion

Imposing B_{1z} at z=0,r=0 gives the familar result from equation (3.25a), namely

$$a_1 = \frac{B_{10}}{B_0} = f(0).$$

Specifying $B_{1\phi}$ at z=0,r=r_0 ($r_0 \neq 0$), multiplying equation (3.25b) by $\cos\phi$ and integrating over $[-\pi,\pi]$ gives

$$\alpha a_1 c_1 = \frac{\tau r_0}{L\pi J_1\left(\frac{\tau r_0}{L}\right)} \int_{-\pi}^{\pi} \cos\phi\, g(r_0,\phi)\, d\phi \equiv \langle g \rangle , \qquad (3.26)$$

where $\langle g \rangle$ is an imposed twist of the field averaged over one period of $\cos\phi$ for a particular r_0. Henceforth, we shall use B_{10} and $\langle g \rangle$ as parameters to characterise the perturbed state.

The solutions may then be written as

$$B_{1z} = B_0 J_1\left(\frac{\tau r}{L}\right)\left(\cos\phi - \frac{B_0\langle g \rangle}{B_{10}\alpha}\sin\phi\right)\exp\left(-\frac{\tau\alpha z}{L}\right),$$

$$B_{1r} = -B_{10}\frac{\alpha}{2}\left(J_0\left(\frac{\tau r}{L}\right) - J_2\left(\frac{\tau r}{L}\right)\right)\left(\cos\phi - \frac{B_0\langle g \rangle}{B_{10}\alpha}\sin\phi\right)\exp\left(-\frac{\tau\alpha z}{L}\right),$$

$$B_{1\phi} = B_{10}\frac{L\alpha}{\tau r} J_1\left(\frac{\tau r}{L}\right)\left(\sin\phi + \frac{B_0\langle g \rangle}{B_{10}\alpha}\cos\phi\right)\exp\left(-\frac{\tau\alpha z}{L}\right),$$

$$p_1 = \frac{-B_0 B_{10}}{\mu}\frac{M_A^2}{1-M^2}\left(\cos\phi - \frac{B_0\langle g \rangle}{B_{10}\alpha}\sin\phi\right)\exp\left(-\frac{\tau\alpha z}{L}\right).$$

Note that B_{1z} and p_1 may be written in the form

$$B_{1z} = B_{10} K J_1\left(\frac{\tau r}{L}\right)\cos\Psi\exp\left(-\frac{\tau\alpha z}{L}\right),$$

$$p_1 = -\frac{B_{10}B_0}{\mu}\frac{M_A^2}{1-M^2} K J_1\left(\frac{\tau r}{L}\right)\cos\Psi\exp\left(-\frac{\tau\alpha z}{L}\right),$$

where

$$\Psi = \phi + \theta$$

and

$$K = \sqrt{1+\frac{B_0^2\langle g \rangle^2}{B_{10}^2\alpha^2}} \; ; \; \tan\theta = \frac{B_0\langle g \rangle}{B_{10}\alpha}.$$

This is the same form the solution took when $c_1=0$. The classification of the solutions will thus be the same, but with ϕ replaced by Ψ. We saw before that the cylindrical region is partitioned into two : in one region a compression occurs, and in the other an expansion. The effect of a non-zero $\langle g \rangle$ is to rotate these

regions through an angle that depends upon the sign and magnitude of $B_0\langle g\rangle/B_{10}\alpha$. In particular, if $B_0\langle g\rangle/B_{10}\alpha>0$ then $0<\theta<\pi/2$, and when $B_0\langle g\rangle/B_{10}\alpha<0$, $3\pi/2<\theta<2\pi$.

By way of illustration, consider the following simple case. Suppose we choose $B_{10}>0$ for $0<v_0<c_T$. Then from Table 3.1, the interaction will be a **slow-mode.**

For $\langle g\rangle=0$, the cylindrical region is partitioned into two regions, as shown in Figure 3.6. Now choose $B_0\langle g\rangle/B_{10}\alpha=1$ (i.e., $\langle g\rangle>>0$), so that $\theta=\pi/4$. The regions have been rotated through an angle of $-\pi/4$ (Figure 3.6b). For $B_0\langle g\rangle/B_{10}\alpha = -1$ (i.e., $\langle g\rangle<0$), the regions are rotated through $\pi/4$ relative to the $\langle g\rangle=0$ case (Figure 3.6c). Note that the boundary between the regions occurs at the zeros of the plasma and magnetic pressure.

Increasing $\langle g\rangle$ increases $B_{1\phi}$ at some ϕ, so that the plasma is expelled from the compression region (decreasing the plasma pressure), thus extending the region of expansion. At $\phi+\Psi$ the reverse process is occurring, so that the regions of compression and expansion undergo an effective rotation.

3.5 Conclusions

In this chapter we have modelled the wide variety of coronal disturbances which may create observed steady coronal structure in a cylindrical geometry. We have shown that in the axisymmetric case, the basic solutions have similar qualitative properties to the rectangular case. That is, the response of the corona to MHD interactions depends upon the parameters B_{10} and β_{10}, which represent the magnetic field and plasma beta of the perturbed state at the base of of the corona. Altering B_{10} and β_{10} can change the interaction from a **slow-mode** to **fast-mode**, and from a **compression** to an **expansion** (and vice-versa). Varying the value of M_A and β, the Alfven Mach number and plasma beta in the uniform basic state changes the strength of the interaction.

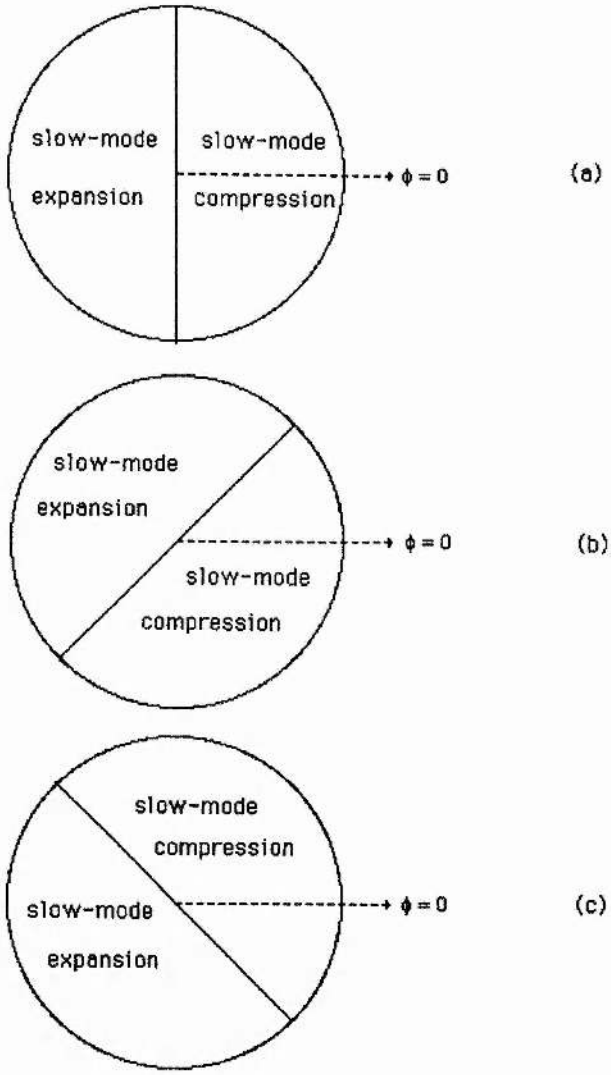

Figure 3.6: The partition of the cylindrical region for $B_{10}>0$, $0<v_0<c_T$, when the averaged imposed twist $\langle g \rangle$ is (a) equal to zero, (b) greater than zero, (c) less than zero, where B_{10} is the value of the imposed longitudinal magnetic field B_{1z} at the origin (r=0, z=0).

There are, however, quantitative differences between the geometries. In the cylindrical case interactions are stronger in the region surrounding r=0 than near the outer boundary, and pressure gradients are smaller.

The ϕ-dependent case exhibits some new interesting features. The region is now partitioned into two semicircular portions (concentric circles in the ϕ-independent case), the orientation of which depends on <g>, a measure of the mean azimuthal field imposed at the base. To determine the response of the corona, one needs to impose B_{10} or β_{10} (along with <g>). This alters the classification of the solutions, which depends upon B_{10} (or β_{10}),M_A and $\cos\phi$.

Chapter 4 : Effect Of Magnetogravity Interactions

4.1 Introduction

In the analysis of the previous two chapters the effect of gravity was neglected. Therefore, in this chapter we extend the model of chapter two to a gravitationally stratified atmosphere in a slab geometry.

We are interested in answering the question: how does gravity alter the basic solutions, and what is the effect on the MHD interactions? We start from a plasma flow along a unidirectional magnetic field, although, by contrast with the previous work, the flow is nonuniform. It turns out that a gravitational correction to the basic solutions increases the maxima of the plasma and magnetic pressures, but the curvature of the fieldlines decreases.

The format of the chapter is as follows. The basic state is investigated in section 4.2, and the governing equation of the perturbed state is derived in section 4.3. Solutions for the first correction due to gravity are developed in section 4.4, and the properties of the fundamental mode are noted in section 4.5. In section 4.6 we discuss these more fully.

4.2 Basic State

Consider the basic state in which

$\mathbf{B}_0 = B_0\hat{\mathbf{z}}$; $\mathbf{v}_0 = v_0\hat{\mathbf{z}}$; $p_0 = p_0(z)$; $\rho_0 = \rho_0(z)$,

such that the atmosphere is isothermal (i.e., the isothermal sound speed $c_s = (p_0/\rho_0)^{1/2}$ is constant) and there is a constant gravitational force with $\mathbf{g} = g\hat{\mathbf{z}}$. The MHD equations reduce to

$$\begin{aligned} &\frac{1}{2}\rho_0\frac{dv_0^2}{dz} = -\frac{dp_0}{dz} - \rho_0 g \,, \\ &\frac{d}{dz}(\rho_0 v_0) = 0 \,, \\ &\frac{d}{dz}\left(\frac{p_0}{\rho_0}\right) = 0 \,. \end{aligned} \tag{4.1}$$

Introducing the dimensionless variable Z=z/L, where L is the half-width of the rectangular region $-1 \le x/L \le 1$, $Z \ge 0$,(Figure 4.1) equations (4.1) may be manipulated into the first-order differential equation in terms of the Mach number M ($=v_0/c_s$). This may be written as

$$\frac{dM^2}{dZ} = \frac{2\delta M^2}{1-M^2}, \tag{4.2}$$

where $\delta=L/\Lambda$ and $\Lambda = c_s^2/g$ is the pressure scale-height. The parameter δ is a measure of the importance of gravitational effects.

Integrating equation (4.2) with respect to Z yields

$$M^2(Z)\exp(-M^2(Z)) = M^2(0)\exp(-M^2(0))\exp(2\delta Z), \tag{4.3}$$

where M(0) is the Mach number evaluated at the coronal base. From equation (4.2) note that for subsonic flow ($M^2(0)<1$), the Mach number increases with height (i.e., $dM^2/dZ>0$), while for supersonic flow ($M^2(0)>1$) it decreases ($dM^2/dZ<0$). Also, dM^2/dZ approaches infinity at the sonic point M(0)=1. The solutions for the subsonic branch are plotted in Figure 4.2. For subsonic M(0), the trajectories converge toward m=1. Note also that there are no solar wind solutions in this model with uniform gravity, though they would of course be found in a spherical geometry with gravity falling off with distance. In our present study we are interested in investigating the effects of gravity for the low corona (Z<2, say).

From equations (4.1) and (4.3) one can deduce that the plasma beta (β) may be written in the form

$$\beta(Z) = \beta(0)\exp\left(-\delta Z + \frac{1}{2}(M^2(0)-M^2(Z))\right), \tag{4.4}$$

$\beta(0)$ ($=2\mu p_0/B_0^2$) is the plasma beta evaluated at the coronal base. This result implies that for subsonic M(0), the plasma pressure decreases more rapidly with increasing Z than in the magnetostatic case. For supersonic M(0), the pressure decreases more slowly than in the magnetostatic case. These results may be explained from a consideration of how energy changes form with increasing Z. In the case of no flow, gravitational energy increases with height, the internal energy

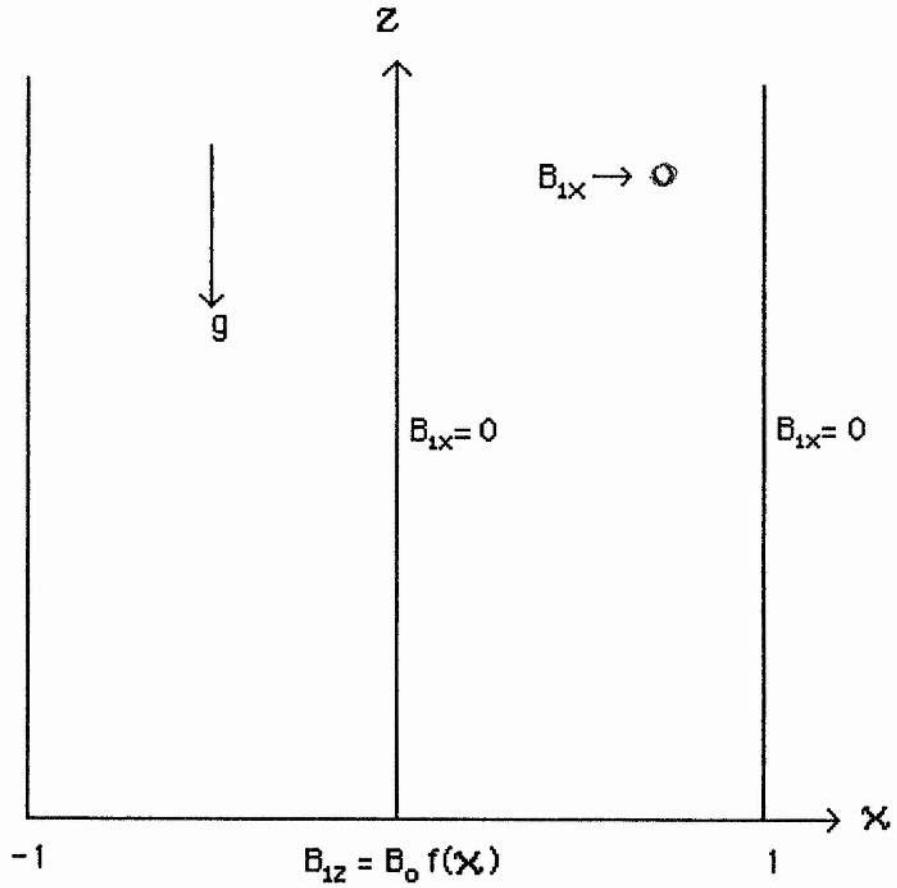

Figure 4.1: Geometric configuration and boundary conditions.

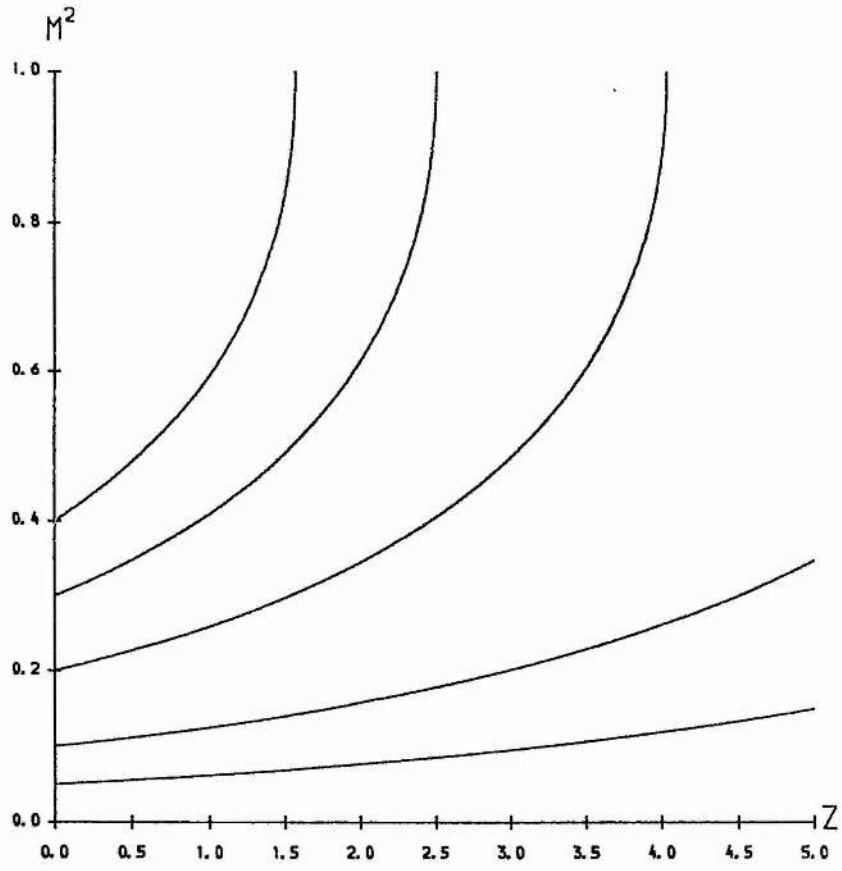

Figure 4.2: Subsonic branch of the Mach number (M) plotted against non-dimensional height (Z).

(and hence the pressure) decreases. For subsonic M(0), the kinetic energy of the plasma increses with increasing height (Z), thus requiring the internal energy (and hence $p_0(Z)$) to decrease more rapidly than in the static case. Finally, for supersonic flows, the kinetic energy decreases with height, requiring the internal energy to decrease more slowly than in the case with no flow.

Another useful result, which will be employed in the next section,is

$$-\frac{\rho_0}{\rho_0'}=\frac{v_0}{v_0'}=\frac{1-M^2(Z)}{\delta}, \tag{4.5}$$

where a dash denotes differentiation with respect to Z. The limit $M\rightarrow 0$, reduces equation (4.5) to the familar magnetostatic result.

4.3 Governing Equation

In this section the equation which governs small perturbations about the basic state (4.1) is derived. As in chapters two and three, linearise the equations (1.11)-(1.15), including a constant gravitational term in the equation of motion, and so obtain;

$$\rho_0 v_0\frac{\partial v_{1x}}{\partial Z}=-\frac{\partial p_1}{\partial X}-\frac{B_0}{\mu}\frac{\partial B_{1x}}{\partial X}+\frac{B_0}{\mu}\frac{\partial B_{1x}}{\partial Z}, \tag{4.6}$$

$$\rho_0 v_0\frac{\partial v_{1z}}{\partial Z}+\rho_0 v_0' v_{1z}+\frac{1}{2}(v_0^2)'\rho_1=-\frac{\partial p_1}{\partial Z}-L\rho_1 g, \tag{4.7}$$

$$\frac{\partial B_{1x}}{\partial X}+\frac{\partial B_{1z}}{\partial Z}=0, \tag{4.8}$$

$$v_{1x}=\frac{v_0}{B_0}B_{1x}, \tag{4.9}$$

$$\rho_0' v_{1z}+\rho_0\left(\frac{\partial v_{1x}}{\partial X}+\frac{\partial v_{1z}}{\partial Z}\right)+v_0\frac{\partial \rho_1}{\partial Z}+v_0'\rho_1=0, \tag{4.10}$$

$$p_1=c_s^2\rho_1, \tag{4.11}$$

where Z=z/L and X=x/L. We define the flux function A_1 by

$$B_{1x}=\frac{\partial A_1}{\partial Z};\quad B_{1z}=-\frac{\partial A_1}{\partial X}.$$

to satisfy the solenoidal condition (4.8). Substituting equations (4.11),(4.9), (4.8) into equation (4.6) yields

$$\frac{\mu c_s^2}{B_0}\frac{\partial \rho_1}{\partial X}=\mathfrak{D}A_1, \tag{4.12}$$

where $\mathfrak{D}$ is the partial differential operator

$$\mathfrak{D} \equiv \frac{\partial^2}{\partial X^2} + \frac{\partial^2}{\partial Z^2} - \frac{\partial}{\partial Z}\left[M_A{}^2 \frac{\partial}{\partial Z}\right]. \qquad (4.13)$$

Eliminating $\partial v_{1z}/\partial Z$ from equations (4.7) and (4.10), and using (4.12) we obtain the relation

$$\rho_0 v_0 \frac{\partial v_{1z}}{\partial X} = -\frac{B_0}{2\mu}\left\{(1-M_T{}^2)\frac{\partial^3 A_1}{\partial X^2 \partial Z} + (1-M^2)\frac{\partial^3 A_1}{\partial Z^3} - (1-M^2)\frac{\partial^2}{\partial Z^2}\left[M_A{}^2 \frac{\partial A_1}{\partial Z}\right]\right\}$$

$$- \frac{B_0 \delta}{2\mu} \mathfrak{D} A_1 . \qquad (4.14)$$

Substituting equation (4.14) into (4.7), and using (4.5) we finally obtain the governing equation

$$\frac{\partial}{\partial Z}\left\{(1-M^2)(1-M_T{}^2)\frac{\partial^3 A_1}{\partial X^2 \partial Z} + (1-M^2)^2 \frac{\partial^2}{\partial Z^2}\left[(1-M_A{}^2)\frac{\partial A_1}{\partial Z}\right]\right\}$$

$$+ \delta \tilde{\mathfrak{D}} A_1 - \delta^2 \mathfrak{D} A_1 = 0 , \qquad (4.15)$$

where

$$\tilde{\mathfrak{D}} \equiv (1-M^2)\frac{\partial \mathfrak{D}}{\partial Z} - (1+M^2)\mathfrak{D} - M^2 \frac{\partial^3}{\partial X^2 \partial Z} .$$

Setting $\delta = 0$ in equation (4.15) we recover the gravity-free equation discussed in chapter 2.

4.4 Correction Due To Gravity

In order to make analytical progress in solving equation (4.15),a correction to the gravity-free case for small δ (a weakly stratified atmosphere) is sought. Although limited in its validity, such a correction will highlight the basic effect of gravity on the MHD interactions. For a more realistic model, the corona aught to be modelled in a spherical geometry with gravity varying with height. Taking $\Lambda \sim 10^8$m for the corona, then $\delta<1$ for structures whose half-width (L) is less than 10Mm. We will consider δ as a small parameter, and expand in powers of δ, neglecting the δ^2 term.

Consider first the basic state described by equation (4.3). Expanding this equation in powers of the small parameter δ, for small changes in M(Z) from M(0), the Mach number at the coronal base, we obtain

$$M^2(Z) = M^2(0) + \left(\frac{2M^2(0)Z}{1-M^2(0)}\right)\delta + O(\delta^2)\,. \tag{4.16}$$

From equation (4.4) it can be shown that

$$\beta(Z) = \beta(0)\left(1 - \frac{Z\delta}{1-M^2(0)}\right),$$

and hence using the relationship $M_A^2 = \beta M^2/2$, we obtain

$$M_A^2(Z) = M_A^2(0) + \left(\frac{M_A^2(0)Z}{1-M^2(0)}\right)\delta + O(\delta^2)\,, \tag{4.17}$$

and

$$M_T^2(Z) = M_T^2(0) + \left(\frac{2M^2(0)+M_A^2(0)}{1-M^2(0)}\right)Z\delta + O(\delta^2)\,, \tag{4.18}$$

where M_A and M_T are the Alfven and cusp Mach numbers respectively. Equations (4.16)-(4.18) will be used to determine the coefficients of the governing equation of the perturbed state.

Returning to the perturbed state, set

$$A_1 = A^{(0)} + A^{(1)}\delta + \ldots$$

and substitute into equation (4.15) (along with equations (4.16)-(4.18)) to yield,

$$O(1):\ \frac{\partial^2}{\partial Z^2}\left[\frac{\partial^2 A^{(0)}}{\partial Z^2} + \alpha^2\frac{\partial^2 A^{(0)}}{\partial X^2}\right] = 0\,, \tag{4.19}$$

$$O(\delta):\ \frac{\partial^2}{\partial Z^2}\left[\frac{\partial^2 A^{(1)}}{\partial Z^2} + \alpha^2\frac{\partial^2 A^{(1)}}{\partial X^2}\right] = \gamma_1 Z\frac{\partial^4 A^{(0)}}{\partial Z^2\partial X^2} + \gamma_2\frac{\partial^3 A^{(0)}}{\partial X^2\partial Z} + \gamma_3\frac{\partial^3 A^{(0)}}{\partial Z^3}\,, \tag{4.20}$$

where

$$\alpha^2 = \frac{1-M_T^2(0)}{(1-M^2(0))(1-M_A^2(0))}\,,$$

$$\gamma_1 = \frac{2M^2(0)\alpha^2}{1-M^2(0)} + \frac{2M^4(0)}{(1-M^2(0))^2}(M_T^2(0)-(1-M^2(0))) + \frac{M^2(0)M_A^2(0)}{(1-M_A^2(0))^2}\,, \tag{4.21a}$$

$$\gamma_2 = \frac{M_A^2(0)}{(1-M^2(0))^2(1-M_A^2(0))^2} + \frac{M^2(0)(2(1-M^2(0))(1-M_A^2(0))+2-3M_A^2(0))}{(1-M^2(0))^2(1-M_A^2(0))^2}\,, \tag{4.21b}$$

$$\gamma_3 = \frac{3M_A^2(0)}{(1-M_A^2(0))^2}\,. \tag{4.21c}$$

Seeking separable solutions to equations (4.19) and (4.20) of the form

$$A_1 = A^{(0)} + \delta A^{(1)} = \Delta(X)(\Gamma^{(0)}(Z)+\delta\Gamma^{(1)}(Z)),$$

we obtain the ordinary differential equations

$$\frac{d^2\Delta}{dX^2} + \omega^2\Delta = 0, \tag{4.22}$$

and

$$O(1): \frac{d^2}{dZ^2}\left[\frac{d^2\Gamma^{(0)}}{dZ^2} - \alpha^2\omega^2\Gamma^{(0)}\right] = 0\,, \tag{4.23a}$$

$$O(\delta): \frac{d^2}{dZ^2}\left[\frac{d^2\Gamma^{(1)}}{dZ^2} - \alpha^2\omega^2\Gamma^{(1)}\right] = \gamma_3\frac{d^3\Gamma^{(0)}}{dZ^3} - \omega^2\left[\gamma_1 Z\frac{d^2\Gamma^{(0)}}{dZ^2} + \gamma_2\frac{d\Gamma^{(0)}}{dZ}\right], \tag{4.23b}$$

where ω^2 is a separation constant. We now proceed to construct solutions to these equations. Note, however, that equations (4.19) and (4.20) possess more general solutions than the separable ones investigated here.

Following the same proceedure as in chapters two and three, we wish to find solutions in the region $-1 \le X \le 1$, $Z \ge 0$ subject to the boundary conditions

$$B_{1x} \to 0 \text{ as } Z \to \infty\,, \tag{4.24a}$$

$$B_{1x} = 0 \text{ on } X = 0\,, \tag{4.24b}$$

$$B_{1x} = 0 \text{ on } X = \pm 1, \tag{4.24c}$$

$$B_{1z} = B_0 f(X) \text{ on } Z = 0. \tag{4.24d}$$

Boundary condition (4.24a) will remove from the solution all terms that are exponentially growing or purely linear in Z. The solution of equation (4.23a) is then

$$\Gamma^{(0)}(Z) = e^{-\alpha\omega z} - \frac{\nu}{\alpha^2\omega^2}\,, \tag{4.25}$$

where ν is an arbitary constant. Substituting equation (4.25) into (4.23b), the equation for $\Gamma^{(1)}(Z)$ becomes

$$\frac{d^2\Gamma^{(1)}}{dZ^2} - \alpha^2\omega^2\Gamma^{(1)} = (\sigma_1 Z+\sigma_2)e^{-\alpha\omega z} + \sigma_3 Z + \sigma_4, \tag{4.26}$$

where

$$\sigma_1 = -\omega^2\gamma_1\,,$$

$$\sigma_2 = \frac{1}{\alpha^2\omega^2}\left[1+\omega^2\alpha\left\{\gamma_2 - \frac{2\alpha^2 M_A^2(0)}{(1-M_A^2(0))}\right\} - \alpha\omega^3\gamma_1\right],$$

and σ_3 and σ_4 are constants of integration. We need only find a particular integral of equation (4.26) and this may be shown to be

$$\Gamma^{(1)}(Z) = Z(s_1 Z+s_2)e^{-\alpha\omega z} - \frac{c}{\alpha^2\omega^2}\,,$$

for some constant c, and where

$$s_1 = \frac{3\omega\gamma_1}{\alpha}\,;\; s_2 = -\frac{\sigma_2}{\alpha}\,.$$

Applying the boundary condition (4.24b)-(4.24c), we can show that

$$A_1 = -\sum_{n=1}^{\infty} \frac{B_0 a_n}{\omega_n} \sin(\omega_n X)\left(e^{-\alpha\omega z} + b_n + \delta\left(Z(s_1 Z + s_2)e^{-\alpha\omega z} + c_n\right)\right)\,,$$

where $\omega_n = n\pi$, (n=1,2,...) and ω is replaced by ω_n in the expressions for the constants s_1 and s_2.

Following the usual prescription, the magnetic field components are found to be

$$B_{1x} = \sum_{n=1}^{\infty} B_0 \alpha a_n \sin(\omega_n X)\left\{1+\delta\left[s_1 Z^2 + \left(s_2 - \frac{2s_1}{\alpha\omega_n}\right)Z - \frac{s_2}{\alpha\omega_n}\right]\right\} e^{-\alpha\omega_n z}\,, \quad (4.27a)$$

and

$$B_{1z} = \sum_{n=1}^{\infty} B_0 a_n \sin(\omega_n X)\left\{e^{-\alpha\omega_n z} + \delta\left[Z(s_1 Z + s_2)e^{-\alpha\omega_n z} + c_n\right]\right\}. \quad (4.27b)$$

Noting that

$$v_{1x} = \frac{v_0(0)}{B_0}\left\{1+\frac{\delta Z}{1-M^2(0)}\right\}B_{1x} + O(\delta^2)\,,$$

then from equation (4.9) we may show that

$$v_{1x} = \sum_{n=1}^{\infty} v_0(0)\alpha a_n \sin(\omega_n X)\left\{1+\delta\left[s_1 Z^2 + \left(\frac{1}{1-M^2(0)} - s_2 - \frac{2s_1}{\alpha\omega_n}\right)Z - \frac{s_2}{\alpha\omega_n}\right]\right\} e^{-\alpha\omega_n z}\,, \quad (4.28)$$

and finally from equation (4.6)

$$p_1 = -\frac{B_0^2}{\mu}\sum_{n=1}^{\infty} a_n \cos(\omega_n X)\left\{b_n + \frac{M_A^2(0)}{1-M^2(0)}e^{-\alpha\omega_n z} + \delta\left[(t_1 + t_2 Z + t_3 Z^2)e^{-\alpha\omega_n z} + c_n\right]\right\}\,, \quad (4.29)$$

where

$$t_1 = -2\left\{\frac{2(1-M^2(0))}{\omega_n}\left(\frac{s_1}{\omega_n} - \alpha s_2\right) + \frac{\alpha M_A^2(0)}{1-M^2(0)}\right\}, \quad (4.30a)$$

$$t_2 = \frac{M_A^2(0)}{1-M^2(0)}(s_2 + \alpha^2) + \frac{4}{\omega_n}(1-M_A^2(0))\alpha s_1 , \qquad (4.30b)$$

$$t_3 = \frac{M_A^2(0)s_1}{1-M^2(0)} . \qquad (4.30c)$$

Not surprisingly, putting $\delta=0$, we recover the gravity-free solutions obtained in chapter two.

Applying the boundary condition (4.24d), and imposing the plasma pressure at the coronal base, leads to the relations

$$a_n(1+b_n+\delta c_n) = 2\int_0^1 f(X)\cos(\omega_n X)dX \equiv I_{n1} ;$$

and

$$a_n\left\{b_n+\delta c_n+\left(\frac{M_A^2(0)}{1-M^2(0)} + \delta t_1\right)\right\} = -\int_0^1 \frac{2\mu p_1(X,0)}{B_0^2}\cos(\omega_n X)dX \equiv I_{n2} ,$$

from which we can find the constants a_n and $(b_n+\delta c_n)$ to be

$$a_n = \frac{I_{n1} - I_{n2}}{\left\{1 - \left(\frac{M_A^2(0)}{1-M^2(0)}+\delta t_1\right)\right\}} ;$$

$$b_n+\delta c_n = \frac{1}{I_{n1}-I_{n2}}\left\{I_{n2} - \left(\frac{M_A^2(0)}{1-M^2(0)}+\delta t_1\right)I_{n1}\right\} .$$

The constant $b_n+\delta c_n$ is the limiting value of the plasma pressure as $Z \to \infty$. We can require this to be zero by choosing $b_n = - c_n$.

The correction due to gravity leads to an alteration in behaviour of the solutions in the certain cases. For example, the type of interaction occurring may now change its nature as we vary the value of Z. Also, a fieldline which is diverging at the coronal base (Z=0) may now become converging (or vice-versa) as we increase Z.

4.5 Fundamental Mode Solutions (n=1)

In order to investigate the properties of the gravitational correction in more detail, we will restrict our attention to the fundamental mode (n=1). These are

$$B_{1x} = B_0\alpha a_1\sin(\pi X)\left\{1+\delta\left[s_1Z^2+\left(s_2 - \frac{s_2}{\alpha\pi}\right)Z - \frac{s_2}{\alpha\pi}\right]\right\}e^{-\alpha\omega_n z} , \qquad (4.31a)$$

$$B_{1z} = B_0 a_1\cos(\pi X)\left\{b_1+e^{-\alpha\omega_n z} +\delta\left[Z(s_1Z+s_2)e^{-\alpha\omega_n z} +c_1\right]\right\} , \qquad (4.31b)$$

$$v_{1x} = v_0\alpha a_1\sin(\pi X)\Big\{1+\delta\Big[s_1Z^2+\Big(\frac{1}{1-M^2(0)}+s_2-\frac{2s_1}{\alpha\pi}\Big)Z - \frac{s_2}{\alpha\pi}\Big]\Big\}e^{-\alpha\omega_n z}, \qquad (4.31c)$$

$$p_1 = -\frac{B_0^2}{\mu}a_1\cos(\pi X)\Big\{b_1+\frac{M_A^2(0)}{1-M^2(0)}e^{-\alpha\omega_n z} + \delta\big[(t_1+t_2Z+t_3Z^2)e^{-\alpha\omega_n z}+c_1\big]\Big\}, \qquad (4.31d)$$

where

$$a_1 = \frac{B_{10}(1+\beta_{10})}{B_{10}}\Big[\frac{1-M^2(0)}{(1-M_T^2(0))-\delta(1-M^2(0))t_1}\Big], \qquad (4.32a)$$

and

$$b_1+\delta c_1 = -(1+\beta_{10})^{-1}\Big[\Big(\beta_{10}+\frac{M_A^2(0)}{1-M^2(0)}\Big)+\delta t_1\Big], \qquad (4.32b)$$

with

$$B_{10} = B_0f(0)\ ,\ \beta_{10} = \frac{\mu p_1(0,0)}{B_0B_{10}}\ .$$

The constants s_1 and s_2 may be written in the form

$$s_1 = \frac{3\pi}{\alpha}\frac{M^2(0)}{(1-M^2(0))^2(1-M_A^2(0))^2}(M_A^2(0)(1-M^2(0))^2 + 2M^2(0)(1-M_A^2(0))^2\{M_T^2(0)-(1-M^2(0))\})+\frac{9\alpha\pi M^2(0)}{1-M^2(0)},$$

$$s_2 = -\frac{\pi}{\alpha^2}\Big[\gamma_1-\gamma_2+\frac{2\alpha^2M_A^2(0)}{(1-M^2(0))^2}\Big]-\frac{1}{\alpha^2\pi^2}\ .$$

For $M_T(0)<1$, it can be shown that $s_1\geq 0$, and to see what is the sign of s_2, write s_2 in the form

$$s_2 = -\frac{1}{\alpha^2}\Big(\pi H+\frac{1}{\alpha\pi}\Big),$$

where

$$H=\frac{1-M_A^2(0)}{(1-M^2(0))^2}\{M_A^2(0)(1-M^2(0))^2(1-M_A^2(0))+2M^4(0)(1-M_A^2(0)) +2M^2(0)\{1-M_T^2(0)(1-M_A^2(0))\}\}+\frac{2M_A^2(0)}{(1-M_A^2(0))(1-M^2(0))^2}\{M_A^2(0)(1-M^2(0)) M^2(0)(1-M_A^2(0))\}+\frac{2M_A^2(0)}{(1-M^2(0))^2}\Big(\frac{2}{\beta(0)}(1-M_A^4(0))-1\Big).$$

For $M_T(0)<1$, a sufficient condition for $s_2<0$ is

$$\frac{2}{\beta(0)}(1-M_A^4(0))-1>0\ .$$

This holds if $\beta<2$, placing the upper bound $M(0)<0.7$ on the Mach number. This is quite acceptable for the parameter range appropriate to our current approximation. Thus, with $s_2<0$, we have $t_1<0$ from equation (4.30a).

Putting $\delta=0$ reduces the solutions back to the case discussed in chapter two. Figure 4.3a,b shows an example of a **slow-mode compression** in the central region, a **slow-mode expansion** near $X=\pm1$, with $\delta=0$. It is noticeable that the Z-dependance is localised to a narrow 'boundary layer' near the base of the corona. This is particularly the case for the plasma pressure p_1 as the exponential term is multiplied by the small constant $M_A^2(0)/(1-M^2(0))$. The width of the boundary layer increases with $M_A(0)$ for $M_T(0)<1$. A similar feature has been reported for twisted flux tubes, for small twist (Lothian and Hood, 1989). When a correction due to gravity is added, the solutions for B_{1z} and p_1 are plotted in Figures 4.3c,d. Observe that the interaction has switched to a **fast-mode compression** about $X=0$, and a **fast-mode compression** near the boundaries $X=\pm1$. Gravity has also stretched out the boundary layer in the the case of p_1, principally because of the non-uniform $p_0(Z)$ in the basic state. This example illustrates that the addition of a gravitational correction can have noticeable effects on the MHD interactions

Note that the equation of the fieldlines is determined from the differential equation

$$\frac{dZ}{dX}=\frac{B_0}{B_{1x}}.$$

Substituting for B_{1x} from equation (4.31a) and integrating, we find that the equation of the fieldline through the point $(X_0,0)$ to be

$$1+\delta\left[\frac{2}{\alpha\pi}\left(\frac{1}{\alpha\pi}-1\right)s_1\right] - \left\{1+\delta\left[s_1Z^2+\left(\frac{2}{\alpha\pi}\left(\frac{2}{\alpha\pi}-1\right)s_1+s_2\right)Z+\frac{2}{\alpha\pi}\left(\frac{1}{\alpha\pi}-1\right)s_1\right]\right\}e^{-\alpha\pi z} = \frac{1}{a_1}\log\left[\frac{\tan\left(\frac{\pi X}{2}\right)}{\tan\left(\frac{\pi X_0}{2}\right)}\right]. \qquad (4.23)$$

Figure 4.3a

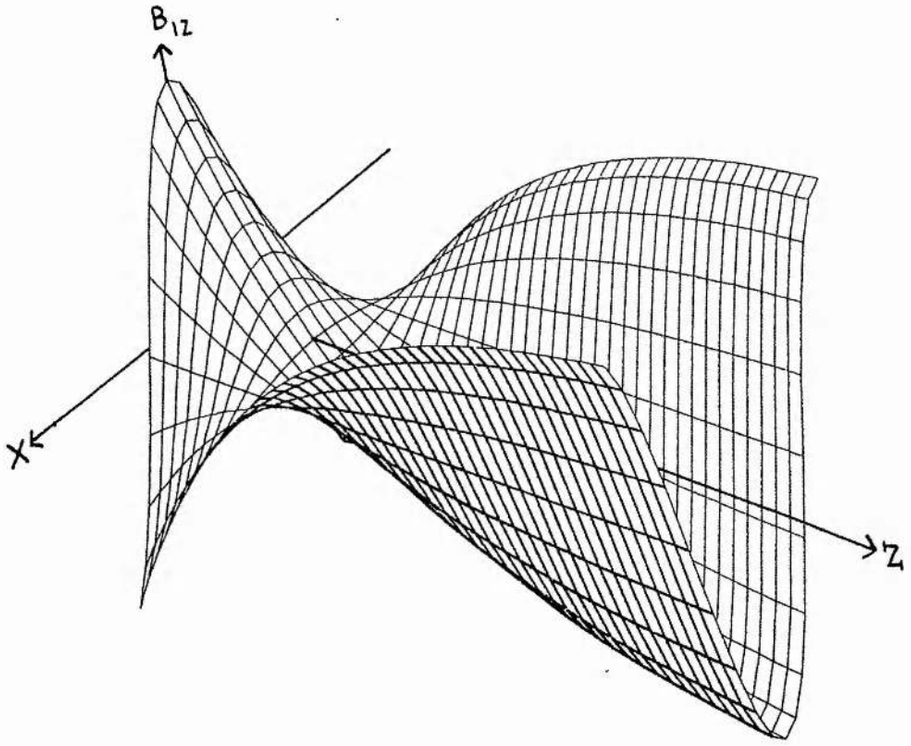

Figure 4.3: Fundamental mode solutions with $M_A^2(0)=0.1,\beta(0)=0.5$, $B_{10}=0.6,\beta_{10}=0.4$ for (a) $B_{1z}(\delta=0)$, (b) $p_1(\delta=0)$, (c) $B_{1z}(\delta=0.05)$,(d) $p_1(\delta=0.05)$ where $0\leq Z\leq 2.0$.

Figure 4.3b

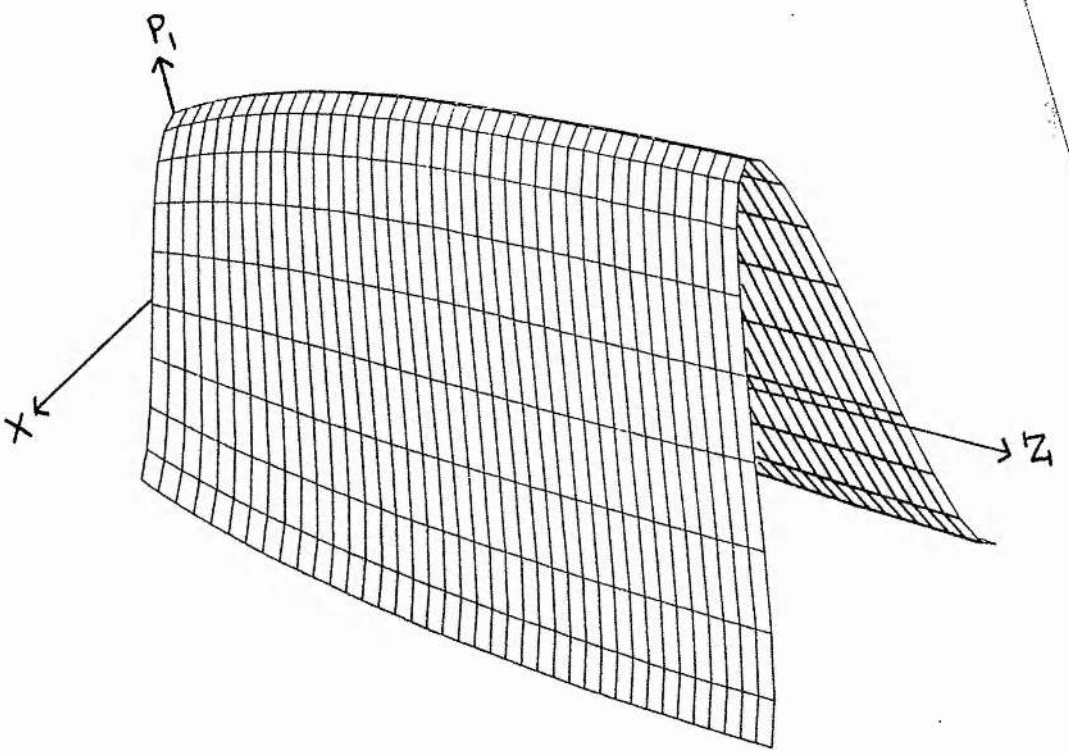

Figure 4.3c

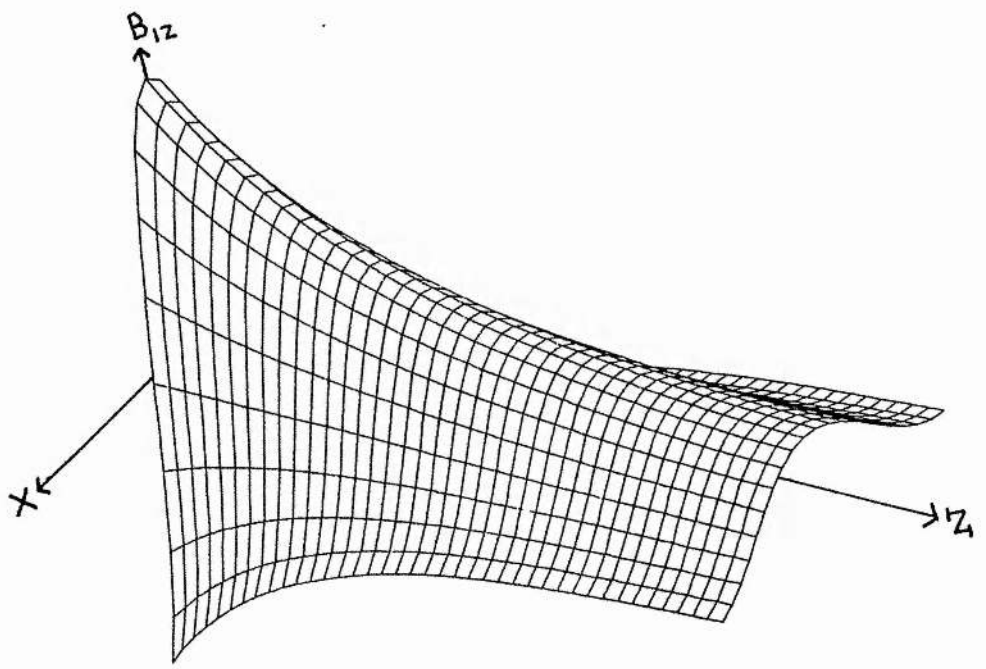

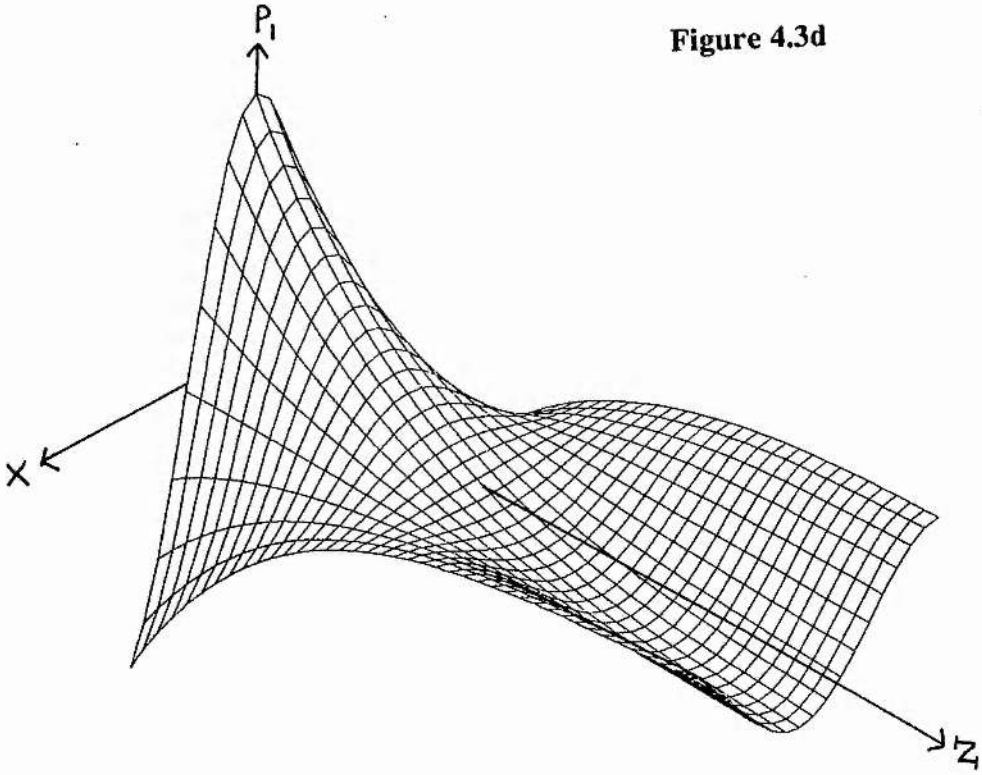

Figure 4.3d

Puttting $\delta=0$ in equation (4.33) recovers the equation of a fieldline in the absence of gravity.

From the differential equation for the fieldlines, we note that the magnetic field topology is basically determined by the transverse component of magnetic field B_{1x}. When $\delta=0$ the fieldlines are either purely diverging or converging, depending upon the sign of a_1. As we saw in chapter two, a coronal hole may be modelled by the diverging field case ($a_1>0$) (Figure 4.4a), while converging fields ($a_1<0$) (Figure 4.4b) may provide a model for plumes of enhanced pressure. The important point to note is that B_{1x} is monotonic in Z.

However, with $\delta\neq0$, the situation is more complicated,as we now have a quadratic multiplying the exponentially decaying term in equation (4.31a). One possibility is that the quadratic term in (4.31a) will be completely dominated by the decaying exponential term, and so B_{1x} remains monotonic, just as before. Such an example is seen in Figure 4.4c. Alternatively, the quadratic term could cause B_{1x} to decrease, then increase before decaying away to zero (Figure 4.4d). Also, we may find that the quadratic has a zero, in which case the sign will change before decaying to zero. In the last two cases we get magnetic fields reminiscent of the overlying magnetic field structure of coronal streamers. The two previous cases may be distinguished by considering the X-coordinate of the fieldline in the limit $Z\rightarrow\infty$ .For the case where B_{1x} is not monotonic, but has no zero, the value of X at $Z\rightarrow\infty$ is greater than X_0, the footpoint of the fieldline. When B_{1x} has a zero, the value of X at $Z\rightarrow\infty$ is less than (or equal to) X_0

Clearly, there exists the possibility of B_{1x} having two roots. We have found that for the parameter values and ranges of Z we have been considering that B_{1x} has at most one root.

4.6 Discussion

4.6.1 Modifications In Solutions For Monotonic $B_{1x}(0.5,Z)$

Figure 4.4a

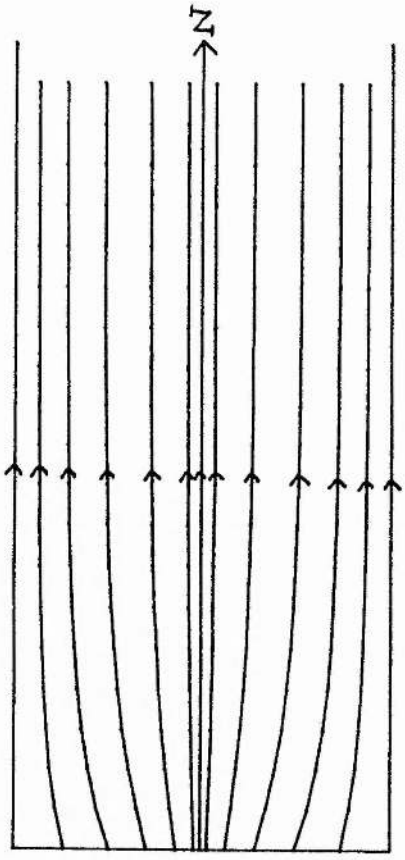

Figure 4.4: Magnetic fieldline plots when $0 \leq Z \leq 2.0$, and

(a) $M_A^2(0)=0.2, \beta(0)=0.5, \delta=0.0, \beta_{10}=0.5, B_{10}=-0.5$,

(b) $M_A^2(0)=0.2, \beta(0)=0.5, \delta=0.0, \beta_{10}=0.5, B_{10}=0.5$,

(c) $M_A^2(0)=0.2, \beta(0)=0.5, \delta=0.1, \beta_{10}=0.5, B_{10}=0.5$,

(d) $M_A^2(0)=0.5, \beta(0)=0.6\ \delta=0.15, \beta_{10}=2.0, B_{10}=1.0$,

(e) $M_A^2(0)=0.5, \beta(0)=0.5, \delta=0.0, \beta_{10}=0.5, B_{10}=0.5$,

(f) $M_A^2(0)=0.4, \beta(0)=0.5, \delta=0.1, \beta_{10}=0.5, B_{10}=0.5$.

Figure 4.4b

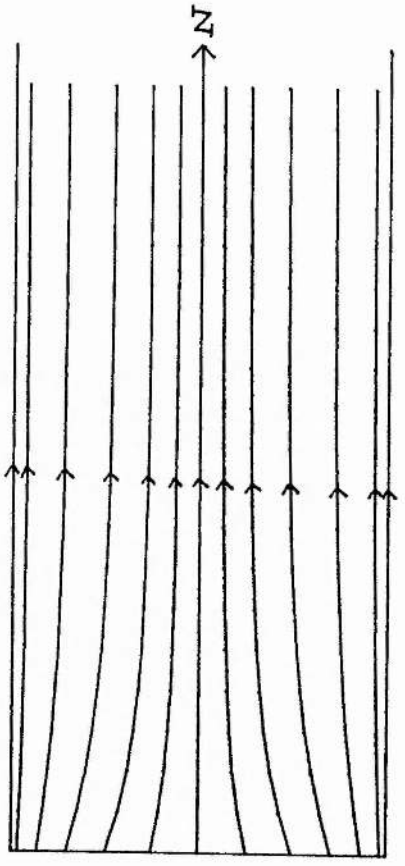

Figure 4.4c

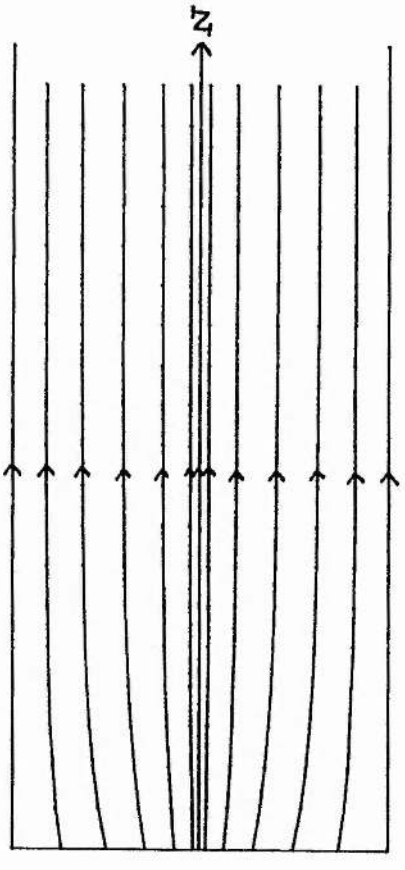

Figure 4.4d

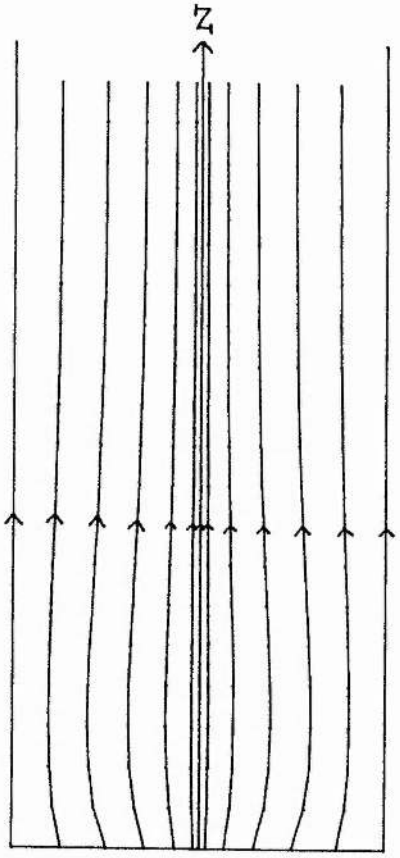

Figure 4.4e

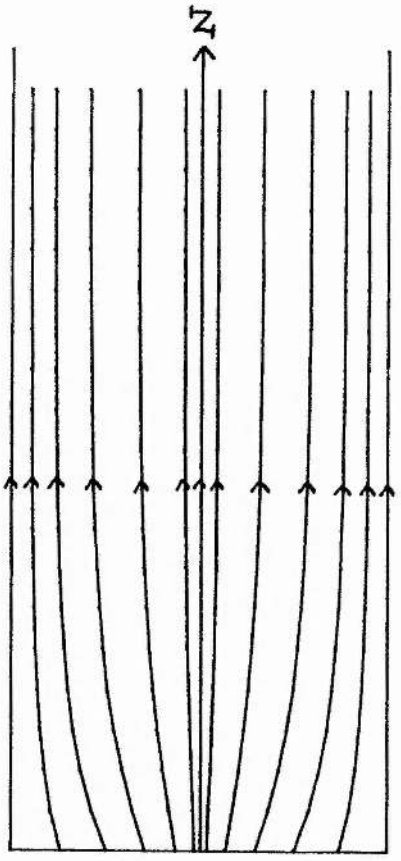

Figure 4.4f

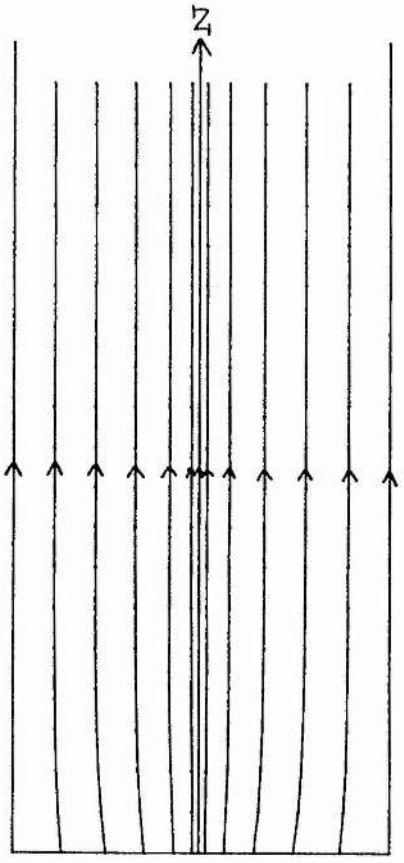

We will now discuss in more detail the modifications due to the gravitational correction in the special case of B_{1x} changing monotonically with height. That is, those cases when the magnetic field is purely diverging or converging. We now address the question of how small changes in $M_A(0)$ and $\beta(0)$ affect the solutions, and consider how the classification of the solutions is altered with gravity present.

Firstly, let us consider the effect of gravity on the maxima/minima of the various perturbed quantities. In the absence of gravity, it was demonstrated in chapter two that increasing $M_A(0)$, for $M_T(0)<1$, resulted in an increase in the maxima of the perturbation quantities B_{1x},B_{1z} and p_1. In particular, this increased the curvature of the fieldlines (compare Figures 4.4a and 4.4e). This arose due to an increase in centrifugal forces causing a corresponding increase in the magnetic tension of the magnetic field line curvature.

Let us now define the maximum of B_{1x},B_{1z} and p_1 by

$$\max[B_{1x}(Z=0,\delta)] = \alpha a_1\left(1- \frac{\delta s_2}{\alpha\pi}\right),$$

$$\max[p_1(Z\rightarrow\infty,\delta)] = \max[p_1(\infty,\delta)] = a_1(b_1+\delta c_1)$$

and

$$\max[B_{1z}(\infty,\delta)] = a_1(b_1+\delta c_1)\,.$$

We are interested in whether the maxima are increased or decreased with the addition of of gravity. Define the quantities

$$\Delta B_{1x} = \max[B_{1x}(0,\delta)] - \max[B_{1x}(0,0)],$$

and

$$\Delta B_{1z} = \max[B_{1z}(\infty,\delta)] - \max[B_{1z}(\infty,0)];$$

then substituting appropriately from equations (4.32a) and (4.32b), it may be shown that

$$\Delta B_{1x} = \frac{-\delta B_{10}(1+\beta_{10})(1-M^2(0))}{B_0(1-M_T^2(0))[(1-M_T^2(0))-\delta(1-M^2(0))t_1]}\left\{2\alpha M_A^2(0) + (1-M^2(0))(1-M_A(0))\left(4s_1- \frac{3\alpha s_2}{\pi}\right)\right\},$$

and

$$\Delta B_{1z} = \frac{-\delta B_{10}(1-M^2(0))^2(1+\beta_{10})t_1}{B_0(1-M_T^2(0))[(1-M_T^2(0))-\delta(1-M^2(0))t_1]}.$$

Clearly for $M_T(0)<1$, $\Delta B_{1x}<0$ while $\Delta B_{1z}>0$ and $\Delta p_1>0$. At first sight, these are somewhat paradoxical. Previously, as the maxima of B_{1x} increased, so did the amount of bunching of the field, and hence the maxima of B_{1z} increased. The presence of gravity alters the situation.

By way of illustration, consider again the case of a diverging field, where B_{1x} is monotonic. When the basic state is perturbed, the footpoints are shifted to give the prescribed magnetic field profile at Z=0. In response, the position of the fieldlines at $Z\rightarrow\infty$ will also change relative to the uniform field in the basic state. For a diverging field, the maxima of B_{1z} is shifted from along X=1 to X=0 with gravity present. To see why this occurs, remember that gravity introduces a pressure gradient along the fieldlines in the basic state. This is largest for small Z. Thus, any perturbation about this basic state will have a greater pressure gradient than in the case with no gravity. This 'additional' pressure gradient acts so as to reduce the tension in the fieldlines, and hence reduces the curvature of the field. Thus, the maximum of B_{1x} is smaller with gravity present. Note that the field strength at Z=0 is independent of gravity, and the fieldlines become bunched around X=0, rather than X=±1. Hence, the maximum of B_{1z} occurs at X=0. Furthermore, this effect is sufficiently large so as to increase the maxima of B_{1z}.

We may examine this a little more formally by decomposing the equation of motion (1.11) along a fieldline ($\hat{\mathbf{s}}$) and normal to the field ($\hat{\mathbf{n}}$). This yields the **s**-component

$$\rho\frac{d}{ds}\left(\frac{1}{2}v^2\right)+\rho g_s = -\frac{dp}{ds},$$

and the **n**-component

$$\frac{\rho v^2}{\mathcal{R}}+\rho g_n = -\frac{d}{dn}\left(p+\frac{B^2}{2\mu}\right),$$

where $\mathcal{R}$ is the radius of curvature of a streamline (and hence a fieldline in this case), g_s is the component of gravity in the the $\hat{s}$-direction, and g_n is the component of gravity in the $\hat{n}$-direction. Linearising these equations we obtain

$$\rho_0 \frac{d}{ds}(v_0.v_1) + \frac{\rho_1}{2}\frac{d}{ds}(v_0^2) + \rho_1 g_s = -\frac{dp_1}{ds}, \qquad (4.34)$$

and

$$\frac{2\rho_0 v_0.v_1}{\mathcal{R}} + \frac{\rho_1 v_0^2}{\mathcal{R}} + \rho_1 g_n = -\frac{dp_T}{dn}, \qquad (4.35)$$

where $p_T = p_1 + \mathbf{B}_0.\mathbf{B}_1/\mu$ is the total pressure perturbation. Adding the gravitational term $\rho_1 g_n$ in (4.35) increases the magnitude of the left-hand side. For force balance, the total pressure gradient normal to the fieldlines increases. This has arisen from the increase in the magnetic pressure, caused by greater bunching of the fieldlines, and hence an increase in the maxima of $\mathbf{B}_1.\hat{\mathbf{s}}$ (or B_{1z}).

In equation (4.34), adding the gravitational term $\rho_1 g_s$ increases the magnitude of the left hand side. To maintain force balance, the longitudinal plasma pressure gradient increases. Since p_1 is fixed at the coronal base (Z=0), this may be accomplished by increasing the value of the maxima of p_1 at $Z \to \infty$. Hence, adding a gravitational correction increases the maxima of B_{1z} and p_1 at $Z \to \infty$.

Increasing $M_A(0)$ ($M_T(0)<1$), with gravity present, reduces the curvature of the fieldlines (compare Figure 4.4c and Figure 4.4f), and hence it reduces the maxima of B_{1x}, but increases the minima of B_{1x} and p_1. To show that this is consistent with the governig equations,we can eliminate ρ_1 from equations (4.34) and (4.35) to give the equation

$$\left(\frac{1dv_0^2}{2\,ds} + g_s\right)\left(\frac{2\rho_0 v_0.v_1}{\mathcal{R}} + \frac{dp_T}{dn}\right) = \left(\frac{v_0^2}{\mathcal{R}} + g_n\right)\frac{dp_1}{ds} + \rho_0 g_n \frac{d}{ds}(v_0.v_1). \qquad (4.36)$$

When v_0 is increased in equation (4.36), it is quite consistent for dp_T/dn, dp_1/ds and $\mathcal{R}$ all to increase. This would imply that the maxima of p_1 and B_{1z} increase as $Z \to \infty$, and the maxima of B_{1x} decreases. Thus the curvature of the fieldlines decreases, and the maximum of the plasma and magnetic pressure increase with increasing $M_A(0)$.

With $\delta=0$, it was found that increasing $\beta(0)$ decreased the maxima of B_{1x},B_{1z} and p_1. When $\delta\neq0$, a similar argument to the one presented above may be used to show that increasing $\beta(0)$ increases the maxima of B_{1x}, and so decreases the maxima of B_{1z} and p_1

The addition of gravity also alters the criteria which govern the classification of the type of MHD interaction occurring in the plasma. When $\delta=0$, the classification of the solutions with $M_T(0)<1$ is summarised in Table 4.1 (as plasma flows along the Z-axis).

When the gravitational correction is added, the critical values of β_{10} become -1 and $-[M_A^2(0)/(1-M^2(0))+\delta t_1]$. First, let us consider the case when

$$\frac{M_A^2(0)}{1-M^2(0)} + \delta t_1 < 1,$$

when $\delta=0$, then including gravity modifies the bounds to

$$-1 < \beta_{10} < -\left(\frac{M_A^2(0)}{1-M^2(0)} + \delta t_1\right), \tag{4.37}$$

or

$$\beta_{10} > -\left(\frac{M_A^2(0)}{1-M^2(0)} + \delta t_1\right). \tag{4.38}$$

That is, the interaction may stay the same for (4.37) or may switch from a **fast-mode compression** to a **slow-mode expansion** with $B_{10}<0$, and from a **slow-mode compression** to a **fast-mode expansion** with $B_{10}>0$. As an example, consider Figure 4.3 where a **slow-mode compression** switches to a **fast-mode expansion** in the neighbourhood of the Z-axis with the addition of gravity. The classification is summarised in Table 4.2.

When

$$\frac{M_A^2(0)}{1-M^2(0)} + \delta t_1 > 1,$$

the classification is summarised in Table 4.3. Hence if $\beta_{10}<-1$ with $\delta=0$, giving a **fast-mode expansion** ($B_{10}<0$) or a **slow-mode expansion** ($B_{10}>0$), then with $\delta\neq0$,

$$-\left(\frac{M_A^2(0)}{1-M^2(0)} + \delta t_1\right) < \beta_{10} < -1, \tag{4.39}$$

Table 1 : Classification of solutions for $M_T(0)<1$ and $\delta=0$.

	$B_{10} < 0$	$B_{10} < 0$
$\beta_{10} > \frac{-M_A^2(0)}{1-M^2(0)}$	slow-mode expansion	fast-mode expansion
$-1 < \beta_{10} < \frac{-M_A^2(0)}{1-M^2(0)}$	fast-mode compression	slow-mode compression
$\beta_{10} < -1$	fast-mode expansion	slow-mode expansion

Table 2 : Classification of solutions for $M_T(0) < 1$ and $M_A^2(0)(1-M^2(0))^{-1} + \delta t_1 < 1$.

	$B_{10} < 0$	$B_{10} > 0$
$\beta_{10} > -\left[\frac{M_A^2(0)}{1-M^2(0)} + \delta t_1\right]$	slow-mode expansion	fast-mode expansion
$-1 < \beta_{10} < -\left[\frac{M_A^2(0)}{1-M^2(0)} + \delta t_1\right]$	fast-mode compression	slow-mode compression
$\beta_{10} < -1$	fast-mode expansion	slow-mode expansion

Table 3 : Classification of solutions for $M_T(0) < 1$ and $M_A^2(0)(1-M^2(0))^{-1} + \delta t_1 > 1$.

	$B_{10} < 0$	$B_{10} > 0$
$\beta_{10} > -1$	slow-mode expansion	fast-mode expansion
$-\left[\frac{M_A^2(0)}{1-M^2(0)} + \delta t_1\right] < \beta_{10} < -1$	fast-mode compression	slow-mode compression
$\beta_{10} < -\left[\frac{M_A^2(0)}{1-M^2(0)} + \delta t_1\right]$	fast-mode expansion	slow-mode expansion

or

$$\beta_{10} < -\left(\frac{M_A^2(0)}{1-M^2(0)} + \delta t_1\right). \tag{4.40}$$

This gives either a **fast-mode compression** ($B_{10}>0$) or a **slow-mode compression** ($B_{10}>0$) for the interval (4.39), and a **fast-mode expansion** ($B_{10}<0$) or a **slow-mode expansion** ($B_{10}>0$) for interval (4.40).

For $\beta_{10} > -1$ with $\delta=0$, we had

$$-1 < \beta_{10} < \frac{-M_A^2(0)}{1-M^2(0)}, \tag{4.41}$$

or

$$\beta_{10} > \frac{-M_A^2(0)}{1-M^2(0)}, \tag{4.42}$$

which maps onto the interval $\beta_{10} > -1$ for $\delta \neq 0$. Hence a **fast-mode compression** ($B_{10}<0$) and a **slow-mode compression** ($B_{10}<0$) map onto a **slow-mode expansion** ($B_{10}<0$) and a **fast-mode expansion** ($B_{10}>0$) respectively with $\delta \neq 0$. Also, a **slow-mode expansion** ($B_{10}<0$) and a **fast-mode expansion** ($B_{10}>0$) are invariant with the inclusion of the gravitational correction for this particular parameter range.

The above discussion illustrates that the effect of gravity is to shift parameter boundaries between various classes of MHD interactions. This changes the nature of the disturbance for some parameter ranges, while it leaves others unchanged.

4.6.2 Non-monotonic $B_{1x}(0.5,Z)$

Let us turn our attention briefly to the case when B_{1x} is not monotonically changing with Z. We now have the possibility of a diverging field becoming converging (Figure 4.5c), or vice-versa (Figure 4.5b), and these solutions are plotted in Figure 4.6. To see why this arises consider the following.

On physical grounds we require

$$p(X,Z) = p_0(Z) + \varepsilon p_1(X,Z) \geq 0 \ (\forall Z),$$

for $\varepsilon << 1$, and from section 4.2 we know that for the basic state $p_0(Z) \rightarrow \infty$. The physical restriction we have imposed restricts the type of perturbation permitted

Figure 4.5a

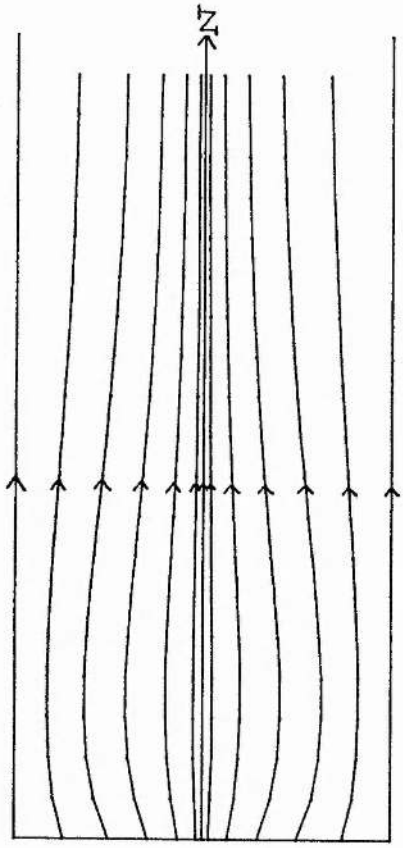

Figure 4.5: Magnetic fieldlines for $0 \leq Z \leq 2.0$, when

(a)$M_A^2(0)=0.65, \beta(0)=0.7, \delta=0.15, \beta_{10}=1.0, B_{10}= 1.0,$

(b)$M_A^2(0)=0.65, \beta(0)=0.7, \delta=0.1, \beta_{10}=1.0, B_{10}= -1.0.$

Figure 4.5b

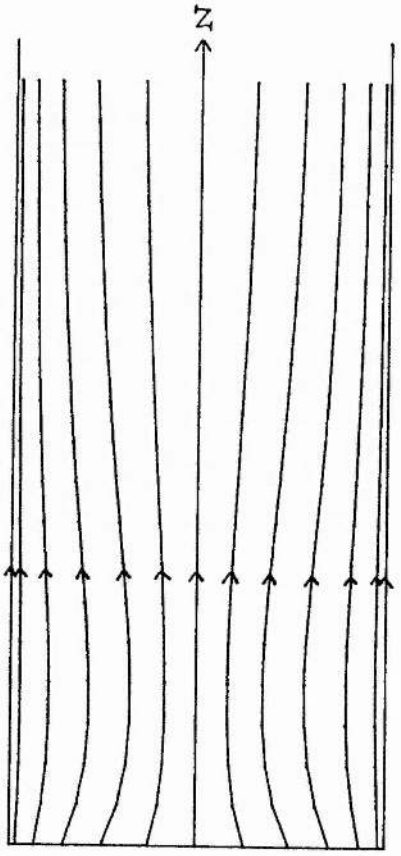

about $p_0(Z)$. In particular, if $p_1(X,0)<0$, then two possibilities arise, namely $p_1(X,Z)\rightarrow\infty$ as $Z\rightarrow\infty$ (i.e., $b_1+\delta c_1 = 0$), or

$$p_1(X,Z) < 0 \text{ for } 0\leq Z\leq h$$

$$\geq 0 \text{ for } h\leq Z.$$

This ensures that $p(X,Z)\geq 0$ ($\forall Z$). Let us now consider a particular example to illustrate the above. Suppose $p_1(X,0)<0$, and the magnetic field is diverging at Z=0, then without gravity we could choose B_{10} and β_{10} such that the pressure maximum would occur along X=0 and the magnetic field maximum along X=1. However, with gravity present there exists a Z_1 such that $p_1(X,Z(>Z_1))$ is positive (i.e., p_1 has a zero). The plasma pressure maximum will now lie along X=1 and the magnetic pressure maximum along X=0. In terms of the fieldlines, this will require the diverging field to become converging.

A particular example of these solutions is plotted in Figure 4.6. Near X=0, a **fast-mode expansion** changes to a **slow-mode expansion**, due to B_{1z} having a stationary point. This illustrates another way in which gravity modifies the basic solutions. That is, the type of disturbance may vary with Z. In principle, B_{1z} and p_1 may have two stationary points in $Z\geq 0$, though we have only detected the case of one stationary point for the parameter range and values of Z investigated. To demonstrate the variety of possible situations which may arise, we consider when B_{1z} and p_1 have at most one stationary point, λ_1 and λ_2 respectively.

Suppose first that B_{1z} only has a stationary point. Then as Z increases we could have either a **fast-mode expansion** changing to a **slow-mode expansion** (Figure 4.7) or a **slow-mode expansion** to a **fast-mode**. When p_1 has a stationary point (and not B_{1z}), then a **fast-mode expansion** would change to a **slow-mode compression,** or a **slow-mode compression** to a **fast-mode expansion**, depending upon the particular values of B_{10} and β_{10} imposed at the coronal base.

When both B_{1z} and p_1 have a stationary point the combinations of interactions become even more complex. For example, suppose that at Z=0, $dp_1/dZ>0$,

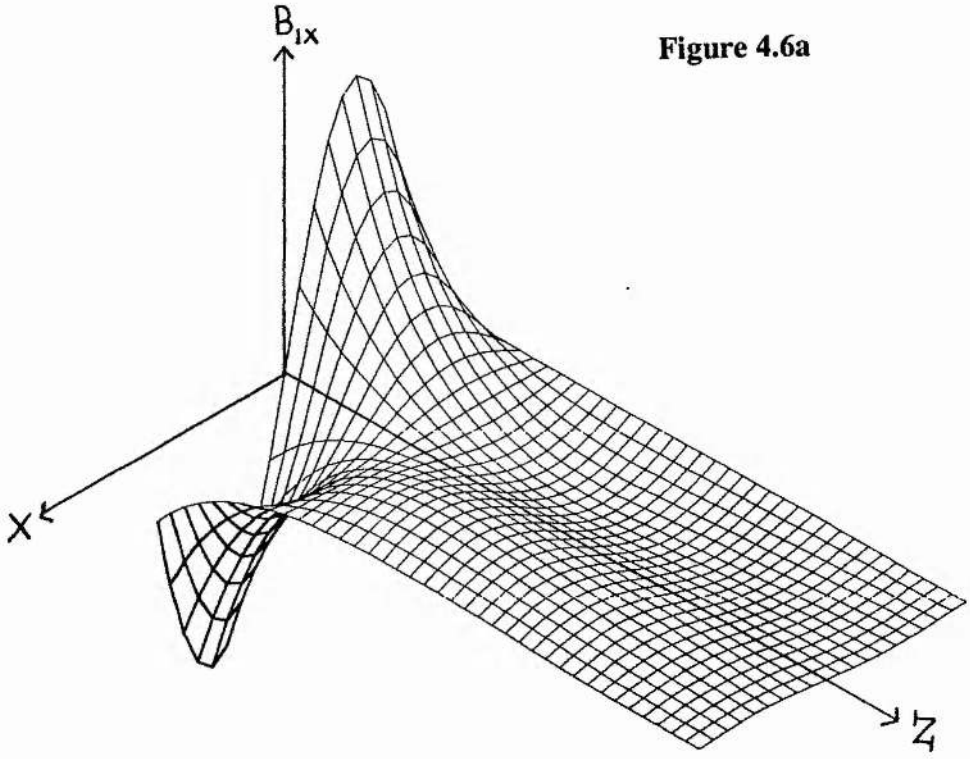

Figure 4.6a

Figure 4.6: Fundamental mode of (a) B_{1x}, (b) p_1, (c) B_{1z} where $0 \leq Z \leq 2.0$ and $M_A^2(0)=0.65, \beta(0)=0.7, \delta=0.15, \beta_{10}=1.0, B_{10}= 1.0$.

Figure 4.6b

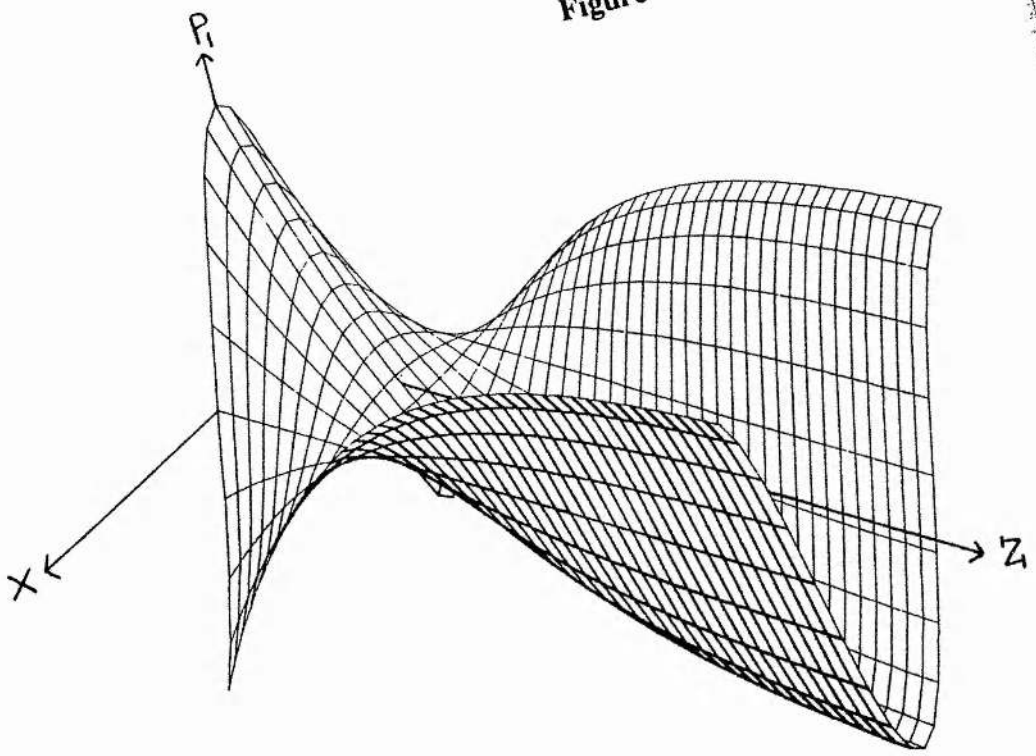

Figure 4.6c

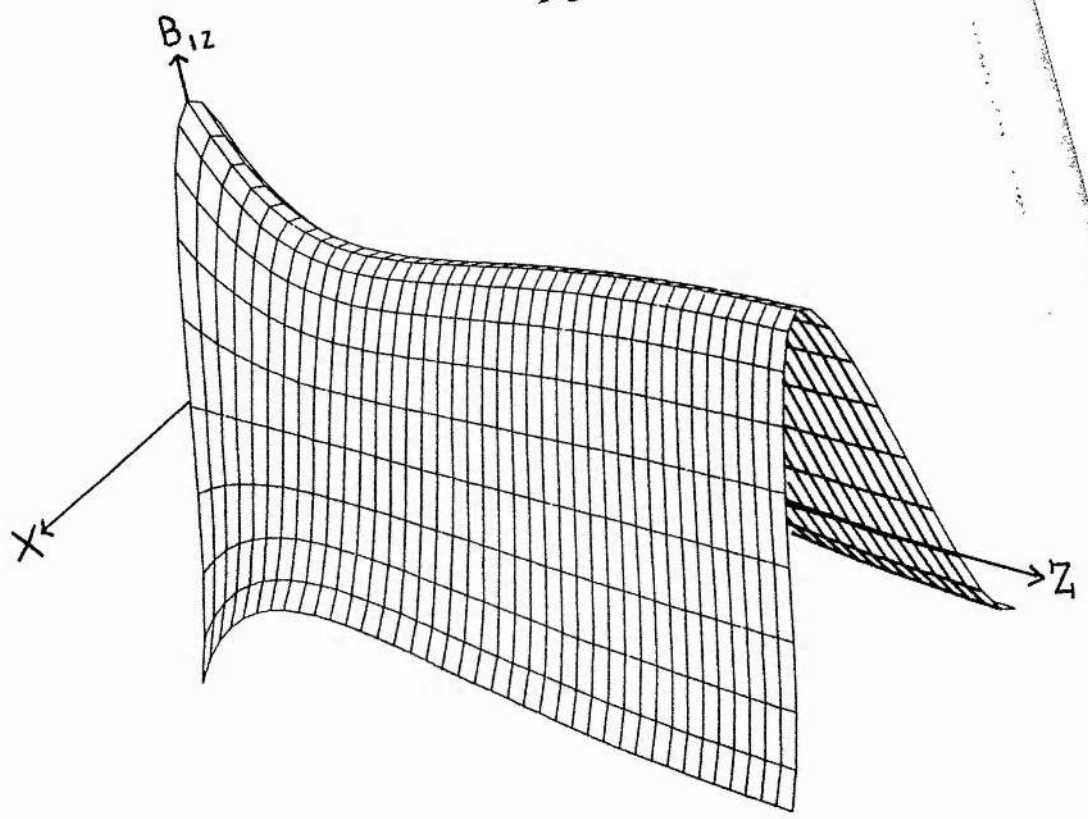

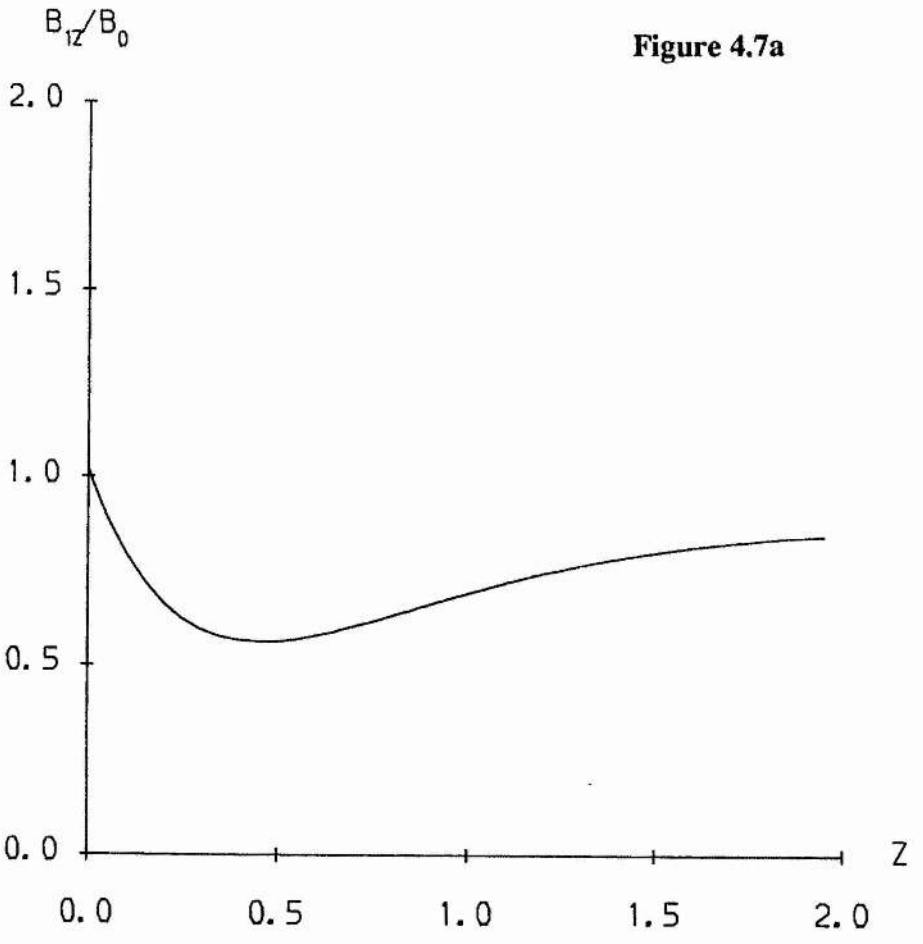

Figure 4.7a

Figure 4.7: Fundamental mode of (a) B_{1z} , (b) p_1, along x=0 for

$M_A^2(0)=0.65, \beta(0)=0.7, \delta=0.15, \beta_{10}=1.0, B_{10}= 1.0.$

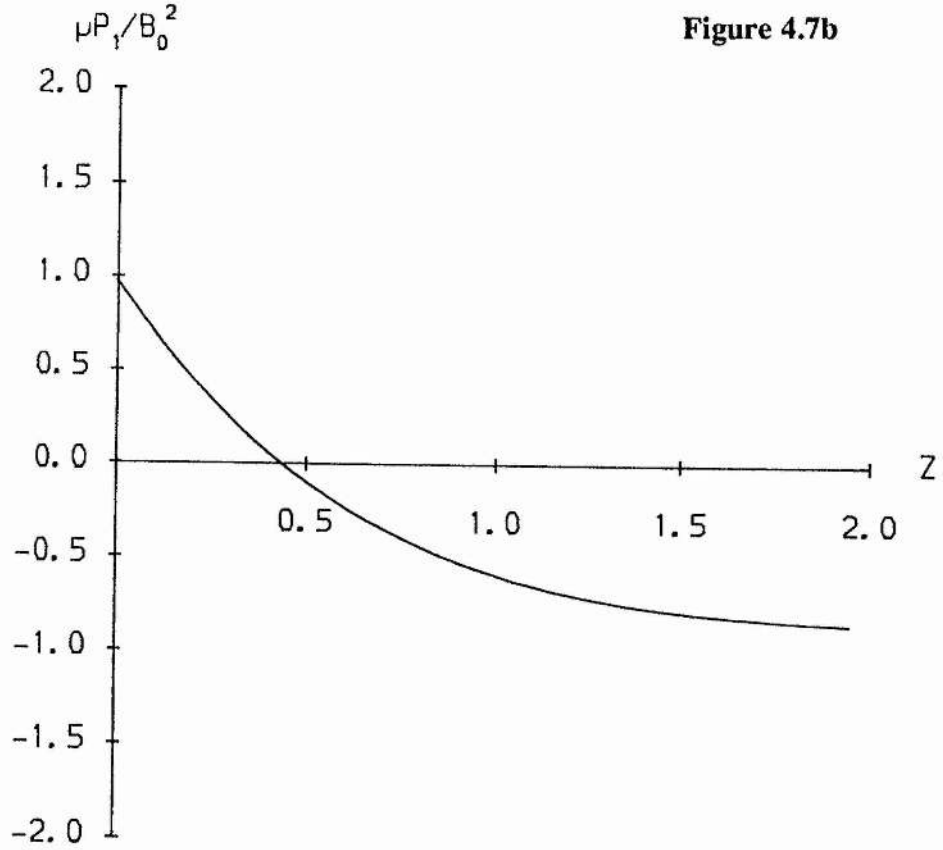

Figure 4.7b

Table 4 :Chains of possible MHD interactions as Z increases when B_{1z} and p_1 have stationary points λ_1 and λ_2 respectively. The following shorthand is adopted: F.C = fast-mode compression, F.E = fast-mode expansion , S.C = slow-mode compression , S.E = slow-mode expansion.

$\left.\frac{dp_1}{dZ}\right\|_{Z=0}$	$\left.\frac{dB_{1z}}{dZ}\right\|_{Z=0}$	$\lambda_1 > \lambda_2$	$\lambda_1 < \lambda_2$
< 0	> 0	F.E ↓ S.C ↓ F.C	F.E ↓ S.E ↓ F.C
> 0	> 0	F.C ↓ S.E ↓ F.E	F.C ↓ S.C ↓ F.E
> 0	< 0	S.C ↓ F.E ↓ S.E	S.C ↓ F.C ↓ S.E
< 0	> 0	S.E ↓ F.C ↓ S.C	S.E ↓ F.E ↓ S.C

$dB_{1z}/dZ<0$, with $\lambda_1<\lambda_2$ then the interaction in the plasma changes from a **slow-mode compression**, and finally to a **slow-mode expansion**, as Z increases. The various chains of interactions possible as Z increases are summarised in Table 4.4. Clearly the addition of gravity can alter the basic solutions in a noticeable way and introduce a wider variety of combinations which may take place.

4.6.3 Conclusions

In this chapter we have benn concerned with modelling MHD interactions in a gravitationally stratified atmosphere for a slab geometry. In section 4.3 we derived the governing equation for small perturbations about the basic state described in section 4.2. This equation is of considerable complexity and in order to make analytical progress we derived a correction due to gravity (section 4.4). This correction demonstrates that the addition of gravity in the equation of motion can have a noticeable effect on the nature of MHD interactions. Considering the fundamental mode we saw that two basic cases arise. Namely, those parameter ranges where the magnetic field structure is effectively the same as for the gravity-free case ($\delta=0$) (i.e., purely converging or diverging fieldlines), and those where the direction of the fieldlines change (i.e., a diverging field becomes converging).

In the former case, the addition of gravity increases the maxima of the plasma and magnetic pressures, but decreases the curvature of the fieldlines. Increasing the Alfven Mach number reduces the curvature of the fieldlines, and increases the maxima of both the plasma and magnetic pressure. These results contrast with the corresponding results for the gravity-free solutions ,where the curvature of the fieldlines also increased with $M_A(0)$ for $M_T(0)<1$. Additionally, the classification of the solutions is altered. For example, for an appropriate choice of B_{10} and β_{10} the interaction could switch from a **slow-mode compression** to a **fast-mode expansion** with the addition of the gravitational correction.

When the magnetic and plasma pressure are no longer monotonic, the type of interaction occurring in the plasma varies with Z. For example, when both magnetic and plasma pressures have a stationary point, we could have the following chain of MHD interactions: **fast-mode compression** to **slow-mode expansion** to **fast-mode expansion**. The magnetic field topologies associated with non-monotonic plasma and magnetic pressures are reminiscent of the global field structure of coronal streamers.

The addition of gravity plays an important role in altering the basic solutions, and the nature of MHD interactions. It also illustrates how a stratified atmosphere can give a more varied selection of magnetic field structures as perturbations on a uniform, unidirectional field. Although the model presented in these chapters is a gross simplification of the corona,we have seen that it is possible to produce coronal -'like' structures as extended standing disturbances.

Part 2

Chapter 5 Exact Solutions For Flows In Arcades

5.1 Introduction

The linear theory presented in the previous three chapters has the restriction that only small departures from the basic state are permitted. Even a cursory glance at an eclipse photograph will show that the corona is certainly non-linear, and so it is desirable to construct more realistic solutions. One possible approach would be to expand the MHD equations byond first order in some small parameter ϵ, and to consider weakly nonlinear solutions. An alternative is to seek exact solutions to the MHD equations. In the remainder of the thesis we present some simple exact solutions which may be useful in modelling the solar atmosphere. Our study is not intended to be exhaustive,but we aim to show the potential of this particular approach.

We follow the method given by Tsinganos (1981,1982) for finding exact solutions. In the first of his two papers (1981), the equations of motion, induction, continuity (mass and magnetic flux) are reduced to a single partial differential equation, with the assunption that the plasma density is a function of the flux function . This derivation was performed separately in cartesian, cylindrical and spherical geometries. Later in this section we give a similar derivation in an orthogonal curvilinear coordinate system. The solutions we present follow from this derivation with the assumption that the density is a function of the flux function. In a later treatment, Tsinganos (1982) shows how two different general equations of state may be included. Restrictions which arise in the solutions following the first method may be overcome by including an equation of state.

5.2 Reduction of MHD Equations

First, we rewrite the MHD equations in dimensionless variables as follows. Define variables

$$\mathbf{Q} = Q_0 \hat{\mathbf{Q}}$$

and

$$q = q_0 \hat{q}$$

where the Q_0 ,q_0's are characteristic values of the various variables. The MHD equations in dimensionless variables are

$$\nabla.\hat{\mathbf{B}} = 0\,, \tag{5.1}$$

$$\nabla.(\hat{\rho}\hat{\mathbf{v}}) = 0\,, \tag{5.2}$$

$$\nabla \times (\hat{\mathbf{v}} \times \hat{\mathbf{B}}) = \mathbf{0}\,, \tag{5.3}$$

$$M_a^2 \hat{\rho}(\hat{\mathbf{v}}.\nabla)\hat{\mathbf{v}} = -\frac{1}{2}\nabla(\beta\hat{p} + \hat{B}^2) + (\hat{\mathbf{B}}.\nabla)\hat{\mathbf{B}} - H\hat{\rho}\nabla\hat{V}\,, \tag{5.4}$$

where the dimensionless parameters M_a,β and H are defined by

$$M_a^2 = \frac{v_0^2 \mu \rho_0}{B_0^2}\ ;\ \beta = \frac{2\mu p_0}{B_0^2}\ ;\ H = \frac{\mu \rho_0 V_0}{l B_0^2}\,,$$

and l is a typical length scale of the plasma. Setting M_a=0, reduces equation (5.1) to the usual magnetostatic equation. Henceforth the 'hats' will be dropped for convenience.

Now consider an orthogonal curvilinear coordinate system $\mathbf{e}_1,\mathbf{e}_2,\mathbf{e}_3$ with the line elements $h_1(x_1,x_2,x_3)$, $h_2(x_1,x_2,x_3)$ and $h_3(x_1,x_2,x_3)$. Henceforth, the special case where x_3 is an ignorable coordinate will be considered, giving $h_i=h_i(x_1,x_2)$ (i=1,2,3).

The conservation equations (5.1) and (5.2) may then be expressed in the form

$$\frac{\partial}{\partial x_1}(h_2h_3B_1) + \frac{\partial}{\partial x_2}(h_1h_2B_2) = 0, \tag{5.5}$$

$$\frac{\partial}{\partial x_1}(h_2h_3\rho v_1) + \frac{\partial}{\partial x_2}(h_1h_2\rho v_2) = 0\,, \tag{5.6}$$

respectively. Equations (5.5) and (5.6) are identically satisfied by defining a flux and streamfunction, respectively, namely

$$h_2h_3B_1 = \frac{\partial A}{\partial x_2}\ ;\ h_1h_3B_2 = -\frac{\partial A}{\partial x_1}\,, \tag{5.7}$$

and

$$h_2h_3\rho v_1 = \frac{\partial \Psi}{\partial x_2} \; ; \; h_1h_3\rho v_2 = -\frac{\partial \Psi}{\partial x_1} . \tag{5.8}$$

From equation (5.3), and using equation (5.7) and (5.8), the $\mathbf{e}_1$ and $\mathbf{e}_2$ components may be recast in the Jacobian notation (see Appendix) to give

$$\frac{\partial}{\partial x_2}\left\{\frac{1}{h_1h_2h_3\rho}\left[A,\Psi\right]\right\} = 0 \; ,$$

and

$$\frac{\partial}{\partial x_1}\left\{\frac{1}{h_1h_2h_3\rho}\left[A,\Psi\right]\right\} = 0.$$

This is equivalent to the single expression

$$\left[A,\Psi\right] = 0 , \tag{5.9}$$

assuming that there is no constant electric field in the $\mathbf{e}_3$ direction. This is a key assumption for what follows, and it is not clear whether this assumption can be relaxed in general. In chapter seven, we present a particular class of solutions with a constant electric field in the ignorable direction. Equation (5.9) has the general solution

$$\Psi = \Psi(A) , \tag{5.10}$$

which expresses physically that the magnetic and stream surfaces coincide. However, in general, the magnetic and streamlines do not coincide due to nonuniform convective components of the fields in the $\mathbf{e}_3$ direction. This arises from the difference in the field components v_3 and B_3.

The $\mathbf{e}_3$ component of equation (5.3) yields the Jacobian relation

$$\left[\frac{v_3}{h_3}, A\right] - \left[\frac{B_3}{h_3\rho}, \Psi\right] = 0 ,$$

and using the fact that $\Psi = \Psi(A)$, this may be written as

$$\left[\left(\frac{v_3}{h_3} - \frac{B_3\Psi_A}{h_3\rho}\right), A\right] = 0 ,$$

where subscript A denotes differentiation with respect to A. The general solution is then

$$\frac{v_3}{h_3} - \frac{B_3\Psi_A}{h_3\rho} = \Phi_A(A) , \tag{5.11}$$

where $\Phi_A(A)$ is an arbitary function of A, which corresponds to the electrostatic potential arising from the induction equation

$$\mathbf{v}\times\mathbf{B} = \nabla\Phi.$$

Now turning our attention to the equation of motion (5.4), the $\mathbf{e}_3$-component can be shown to be

$$M_a^2\rho(\mathbf{v}.\nabla)v_3 = (\mathbf{B}.\nabla)B_3.$$

Using the vector identity

$$(\mathbf{F}.\nabla)\mathbf{F} = (\nabla\times\mathbf{F})\times\mathbf{F} + \nabla\left(\frac{1}{2}|\mathbf{F}|^2\right),$$

this component becomes

$$M_a^2\rho(\mathbf{v}\times\nabla\times\mathbf{v}).\mathbf{e}_3 = (\mathbf{B}\times\nabla\times\mathbf{B}).\mathbf{e}_3 ,$$

or in Jacobian notation

$$[h_3B_3,A] - [M_a^2h_3v_3, \Psi] = 0.$$

Again using the result $\Psi=\Psi(A)$, we obtain

$$\left[h_3\left(B_3 - M_a^2\Psi_A v_3\right),\ A\right] = 0 ,$$

which has the general solution

$$h_3\left(B_3 - M_a^2\Psi_A v_3\right) = \Omega(A) , \tag{5.12}$$

where $\Omega(A)$ is an arbitary function of A.

From equations (5.11) and (5.12) one can easily show that

$$v_3\left(1 - \frac{M_a^2\Psi_A^2(A)}{\rho}\right) = h_3\Phi_A(A) + \frac{\Psi_A(A)\Omega(A)}{h_3\rho}, \tag{5.13}$$

$$B_3\left(1 - \frac{M_a^2\Psi_A^2(A)}{\rho}\right) = h_3M_a^2\Phi_A(A)\Psi_A(A) + \frac{\Omega(A)}{h_3}, \tag{5.14}$$

and

$$\frac{1}{2}h_3^2\left(M_a^2\rho v_3^2 - B_3^2\right) = \frac{\frac{1}{2}h_3^2}{\left(1 - \frac{M_A^2\Psi_A^2(A)}{\rho}\right)}\left\{M_a^2\rho h_3^2\Phi_A^2 - \frac{\Omega^2}{h_3^2}\right\}. \tag{5.15}$$

Considering again the equation of motion (5.4), we choose to write it in the form

$$\nabla\left(\frac{1}{2}\beta p+\frac{1}{2}M_a^2\rho|v|^2+H\rho V\right) = (\nabla\times\mathbf{B})\times\mathbf{B} + M_a^2\rho\mathbf{v}\times(\nabla\times\mathbf{v})$$

$$+\left(HV+\frac{1}{2}M_a^2|v|^2\right)\nabla\rho. \qquad (5.16)$$

Defining the modified Bernoulli pressure

$$\Pi=\frac{1}{2}\beta p+\frac{1}{2}M_a^2\rho|v|^2+\rho HV-\frac{h_3^2M_a^2\rho\Phi_A^2(A)}{\left(1-\frac{M_a^2\Psi_A^2(A)}{\rho}\right)}, \qquad (5.17)$$

the e_1-component of equation (5.16) may be written as

$$\frac{\partial\Pi(x_1,x_2)}{\partial x_1}=-\left(1-\frac{M_a^2\Psi_A^2(A)}{\rho(x_1,x_2)}\right)\frac{\partial A}{\partial x_1}\Delta A-\frac{h_3^2}{2}\frac{\partial}{\partial x_1}\left(\frac{M_a^2\rho(x_1,x_2)\Phi_A^2(A)}{1-\frac{M_a^2\Psi_A^2(A)}{\rho(x_1,x_2)}}\right)$$

$$-\frac{1}{2h_3^2}\frac{\partial}{\partial x_1}\left(\frac{\Omega^2(A)}{1-\frac{M_a^2\Psi_A^2(A)}{\rho(x_1,x_2)}}\right)$$

$$+M_a^2\Psi_A\frac{\partial}{\partial x_1}\left[\frac{1}{h_1^2h_2^2}\frac{\partial A}{\partial x_1}\frac{\partial}{\partial x_1}\left(\frac{\Psi_A}{\rho}\right)+\frac{1}{h_2^2h_3^2}\frac{\partial A}{\partial x_2}\frac{\partial}{\partial x_2}\left(\frac{\Psi_A}{\rho}\right)\right]\frac{\partial A}{\partial x_1}$$

$$+\left(HV+\frac{1}{2}M_a^2\left[|v|^2-v_3^2\right]\right)\frac{\partial\rho(x_1,x_2)}{\partial x_1}, \qquad (5.18)$$

where we have made use of equation (5.15) and

$$\Delta A=\frac{1}{h_1h_2h_3}\left(\frac{\partial}{\partial x_1}\left(\frac{h_2}{h_1h_3}\frac{\partial A}{\partial x_1}\right)+\frac{\partial}{\partial x_2}\left(\frac{h_1}{h_2h_3}\frac{\partial A}{\partial x_2}\right)\right).$$

Similary the e_2-component of equation (5.16) may be written as

$$\frac{\partial\Pi(x_1,x_2)}{\partial x_2}=-\left(1-\frac{M_a^2\Psi_A^2(A)}{\rho(x_1,x_2)}\right)\frac{\partial A}{\partial x_2}\Delta A$$

$$-\frac{h_3^2}{2}\frac{\partial}{\partial x_2}\left(\frac{M_a^2\rho(x_1,x_2)\Phi_A^2(A)}{1-\frac{M_a^2\Psi_A^2(A)}{\rho(x_1,x_2)}}\right)-\frac{1}{2h_3^2}\frac{\partial}{\partial x_2}\left(\frac{\Omega^2(A)}{1-\frac{M_a^2\Psi_A^2(A)}{\rho(x_1,x_2)}}\right)$$

$$+M_a^2\Psi_A\left[\frac{1}{h_1^2h_3^2}\frac{\partial A}{\partial x_1}\frac{\partial}{\partial x_1}\left(\frac{\Psi_A}{\rho}\right)+\frac{1}{h_2^2h_3^2}\frac{\partial A}{\partial x_2}\frac{\partial}{\partial x_2}\left(\frac{\Psi_A}{\rho}\right)\right]\frac{\partial A}{\partial x_2}$$

$$+\left(HV+\frac{1}{2}M_a^2\left[|v|^2-v_3^2\right]\right)\frac{\partial\rho(x_1,x_2)}{\partial x_2}. \qquad (5.19)$$

To make further progress we assume that the plasma density is a function of A alone, i.e., $\rho=\rho(A)$. We now wish to show that the modified Bernoulli pressure Π is a function of A alone, i.e., $\Pi=\Pi(A)$. To do this note the following relations for a differentiable function T;

$$\frac{\partial T(x_1,x_2)}{\partial x_1} = \frac{\partial T(x_1,A)}{\partial x_1} + \frac{\partial A}{\partial x_1}\frac{\partial T(x_1,A)}{\partial A} = \frac{\partial A}{\partial x_1}\frac{\partial T(x_2,A)}{\partial A}, \qquad (5.20)$$

$$\frac{\partial T(x_1,x_2)}{\partial x_2} = \frac{\partial T(x_2,A)}{\partial x_2} + \frac{\partial A}{\partial x_2}\frac{\partial T(x_2,A)}{\partial A} = \frac{\partial A}{\partial x_2}\frac{\partial T(x_1,A)}{\partial A}, \qquad (5.21)$$

and transform equation (5.19) into coordinates (x_1,A) using (5.21) to yield

$$\frac{\partial \Pi(x_1,A)}{\partial A} + \left(1 - \frac{M_a^2\Psi_A^2(A)}{\rho}\right)\Delta A$$
$$+ \frac{h_3^2(x_1,A)}{2}\frac{d}{dA}\left(\frac{M_a^2\rho\Phi_A^2(A)}{1 - \frac{M_a^2\Psi_A^2(A)}{\rho}}\right) + \frac{1}{2h_3^2(x_1,A)}\frac{d}{dA}\left(\frac{\Omega^2(A)}{1 - \frac{M_a^2\Psi_A^2(A)}{\rho}}\right)$$
$$-M_a^2\Psi_A\left[\frac{1}{h_1^2h_3^2}\frac{\partial A}{\partial x_1}\frac{\partial}{\partial x_1}\left(\frac{\Psi_A}{\rho}\right) + \frac{1}{h_2^2h_3^2}\left(\frac{\partial A}{\partial x_2}\right)^2\frac{d}{dA}\left(\frac{\Psi_A}{\rho}\right)\right]$$
$$-\left(HV + \frac{1}{2}M_a^2\left[|v|^2 - v_3^2\right]\right)\frac{d\rho}{dA} = 0. \qquad (5.22)$$

assuming that $\partial A/\partial x_2$ is non-zero. Now transforming equation (5.18) into variables (x_1,A) using (5.20) we obain

$$\frac{\partial \Pi(x_1,A)}{\partial x_1} + \frac{\partial A}{\partial x_2}\left\{\frac{\partial \Pi(x_1,A)}{\partial A} + \left(1 - \frac{M_a^2\Psi_A^2(A)}{\rho}\right)\Delta A\right.$$
$$+ \frac{h_3^2(x_1,A)}{2}\frac{d}{dA}\left(\frac{M_a^2\rho\Phi_A^2(A)}{1 - \frac{M_a^2\Psi_A^2(A)}{\rho}}\right) + \frac{1}{2h_3^2(x_1,A)}\frac{d}{dA}\left(\frac{\Omega^2(A)}{1 - \frac{M_a^2\Psi_A^2(A)}{\rho}}\right)$$
$$-M_a^2\Psi_A\left[\frac{1}{h_1^2h_3^2}\frac{\partial A}{\partial x_1}\frac{\partial}{\partial x_1}\left(\frac{\Psi_A}{\rho}\right) + \frac{1}{h_2^2h_3^2}\left(\frac{\partial A}{\partial x_2}\right)^2\frac{d}{dA}\left(\frac{\Psi_A}{\rho}\right)\right]$$
$$\left. - \left(HV + \frac{1}{2}M_a^2\left[|v|^2 - v_3^2\right]\frac{d\rho}{dA}\right)\right\} = 0. \qquad (5.23)$$

Substituting equation (5.22) into (5.23) we have

$$\frac{\partial \Pi(x_1,A)}{\partial x_1} = 0,$$

and hence $\Pi = \Pi(A)$. Similarly we could have transformed them into variables (x_2,A) and deduced that

$$\frac{\partial \Pi(x_2,A)}{\partial x_2} = 0,$$

assuming that $\partial A/\partial x_1$ is non-zero.

Rearranging either (5.21) or (5.22) we can obtain the single non-linear partial differential equation

$$\left(1 - \frac{M_a^2\Psi_A^2(A)}{\rho}\right)\Delta A - \frac{1}{2}\frac{M_a^2}{h_3^2}\left[\frac{1}{h_1^2}\left(\frac{\partial A}{\partial x_1}\right)^2 + \frac{1}{h_2^2}\left(\frac{\partial A}{\partial x_2}\right)^2\right]\frac{d}{dA}\left(\frac{\Psi_A^2}{\rho}\right)$$

$$+\frac{h_3^2}{2}\frac{d}{dA}\left(\frac{M_a^2\rho\Phi_A^2(A)}{1 - \frac{M_a^2\Psi_A^2(A)}{\rho}}\right)+\frac{1}{2h_3^2}\frac{d}{dA}\left(\frac{\Omega^2(A)}{1 - \frac{M_a^2\Psi_A^2(A)}{\rho}}\right)$$

$$- HV\frac{d\rho}{dA} + \frac{d\Pi}{dA} = 0. \qquad (5.24)$$

The object now is to choose the arbitary functions Π,Φ,Ω, and ρ of A, and then seek solutions of the resulting partial differential equation.

In the magnetostatic limit ($M_a \to 0$) equation (5.24) reduces to

$$\Delta A + \frac{1}{2h_3^2}\frac{d\Omega^2}{dA} - HV\frac{d\rho}{dA} + \frac{d\Pi}{dA} = 0\,,$$

and when gravity is absent (H=0) the above equation simplifies further to

$$\Delta A + \frac{1}{2h_3^2}\frac{dB_3^2}{dA} + \frac{1}{2}\beta\frac{dp}{dA} = 0.$$

In the low-beta limit ($\beta \to 0$) we obtain the force-free equation

$$\Delta A + \frac{1}{2h_3^2}\frac{dB_3^2}{dA} = 0\,,$$

which reduces to the potential case when $B_3=0$, namely

$$\Delta A = 0.$$

5.3 Flows In Arcades

The modelling presented in the previous chapters concentrated on open magnetic field structures, such as plumes and coronal holes. However it is clear from observations that closed structure also exists, in the form of loops or arcades of magnetic fields. The solutions of the previous chapters focused on the corona, the solutions presented here may have wider application to the photosphere and chromosphere.

Most theoretical studies of closed magnetic structures in the solar atmosphere have assumed them to be in magnetostatic equilibrium. For example, models for magnetic arcades have been generalised from the familar force-free solutions (see

for example Priest, 1984) to include plasma pressure and gravitational effects (for example, Zweibel and Hundhausen, 1982).

However, observations have shown that plasma flows do often exist in these structures as described in e.g, Bruzek and Durrant (1977). Thus, it is desirable to contruct models to include flows. Steady flows in single loops have been modelled by several authors. For example, Cargill and Priest (1980,1982) extended the theory of Meyer and Schmidt (1968) for photospheric Evershed flow to flow along coronal magnetic loops. These models assumed the loops to be rigid, although the cross-sectional area is allowed to vary in a prescribed way. This assumption has recently been relaxed by Thomas (1988), Montesinos and Thomas (1989) and Degenhart (1990), who include a variation of the cross-sectional area of the tube in a way that depends upon the size of the flow speed.

In this chapter we present a class of exact solutions using the method of section 5.2, which may model subsonic steady flows along an arcade of magnetic fieldlines. Two sets of solutions are given, first for a symmetric arcade, the second for non-symmetric arcades. In the latter case the plasma pressure, magnetic field and velocity differences may be imposed across the arcade. These solutions may provide a model for subsonic flow in magnetic arcades.

In a cartesian geometry and neglecting gravity (H=0) equation (5.24) reduces to

$$\left(1 - \frac{M_a^2 \Psi_A^2}{\rho}\right)\nabla^2 A - \frac{1}{2} M_a^2 \left[\left(\frac{\partial A}{\partial x}\right)^2 + \left(\frac{\partial A}{\partial z}\right)^2\right]\frac{d}{dA}\left(\frac{\Psi_A^2}{\rho}\right)$$
$$+ \frac{1}{2}\frac{d}{dA}\left(\frac{M_a^2 \rho \Phi_A^2 + \Omega^2}{1 - \frac{M_a^2 \Psi_A^2}{\rho}}\right) + \frac{d\Pi}{dA} = 0 . \qquad (5.25)$$

Tsinganos (1981,1982) presented solutions with constant density, and we here present a new class of solutions with nonuniform density.

We make the following prescription for the arbitary functions of A;

$$\rho = A^2,\ \Psi = \frac{1}{2}A^2,\ \Phi = \Phi_0,\ \Omega = \Omega_0 A,\ \Pi = -\Pi_0 A + \Pi_1 , \qquad (5.26)$$

where Φ_0, Ω_0, Π_0 and Π_1 are constants. The choice $\Phi=\Phi_0$, implies that the fieldlines are parallel to the streamlines. The generalised Bernoulli pressure Π,is chosen to be linear in A, and the density to vary as the square of A. Since the plasma flow is along the fieldlines and the density is constant along curves of constant A, then the flow is incompressible, though the value of the density varies from fieldline to fieldline. There are clearly many choices for the arbitrary functions of A, but with the particular choice (5.26), equation (5.25) reduces to the linear elliptic equation,

$$\nabla^2 A + \alpha^2 A = \bar{\Pi}, \tag{5.27}$$

where

$$\alpha^2 = \frac{\Omega_0^2}{(1-M_a^2)^2} \; ; \; \bar{\Pi} = \frac{\Pi_0}{(1-M_a^2)},$$

and ∇^2 is the two-dimensional Laplacian operator.

Setting $M_a=0$ and $\bar{\Pi}=0$ (i.e., no flows and variations in the generalised Bernoulli pressure) reduces equation (5.27) to the familiar equation for linear force-free fields. Setting also $\alpha=0$ (i.e., $\Omega_0=0$) we obtain the potential case, and the B_y -component of the magnetic field is zero. The inclusion of the centrifugal force terms in the equation of motion modifies the value of α^2, but for the particular choice (5.26), the magnetic field topology is similar to the magnetostatic case. Thus, the solutions to equation (5.27) will give steady flows parallel to the fieldlines in magnetic arcades. It should of course be noted that more general fields may be possible for general choices of ρ, Ω, Φ, Ψ and Π. In the next section we consider the case of symmetric arcades.

5.4 Symmetric Arcades

Turning our attention to equation (5.27), we note that a particular integral is

$$A_p = \frac{\bar{\Pi}}{\alpha^2}.$$

Consider now the homogeneous version of equation (5.27) and look for separable solutions of the form

$A_c(x,z) = X(x)Z(z)$,

subject to the boundary conditions

$$B_x \to 0 \text{ as } z \to \infty , \tag{5.28a}$$

$$B_z = f(x) \text{ on } z = 0 . \tag{5.28b}$$

Imposing condition (5.28a) we obtain the solution

$$A=A_c+A_p = [a\cos\sigma x + b\sin\sigma x]e^{-\nu z} + \frac{\Pi}{\alpha^2} , \tag{5.29}$$

where $\nu^2 = \sigma^2 - \alpha^2$, σ^2 is a separation constant and a,b are arbitary constants.

Two further boundary conditions are necessary, and we take

$B_z = 0$ on $x=0$,

$B_x = 0$ on $x= \pm 1$,

which ensures that the magnetic field is symmetric about x=0. Imposing these conditions to solution (5.29) gives b=0 and $\sigma = (n-1/2)\pi$ where n is a positive integer, thus giving the solution for A to be

$$A = \sum_{n=1}^{\infty} \frac{a_n}{(n-1/2)\pi} \cos[(n-1/2)\pi x]e^{-\nu z} + \frac{\Pi}{\alpha^2} .$$

From the equations (5.7) the magnetic field components may be deduced to be

$$B_x = - \sum_{n=1}^{\infty} \frac{a_n \nu}{(n-1/2)\pi} \cos[(n-1/2)\pi x]e^{-\nu z}, \tag{5.30a}$$

$$B_z = \sum_{n=1}^{\infty} a_n \sin[(n-1/2)\pi x]e^{-\nu z} , \tag{5.30b}$$

and from equation (5.14)

$$B_y = \frac{\Omega_0}{(1-M_a^2)} \left\{ \sum_{n=1}^{\infty} \frac{a_n}{(n-1/2)\pi} \cos[(n-1/2)\pi x]e^{-\nu z} + \frac{\Pi}{\alpha^2} \right\} . \tag{5.30c}$$

Similarly, the components of the velocity may be found from equations (5.8) and (5.13) to be

$$v_x = \frac{-\sum_{n=1}^{\infty} \frac{a_n \nu}{(n-1/2)\pi} \cos[(n-1/2)\pi x] e^{-\nu z}}{\sum_{n=1}^{\infty} \frac{a_n}{(n-1/2)\pi} \cos[(n-1/2)\pi x] e^{-\nu z} + \frac{\Pi}{\alpha^2}}, \qquad (5.31a)$$

$$v_z = \frac{\sum_{n=1}^{\infty} a_n \sin[(n-1/2)\pi x] e^{-\nu z}}{\sum_{n=1}^{\infty} \frac{a_n}{(n-1/2)\pi} \cos[(n-1/2)\pi x] e^{-\nu z} + \frac{\Pi}{\alpha^2}}, \qquad (5.31b)$$

$$v_y = \frac{\Omega_0}{(1-M_a^2)}. \qquad (5.31c)$$

Using equation (5.17), the plasma pressure may be shown to be

$$\frac{1}{2}\beta p = \Pi_1 - \Pi_0 \left\{ \sum_{n=1}^{\infty} \frac{a_n}{(n-1/2)\pi} \cos[(n-1/2)\pi x] e^{-\nu z} + \frac{\Pi}{\alpha^2} \right\}$$

$$- \frac{1}{2} M_a^2 \left\{ \left[\sum_{n=1}^{\infty} \frac{a_n \nu}{(n-1/2)\pi} \cos[(n-1/2)\pi x] e^{-\nu z} \right]^2 \right.$$

$$+ \left[\sum_{n=1}^{\infty} a_n \sin[(n-1/2)\pi x] e^{-\nu z} \right]^2$$

$$\left. + \alpha^2 \left[\sum_{n=1}^{\infty} \frac{a_n}{(n-1/2)\pi} \cos[(n-1/2)\pi x] e^{-\nu z} + \frac{\Pi}{\alpha^2} \right]^2 \right\}, \qquad (5.32)$$

and the plasma density is

$$\rho = \left\{ \sum_{n=1}^{\infty} \frac{a_n}{(n-1/2)\pi} \cos[(n-1/2)\pi x] e^{-\nu z} + \frac{\Pi}{\alpha^2} \right\}^2. \qquad (5.33)$$

Imposing the boundary condition (5.28b) yields

$$a_n = \int_0^1 f(x) \sin[(n-1/2)\pi x] dx .$$

The solutions (5.30)-(5.33) are clearly fairly complicated, and so to investigate some of their properties we consider only the fundamental mode (n=1).

5.4.1 Fundamental Mode

The fundamental mode solutions may be written as

$$B_x = -\frac{2a_1\nu}{\pi}\cos\left(\frac{\pi x}{2}\right)e^{-\nu z}, \tag{5.34a}$$

$$B_z = a_1\sin\left(\frac{\pi x}{2}\right)e^{-\nu z}, \tag{5.34b}$$

$$B_y = \frac{\Omega_0}{(1-M_a^2)}\left\{\frac{2a_1}{\pi}\cos\left(\frac{\pi x}{2}\right)e^{-\nu z} + \frac{\Pi}{\alpha^2}\right\}, \tag{5.43c}$$

$$v_x = \frac{B_x}{\left\{\frac{2a_1}{\pi}\cos\left(\frac{\pi x}{2}\right)e^{-\nu z} + \frac{\Pi}{\alpha^2}\right\}}, \tag{5.34d}$$

$$v_z = \frac{B_z}{\left\{\frac{2a_1}{\pi}\cos\left(\frac{\pi x}{2}\right)e^{-\nu z} + \frac{\Pi}{\alpha^2}\right\}}, \tag{5.34e}$$

$$v_y = \frac{\Omega_0}{(1-M_a^2)}, \tag{5.34f}$$

$$\beta p = \left\{2\Pi_1 - (2-M_a^2)\frac{\Pi_0^2}{\Omega_0^2}\right\} - \frac{4a_1}{\pi}\frac{\Pi_0}{(1-M_a^2)}\cos\left(\frac{\pi x}{2}\right)e^{-2\nu z} - M_a^2a_1^2e^{-2\nu z}, \tag{5.34g}$$

$$\rho = \left\{\frac{2a_1}{\pi}\cos\left(\frac{\pi x}{2}\right)e^{-\nu z} + \frac{\Pi}{\alpha^2}\right\}^2. \tag{5.34h}$$

The equation of a fieldline is A=constant, and for the fieldline passing through the point $(x_0,0)$ we have

$$z = \frac{1}{\nu}\log\left[\frac{\cos\left(\frac{\pi x}{2}\right)}{\cos\left(\frac{\pi x_0}{2}\right)}\right]. \tag{5.35}$$

Along the base (z=0) of the region under consideration we impose the following conditions

$B_z(1,0) = B_m$,

$v_z(1,0) = v_m$,

$p(0,0) = p_1$,

$$p(1,0) = p_2,$$

from which we find that

$$a_1 = B_m ,$$

$$\Pi_0 = \beta\delta p(1-M_a^2)\frac{\pi}{4B_m} ,$$

and

$$\Omega_0^2 = \beta\delta p(1-M_a^2)2\frac{v_m\pi}{4B_m^2} ,$$

where $\delta p = p_2-p_1$ is the pressure difference between the centre and the edge of the rectangular region under consideration along the base (z=0). In addition we deduce that

$$\nu^2 = \frac{\pi}{4}\left\{\pi - \frac{\beta\delta p v_m}{B_m^2}\right\}, \tag{5.36}$$

which must be positive, giving the condition

$$\delta p v_m < \frac{\pi B_m^2}{\beta}. \tag{5.37}$$

Since $\Omega_0^2>0$, we are further restricted to having

$$\delta p v_m > 0,$$

and so δp and v_m have the same sign.

The plasma density and pressure may now be written as

$$\rho = \left\{\frac{2}{\pi}\cos\left(\frac{\pi x}{2}\right)e^{-\nu z}+\frac{1}{v_m}\right\}^2 ,$$

and

$$\beta p = \beta p_1 + M_a^2 B_m^2(1- e^{-2\nu z}) - \beta\delta p\cos\left(\frac{\pi x}{2}\right)e^{-2\nu z},$$

respectively.

Before discussing the properties of the fundamental mode solutions, let us consider the magnetic topology. The magnetic fieldlines are plotted in Figure 5.1 and can be seen to form an arcade. The magnetic field structure is similar to that of a linear force-free field,but now both plasma pressure and inertial effects are included. In particular, there will be a flow of plasma along the magnetic fieldlines.

Figure 5.1(a)

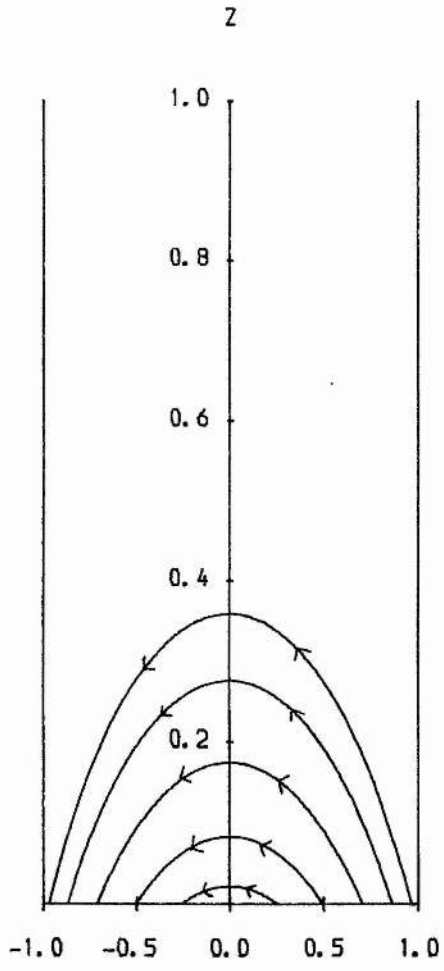

Figure 5.1(a)-(c): Magnetic fieldline plots when β=1.0,δp=1.0 and B_m=1.0

(a) v_m=0.0, (b) v_m=1.0,(c) v_m= 2.0.

Figure 5.1(b)

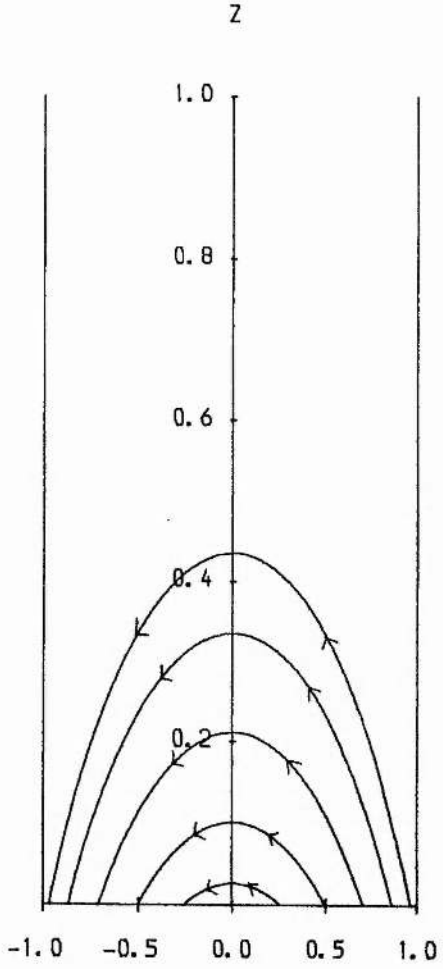

Figure 5.1(c)

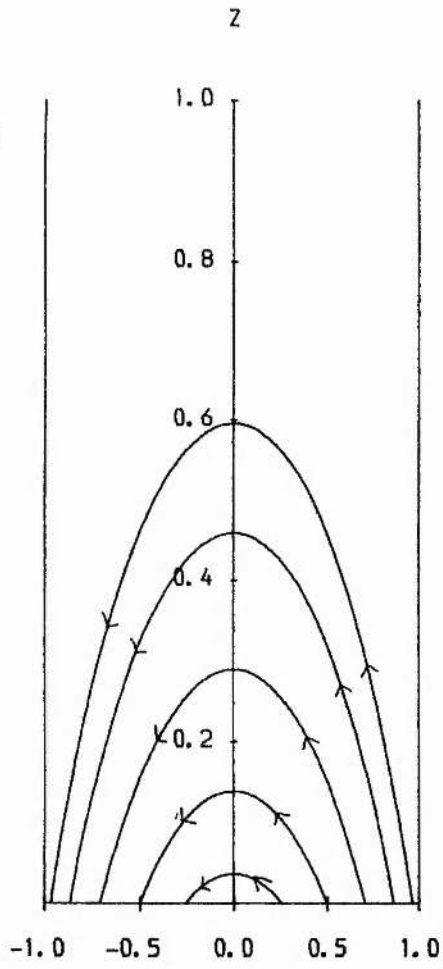

From equation (5.35) we note that the maximum height of the arcade h varies as v^{-1}. Thus, from equation (5.36) increasing v_m the flow speed at x=1 (subject to inequality (5.37)) increases the height of the arcade. This is illustrated in Figure 5.1 for three different values of v_m with $\delta p, B_m$ and β fixed. This effect is due to the presence of a centrifugal force which was not present in previous static models. Continuing to increase v_m until $\delta p v_m = \pi B_m^2/\beta$, the arcade erupts and the magnetic field becomes vertical. It is interesting to note that the imposed velocity and pressure difference is coupled together in these solutions. This is due to our choice of the arbitary functions of A. Had we made a slightly more general choice, say

$$\Omega = \Omega_0 A + \Omega_1 \, , \, \Pi = -\Pi_0 A + \Pi_1 + \Pi_2 A^2 \, ,$$

then there would be separate terms depending upon δp and v_m .

Note that increasing the pressure difference δp between x=0 and x=1, also has the effect of increasing the height of the arcade. As δp is increased, we can see that greater magnetic tension is reqired for force balance. This is produced by an increase in arcade height.

Increasing B_m has the effect of decreasing the height of the arcade. In this case, the footpoints in x>1/2 will shift towards x=1 increasing the field maxima. However the minimum of B_z at x=0 will decreae, while the maximum will increase. This will lead to a net lowering of the arcade.

Increasing the dominance of the plasma pressure foreces over magnetic forces (i.e., increase β) will also cause the arcade to rise,

The fundamental mode profiles are plotted at different heights (z) in Figures 5.2 and 5.3. In both cases B_m is chosen to be positive while inFigure 5.3, they are both negative.

Consider first Figure 5.2, and observe that B_x and V_x have maximum magnitudes along x=0 (a direct consequence of the symmetry of the solutions). The profile of v_x is flattened (compared with B_x) by the presence of a non-unity denominator in the solution. The vertical components (B_z,v_z) of field and flow

Figure 5.2(a)

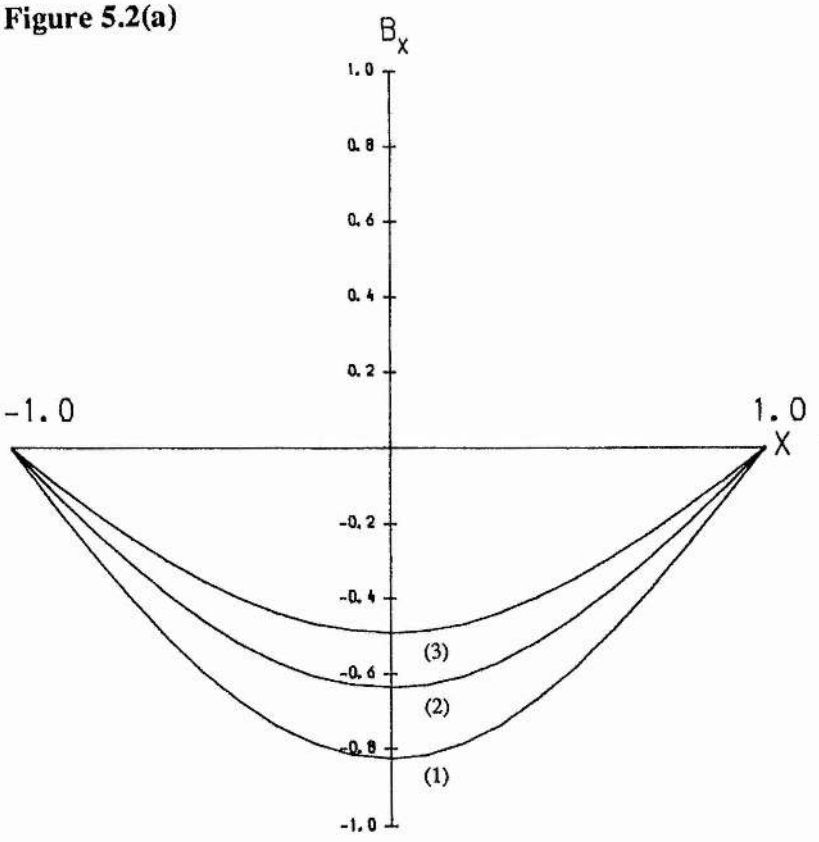

Figure 5.2: The variation with x of the fundamental mode solutions of (a) B_x, (b) B_z, (c) v_x, (d) v_z, (e) βp, (f) ρ when M_a=0.5, β=1.0, B_m=1.0, v_m=1.0,δp=1.0,p_1=1.0 for various values of z, namely (1) z=0.0, (2) z=0.5 and (3)z=1.0. (g) and (h) show the corresponding variations of ρ and βp with height z along x=0.

Figure 5.2(b)

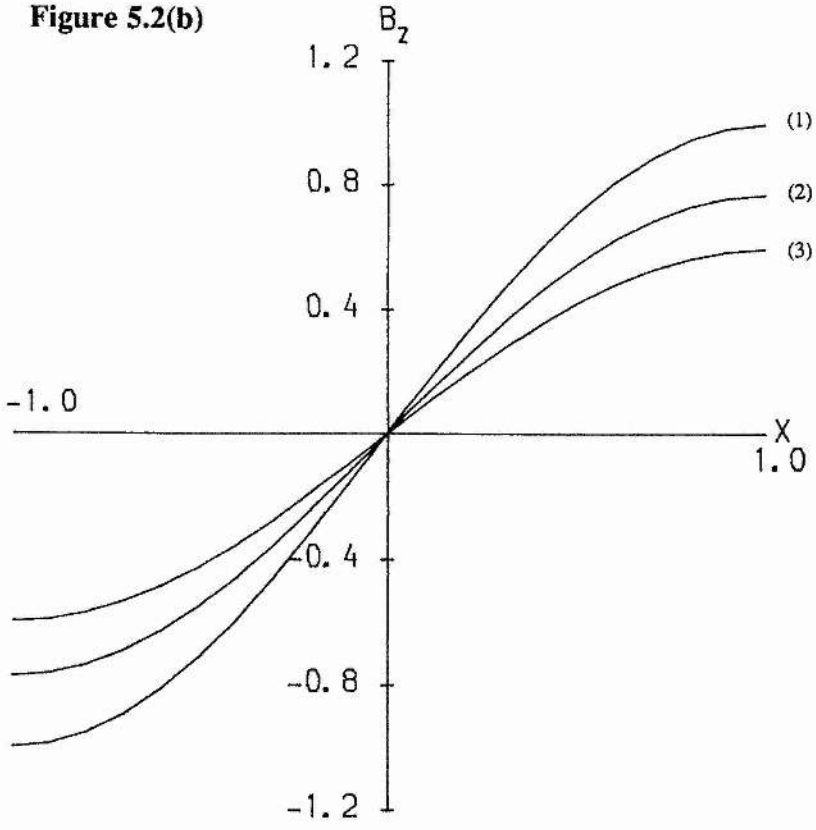

Figure 5.2(c)

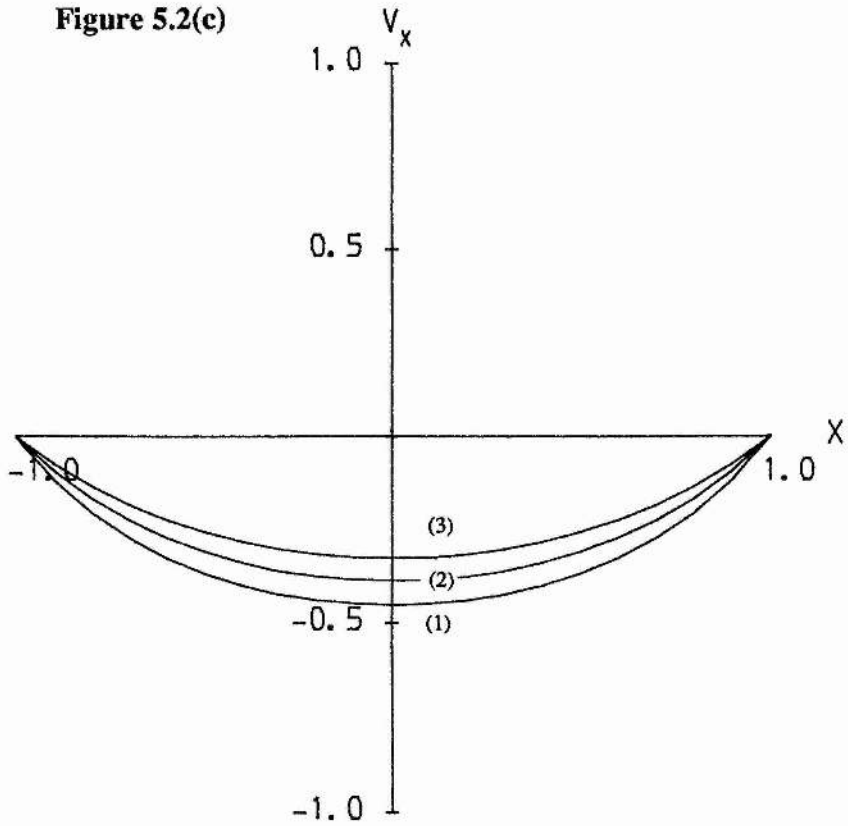

Figure 5.2(d)

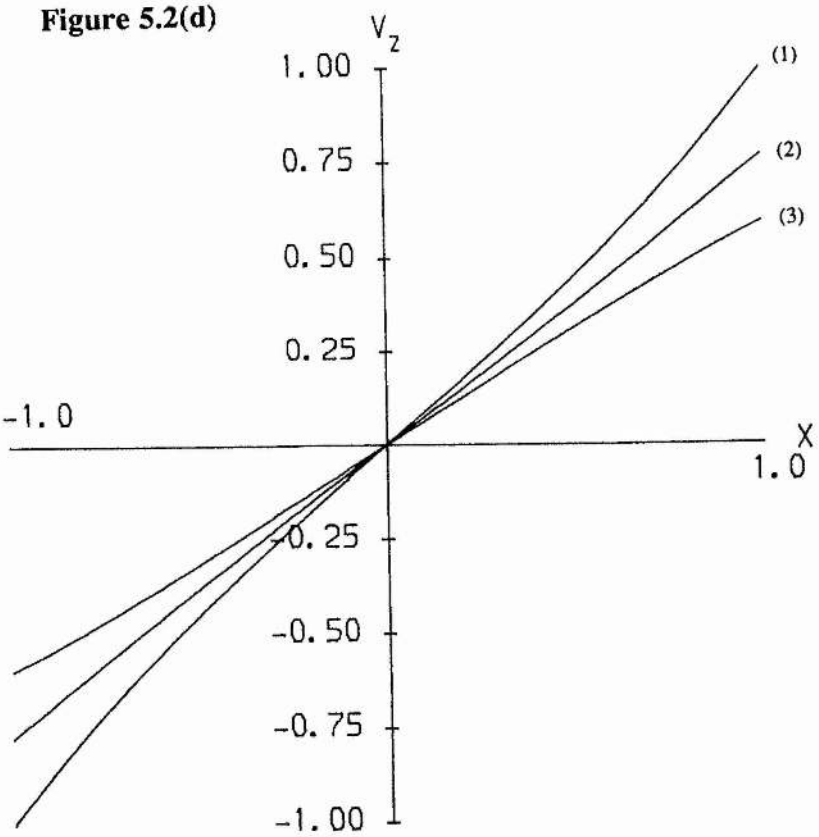

Figure 5.2(e)

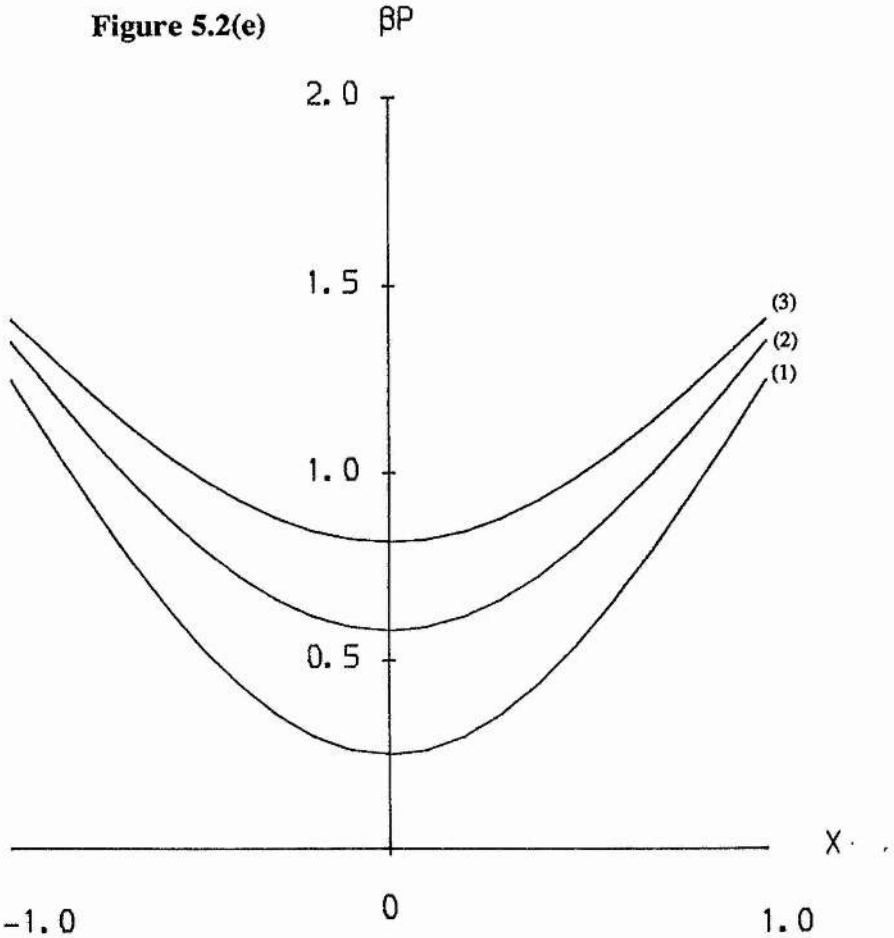

Figure 5.2(f)

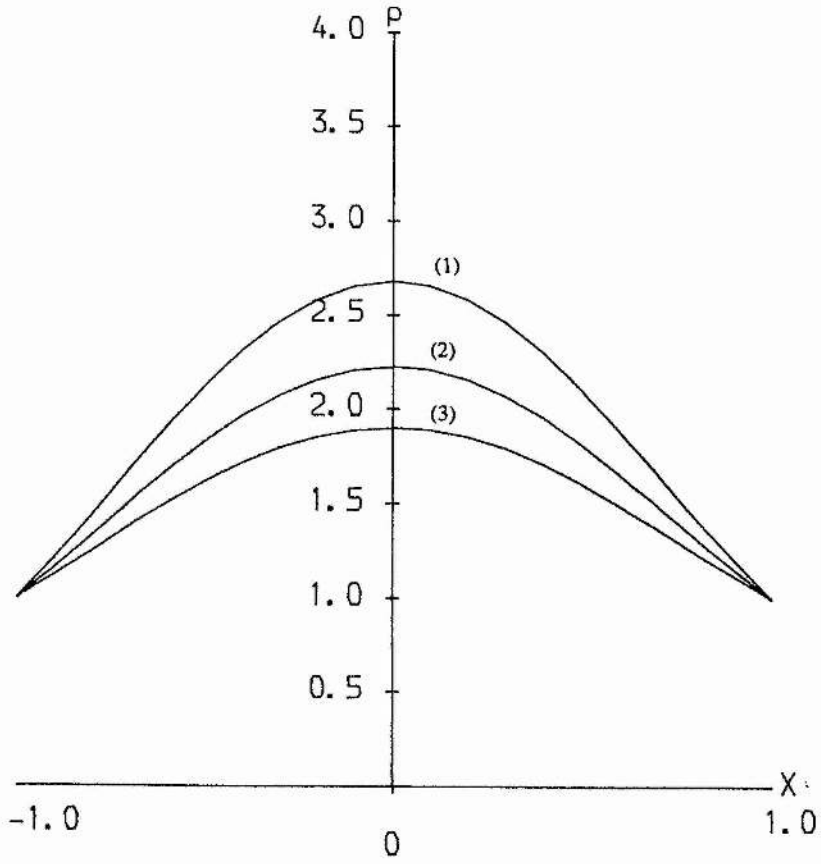

Figure 5.2(g)

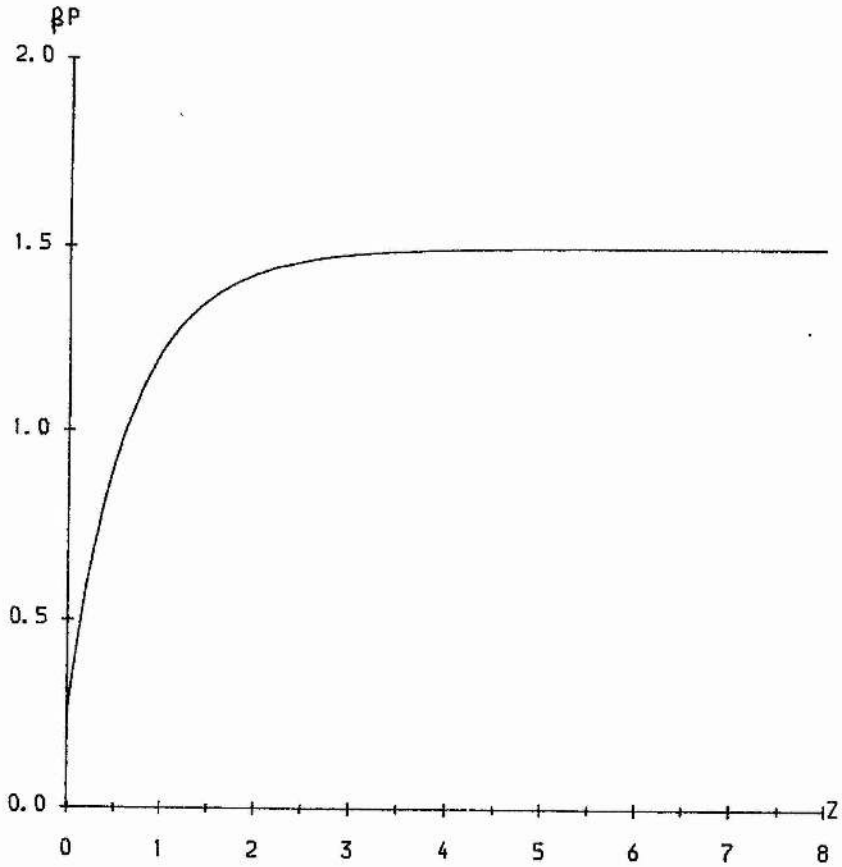

Figure 5.2(h)

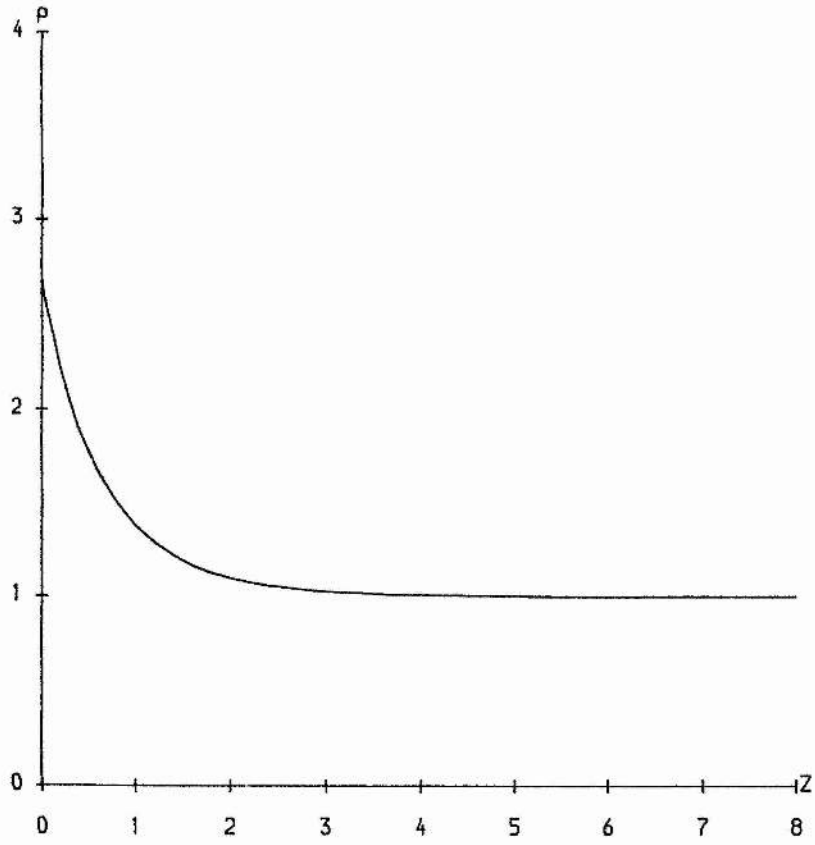

have maximum magnitudes at x=±1. Notice that the denominator in the solution for v_z straightens out the profile. As z increases, the curve changes from concave upward to concave downward, and it becomes more like B_z in shape. The plasma density has a maximum at x=0. Thus, as the plasma raises up the arcade (x>0), it experiences an expansion, but it is compressed as it moves back down the arcade (x<0). From Figure 5.2g and 5.2h we see that the plasma pressure increases to a constant value as z increases, while the plasma density decreases. This reveals a limitation of these solutions in that it is not possible for both pressure and density to decrease with increasing z for the same parameter set. This is due to our neglect of gravitational effects. Thus, our solutions may model arcades low in the corona, with arcade heights less than the coronal scale height.Gravity could easily be added as an extension of this work.

Now let us turn our attention to Figure 5.3, and the case when $v_m$and δp are chosen to be negative. The profiles of the components of the magnetic field B_x and B_z are essentially the same with the maxima and minima being reversed. Notice now that the plasma pressure deceases with z to a constant value, while the plasma density increases. The components of velocity v_x and v_z experience a change in their profiles. For small z, v_x becomes strongly peaked at x=0, while v_z has a maxima (minima) between x= -1,0 (x = 0,1). As z increases, the maxima (minima) move towards the edge of the arcade, and the profile is similar to that when v_m>0. Observe that v_z has sharp gradients about x=0, due to the fact that the denominator in the solutions for the velocity becomes small. In fact, we could choose v_m so that v_z and v_x have asymptotes, which leads to unphysical solutions. This cannot arise when v_m>0, which is the more physically realistic case.

5.5 Flows In Non-symmetric Arcades

Since the solutions in the previous section were symmetric about x=0, the plasma pressure at each footpoint of a fieldline is the same. Thus, such flows

Figure 5.3(a)

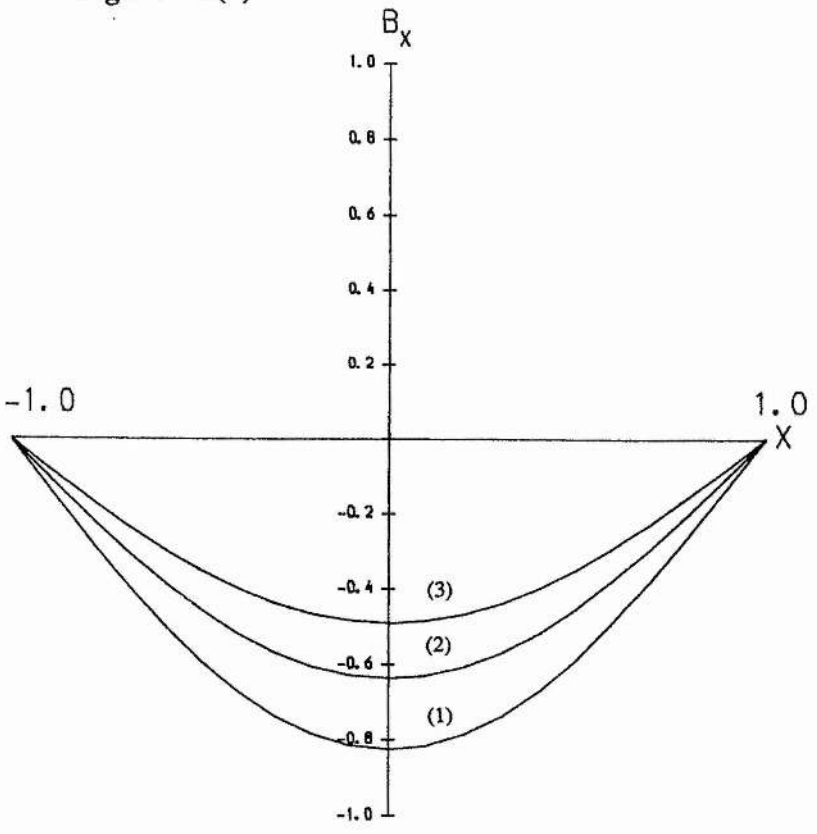

Figure 5.3 : The solutions similar to Figure 5.3 but with v_m=-1.0 and δp = -1.0.

Figure 5.3(b)

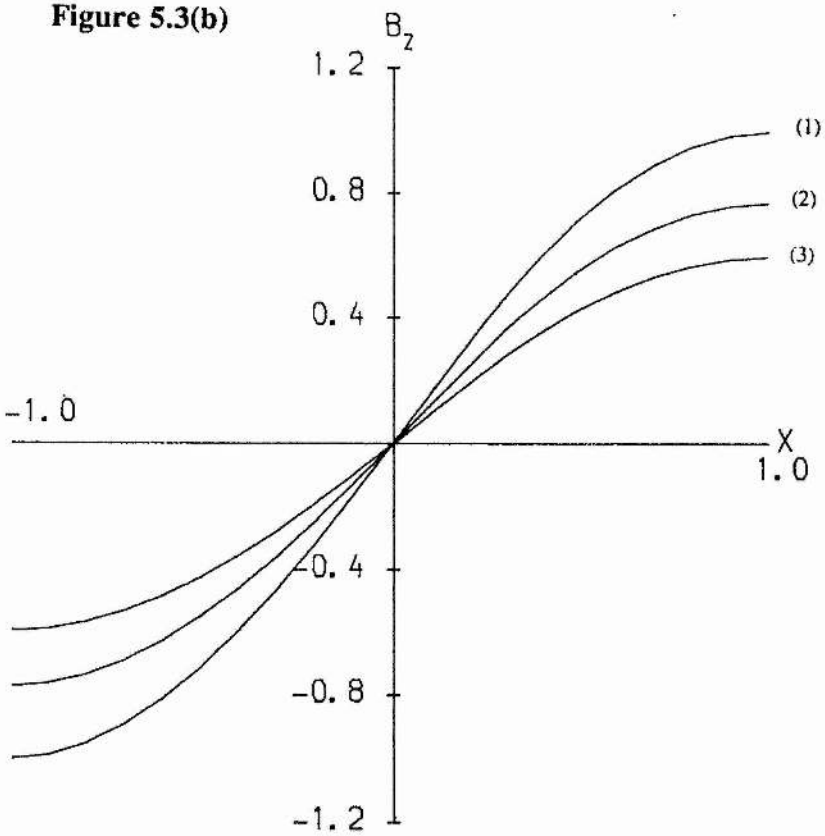

Figure 5.3(c)

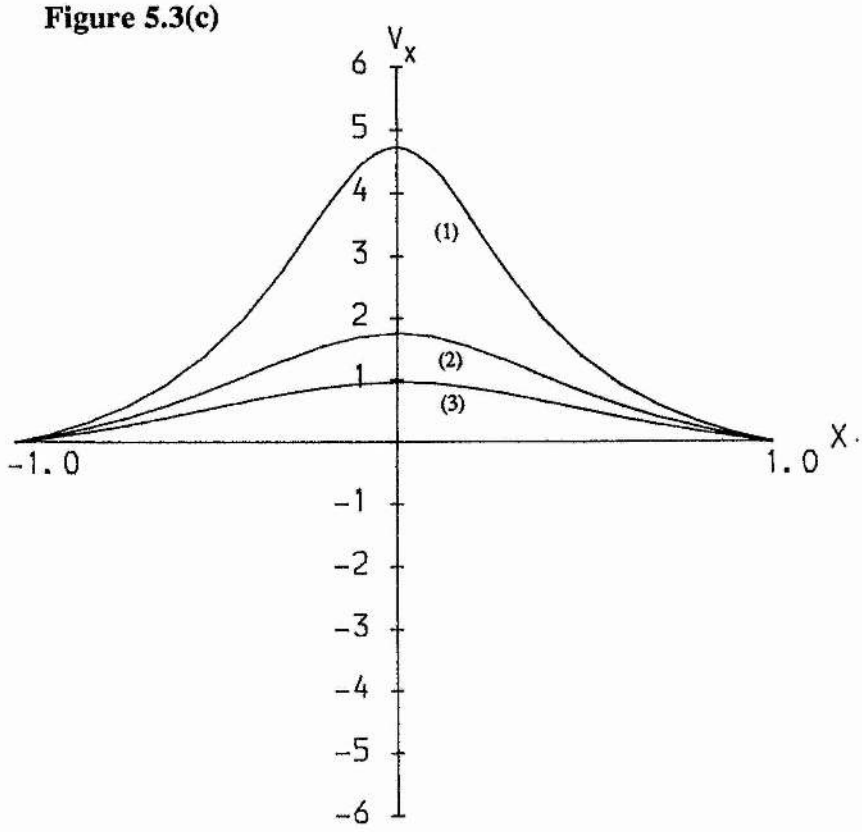

Figure 5.3(d)

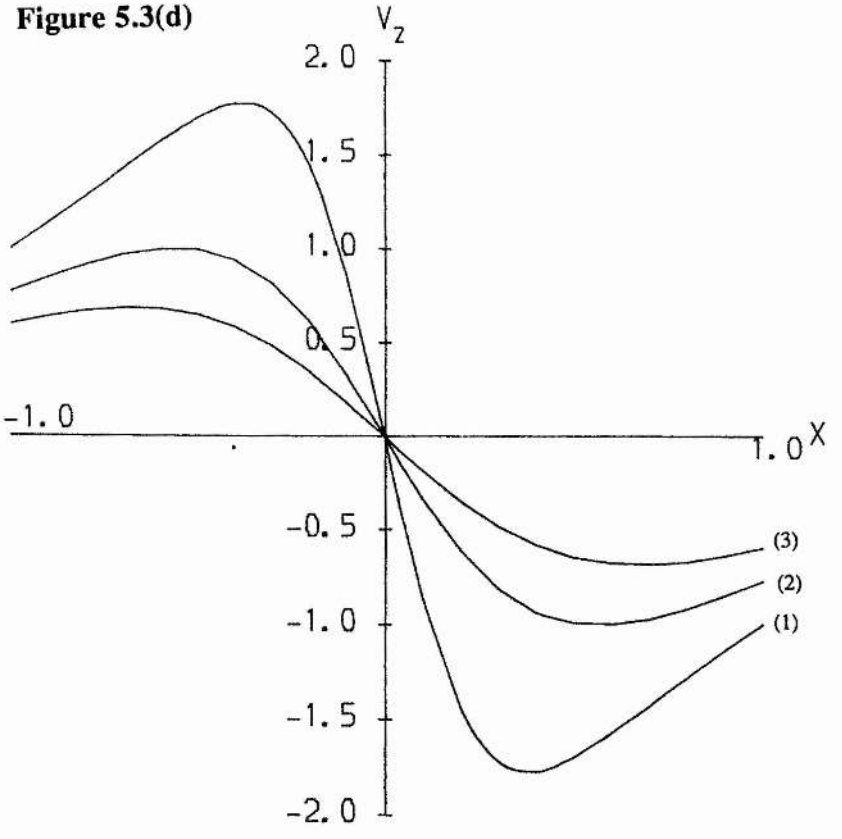

Figure 5.3(e)

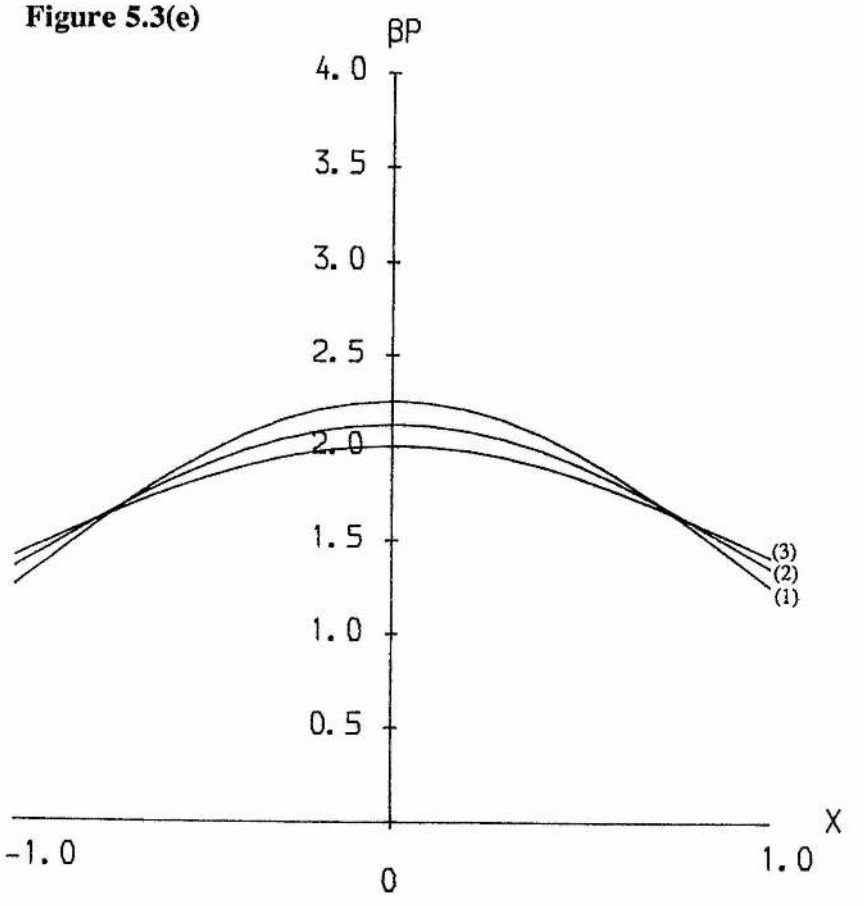

Figure 5.3(f)

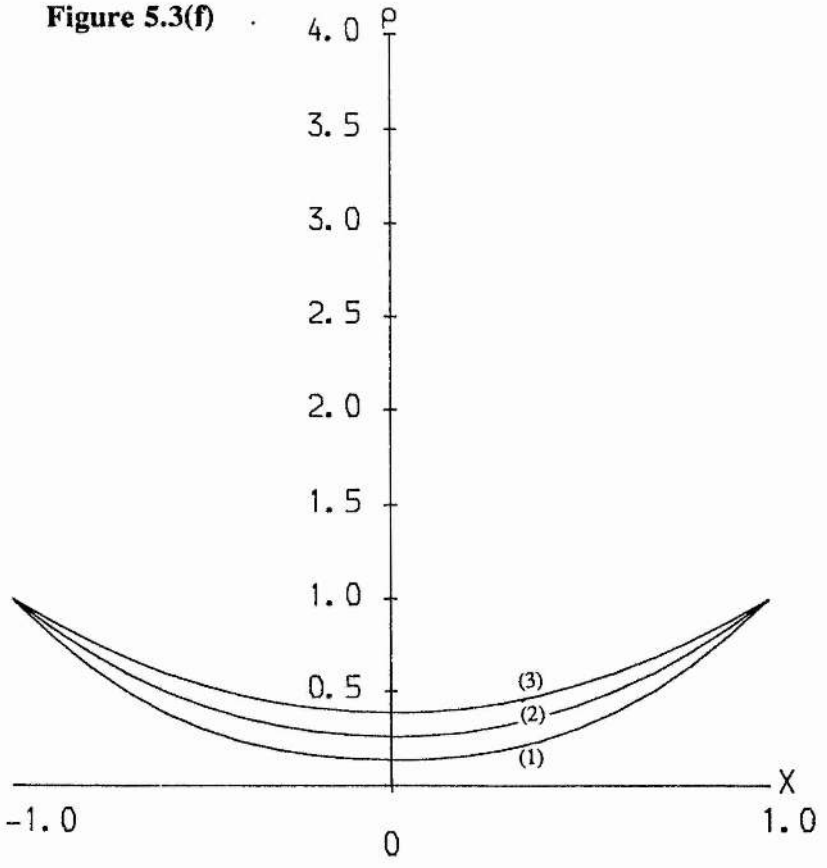

Figure 5.3(g)

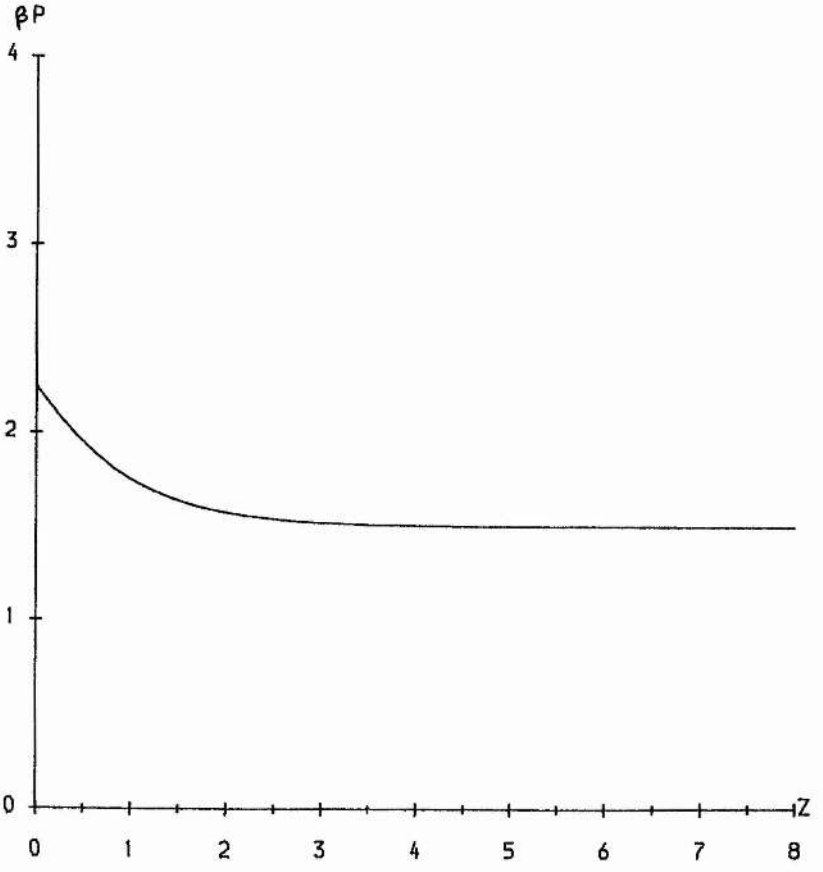

Figure 5.3(h)

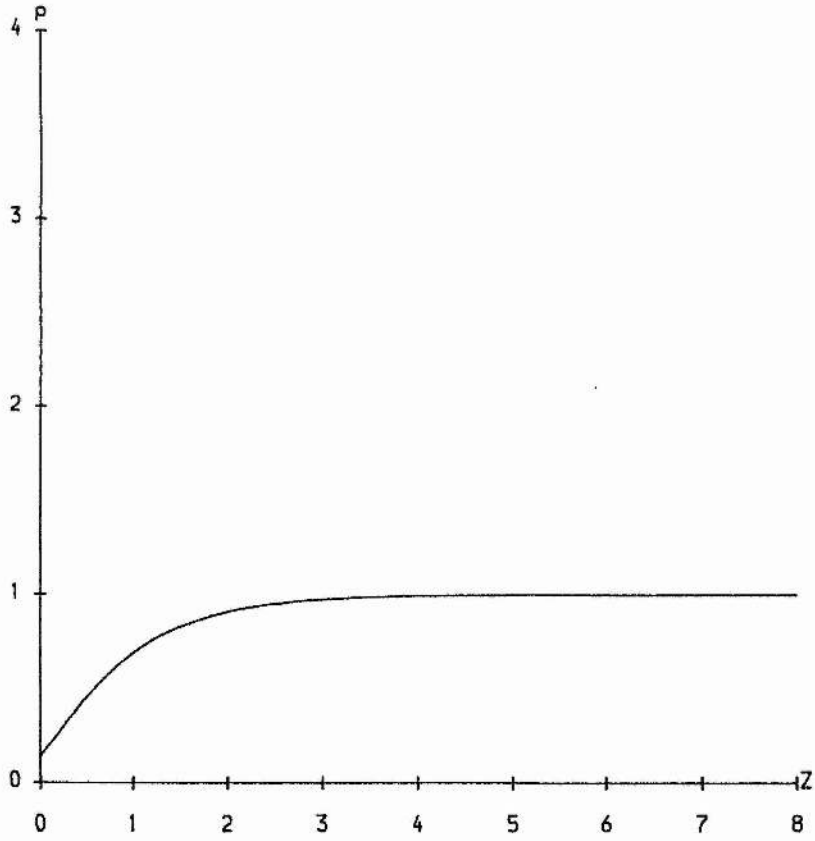

cannot be strictly termed 'siphon' flow, driven by footpoint plasma pressure differences. In this section we see how to construct a solution which allows plasma pressure differences between any two footpoints of a particular fieldline. For this we must introduce some asymmetry into the solution.

For example, observe that

$$A = [a_1\cos\sigma x+b_1\sin\sigma x]e^{-\nu z}+[a_2x+b_2]e^{-\alpha z}+\frac{\Pi}{\alpha^2} ,$$

is a solution to equation (5.27). The new term is the separable solution found by choosing the separation constant to be zero. The x-component B_x and z-component B_z of the magnetic field can be easily shown to be

$$B_x = -\nu[a_1\cos\sigma x+b_1\sin\sigma x]e^{-\nu z} - \alpha[a_2x+b_2]e^{-\alpha z} , \qquad (5.38a)$$

and

$$B_z = \sigma[a_1\sin\sigma x-b_1\cos\sigma x]e^{-\nu z} - a_2e^{-\alpha z} . \qquad (5.38b)$$

The components of the plasma velocity can be found in the same way as before and are given by

$$v_x = \frac{B_x}{A} , \qquad (5.38c)$$

and

$$v_z = \frac{B_z}{A} . \qquad (5.38d)$$

Also, the plasma density is

$$\rho = \left\{[a_1\cos\sigma x+b_1\sin\sigma x]e^{-\nu z}+[a_2x+b_2]e^{-\alpha z}+\frac{\Pi}{\alpha^2}\right\}^2 , \qquad (5.38e)$$

and the plasma pressure may be shown to be

$$\beta p = \left[2\Pi_1 - (2-M_a^2)\frac{\Pi_0^2}{\Omega_0^2}\right] + \left[\frac{2M_a^2\Pi_0}{1-M_a^2}\right][(a_1\cos\sigma x+b_1\sin\sigma x)e^{-\nu z}$$

$$+(a_2x+b_2)e^{-\alpha z}] - M_a^2\sigma^2(a_1^2+b_1^2)e^{-2\nu z} - M_a^2\alpha^2[2(a_2x+b_2)^2+a_2^2]e^{-2\alpha z}$$

$$-2M_a^2[\alpha(1+\nu)(a_2x+b_2)(a_1\cos\sigma x+b_1\sin\sigma x)-a_2\sigma(a_1\sin\sigma x-b_1\cos\sigma x)]e^{-(\nu+\alpha)z}. \qquad (5.38f)$$

To simplify the algebra we will consider the special case when $b_2=0$.

Firstly, we require

$$B_x(\pm1,z) = 0,$$

from which we deduce the system of equations

$$\begin{bmatrix} (a_1\cos\sigma - b_1\sin\sigma)\nu & -\alpha a_2 \\ (a_1\cos\sigma + b_1\sin\sigma)\nu & \alpha a_2 \end{bmatrix} \begin{bmatrix} e^{-\nu z} \\ e^{-\alpha z} \end{bmatrix} = \mathbf{0}. \tag{5.39}$$

The system (5.39) has non-trivial solutions when $\cos\sigma = 0$, that is $\sigma=\pi/2$ (in general $\sigma = (n-1/2)\pi$, but we will only deal with the fundamental mode n=1). Substituting back into equation (5.39) we deduce that

$$e^{-\nu z} = \frac{-\alpha a_2}{\nu b_1} e^{-\alpha z}. \tag{5.40}$$

Consider now the longitudinal component of magnetic field B_z, and impose the following boundary conditions:

$$B_z(-1,0) = B_1 \, , \; B_z(1,0) = B_z \, ,$$

from which we obtain

$$a_1 = -\frac{1}{\pi}(B_1+B_2) \, , \tag{5.41a}$$

and

$$a_2 = -\frac{1}{2}(B_1 - B_2) \, . \tag{5.41b}$$

Using equation (5.38d) and imposing

$$v_z(-1,0) = v_1 \, , \; v_z(1,0) = v_2$$

it may be shown that

$$\frac{\Pi}{\alpha^2} = \frac{1}{2}\left(\frac{B_1}{v_1} + \frac{B_2}{v_2}\right), \tag{5.42}$$

and

$$b_1 = \frac{1}{2}\left\{B_1\left(1 - \frac{1}{v_1}\right) + B_2\left(1 + \frac{1}{v_2}\right)\right\}. \tag{5.43}$$

Finally, from equation (5.38f) and imposing

$$p(-1,0) = p_1 \; ; \; p(1,0) = p_2,$$

we find that

$$\Pi_0 = \frac{(1-M_a^2)}{M_a^2}\left(\frac{B_1}{v_1} - \frac{B_2}{v_2}\right)^{-1} \left\{M_a^2\delta B - \beta\delta p\right\}$$

where

$$\delta B = B_1^2 - B_2^2 \, , \; \delta p = p_1 - p_2.$$

Also, we can simply show that

$$\alpha^2 = \frac{1}{M_a^2}\left\{\frac{M_a^2\delta B - \beta\delta p}{\delta m}\right\},$$

where

$$\delta m = \left(\frac{B_1^2}{v_1^2} - \frac{B_2^2}{v_2^2}\right),$$

and

$$\beta p_f = \left[2\Pi_1 - (2-M_a^2)\frac{\Pi_0^2}{\Omega_0^2}\right] = \frac{1}{2}\beta(p_0+p_1) + \frac{\pi^2}{16}M_a^2(B_1+B_2)^2$$

$$+3(B_1-B_2)^2\left\{\frac{M_a^2\delta B-\beta\delta p}{\delta m}\right\}+M_a^2(B_1+B_2)\left\{B_1(1+v_1^{-1}) + B_2(1+v_2^{-1})\right\}$$

$$+\left\{\frac{M_a^2\delta B-\beta\delta p}{\delta m}\right\}\left\{\frac{\pi^2}{4} - \left(\frac{M_a^2\delta B-\beta\delta p}{\delta m}\right)\right\}^{1/2}.$$

We can now rewrite the solutions in the more convenient form

$$A = a_2\left[x - \frac{\alpha k}{\nu}\sin\left(\frac{\pi x}{2}+\theta\right)\right]e^{-\alpha z} + \frac{\Pi}{\alpha^2},$$

$$B_x = \alpha a_2\left[k\sin\left(\frac{\pi x}{2}+\theta\right) - x\right]e^{-\alpha z},$$

$$B_z = a_2\left[\frac{\alpha\pi}{2\nu}k\cos\left(\frac{\pi x}{2}+\theta\right) - 1\right]e^{-\alpha z},$$

and

$$v_x = \frac{B_x}{A};\ v_z = \frac{B_z}{A};\ \rho = A^2,$$

$$\beta p = \beta p_f + (B_1+B_2)\left(\frac{B_1}{v_1} - \frac{B_2}{v_2}\right)^{-1}\left[x + \frac{\theta k}{\nu}\sin\left(\frac{\pi x}{2}+\theta\right)\right]e^{-\alpha z}$$

$$+\frac{1}{2}M_a^2(B_1+B_2)^2\left\{\frac{1}{4}\frac{\alpha^2}{\nu^2}(1-k^2) - \frac{\alpha^4}{\nu^2 b_1^2}(B_1+B_2)(2x+1)\right\}e^{-2\alpha z}$$

$$+\frac{1}{2}M_a^2(B_1+B_2)^2\left\{2\alpha k x\sin\left(\frac{\pi x}{2}+\theta\right)+\frac{\pi\alpha k}{\nu}\cos\left(\frac{\pi x}{2}+\theta\right)\right\}e^{-2\alpha z},$$

where

$$k = \left(1+\frac{a_1^2}{b_1^2}\right)^{1/2};\ \tan\theta = \frac{a_1}{b_1}.$$

For these to exist, it is clear that we require $\alpha^2>0$, and $\nu^2>0$, for which the following inequalities must hold,

$$\frac{M_a^2\delta B - \beta\delta p}{\delta m} > 0, \qquad (5.44)$$

and

$$\frac{4M_a^2}{\pi^2} > \frac{M_a^2\delta B - \beta\delta p}{\delta m}. \qquad (5.45)$$

Combining (5.44) and (5.45) we must have

$$0 < \frac{M_a^2\delta B - \beta\delta p}{\delta m} < \frac{4M_a^2}{\pi^2}. \qquad (5.46)$$

For $\delta m > 0$ (i.e., $B_1^2/B_2^2 < v_1^2/v_2^2$) inequality (5.46) may rearranged to give

$$\frac{\beta\delta p}{M_a^2} < \delta B < \frac{4\delta m}{\pi^2}\frac{\beta\delta p}{M_a^2}. \qquad (5.47)$$

For $\delta m < 0$ (i.e., $B_1^2/B_2^2 < v_1^2/v_2^2$) the inequality becomes

$$\frac{4\delta m}{\pi^2}\frac{\beta\delta p}{M_a^2} < \delta B < \frac{\beta\delta p}{M_a^2}. \qquad (5.48)$$

Before discussing more fully the consequences of inequalities (5.47) and (5.48), we note that the magnetic topology of the solutions (always choosing $B_1$and B_2 with opposite signs) is a non-symmetric magnetic arcade (Figure 5.4) with plasma flow along the fieldlines. Note that the summit of the arcade need not be at x=0. In fact the position of the arcade summit x^* is given by

$$x^* = \frac{2}{\pi}\left\{\cos^{-1}\left(\frac{2}{\alpha\pi k}\right) - \tan^{-1}\left(\frac{a_1}{b_1}\right)\right\},$$

and thus depends upon the boundary conditions imposed at the base (z=0).

The solutions corresponding to the arcade in Figure (5.4) are plotted for various z in Figure (5.5). In this case plasma flows along the arcade from left to right and experiences a net compression. The transverse component of magnetic field B_{1x} is no longer symmetric about x=0, which is also the case with v_x. The longitudinal components of magnetic field and velocity now have quite different profiles compared with the symmetric case. Both have stationnary points which no longer, in general, have the value of x being ±1, with this effect most marked for small z. There is also a curious difference between v_z and B_z for x<0. Starting at x=-1 and moving towards x=0, we note that $\partial v_z/\partial x$ decreases, while $\partial B_z/\partial x$ increases. This is due to the non-unity denominator in the velocity components. The density profile exhibits a maximum at the summit of the arcade in this case,

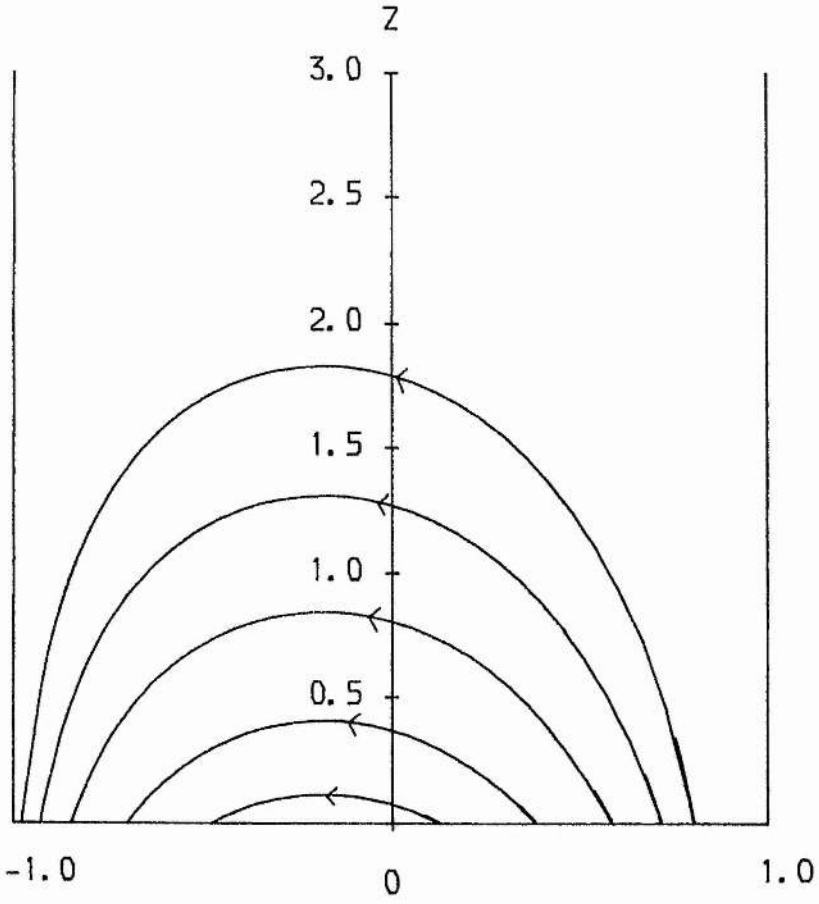

Figure 5.4: Magnetic fieldlines for a non-symmetric arcade with M_a =0.5 β=0.5, B_1=-2.0, B_2= 1.0, v_1 =-1.5, v_2=1.0,p_1=2.0, p_2=1.0.

Figure 5.5(a)

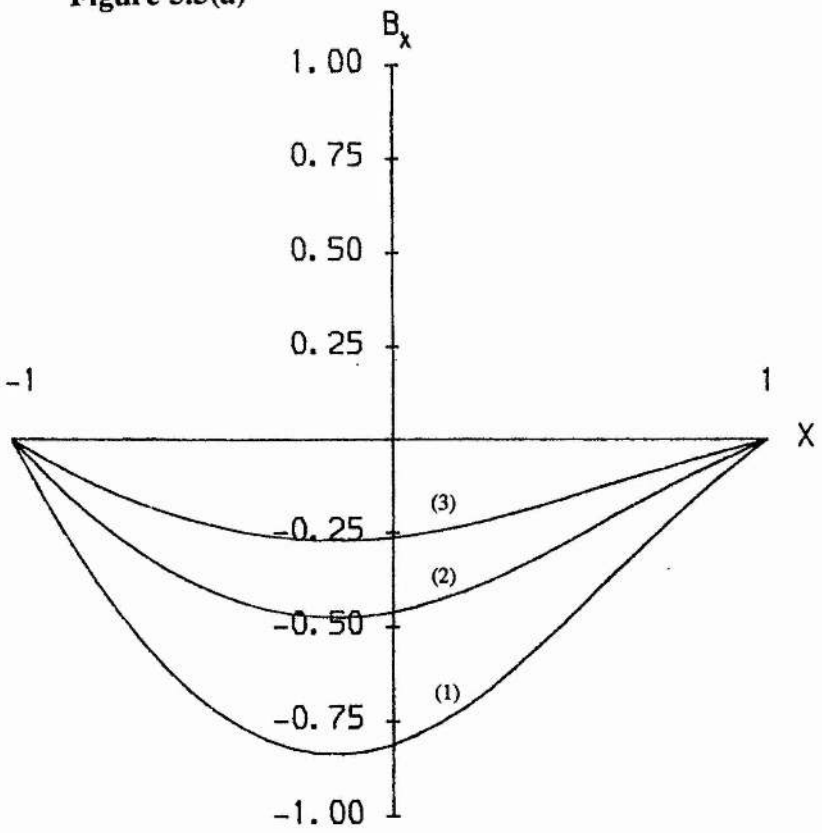

Figure 5.5: The variation with x of the fundamental mode solutions for the non-symmetric arcade in Figure 5.4 of (a) B_x, (b) B_z, (c) v_x, (d) v_z, (e) ρ, (f) βp, when z takes the values (1) 0.0, (2) 0.5 and (3) 1.0 .

Figure 5.5(b)

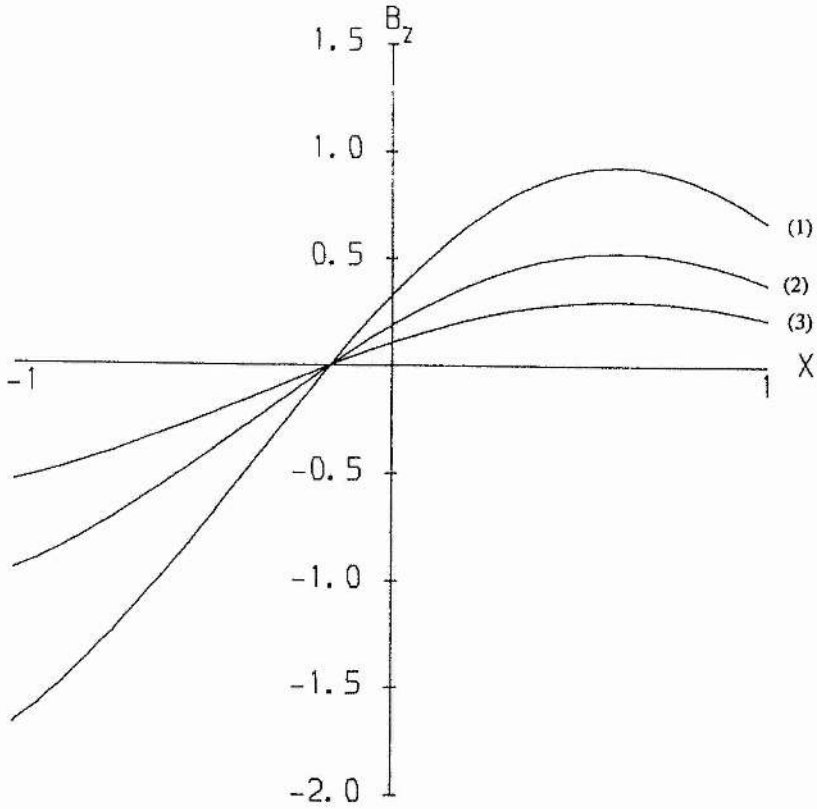

Figure 5.5(c)

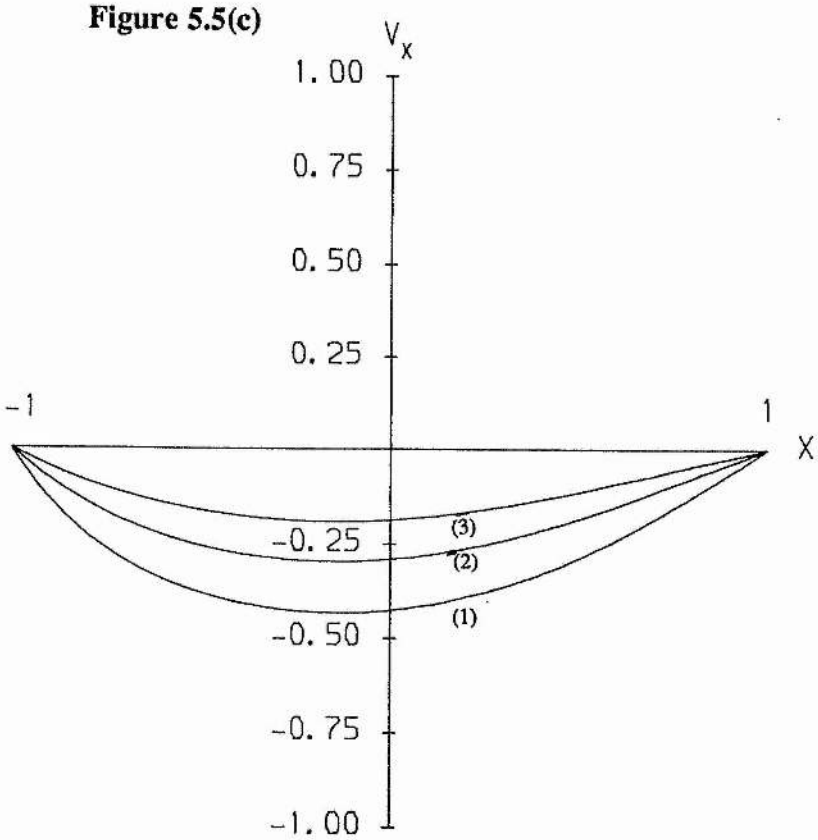

Figure 5.5(d)

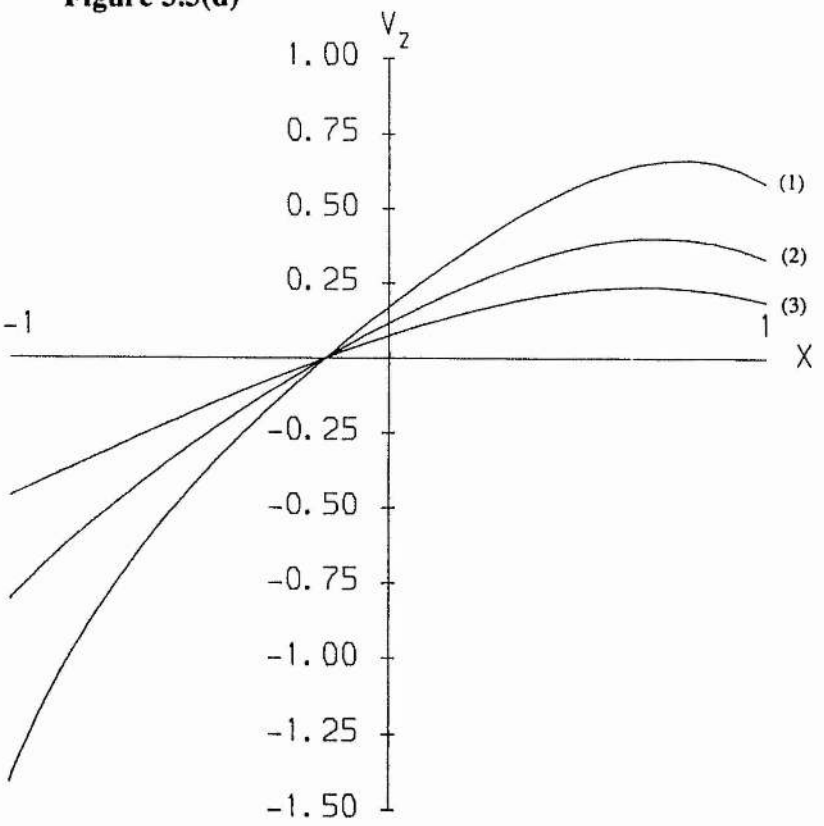

Figure 5.5(e)

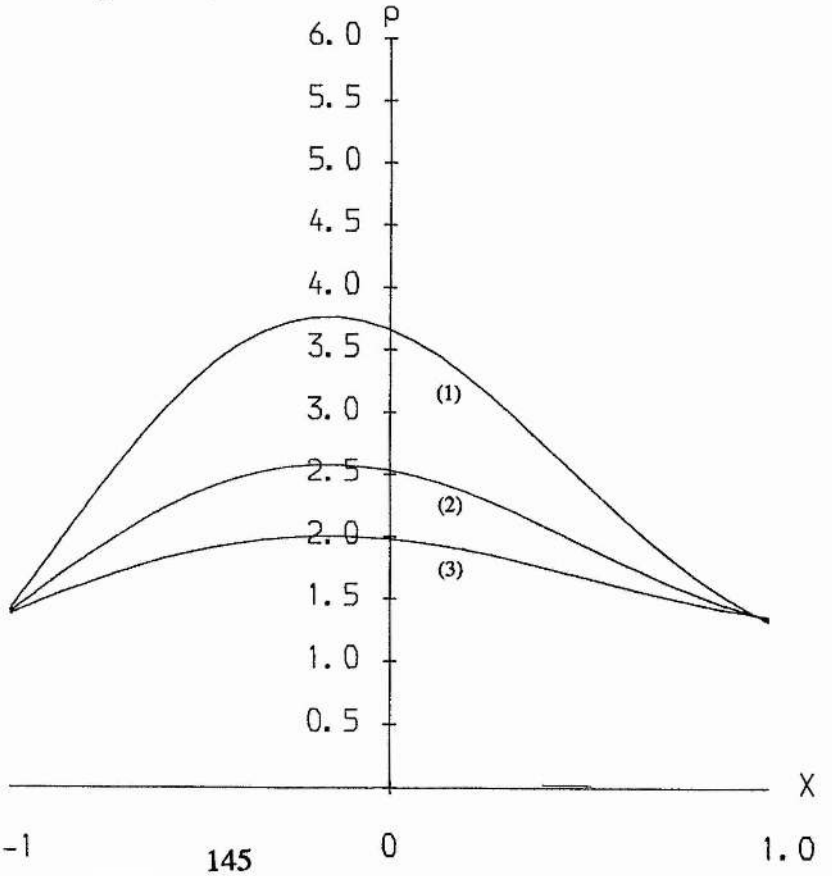

Figure 5.5(f)

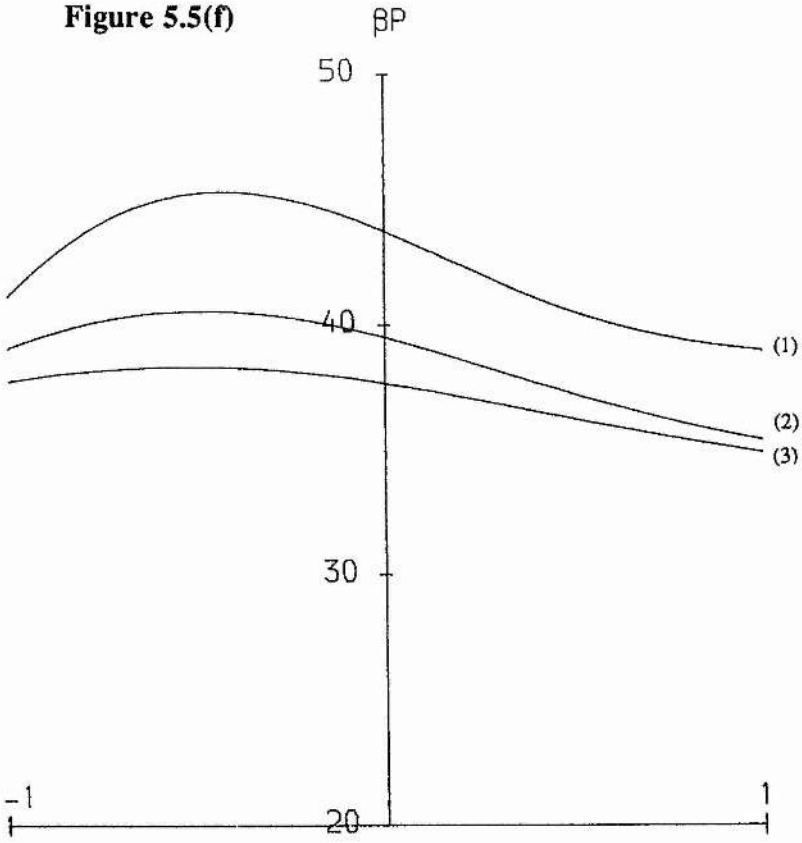

with the value of the maximum decreasing with increasing z. These solutions now permit both density ρ and the plasma pressure p to decrease with increasing z.

Setting $\delta B=0$, we see that the solutions reduce back to the symmetric arcade case. Putting $\delta p = 0$, but keeping $\delta B\neq 0$, it is still possible to have a non-symmetric arcade. Similarly, with $v_1=-v_2$, but $\delta B\neq 0$, it is again possible to find non-symmetric solutions. Thus, the critical parameter is δB, with $\delta B=0$ corresponding to the symmetric arcades and $\delta B\neq 0$ corresponding to the non-symmetric case. Suppose we consider two neighbouring fieldlines, then we may think of them as forming a tube whose cross-section at either end is different providing $\delta B\neq 0$.

5.5.1 Classification Of Solutions

We would now like a way of classifying the solutions which reflects the change in the properties of the flow between when the plasma enters the arcade (at x=-1, say) and when it leaves the arcade. To do this, consider the case in which plasma emerges from the base at z=0 at x=-1, and travels along the arcade to z=0, x=1. We say that the flow is **compressive** if the plasma experiences a net increase in plasma pressure between the two ends of the arcades, an **expansion** otherwise. When the net change in the magnetic field strength between the footpoints is in phase with the change in plasma pressure, we say that the flow is a **fast-mode**, otherwise **slow-mode.** When the plasma leaves the arcade with a greater speed than it enters, we say that the flow is **accelerated**, otherwise **decelerated.** It is to be stressed that we are classifying the solutions according to the 'net' change in behaviour of the plasma between the points x=-1 and x=1. The behaviour along a fieldline may be complex, with the plasma experiencing several compressions and expansions in its journey through the arcade.

Consider the case $v_1>0, v_2<0$ for which the plasma flows from left to right along the magnetic arcade. Returning to inequality (5.47), we note that if $\delta p>0$ then $\delta B<0$. Set $k=B_1^2/B_2^2$ and $k^*=v_1^2/v_2^2$. In the case $k>1$, and since $\delta m>0$,

Table 1 : Classification of solutions for $\delta m > 0$ where $k = (B_1/B_2)^2$, $k^* = (v_1/v_2)^2$ and we use the shorthand : fast mode compression - (FC), fast mode expansion (FE), slow mode compression - (SC), slow mode expansion - (SE), accelerated flow - ($\mathcal{A}$), decelerated flow - ($\mathcal{D}$).

δp	δB	$0 < k^* < 1$		$1 < k^* < k$		$k^* < k < 1$	
		$v_1 > 0$ $v_2 < 0$	$v_1 < 0$ $v_2 > 0$	$v_1 > 0$ $v_2 < 0$	$v_1 < 0$ $v_2 > 0$	$v_1 > 0$ $v_2 < 0$	$v_1 < 0$ $v_2 > 0$
$\delta p > 0$	$\delta B > 0$	FE$\mathcal{A}$	FC$\mathcal{D}$	FE$\mathcal{D}$	FC$\mathcal{A}$	-	-
$\delta p > 0$ and $\frac{4\delta m}{\pi^2} < \left\lvert\frac{\beta\delta p}{M_A^2}\right\rvert$	$\delta B < 0$	-	-	-	-	FC$\mathcal{A}$	FE$\mathcal{D}$
$\frac{4\delta m}{\pi^2} > \frac{\beta\delta p}{M_A^2} > 0$	$\delta B < 0$	-	-	-	-	FC$\mathcal{A}$	FE$\mathcal{D}$
$\frac{4\delta m}{\pi^2} > \frac{\beta\delta p}{M_A^2} > 0$	$\delta B > 0$	SC$\mathcal{A}$	SE$\mathcal{D}$	SC$\mathcal{D}$	SE$\mathcal{A}$		

Table 2 : Classification of solutions for $\delta m < 0$ (using the same shorthand as in Table 1)

δp	δB	$k < k^* < 1$		$1 < k^*$	
		$v_1 > 0$ $v_2 < 0$	$v_1 < 0$ $v_2 > 0$	$v_1 > 0$ $v_2 < 0$	$v_1 < 0$ $v_2 > 0$
$\delta p > 0$	$\delta B < 0$	FCλ	FEλ	FCλ	FEλ
$\frac{\beta\delta p}{M_A^2} > \left\|\frac{4\delta m}{\pi^2}\right\| > 0$	$\delta B > 0$			FEλ	FCλ
$\left\|\frac{4\delta m}{\pi^2}\right\| > \frac{\beta\delta p}{M_A^2} > 0$	$\delta B > 0$			FEλ	FCλ
$\left\|\frac{4\delta m}{\pi^2}\right\| > \frac{\beta\delta p}{M_A^2} > 0$	$\delta B < 0$	SEλ	SCλ	SEλ	SCλ

$k>k^*$. Two cases of interest arise, namely $0<k^*<1$ and $1<k^*<k$. For the former, the flow is a **fast expansive accelerated** flow, and in the latter, a **fast expansive decelerated** flow. The case when $0<k^*<1$ corresponds to a siphon flow, but now along an arcade of magnetic fieldlines.

When $\delta p>0$, two cases must be considered, namely;

(A) $\frac{4\delta m}{\pi^2} < \frac{\beta\delta p}{M_a^2}$,

(B) $\frac{4\delta m}{\pi^2} > \frac{\beta\delta p}{M_a^2}$.

For (A) we have $\delta B<0$ and so $k<1$ and $k^*<k<1$. Thus the flow is a **fast compressive accelerated** flow. For (B) we may have $\delta B<0$ or $\delta B>0$, depending on the particular choice of B_1 and B_2. When $\delta B<0$, then $k^*<k<1$, and the flow is a **fast compressive accelerated** flow. For $\delta B>0$, we either have $0<k^*<1$ or $1<k^*<k$. The former gives a **slow compressive accelerated** flow, the latter a **slow compressive decelerated** flow.

The flows with $v_1<0, v_2>0$ may be treated in a similar way, the classification being summarised in Table 5.1. Likewise, we may classify the solutions when inequality (5.48) holds, and these are summarised in Table 5.2. The point we wish to note in this discussion is that the nature of the plasma flow can alter significantly by passing along the arcade. The precise nature of these changes in behaviour depends upon the particular properties of the magnetic arcade.

5.6 Conclusions

In this chapter we have shown how the MHD equations may be reduced to a single equation, so that exact solutions may be found. A class of exact solutions is presented, which may model subsonic flows in magnetic arcades. Two cases arise, namely, symmetric and non-symmetric arcades. In the former the basic result is that the presence of a flow increases the summit height of the arcade compared with the static case. For the latter case, we saw that we can produce solutions which may, as a special case, model siphon flow in a magnetic arcade.

We also saw that the behaviour of the plasma can alter significantly as a result of flowing along the arcade, in a way that depends upon the particular characteristics of the arcade. We have provided a classification of the various types of flow.

These solutions provide the basis for developing more realistic analytical models for flows in arcades, such as one might find in the solar atmosphere. In the future the incompressible assumption could be relaxed, allowing supersonic flow, and gravitational effects could be included.

Chapter 6 : Flows In Closed And Partially Open Magnetic Structures.

6.1 Introduction

As noted in chapter one, the magnetic field in the solar atmosphere can be classified as being either 'closed' or 'open'. In the former category we have coronal loops and arcades, in the latter, coronal holes and plumes. Some structures are observed to have elements of both categories. The classic example is a helmet streamer, with a closed field region forming an arcade at the base, and an overlying magnetic field. In principle one may model this by finding a solution for the open and closed regions separately, and then match them at a free surface separating the regions. Usually a numerical treatment is needed (Pneumann and Kopp, 1970). In this chapter we derive a class of exact solutions following the method of the previous chapter, which models closed, open and partially open magnetic fields. The closed magnetic field configuration may model the field one might expect above a sunspot with steady flows along the fieldlines. For the open fields, these solutions may model plumes or coronal holes. In certain parameter regimes the solutions give a closed region of fieldlines, with an open overlying field, again with plasma flowing along the fieldlines. These solutions may provide simple models for coronal streamers, for flows in X-ray bright points and their overlying coronal plumes or for the structure at a coronal hole boundary.

$$\left(1 - \frac{M_a^2\Psi_A^2}{\rho}\right)\Delta A - \frac{1}{2}\frac{M_a^2}{r^2}\left[\left(\frac{\partial A}{\partial r}\right)^2 + \left(\frac{\partial A}{\partial z}\right)^2\right]\frac{d}{dA}\left(\frac{\Psi_A^2}{\rho}\right)$$

$$+\frac{r^2}{2}\frac{d}{dA}\left(\frac{M_a^2\rho\Phi_A^2}{1 - \frac{M_a^2\Psi_A^2}{\rho}}\right) + \frac{1}{2r^2}\frac{d}{dA}\left(\frac{\Omega^2}{1 - \frac{M_a^2\Psi_A^2}{\rho}}\right) + \frac{d\Pi}{dA} = 0, \qquad (6.1)$$

where

$$\Delta A = \frac{1}{r}\left[\frac{\partial}{\partial r}\left(\frac{1}{r}\frac{\partial A}{\partial r}\right) + \frac{1}{r}\frac{\partial^2 A}{\partial z^2}\right],$$

and we have neglected the effect of gravity (H=0).

To proceed we choice the arbitrary functions of A to be

$$\Psi = \frac{1}{2}A^2 + kA\,,$$

$$\rho = (A+k)^2,$$

$$\Omega = \Omega_0 A\,, \qquad (6.2)$$

$$\Pi = -\Pi_0 A + \Pi_1,$$

$$\Phi = \Phi_0,$$

where $k, \Omega_0, \Pi_0, \Pi_1$ and Φ_0 are constants. This is similar to the choice in chapter five except for the inclusion of a constant k, to ensure that the density is never zero.

With this choice of the arbitary functions of A, equation (6.1) reduces to

$$\frac{1}{r}\frac{\partial}{\partial r}\left(\frac{1}{r}\frac{\partial A}{\partial r}\right) + \frac{1}{r^2}\frac{\partial^2 A}{\partial z^2} + \frac{\alpha^2}{r^2}A = \Pi_2\,, \qquad (6.3)$$

where

$$\alpha^2 = \frac{\Omega_0^2}{(1-M_a^2)^2}\ ;\ \Pi_2 = \frac{\Pi_0}{(1-M_a^2)}\ .$$

In addition, it is useful to note that for the prescription (6.2),

$$v_r = \frac{B_r}{A+k}\ ;\ v_z = \frac{B_z}{A+k}\,, \qquad (6.4)$$

and

$$\rho|v|^2 = \frac{1}{r^2}\left[B_r^2 + B_z^2 + \alpha^2 A^2\right]. \qquad (6.5)$$

In the next section we find separable solutions to equation (6.3).

6.2: Separable Solutions

Turning our attention to equation (6.3) we note that a particular integral is

$$A_p = \frac{\Pi_2}{\alpha^2} r^2. \tag{6.6}$$

For the homogeneous version of equation (6.3) we look for solutions of the form

$$A = R(r)Z(z),$$

and so obtain the ordinary differential equations

$$Z'' - \nu^2 Z = 0, \tag{6.7}$$

and

$$U^2W''(U) + UW'(U) + (U^2-1)W(U) = 0, \tag{6.8}$$

where

$$R = (\alpha^2 + \nu^2)^{-1/2}\, UW((\alpha^2 + \nu^2)^{-1/2}U), \tag{6.9}$$

with $U = (\alpha^2 + \nu^2)^{1/2}r$ and $\nu^2$is a separation constant.

The solution of equation (6.8) is a Bessel function of first order. Subject to the conditions $B_r \to 0$ as $z \to \infty$, and $B_r = 0$ at $r = 0$ and $r = 1$, the corresponding solution to equation (6.3) is

$$A = -\sum_{n=1}^{\infty} \frac{a_n}{\mu_{1,n}} rJ_1(\mu_{1,n}\, r)e^{-\nu z} + \frac{\Pi_2}{\alpha^2} r^2, \tag{6.10}$$

where $\mu_{1,n}$ is the n'th zero of the Bessel function J_1 and

$$\nu^2 = \mu_{1,n}^2 - \alpha^2.$$

For equation (6.10) to be valid we require that $\alpha^2 > 0$ and $\nu^2 > 0$, and thus we must have $\mu_{1,n}^2 > \alpha^2$. From equations (6.7) the r- and z-components of the components of the magnetic field may then be shown to be

$$B_r = \sum_{n=0}^{\infty} \frac{a_n}{\mu_{1,n}} \nu J_1(\mu_{1,n} r) e^{-\nu z}, \tag{6.11}$$

and

$$B_z = \sum_{n=1}^{\infty} a_n J_0(\mu_{1,n} r) e^{-\nu z} - \frac{2\Pi_2}{\alpha^2}. \tag{6.12}$$

By imposing $B_z = f(r)$ along $z = 0$, and using the orthogonality property of Bessel functions, an expression for the coefficients of the series a_n may be found.

Note that in the limit $z \to \infty$, $B_z \to \Pi_2/\alpha^2$, which will give open fieldlines for $\Pi_2 \neq 0$. This is more general than was possible for a similar analysis in a cartesian geometry (chapter five).

In the interests of simplicity, the remainder of our discussion will centre on the fundamental mode of the solutions (6.10)-(6.12), namely

$$A = -\frac{a_1}{\mu_1} r J_1(\mu_1 r) e^{-\nu z} + \frac{\Pi_2}{\alpha^2} r^2, \tag{6.13}$$

$$B_r = \frac{a_1}{\mu_1} \nu J_1(\mu_1 r) e^{-\nu z}, \tag{6.14}$$

$$B_z = a_1 J_0(\mu_1 r) e^{-\nu z} - \frac{2\Pi_2}{\alpha^2}, \tag{6.15}$$

where $\mu_1 \equiv \mu_{1,1}$. From equations (6.4), the r- and z-components of the plasma velocity are

$$v_r = \frac{a_1}{\mu_1} \nu J_1(\mu_1 r) e^{-\nu z} \Big/ \left\{ - \frac{a_1}{\mu_1} r J_1(\mu_1 r) e^{-\nu z} + \frac{\Pi_2}{\alpha^2} r^2 + k \right\}, \tag{6.16}$$

and

$$v_z = \left\{ a_1 J_0(\mu_1 r) e^{-\nu z} - \frac{2\Pi_2}{\alpha^2} \right\} \Big/ \left\{ - \frac{a_1}{\mu_1} r J_1(\mu_1 r) e^{-\nu z} + \frac{\Pi_2}{\alpha^2} r^2 + k \right\}. \tag{6.17}$$

From equations (5.13) and (5.14) the angular components of the magnetic field and velocity may be determined to be

$$B_\theta = - \alpha \left\{ \frac{a_1}{\mu_1} J_1(\mu_1 r) e^{-\nu z} - \frac{\Pi_2}{\alpha^2} r \right\}, \tag{6.18}$$

and

$$v_\theta = \alpha \left\{ - \frac{a_1}{\mu_1} J_1(\mu_1 r) e^{-\nu z} + \frac{\Pi_2}{\alpha^2} r \right\} \Big/ \left\{ - \frac{a_1}{\mu_1} r J_1(\mu_1 r) e^{-\nu z} + \frac{\Pi_2}{\alpha^2} r^2 + k \right\}. \tag{6.19}$$

Finally, the plasma density ρ is given by

$$\rho = \left\{ - \frac{a_1}{\mu_1} r J_1(\mu_1 r) e^{-\nu z} + \frac{\Pi_2}{\alpha^2} r^2 + k \right\}^2, \tag{6.20}$$

and, by using equations (5.17) and (6.5), the plasma pressure is

$$\beta\rho = 2 \left[\Pi_1 - 2(1 - M_a^2)^2 M_a^2 \frac{\Pi_0^2}{\Omega_0^4} \right] - \frac{\Pi_0^2}{\Omega_0^2} (2 - M_a^2) r^2$$

$$+ 2\Pi_0 a_1 \left[\frac{r J_1(\mu_1 r)}{\mu_1 (1 - M_a^2)} + \frac{2 M_a^2 (1 - M_a^2)}{\Omega_0^2} J_0(\mu_1 r) \right] e^{-\nu z}$$

$$- M_a^2 a_1^2 \left\{ \left(1 - \frac{\alpha^2}{\mu_1^2} \right) J_1^2(\mu_1 r) + \left(1 + \frac{\alpha^2}{\mu^2} \right) J_0^2(\mu_1 r) \right\} e^{-2vz}. \qquad (6.21)$$

The magnetic topology of these solutions depends upon the constant Π_2. For $\Pi_2 \equiv 0$, the field lines are closed and may model, for example, the magnetic field structure above a sunspot. When $\Pi_2 \neq 0$, we would have the possibility of open field lines which will be treated in section 6.5

6.3 Closed Magnetic Structures ($\Pi_2 = 0$)

We consider the cylindrical region $z \geq 0$, $0 \leq r \leq 1$, $0 \leq \theta < 2\pi$, and impose the following conditions

$$v_z(0,0) = v_0, \qquad (6.22)$$

$$B_\theta \left(\frac{\mu_0}{\mu_1}, 0 \right) = B_{\theta 1}, \qquad (6.23)$$

$$p(0,0) = p_0, \qquad (6.24)$$

$$p(1,0) = p_1, \qquad (6.25)$$

where $r = \mu_0/\mu_1$ is the value of r at the summit of the arcade, and μ_0 is the first zero of the Bessel function J_0. $B_{\theta 1}$is the value of $B_\theta$the value of r corresponding to the maximum of B_r.

Conditions (6.24) and (6.25) lead immediately to the relations

$$\beta(p_0 - p_1) = - M_a^2 a_1^2 (1 - J_0^2(\mu_1)) \left(1 + \frac{\alpha^2}{\mu_1^2} \right), \qquad (6.26)$$

and

$$\beta(p_0 + p_1) = 2(2\Pi_1) - M_a^2 a_1^2 \left(1 + \frac{\alpha^2}{\mu_1^2}\right)(1 + J_0^2(\mu_1)). \tag{6.27}$$

From equations (6.22) and (6.23) we deduce that

$$k = \frac{a_1}{V_0}, \tag{6.28}$$

$$\alpha = -\frac{\mu_1 B_{\theta 1}}{a_1 J_1(\mu_0)}, \tag{6.29}$$

respectively. Substituting (6.29) into equation (6.26) we obtain

$$a_1^2 = \frac{\beta(p_1 - p_0)}{M_a^2(1 - J_0^2(\mu_1))} - \frac{B_{\theta 1}^2}{J_1^2(\mu_0)}, \tag{6.30}$$

and so, since a_1 is real, we require the condition

$$\frac{B_{\theta 1}^2}{(p_1 - p_0)} < \frac{\beta J_1^2(\mu_1)}{M_a^2(1 - J_0^2(\mu_1))}. \tag{6.31}$$

This implies that the plasma pressure at r = 1 must be greater than at r = 0, for p_1-p_0 to be positive. This is consistent with what we would expect for a sunspot. Equation (6.28) then gives

$$k = \pm \frac{1}{v_0}\left\{\frac{\beta(p_1 - p_0)}{M_a^2(1 - J_0^2(\mu_1))} - \frac{B_{\theta 1}^2}{J_0^2(\mu_1)}\right\}^{1/2}, \tag{6.32}$$

on substituting for a_1, and from equation (6.27) it is easy to see that

$$2\Pi_1 = \frac{\beta}{(1 - J_0^2(\mu_1))}\{p_1 - J_0^2(\mu_1)p_0\}. \tag{6.33}$$

Finally from equation (6.31) we note that

$$\alpha^2 = \frac{\mu_1^2 B_{\theta 1}^2}{J_1^2(\mu_0)} \left\{ \frac{\beta(p_1 - p_0)}{M_a^2(1 - J_0^2(\mu_1))} - \frac{B_{\theta 1}^2}{J_1^2(\mu_0)} \right\}^{-1} \tag{6.34}$$

and hence

$$\nu^2 = \mu_1^2 \left\{ 1 - \frac{B_{\theta 1}^2}{J_1^2(\mu_0)} M_a^2(1 - J_0^2(\mu_1)) \left[\beta(p_1 - p_0) - \frac{M_a^2 B_{\theta 1}^2}{J_1^2(\mu_0)} (1 - J_0^2(\mu_1)) \right]^{-1} \right\}. \tag{6.35}$$

We have now found all the arbitrary constants in terms of the imposed quantities v_0, $B_{\theta 1}$, p_0 and p_1. Since we require $\nu^2 > 0$ as well as $\alpha^2 > 0$, we must have

$$\frac{B_{\theta 1}^2}{(p_1 - p_0)} < \frac{1}{2} \frac{\beta J_1^2(\mu_0)}{(1 - J_0^2(\mu_1))}, \tag{6.36}$$

which is a more stringent condition than inequality (6.31).

Substituting the appropriate constants into the expression for the plasma pressure, we obtain

$$p = \frac{1}{1 - J_0^2(\mu_1)} \left\{ p_1 - J_0^2(\mu_1) p_1 - (p_1 - p_0)(J_1^2(\mu_1 r) + J_0^2(\mu_1 r)) e^{-2\nu z} + \frac{2M_a^2 B_{\theta 1}^2}{J_1^2(\mu_0)} J_0^2(\mu_1 r) e^{-2\nu z} \right\}, \tag{6.37}$$

and observe that the coupled effect of a non-zero $B_{\theta 1}$ and the presence of inertial forces is to add an extra positive term to equation (6.37).

The equation of a fieldline projected in the r-z plane and passing through the footpoint $(r_0, 0)$ is

$$z = \frac{1}{\nu} \log \left[\frac{r\, J_1(\mu_1 r)}{r_0\, J_1(\mu_1 r_0)} \right]. \qquad (6.37)$$

A set of fieldlines is plotted in Figure 6.1 and has the topology of a magnetic arcade (with symmetry about the z axis), which may model the magnetic field above a sunspot. The new feature with these solutions is the presence of a steady flow of plasma along the arcade.

Typical profiles of the solutions, plotted for various z, are shown in Figure 6.2. The presence of Bessel functions in the solution has the immediate consequence that the maximum and minimum values of B_z have different magnitudes, compared with the solutions in a cartesian geometry where they are the same (chapter five). Note also that the zero of B_z is closer to $r = 1$ than to $r = 0$, which implies that the summit position is no longer midway between the footpoints of the fieldlines. This gives the magnetic field an asymmetric appearance. The lack of symmetry in the arcade profile is also due to the fact that the value of r for which B_r is a maximum is not the same as that for which B_z vanishes. The value of B_θ, the shear component of magnetic field, is zero at $r = 0$ and $r = 1$, taking its maximum value at the summit of the arcade. The size of B_θ decreases to zero with increasing z, so the arcade becomes less sheared with increasing height. The velocity components have similar profiles to the magnetic field. However, note that the minimum of v_z does not occur at $r = 1$ for $z = 0$, and the position of the minimum tends to $r = 1$ as z increases. The plasma density has a minimum at approximately the position of the summit of each fieldline, the density increasing with z to a constant value. The plasma pressure also increases

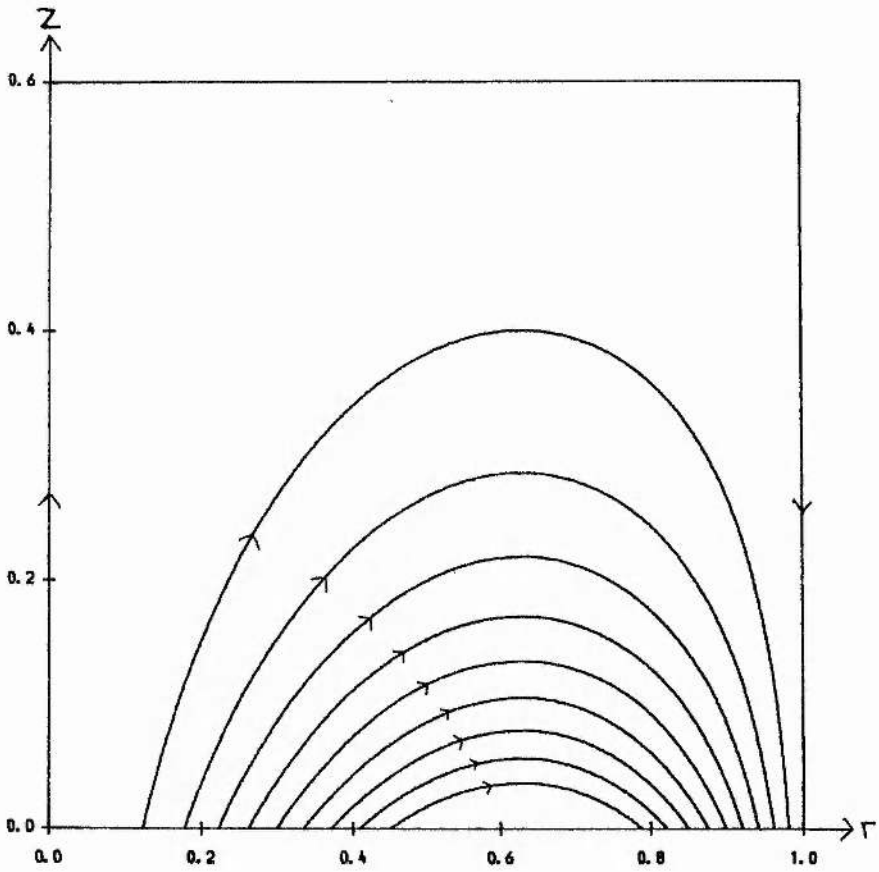

Figure 6.1 : Magnetic fieldline plot when M_a=0.5, β=1.0, v_0=2.0, p_0=1.0 p_1=3.0, $B_{\theta 1}$=0.5.

Figure 6.2a

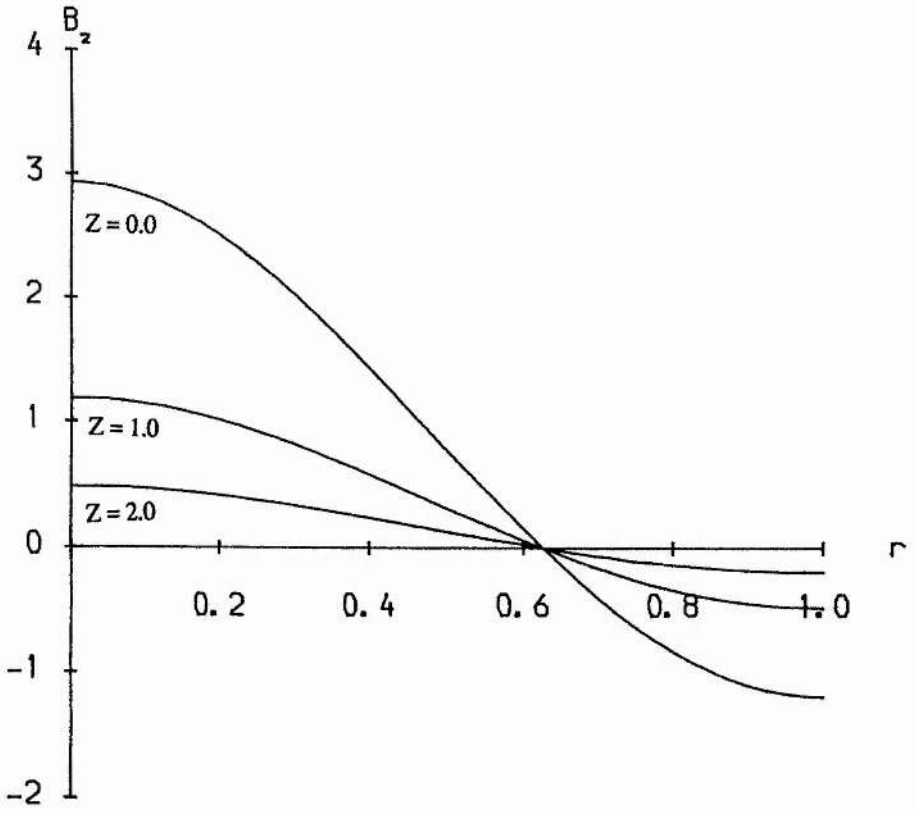

Figure 6.2 : The variation with r of the fundamental mode solution of (a) B_z, (b) B_r, (c) B_θ, (d) v_z,(e) v_r, (f) v_θ, (g) ρ and (h) βp for various values of z. The parameters are the same as in Figure 6.1.

Figure 6.2b

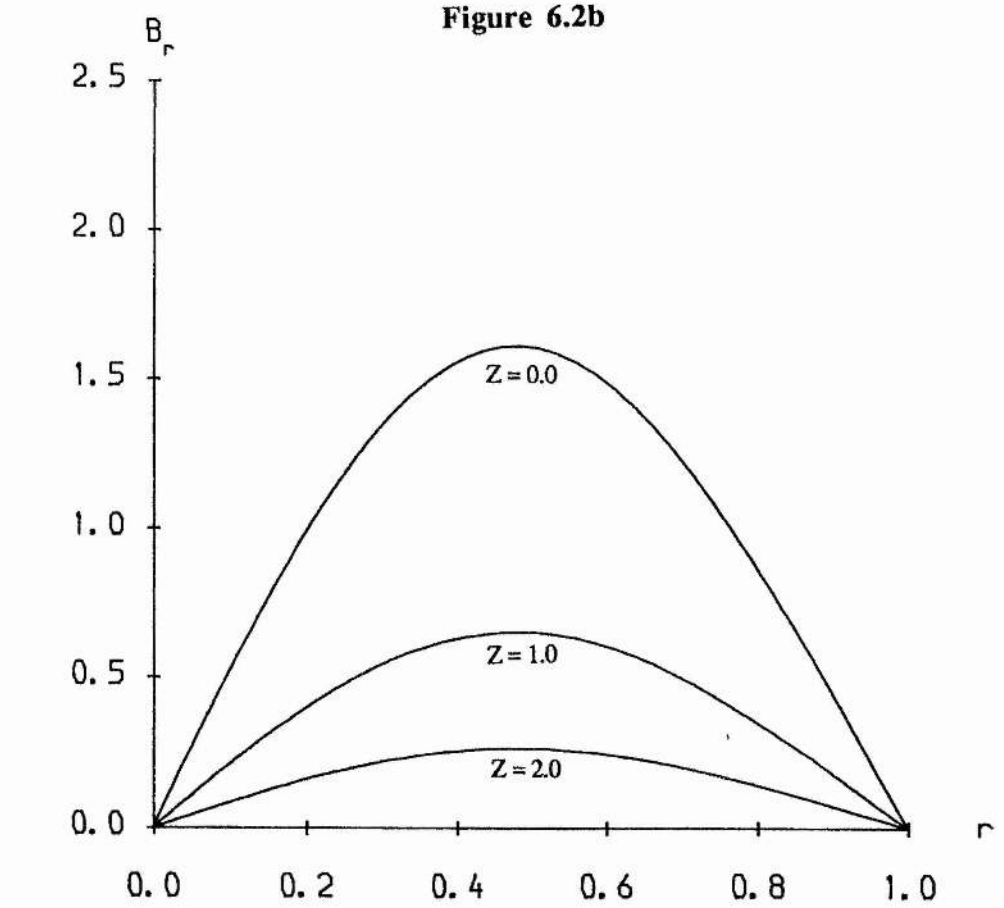

Figure 6.2c

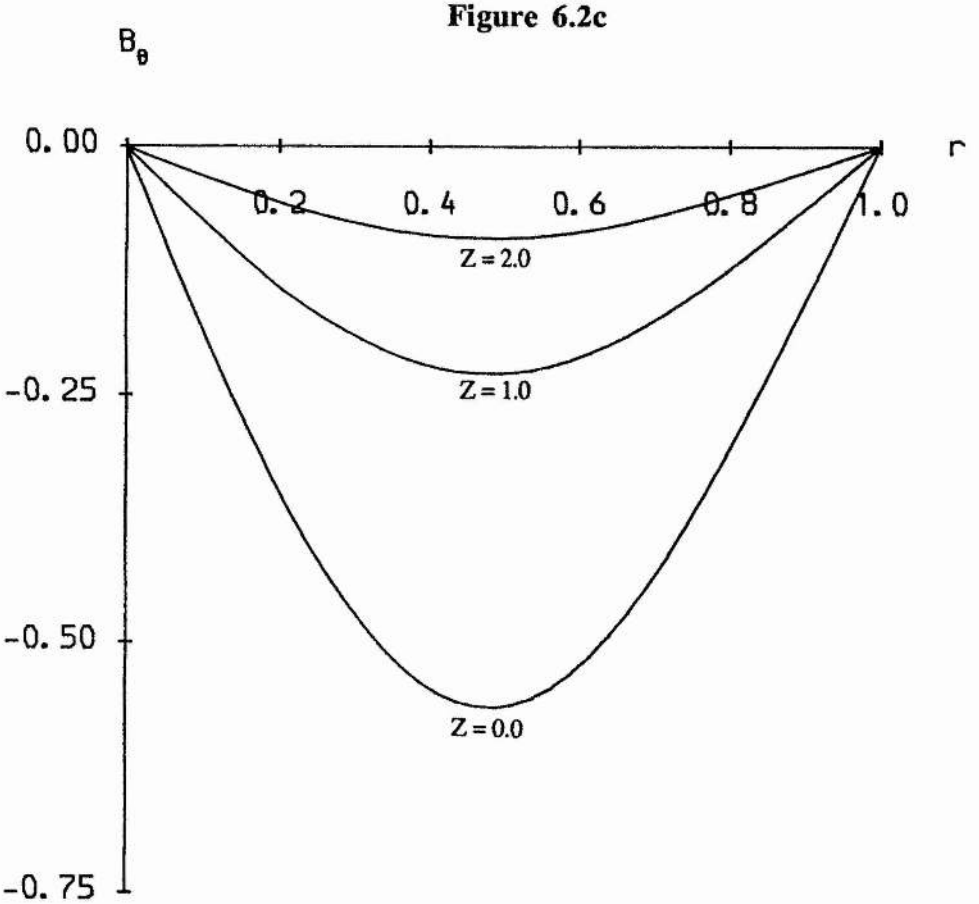

Figure 6.2d

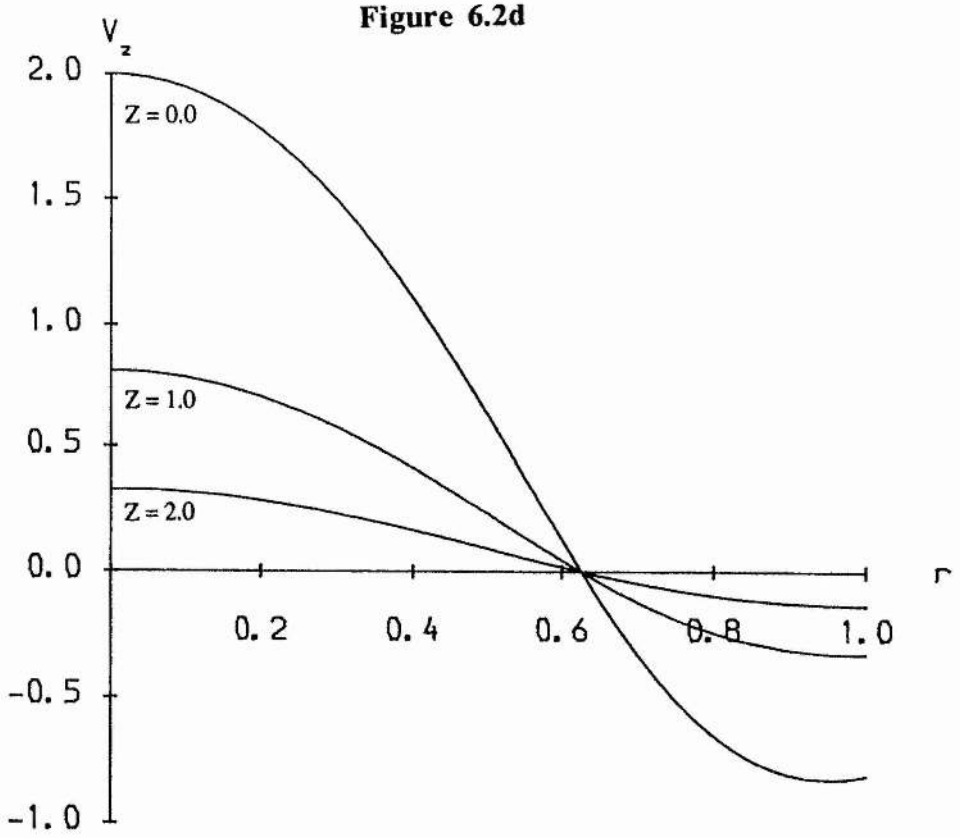

Figure 6.2e

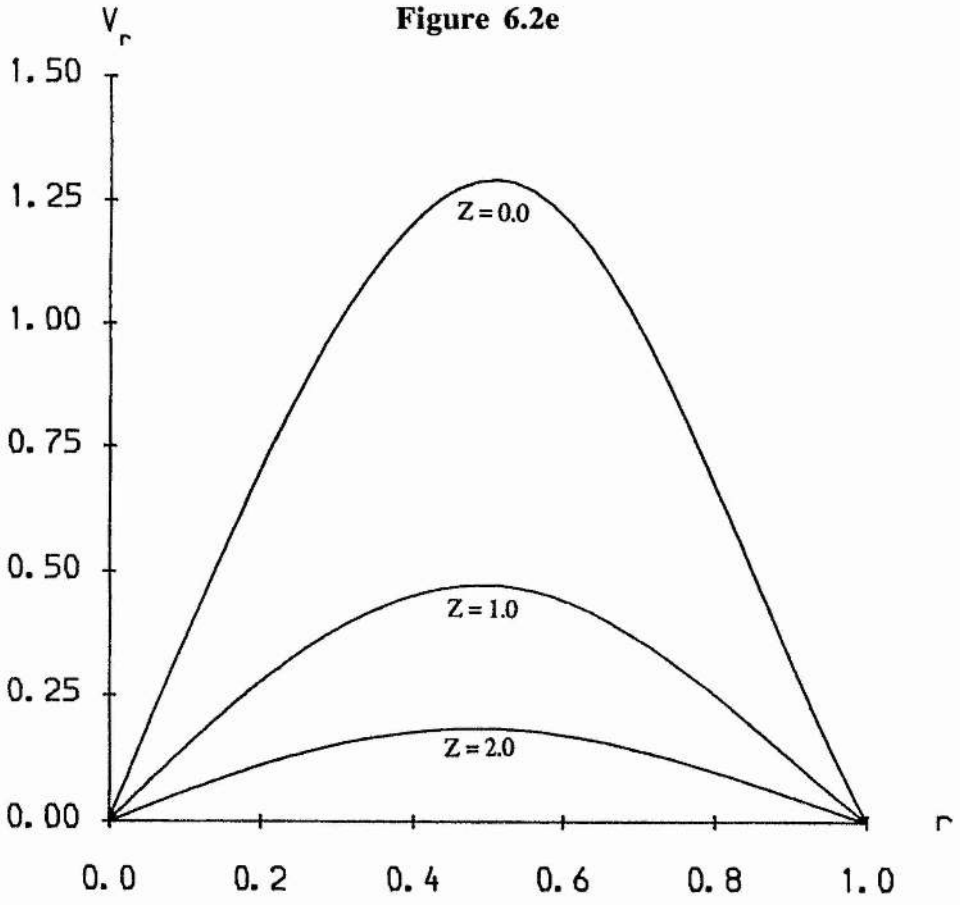

Figure 6.2f

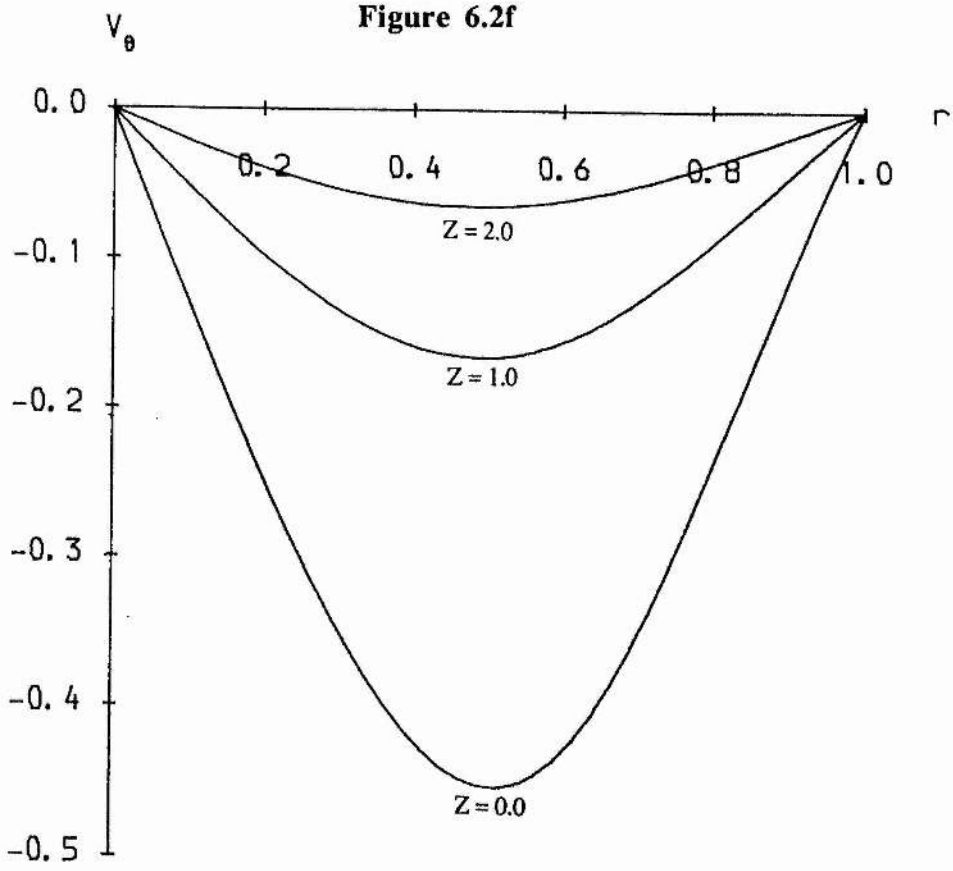

Figure 6.2g

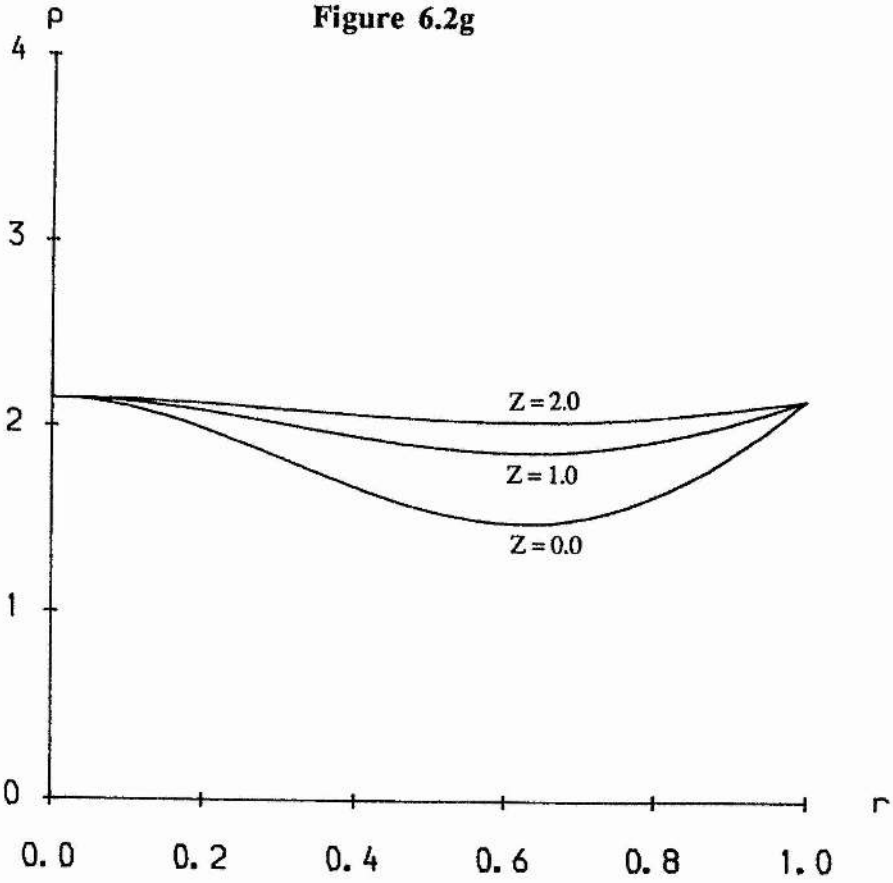

Figure 6.2h

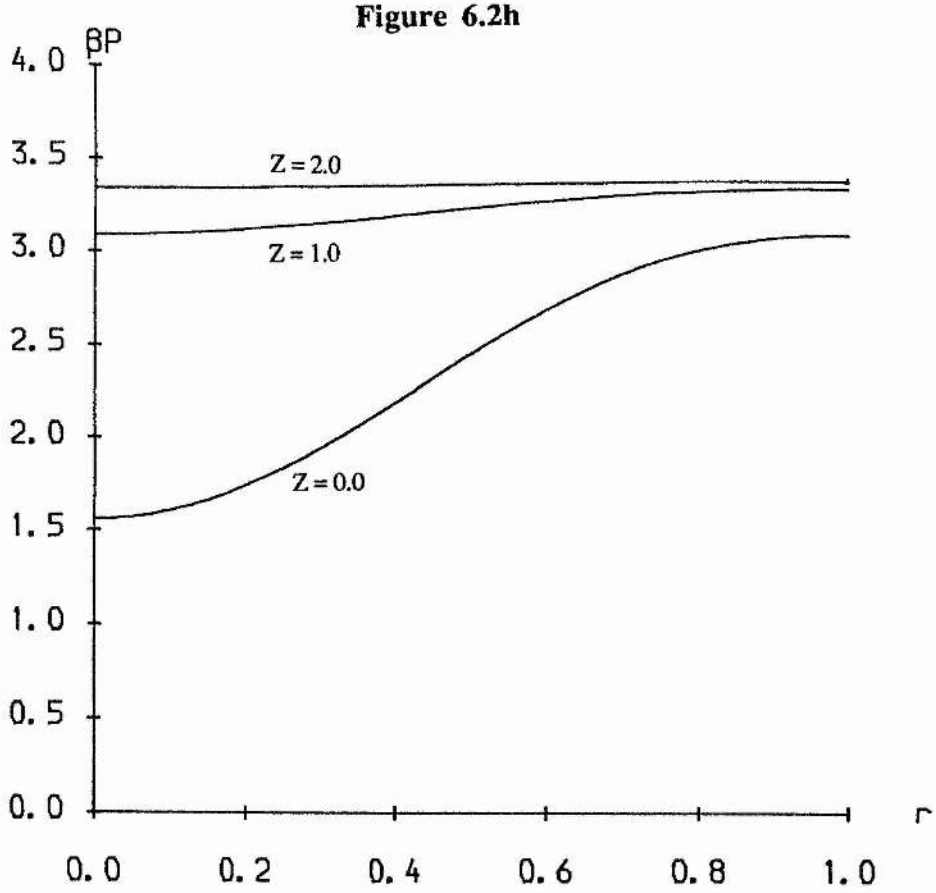

with height to a constant value, flattening out the imposed pressure gradient at z = 0.

Defining the new parameters

$$M_a^{*2} = M_a^2 B_{\theta 1}^2, \qquad \beta^* = \beta(p_1 - p_0),$$

equation (6.38) may be rewritten as

$$\nu^2 = \mu_1^2 \left\{ 1 - M_a^{*2} \frac{(1 - J_0^2(\mu_1))}{J_1^2(\mu_0)} \left[\beta^* - M_a^{*2} \frac{(1 - J_0^2(\mu_1))}{J_1^2(\mu_0)} \right]^{-1} \right\}. \quad (6.39)$$

Then note that from (6.38) that the summit height of a fieldline, and hence the arcade height ,varies with ν^{-1}. For a typical fieldline the variation of the summit height with M_a^2, for different values of β^* is plotted in Figure 6.3. Increasing the parameter M_a^2 increases the summit height of the arcade. Note that when $M_a^2 = 0$ the summit height is independent of the Alfvén Mach number M_a and $B_{\theta 1}$. When $B_{\theta 1} \neq 0$, the presence of inertial forces increases the height of the arcade compared with the static case. Increasing the size of the inertial force (increasing M_a, and hence M_a^*), subject to inequality (6.36), increases the arcade summit height, since a greater centrifugal force requires greater magnetic tension (and hence a more curved field) for force balance. Continuing to increase M_a will eventually cause the arcade to erupt, corresponding to the asymptotes in the graph. Putting $\nu = 0$ in (6.39), the critical calue of M_a^2 for which the arcade erupts is given by

$$M_{crit}^* = \frac{1}{2} \frac{J_1^2(\mu_0)}{(1 - J_0^2(\mu_1))} \beta^*.$$

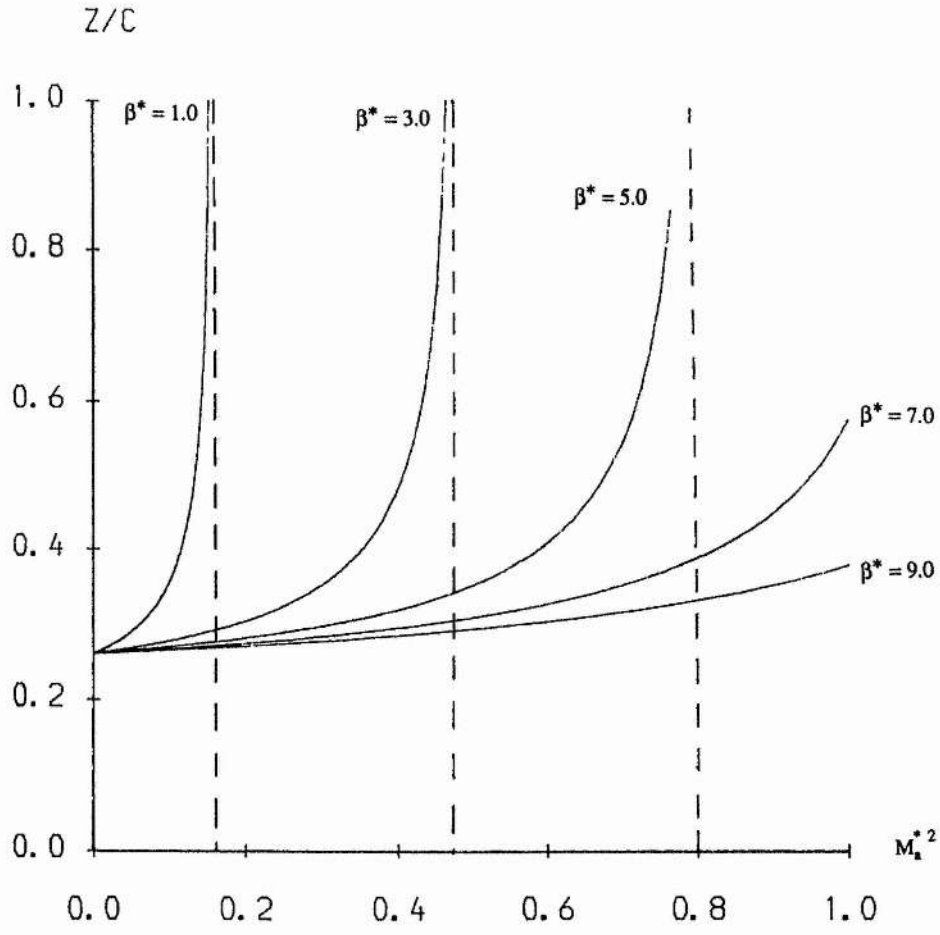

Figure 6.3 : The variation of z/c, the normalised summit height with M_a^* for various values of β^*, where $c=\log[rJ_1(\mu_1 r)/r_0 J_1(\mu_1 r_0)]$.

The greater the value of β^*, the larger the range of M_a^2 before eruption occurs.

Increasing the shear component of the field $B_{\theta 1}$ increases the arcade height, and greater magnetic tension is required for force balance. The greater the value of $B_{\theta 1}$, the smaller the range of possible values of M_a before the arcade erupts. Note also that increasing the value of β^* for a fixed M_a^*, has the effect of lowering the height of the arcade. Increasing the plasma beta (and hence β^*) will increase the effective magnitude of the plasma pressure. One way of maintaining force balance, is to have a corresponding increase in the magnetic pressure. For this we require an increase in the magnetic field strength, that is, the fieldlines have to be brought closer together. In the arcade this can occur by decreasing the height of the arcade, and effectively, 'squashing' the field to give greater magnetic pressure.

6.4 Evershed Flow

Plasma flows have been observed in the penumbra and superpenumbra of a sunspot called Evershed flow. We suggest that the analytical solutions presented in this paper may provide a simple self-consistent model for these flows, in which the reaction of the flow on the field is included rather than treating the field lines as rigid tubes.

In the penumbra it is known that the flow is outward, with the velocity ranging up to 6 kms^{-1} (e.g. Moore and Rabin, 1985) while in the superpenumbra the flow is directed in towards the spot with velocities up to 20 kms^{-1}. This flow is usually called the inverse Evershed flow.

The particular parameter values which pertain to this region of the solar atmosphere are still in doubt. In the penumbra the Alfvén speed is likely to be of

Figure 6.4a

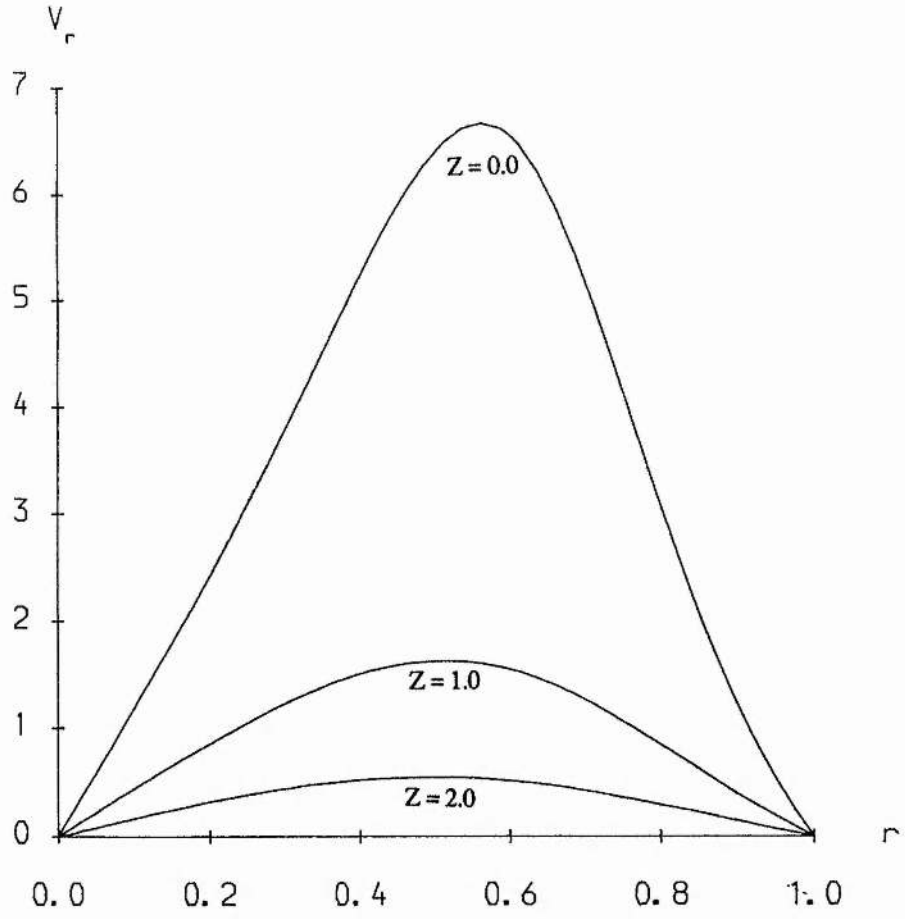

Figure 6.4 : The variation with r of (a) v_r, (b) v_z of the fundamental mode solutions for various values of z with M_a=0.3, β=1.0, v_0=6.0, p_0=1.0, p_1=4.0, $B_{\theta 1}$ =0.05, typical of Evershed flow.

Figure 6.4b

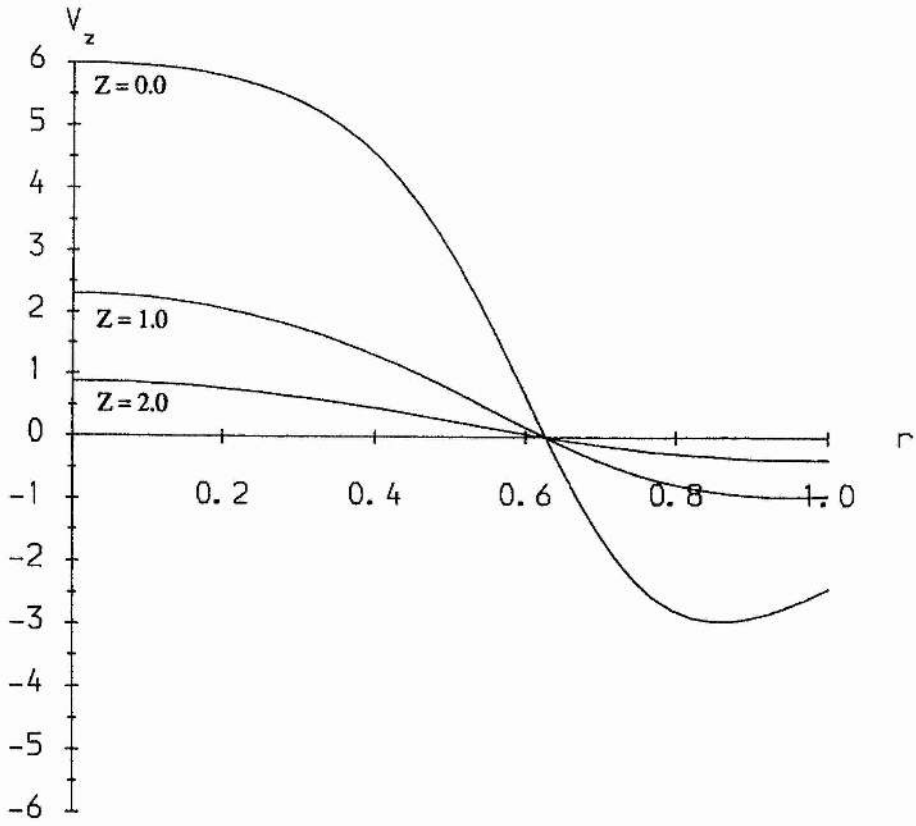

the order of about 30 kms^{-1}, while in the superpenumbra the value will be much greater, say about 80-100 kms^{-1}. The plasma beta will be of order 1 in the penumbra with a smaller value, say 0.1, in the superpenumbra. The precise values of these parameters are not vital, but, by adopting the above values, we may model Evershed and inverse Evershed flow.

For the flow in the penumbra we take $M_a \sim 0.3$, $\beta \sim 1.0$ along with $B_{\theta 1} = 0.05$, $p_0 = 1.0$ and $p_1 = 4.0$. The profiles for the velocity are shown in Figure 6.4. In the penumbra the radial component has a sharp maximum which decreases rapidly in value with increasing z, the position of the maximum shifting inwards towards the z-axis. The value of the z-component of velocity remains fairly constant for $0 \leq r \leq 0.3$, and then decreases rapidly to a minimum at beyond $r \approx 0.85$. Note that here the plasma flow is outward, that is, flowing from $r = 0$ to $r = 1$ ($v_0 > 0$).

The profiles for an inflow, such as we might expect for the inverse Evershed flow exhibit differences in their velocity profiles from those of the outflow. In Figure 6.5 with $v_0 = -20$, the radial component has a minimum much closer to the origin, with the position of the minimum moving outwards away from the z-axis with increasing z. The z-component has a sharp minimum at $r = 0$ and a maximum at $r = 1$, in contrast with the outflow. The arcade associated with the outflow also has a greater summit than the outflow.

6.5 Properties of Solutions

Before determining the various arbitrary constants by imposing various quantities on the base $z = 0$, we examine the physical régimes that are possible in terms of the magnetic field and plasma pressure behaviour.

Firstly, consider the magnetic field structure, when $\Pi_2 \neq 0$ and seek the criteria to determine whether a particular fieldline is open or closed.

Figure 6.5a

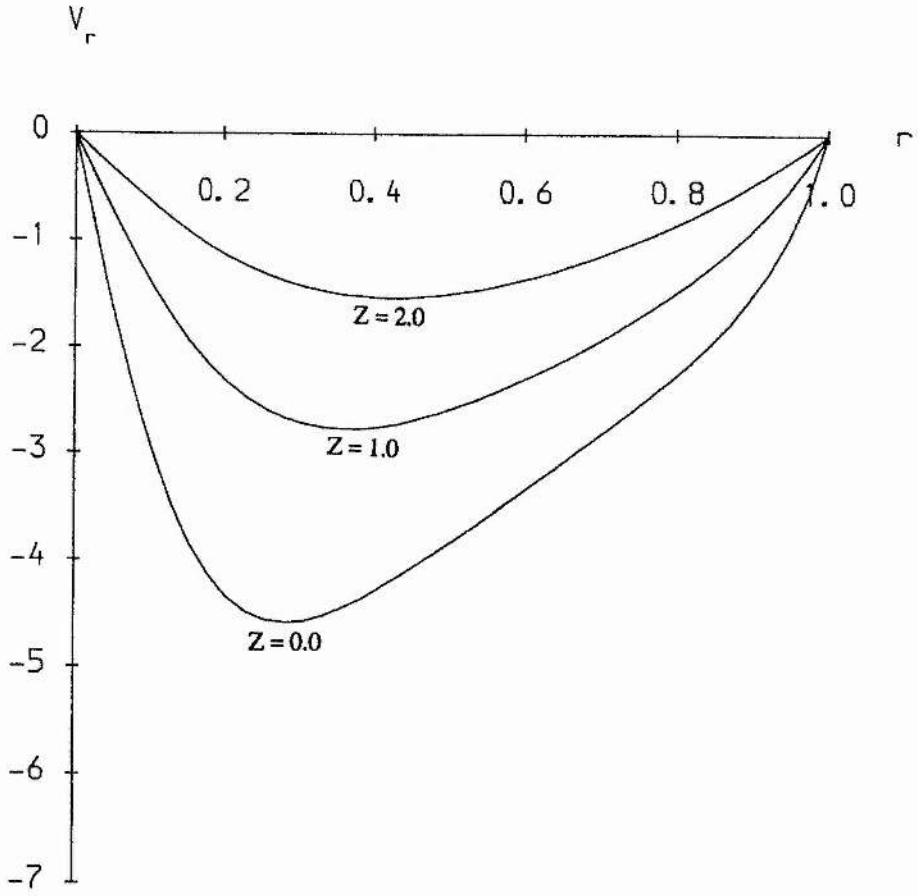

Figure 6.5: The variation with r of (a) v_r, (b) v_z of the fundamental mode solutions for various values of z with M_a=0.2, β=0.1, v_0=-20.0, p_0=1.0, p_1=4.0, $B_{\theta 1}$ =0.1, typical of inverse Evershed flow.

Figure 6.5b

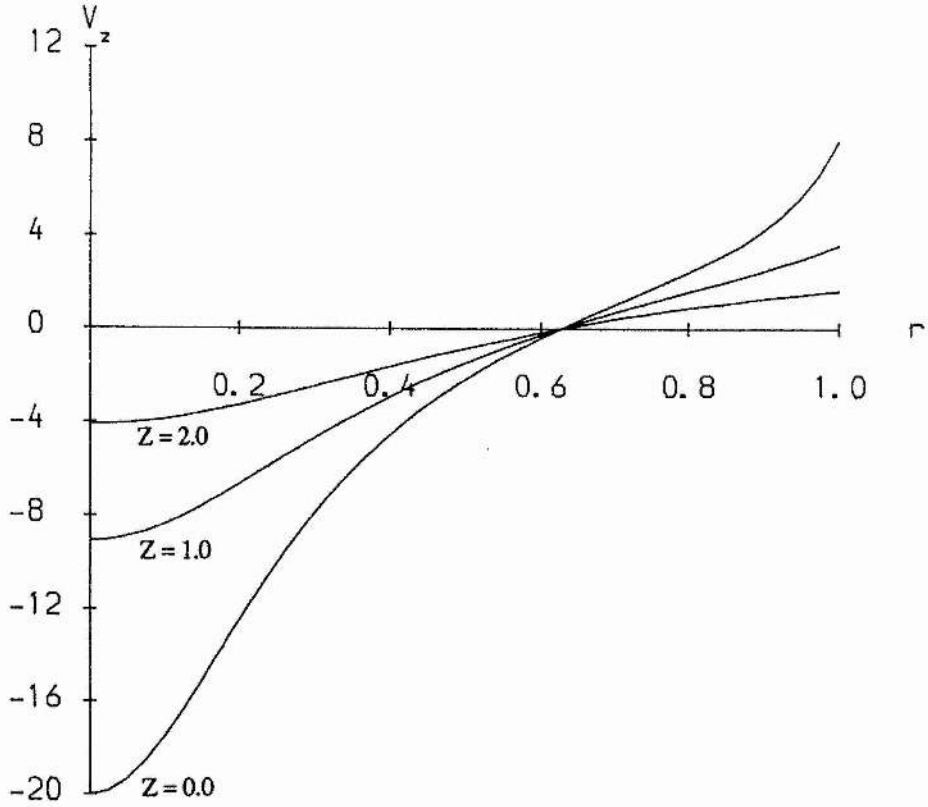

Note first that the equation of a fieldline is the solution of

$$B_r \frac{dz}{dr} = B_z, \tag{6.40}$$

or on substituting for B_r and B_z from (6.14) and (6.15), respectively,

$$\left[\frac{\nu J_1(\mu_1 r)}{\mu_1}\right]\frac{dz}{dr} = \left[J_0(\mu_1 r) - \frac{2\Pi_2}{a_1\alpha^2} e^{\nu z}\right]. \tag{6.41}$$

For a fieldline with footpoint $(r_0,0)$ the integral of equation (6.41) gives

$$\frac{a_1}{\mu_1}\left(r_0 J_1(\mu_1 r_0) - r J_1(\mu_1 r) e^{-\nu z}\right) = \frac{\Pi_2}{\alpha^2}(r_0^2 - r^2). \tag{6.42}$$

In the limit $z \rightarrow \infty$ equation (6.42) reduces to

$$r^2 = r_0\left[r_0 - \frac{\alpha^2 a_1}{\mu_1 \Pi_2} J_1(\mu_1 r_0)\right]. \tag{6.43}$$

For a fieldline to be open, the limit (6.43) must exist and give a real value of r, and so the condition

$$r_0 > \frac{\alpha^2 a_1}{\mu_1 \Pi_2} J_1(\mu_1 r_0) \tag{6.44}$$

holds. For closed fieldlines the limit does not exist, and thus

$$r_0 < \frac{\alpha^2 a_1}{\mu_1 \Pi_2} J_1(\mu_1 r_0). \tag{6.45}$$

Condition (6.44) may be recast in an even simpler form by multiplying by $\mu_1^2 r_0$ and then differentiating with respect to $(\mu_1 r_0)$ to give

$$\frac{\alpha^2 a_1}{2\Pi_2} J_0(\mu_1 r_0) < 1, \tag{6.46}$$

for open fieldlines, and

$$\frac{\alpha^2 a_1}{2\Pi_2} J_0(\mu_1 r_0) > 1, \tag{6.47}$$

for closed fieldlines.

Consider the case where $\alpha^2 a_1/2\Pi_2 > 0$. Two distinct cases arise, namely $2\Pi_2/\alpha^2 a_1 > 1$ and $0 < 2\Pi_2/\alpha^2 a_1 < 1$. Firstly, when $2\Pi_2/\alpha^2 a_1 > 1$ the inequality (6.46) holds for all footpoint positions r_0 in the interval (0,1), giving purely open fieldlines.

Secondly, when $0 < 2\Pi_2/\alpha^2 a_1 < 1$, there exists an r* such that

$$J_0(\mu_1 r^*) = \frac{2\Pi_2}{\alpha^2 a_1}.$$

Then, for $0 < r_0 < r^*$, we have

$$J_0(\mu_1 r_0) > \frac{2\Pi_2}{\alpha^2 a_1},$$

giving closed field lines. For $r^* < r < \mu_0/\mu_1$, we have

$$J_0(\mu_1 r_0) < \frac{2\Pi_2}{\alpha^2 a_1},$$

which indicates that the fieldlines are open. A typical fieldline plot for this particular case is shown in Figure 6.6a. This illustrates an interesting feature of these solutions, namely, that one self-consistent solution gives both regions of closed and open fieldlines, with plasma flows along them.

The second case is when $\alpha^2 a_1/2\Pi_2 < 0$, which implies that the condition for open fieldlines becomes

$$J_0(\mu_1 r_0) > \frac{2\Pi_2}{\alpha^2 a_1}, \tag{6.48}$$

and

$$J_0(\mu_1 r_0) < \frac{2\Pi_2}{\alpha^2 a_1}, \tag{6.49}$$

for closed fieldlines. When

$$\frac{2\Pi_2}{\alpha^2 a_1} < J_0(\mu_1),$$

inequality (6.48) clearly holds, and so the fieldlines are purely open for each r_0. Now choose

$$J_0(\mu_1) < \frac{2\Pi_2}{\alpha^2 a_1} < 0,$$

and consider $0 < r_0 < r^*$ ($r^* > \mu_0/\mu_1$), and we find that (6.48) holds, giving open fieldlines. Then, for $r^* < r_0 < 1$, it can be seen that inequality (6.49) holds, giving closed fieldlines. This is another example of both open and closed fieldlines, a typical case being plotted in Figure 6.6b. Here, the closed region is closer to the outer boundary, with the overlying open field having footpoints closer to the origin. This is the opposite to the example plotted in Figure 6.6a. The magnetic field in Figure 6.6a may model a coronal streamer, while Figure

6.6b may provide a model for a coronal hole including the closed structure at the hole boundary.

Turning attention to the case of purely open fieldlines, consider the condition

$$\frac{2\Pi_2}{\alpha^2 a_1} > 1,$$

where we must have Π_2 and a_1 of the same sign. This gives $dz/dr < 0$, and so the fieldlines are converging to give a plume-like magnetic field structure (Figure 6.6c).

When

$$\frac{2\Pi_2}{\alpha^2 a_1} < J_0(\mu_1),$$

we need Π_2 and a_1 to be of opposite signs, and this gives $dz/dr > 0$ for every fieldline, resulting in a diverging magnetic field structure, such as one might expect in a coronal hole (Figure 6.6d).

The classification of the possible magnetic field structures is summarised in Table 6.1. The type of magnetic field will depend upon the constant $2\Pi_2/\alpha^2 a_1$, and in the next section we show how this is related to the flow at the base of the region under consideration.

Now consider the plasma pressure, which we wish to have the property that its value at $z = 0$ is greater than at $z \to \infty$. This is clearly desirable on physical grounds, and mathematically may be written in the form

$$\beta(p(r,0) - p(r, z\to\infty)) = \beta\Delta p(r)$$

Figure 6.6a

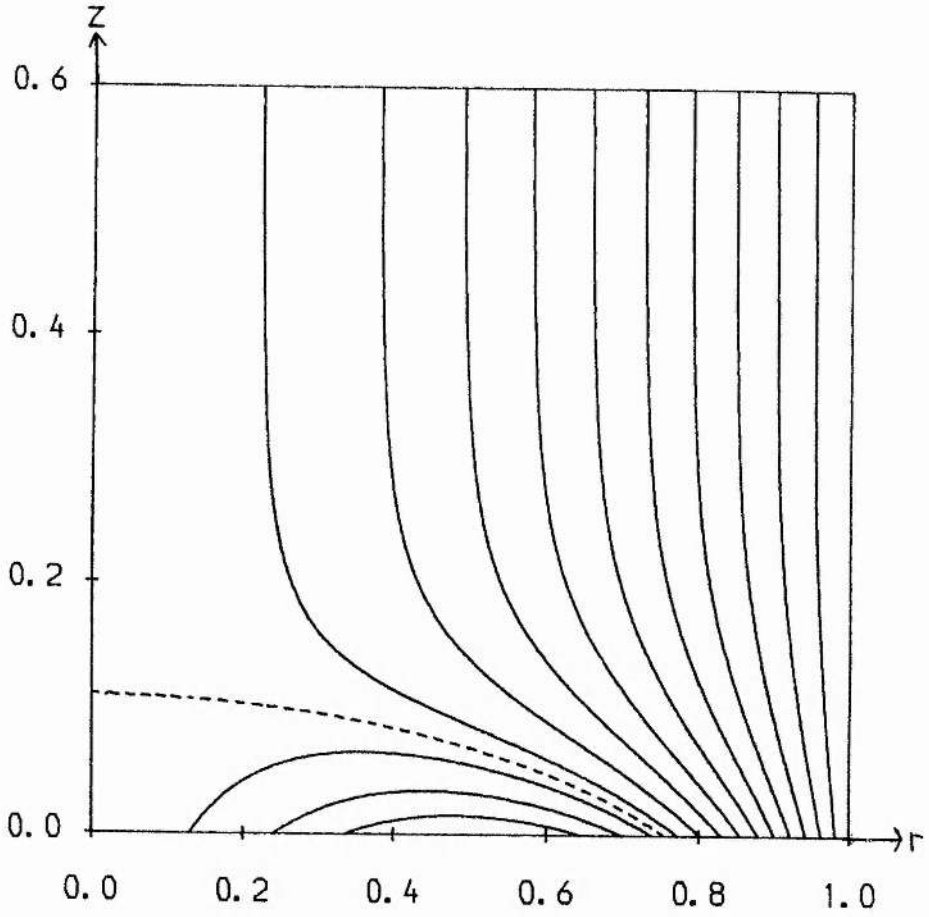

Figure 6.6 : Magnetic fieldline plots with M_a=0.5, $\beta(p_0-p_1)$=1.0 and

a) v^*=2.0, $B_{\theta 1}$=0.5, b) v^*=-2.4, $B_{\theta 1}$=1.0, c) v^*=1.0, $B_{\theta 1}$=0.5,

d)v^*=-0.4, $B_{\theta 1}$=1.0.

Figure 6.6b

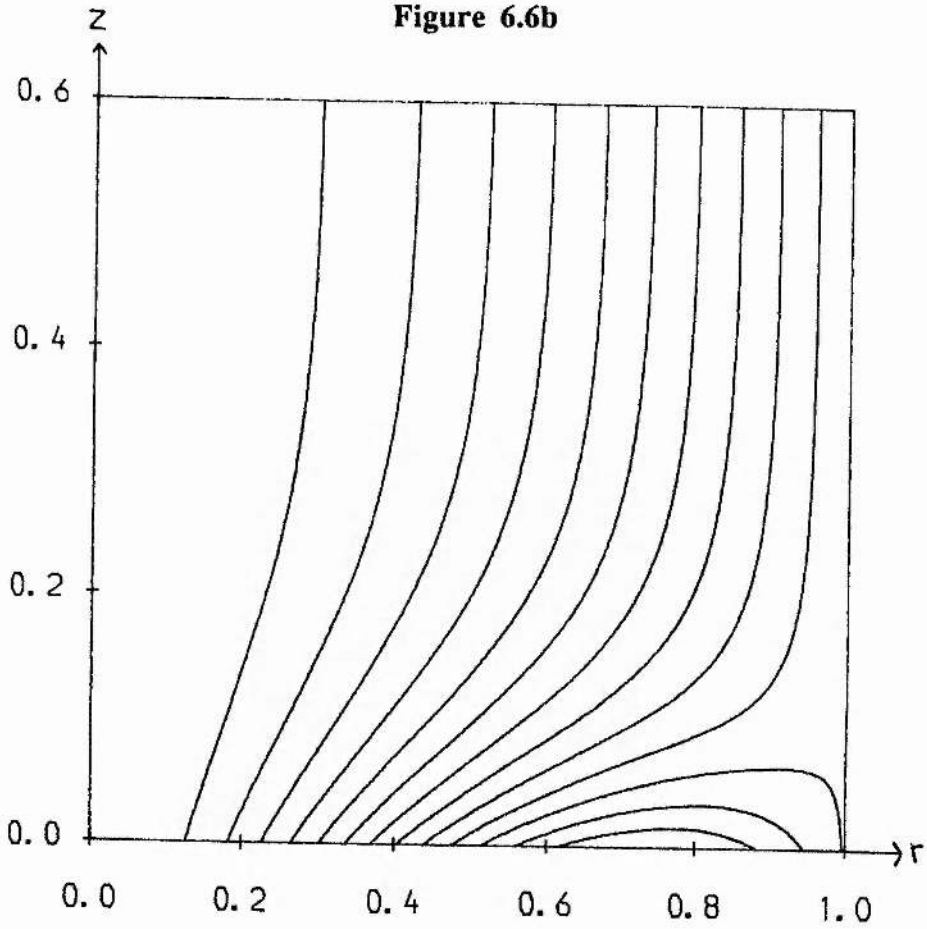

Figure 6.6c

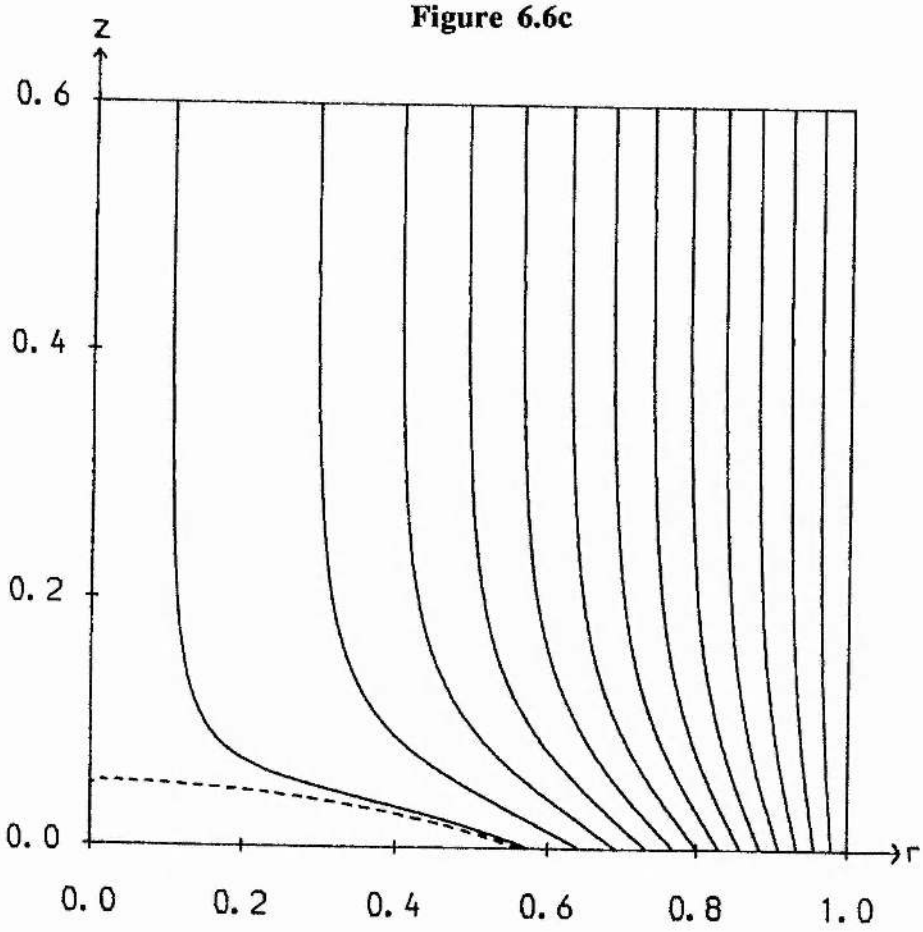

Figure 6.6d

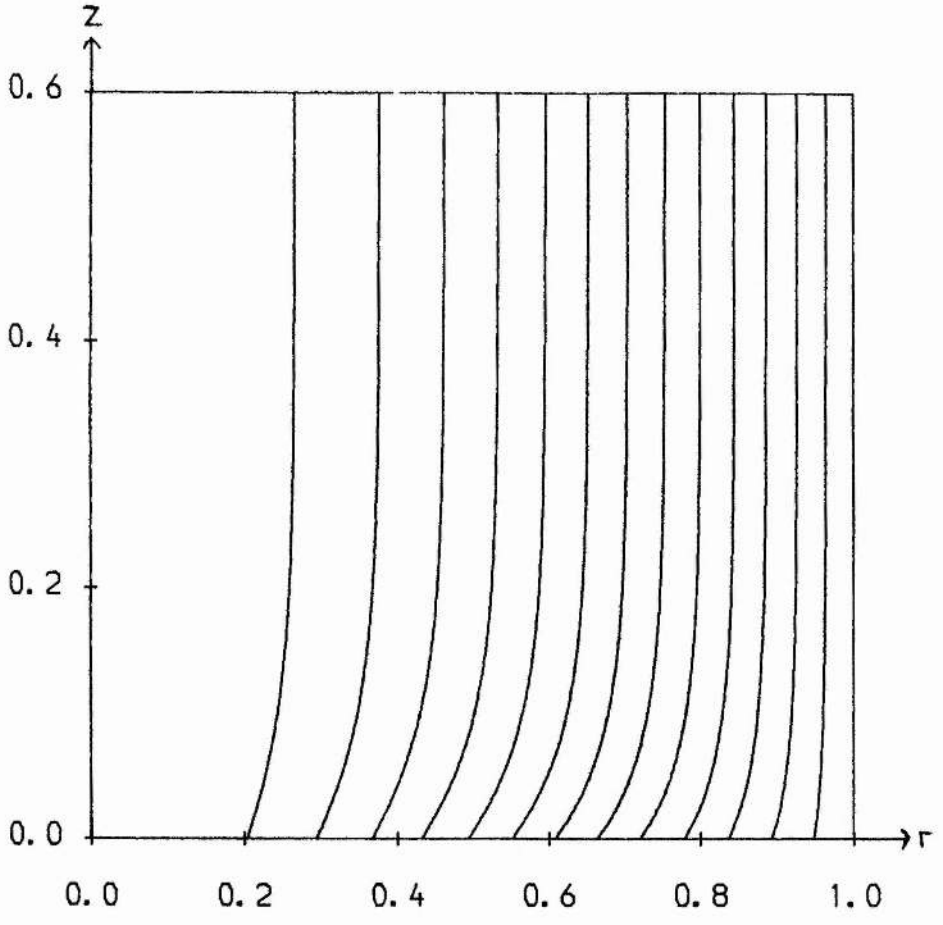

Table 1: Classification of possible magnetic configurations, depending upon the magnitude and sign of $2\Pi_2/\alpha^2 a_1$

Interval of $\frac{2\Pi_2}{\alpha^2 a_1}$	$\frac{2\Pi_2}{\alpha^2 a_1} < J_0(\mu_1)$	$J_0(\mu_1) < \frac{2\Pi_2}{\alpha^2 a_1} < 0$		$0 < \frac{2\Pi_2}{\alpha^2 a_1} < 1$		$\frac{2\Pi_2}{\alpha^2 a_1} > 1$
Interval for r_0	$\forall r_0 \in (0,1)$	$0 < r_0 < r^*$	$r^* < r_0 < \frac{\mu_0}{\mu_1}$	$0 < r_0 < r^*$	$r^* < r_0 < 1$	$\forall r_0 \in (0,1)$
Nature of field	open	open	closed	closed	open	open
Converging or Diverging	diverging	diverging	-	-	converging	converging

$$= M_a^2 a_1^2 \left[\left(1 - \frac{\alpha^2}{\mu_1^2} \right) J_1^2(\mu_1 r) + \left(1 + \frac{\alpha^2}{\mu_1^2} \right) J_0^2(\mu_1 r) \right]$$

$$- 2\Pi_0 a_1 \left[\frac{r\, J_1(\mu_1 r)}{\mu_1 (1 - M_A^2)} + \frac{2M_a^2 (1 - M_a^2)}{\Omega_0^2} J_0(\mu_1 r) \right]. \qquad (6.50)$$

Let us examine when

$$\Delta p(r) > 0$$

along $r = 0$ and $r = 1$, the centre and boundary of the region under consideration. From (6.50)

$$\beta \Delta p(0) = M_a^2 a_1^2 \left(1 + \frac{\alpha^2}{\mu_1^2} \right) - 4\Pi_2 a_1 \frac{M_a^2}{\alpha^2} \qquad (6.51)$$

and

$$\beta \Delta p(1) = M_a^2 a_1^2 \left(1 + \frac{\alpha^2}{\mu_1^2} \right) J_0^2(\mu_1) - 4\Pi_2 a_1 \frac{M_a^2}{\alpha^2} J_0(\mu_1), \qquad (6.52)$$

and when these both hold

$$\beta(\Delta p(0) + \Delta p(1)) > 0$$

$$\Leftrightarrow \frac{2\Pi_2}{a_1 \alpha^2} < \frac{1}{2} \left(\frac{1 + J_0^2(\mu_1)}{1 + J_0(\mu_1)} \right) \left(1 + \frac{\alpha^2}{\mu_1^2} \right). \qquad (6.53)$$

In addition, when the plasma pressure along $r = 0$ is greater than at $r = 1$, then

$$\beta(\Delta p(0) - \Delta p(1)) > 0,$$

which gives

$$\frac{2\Pi_2}{a_1\alpha^2} < \frac{1}{2}(1 + J_0(\mu_1))\left(1 + \frac{\alpha^2}{\mu_1^2}\right). \tag{6.54}$$

Combining inequalities (6.53) and (6.54), the plasma pressure has a greater value along r = 0 (compared with r = 1) when

$$\frac{2\Pi_2}{a_1\alpha^2} < \frac{1}{2}(1 + J_0)\left(1 + \frac{\alpha^2}{\mu_1^2}\right). \tag{6.55}$$

When the plasma pressure is greater along r = 1, than r = 0, then

$$\frac{1}{2}(1 + J_0(\mu_1))\left(1 + \frac{\alpha^2}{\mu_1^2}\right) < \frac{2\Pi_2}{\alpha^2 a_1} < \frac{1}{2}\left(\frac{1 + J_0^2(\mu_1)}{1 + J_0^2(\mu_1)}\right)\left(1 + \frac{\alpha^2}{\mu_1^2}\right). \tag{6.56}$$

Combining these results with those for the magnetic field, we see that when the field is purely diverging ($2\Pi_2/\alpha^2 a_1 < J_0(\mu_1)$) and when $J_0(\mu_1) < 2\Pi_2/\alpha^2 a_1 < 0$ the plasma pressure along r = 0 is greater than along r = 1.

When $0 < 2\Pi_2/\alpha^2 a_1 < 1$ and $2\Pi_2/\alpha^2 a_1 > 1$, we may have either a maximum or minimum along r = 0 depending upon the values of α^2. Altering the value of $2\Pi_2/\alpha^2 a_1$ not only changes the magnetic field structure but also alters the plasma pressure behaviour.

Consider now the variation of plasma pressure with z. A condition for $p(r,0) > p(r,\infty)$ has already been deduced which implies that the plasma

experiences a net expansion. However it is now shown that the actual behaviour of the plasma is more complex.

Firstly, to determine the stationary points of the plasma pressure, note that

$$\frac{\partial(\beta p)}{\partial z} = -2\Pi_0 a_1 \nu \left[\frac{r J_1(\mu_1 r)}{\mu_1(1 - M_a^2)} + \frac{2M_a^2(1 - M_a^2)}{\Omega_0^2} J_0(\mu_1 r) \right] e^{-\nu z}$$

$$+ 2M_a^2 \nu a_1^2 \left[\left(1 - \frac{\alpha^2}{\mu_1^2} \right) J_1^2(\mu_1 r) + \left(1 + \frac{\alpha^2}{\mu_1^2} \right) J_0^2(\mu_1 r) \right] e^{-2\nu z} , \qquad (6.57)$$

and

$$\frac{\partial^2(\beta p)}{\partial z^2} = 2\Pi_0 \nu^2 a_1 \left[\frac{r J_1(\mu_1 r)}{\mu_1(1 - M_a^2)} + \frac{2M_a^2(1 - M_a^2)}{\Omega_0^2} J_0(\mu_1 r) \right] e^{-\nu z}$$

$$+ 4M_a^2 \nu^2 a_1^2 \left[\left(1 - \frac{\alpha^2}{\mu_1^2} \right) J_1^2(\mu_1 r) + \left(1 + \frac{\alpha^2}{\mu_1^2} \right) J_0^2(\mu_1 r) \right] e^{-2\nu z}. \qquad (6.58)$$

Along $r = 0$, the plasma pressure has a stationary point if

$$\left. \frac{\partial p}{\partial z} \right|_{r=0} = 0$$

and this yields

$$e^{-\nu z} = \frac{2\Pi_2}{a_1 \alpha^2} \left[1 + \frac{\alpha^2}{\mu_1^2} \right]^{-1} . \qquad (6.59)$$

Assuming for the moment that (6.59) has real solutions for z, and substituting into (6.58), one can show that the stationary point is a maximum for $M_a < 1$ and

is minimum for $M_a > 1$. For (6.59) to have a real positive solution, we require that

$$0 < \frac{2\Pi_2}{a_1\alpha^2}\left[1 + \frac{\alpha^2}{\mu_1^2}\right]^{-1} < 1$$

or

$$0 < \frac{2\Pi_2}{\alpha^2 a_1} < \left[1 + \frac{\alpha^2}{\mu_1^2}\right]. \tag{6.60}$$

In the light of inequality (6.53), inequality (6.60) is modified to

$$0 < \frac{2\Pi_2}{\alpha^2 a_1} < \frac{1}{2}\left(\frac{1 + J_0^2(\mu_1)}{1 - J_0(\mu_1)}\right)\left(1 + \frac{\alpha^2}{\mu_1^2}\right). \tag{6.61}$$

We consider now the physical consequences of this result, and show that three distinct cases may arise.

When $2\Pi_2/\alpha^2 a_1 < 0$, there is no stationary point (as plasma travels along r = 0), and so the plasma experiences an expansion. When $2\Pi_2/\alpha^2 a_1$ satisfies (6.61) and $M_a < 1$, the plasma pressure is compressed until the plasma maximum is reached, and is then expanded. Alternatively, if $M_a > 1$, the plasma pressure experiences an expansion until the plasma pressure minimum occurs, and is then compressed. However, overall, the plasma experiences an expansion.

6.6 Relating Arbitrary Constants To Boundary Values

We now relate the work of the previous section to a particular set of boundary values. It should be noted that this is not a unique choice.

The following quantities are imposed along the base (z = 0) of the region of interest, namely,

$$\begin{aligned} &v_z(0,0) = v_0 \\ &v_z(1,0) = v_1 \\ &B_\theta(1,0) = B_{\theta 1} \\ &p(0,0) = p_0 \\ &p(1,0) = p_1. \end{aligned} \qquad (6.62)\text{-}(6.66)$$

Conditions (6.62) and (6.63) impose the value of the z-component of velocity along z = 0, (6.65) and (6.66) the value of the plasma pressure at the same points. On the outer boundary, the value of the twist component (B_θ) of magnetic field is specified (condition (6.64)). As an alternative, the angular component of velocity could be imposed at this point instead.

Equations (6.62) and (6.63) give

$$kv_0 = a_1 - \frac{2\Pi_2}{\alpha^2},$$

and

$$\left(k + \frac{\Pi_2}{\alpha^2}\right) v_1 = a_1 J_0(\mu_1) - \frac{2\Pi_2}{\alpha^2},$$

respectively, from which we deduce that

$$a_1 = \frac{\Pi_2}{\alpha^2} v^* \qquad (6.67)$$

where

$$v^* = \frac{2v_1 - 2v_0 - v_0 v_1}{v_1 - v_0 J_0(\mu_1)} \qquad (6.68)$$

on elimination of k. From condition (6.64), we have

$$B_{\theta 1} = \frac{\Pi_2}{\alpha},$$

so that equation (6.67) becomes

$$a_1 = \frac{B_{\theta 1}}{\alpha} v^*. \tag{6.69}$$

Using (6.65) and (6.66) the relations

$$2\left[\Pi_1 - 2(1 - M_a^2)M_a^2 \frac{\Pi_0^2}{\Omega_0^4}\right] = \frac{1}{2}\left\{\beta(p_0+p_1) + B_{\theta 1}^2(2 - M_a^2)\right.$$

$$\left. + M_a^2 \frac{B_{\theta 1}^2 v^{*2}}{\alpha^2}\left(1 + \frac{\alpha^2}{\mu_1^2}\right)(1 + J_0^2(\mu_1)) - \frac{4B_{\theta 1}^2 v^* M_a^2}{\alpha^2}(1 + J_0(\mu_1))\right\}, \tag{6.70}$$

and

$$\alpha = \pm \left\{ \frac{M_a^2 v^*[4(1 - J_0(\mu_1)) - (1 - J_0^2(\mu_1))v^*]}{\delta\beta + \left[\frac{M_a^2}{\mu_1^2}(1 - J_0^2(\mu_1)) - (2 - M_a^2)\right]} \right\}^{1/2}, \tag{6.71}$$

may be deduced where

$$\delta\beta = \frac{\beta(p_0 - p_1)}{B_{\theta 1}^2}.$$

From the above it is easily seen that

$$\frac{2\Pi_2}{\alpha^2 a_1} = \frac{2}{v^*} = \frac{2(v_1 - v_0 J_0(\mu_1))}{2v_1 - 2v_0 - v_0 v_1}, \tag{6.72}$$

and so the classification of the various magnetic field topologies depends upon the plasma velocity at the base, and in particular at $r = 0$ and $r = 1$.

It is now possible to determine the possible ranges of velocities at the base ($z = 0$) appropriate to each magnetic field classification.

Firstly, when the magnetic field is purely diverging, we require for the corona $v_0 > 0$, $v_1 > 0$, and so

$$\frac{2\Pi_2}{\alpha^2 a_1} < J_0(\mu_1)$$

gives

$$0 < v_1 < \frac{2v_0}{2 - v_0} \quad \text{if} \quad 0 < v_0 < 2 \tag{6.73}$$

and

$$v_1 > 0 \quad \text{if} \quad 2 < v_0 < -\frac{2}{J_0(\mu_1)}(1 - J_0(\mu_1)). \tag{6.74}$$

When the fieldlines are purely converging, it is again necessary to have $v_0, v_1 > 0$ along with

$$\frac{2\Pi_2}{\alpha^2 a_1} > 1,$$

which is satisfied only if

$$v_1 > \frac{2v_0}{2 - v_0} \quad \text{and} \quad 0 < v_0 < 2. \tag{6.75}$$

Turning our attention to the partially open magnetic field structure, and the case when

$$J_0(\mu_1) < \frac{2\Pi_2}{\alpha^2 a_1} < 0,$$

an example of which is shown in Figure 6.6b. For the plasma to be outward flowing in the open field region we need $v_0 > 0$, and hence for consistency $v_1 < 0$ (taking into account that the velocity can have at most one zero). This gives the restrictions

$$v_1 < 2(J_0(\mu_1) - 1) \quad \text{when} \quad 2\left(1 - \frac{1}{J_0(\mu_1)}\right) < v_0 \tag{6.76}$$

and

$$2(J_0(\mu_1) - 1) < v_1 < 0 \quad \text{when} \quad 0 < v_0 < 2\left(1 - \frac{1}{J_0(\mu_1)}\right). \tag{6.77}$$

Finally, for

$$0 < \frac{2\Pi_2}{\alpha^2 a_1} < 1,$$

which corresponds to the magnetic field topology illustrated in Figure 6.6a, for outflowing plasma in the open field region we need, $v_1 > 0$, and so $v_0 < 0$. This condition is satisfied when

$$\frac{1}{2}[J_0(\mu_1)(v_0 + 2) - 2] < v_1. \tag{6.78}$$

Now consider the effect of varying the values of v_0 and v_1, for the particular example when

$$J_0(\mu_1) < \frac{2\Pi_2}{\alpha^2 a_1} < 0.$$

From equations (6.76) and (6.77), it can be seen that two regimes exist; namely a 'fast' regime given by inequalities (6.76), and a 'slow' regime given by inequalities (6.77). In Section 6.5, we saw that decreasing the value of $2\Pi_2/\alpha^2 a_1$ when $2\Pi_2/\alpha^2 a_1 < 0$ increased the number of open fieldlines. To investigate how this relates to v_0 and v_1 define the function f by

$$f(v_0, v_1) = \frac{2\Pi_2}{\alpha\, a_1} = \frac{2(v_1 - v_0 J_0(\mu_1))}{2v_1 - 2v_0 - v_0 v_1}, \tag{6.79}$$

and note that

$$\frac{\partial f}{\partial v_0} = \frac{2v_1[2(1 - J_0(\mu_1)) + v_1]}{[2v_1 - 2v_0 - v_0 v_1]^2}, \tag{6.80}$$

and

$$\frac{\partial f}{\partial v_1} = \frac{2v_0[v_0 J_0 - 2v_1 - 2(1 - J_0(\mu_1))]}{[2v_1 - 2v_0 - v_1 v_0]^2}. \tag{6.81}$$

Consider the effect of varying v_0; from (6.80) it is evident that for the 'fast' regime (6.76), increasing v_0 decreases the number of open fieldlines ($\partial f/\partial v_0 > 0$). However, for the 'slow' regime (6.77), increasing v_0 increases the number of open fieldlines (i.e. $\partial f/\partial v_0 < 0$).

There seem to be two different ways in which force balance is maintained, depending upon the regime. In both cases, increases in v_0 will increase the centrifugal forces in the plasma flows along the closed fieldlines. For the 'slow'

regime, the centrifugal force is sufficiently large to strip away closed fieldlines. Here the centrifugal force is balanced by an increase in the magnetic pressure in the overlying field, hence the increase in number of open fieldlines. In the 'fast' regime the centrifugal forces are again increased, with force balance maintained by an increase in magnetic tension in the closed structure, which may come about by increasing the number of closed fieldlines and an increase in the curvature of the field (which will increase the height of the arcade). This effect can be seen by comparing Figure 6.7a and 6.7b.

From this analysis, it becomes clear that the ratio of open to closed flux is a function of the plasma velocity. In the 'slow' regime, increasing v_0 increases the amount of 'closed' flux, whereas in the 'fast' regime, an increase in v_0 increases the proportion of 'open' flux. The ratio R of open flux to the flux entering the region is given by

$$R(v^*) = \mu_1^{+2} [(\mu_1 r^*)^2 - v^*(\mu_1 r^*) J_1(\mu_1 r^*)]^{-1}, \qquad (6.82)$$

where r^* is the solution of the equation

$$J_0(\mu_1 r^*) = \frac{2}{v^*} .$$

When $r^* = 1$, corresponding to purely open fieldlines, then $R = 1$. Equation (6.82) is derived assuming the topology shown in Figure 6.6b. The limit of completely closed magnetic field is found by letting $v^{*-1} \rightarrow 0$, which gives $R = 0$, i.e. no open magnetic flux.

From the expression for α in equation (6.71), it can be seen that the magnetic field topology depends upon the value of the twist component of the magnetic field at $r = 1$, namely $B_{\theta 1}$. Increasing $B_{\theta 1}$ increases the height of the arcade, and causes the field strength at $r = 1$ to increase for the open fieldlines

Figure 6.7a

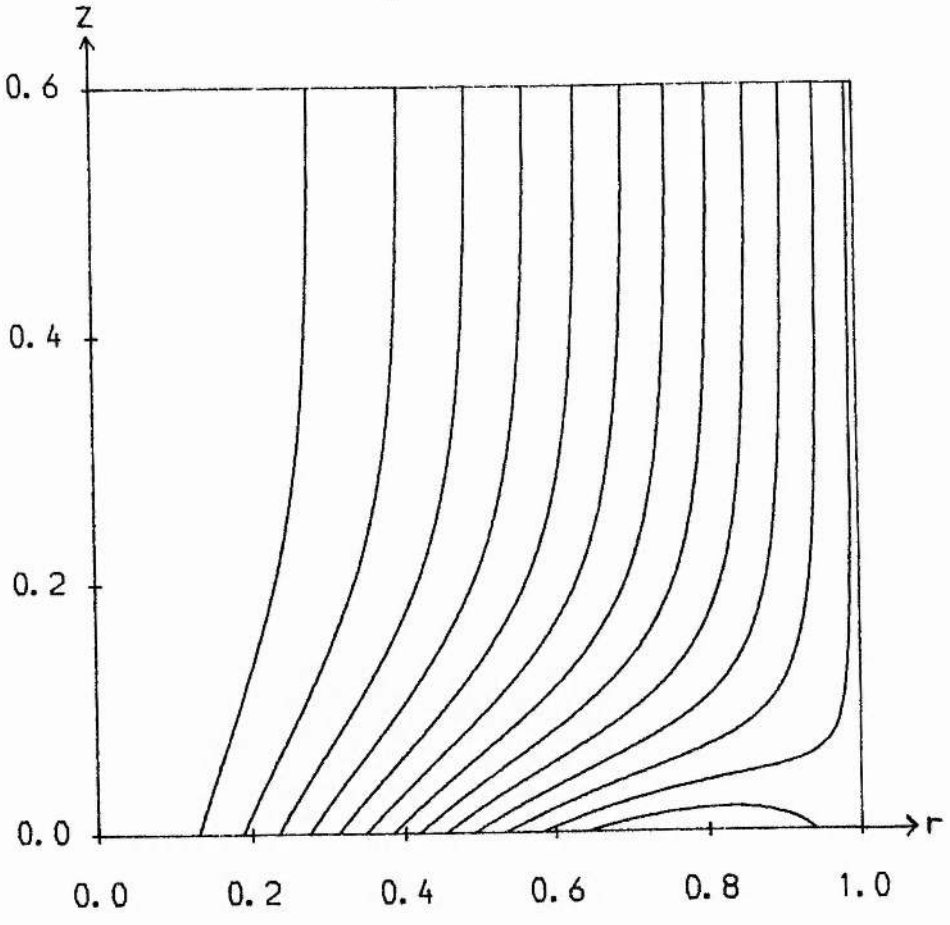

Figure 6.7 : Magnetic fieldline plots with M_a=1.5, $\beta(p_0-p_1)$ = -1.0, $B_{\theta 1}$=0.4 and a) v^*=-2.0, b)v^*=-3.25.

Figure 6.7b

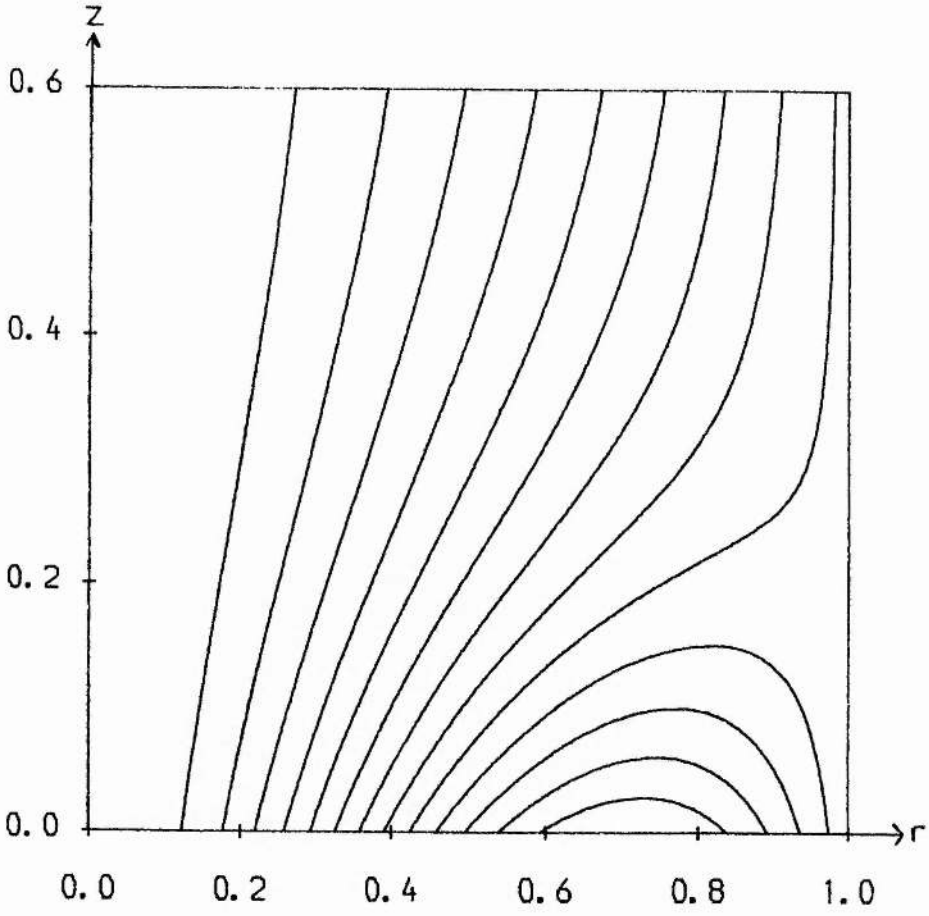

when $0 < 2\Pi_2/\alpha^2 a_1 < 1$, as seen in Figures 6.8a and 6.8b. Note however, that the ratio of closed to open fieldlines remains constant as this depends solely on v^*. Continuing to increase $B_{\theta 1}$, we will reach a value when $v = 0$, corresponding to the eruption of the arcade. Mathematically, the solutions lose their z-dependence, and the fieldlines become vertical, with $B_r \equiv 0$. A similar effect can be achieved by altering the plasma pressure difference between $r = 0$ and $r = 1$. Again, the ratio of open to closed fieldlines is unchanged as the plasma pressure difference varies.

6.7 Conclusions

In this chapter we have shown that the exact solutions presented give a wide range of possible magnetic topologies which may be applicable in modelling the solar atmosphere . In each of these cases there is a flow of plasma along the magnetic fieldlines.

The magnetic field may be closed, open (converging or diverging) or partially open (an arcade with an overlying field). The proportion of open fieldlines depends upon the flow of plasma at the base of the region. In the case discussed it was seen that two parameter regimes existed, ('fast' and 'slow'). Increasing the flow in the open region increases the number of open fieldlines in the 'slow' regime and decreases the open flux in the 'fast' regime. In addition, increasing the twist component of the magnetic field imposed at the base results in the arcade of closed fieldlines rising, before it eventually erupts.

The magnetic field topologies are reminiscent of some of the structures that are observed in the solar corona. The closed magnetic solutions ($\Pi_2=0$) could model the field above sunspot, with Evershed flow along the fieldlines. When Π_2 is non-zero the solutions may model several different solar structures. For example, plumes are ray-like structures found at the polar regions of the sun, and are thought to be associated with open magnetic fields. Such structures may be modelled by the solutions presented here when all the magnetic fieldlines are

Figure 6.8a

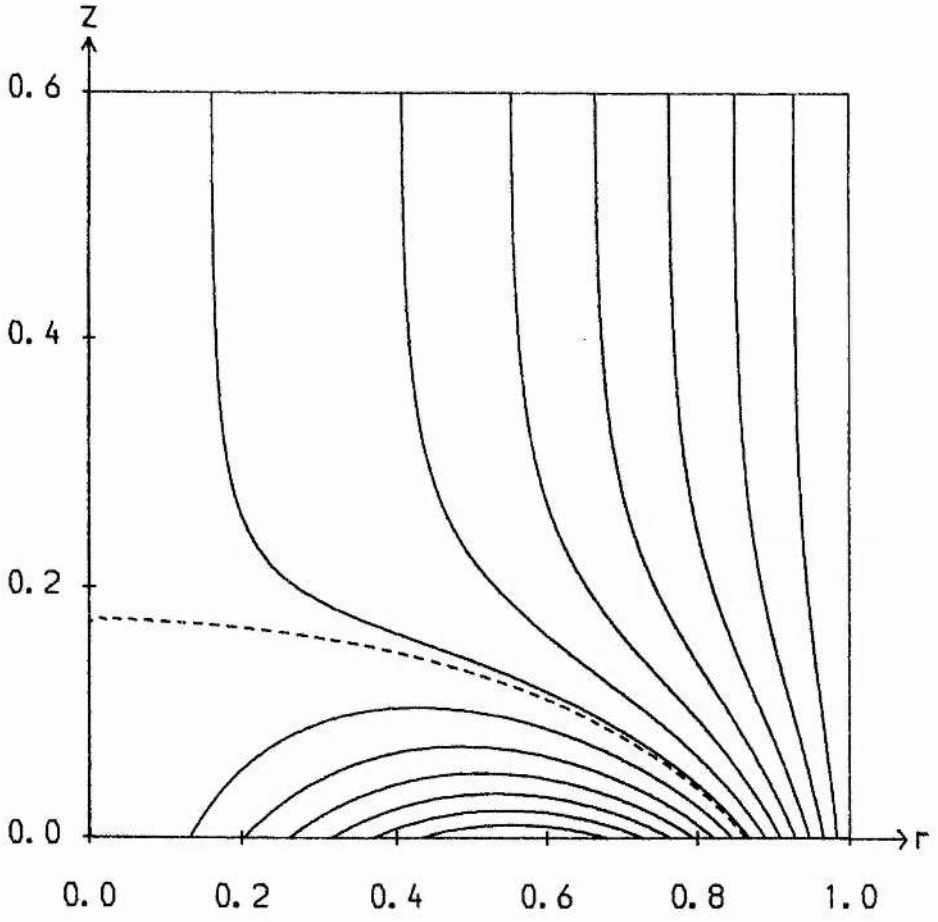

Figure 6.8 : Magnetic fieldline plots with M_a=1.5, $\beta(p_0-p_1)$=1.0, v^*=4.0 and

a) $B_{\theta 1}$=1.0, b) $B_{\theta 1}$=4.0.

Figure 6.8b

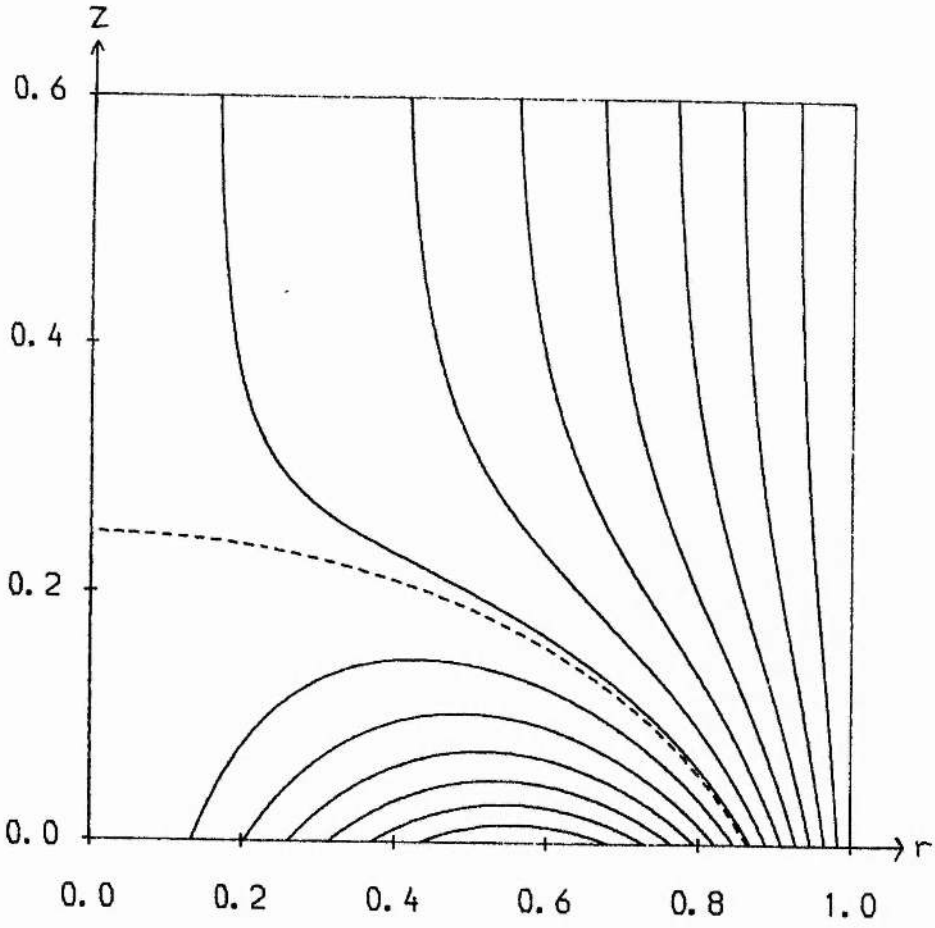

open, as in Figure 6.6d. Coronal streamers consist of both open and closed regions of magnetic fieldlines, such as that shown in Figure 6.6a. As we have seen, these solutions have the feature that both open and closed field is modelled by the same solutions, without the need for matching between regions. Coronal holes are regions of open, diverging magnetic field, associated with the origin of the high-speed solar wind. At the boundary of a hole, it is thought that the magnetic field forms arcades or loops of closed magnetic field. Figure 6.6b shows a topology that has both of these features, and may be applicable to coronal holes. Finally, X-ray bright points are relatively short-lived regions (~ 8 hours) of closed magnetic field associated with emerging flux. Observations of the solar limb show that there is an overlying open magnetic field above the closed field. The magnetic topology shown in Figure 6.6a may represent the field found in such structures. In this case there is a concentration of flux of one polarity around $r = 0$, and a sea of opposite polarity around the outer edge of the cylindrical region.

To make a more direct comparison, these solutions require to be extended to include gravity and density variations along fieldlines.

Chapter 7 : Exact Solutions In An Isothermal Stratified Atmosphere.

7.1 Introduction

The method for finding exact solutions presented in chapter five relied upon the assumption that there is no constant electric field in the ignorable direction. In this chapter we explore the possibility of constructing solutions for which this assumption is relaxed. In general, it is a formidable task , but we show that it is possible to find particular classes of solutions.

The method employed is an extension of that used in the magnetostatic case by several authors (e.g., Dungey, 1953; Kippenhahn and Schluter, 1957; Zweibel and Hundhausen, 1982). For simplicity we work in cartesian coordinates (x,z), though a similar analysis is possible in general orthogonal coordinates. Having described the method in section 7.2, we construct particular solutions in the following sections. In this chapter we are not interested in any detailed investigation of the properties of the solutions, but simply on how the solutions may be constructed.

7.2 Method Of Solution

In dimensionless variables, we consider the usual steady MHD equations, namely,

$$M_a^2 \rho(\mathbf{v}.\nabla)\mathbf{v} = -\frac{1}{2}\beta\nabla p + \mathbf{j}\times\mathbf{B} - H\rho\hat{\mathbf{z}}, \tag{7.1}$$

$$\nabla.\mathbf{B} = 0, \tag{7.2}$$

$$\nabla.(\rho\mathbf{v}) = 0\,, \tag{7.3}$$

$$\nabla\times(\mathbf{v}\times\mathbf{B}) = \mathbf{0}\,, \tag{7.4}$$

$$\mathbf{v}.\nabla\left(\frac{p}{\rho}\right) = 0\,, \tag{7.5}$$

where the constant gravitational force is in the z-direction, and the gravitational constant g is contained in the dimensionless parameter H.

In addition, we define the dimensionless current **j** by

$$\mathbf{j} = \nabla \mathrm{x} \mathbf{B} \,, \tag{7.6}$$

and to satisfy the solenoidal condition (7.2) we follow the usual proceedure of defining a flux function A, by

$$\mathbf{B} = \hat{\mathbf{y}} \mathrm{x} \nabla A \,, \tag{7.7}$$

where $\hat{\mathbf{y}}$ is the unit vector in the ignorable direction. Substituting equation (7.7) into (7.6), we obtain

$$j = \nabla^2 A \,. \tag{7.8}$$

In order to satisfy identically the mass continuity equation we define a compressible stream function Ψ by

$$\rho \mathbf{v} = \hat{\mathbf{y}} \mathrm{x} \nabla \Psi \,. \tag{7.9}$$

Note that for simplicity it has been assumed that the field components in the ignorable direction are identically zero.

Having dealt with equations (7.2) and (7.3), let us now turn our attention to the energy equation (7.5), and note that on substituting for v from (7.9), it may be rewritten in the Jacobian notation

$$\left[\Psi, \frac{p}{\rho}\right] = 0 \,. \tag{7.10}$$

Thus, we immediately deduce that the general solution is

$$\frac{p}{\rho} = \mu(\Psi) \,, \tag{7.11}$$

for some function μ, although for simplicity we take

$$\frac{p}{\rho} = \text{constant} = c_s^2, \tag{7.12}$$

for the remainder of this work. We may identify the constant c_s^2, as the dimensionless square of the isothermal sound speed.

Next, let us consider the induction equation (7.4). On substituting for **B** and v from equations (7.7) and (7.9), respectively, the following Jacobian relation results :

$$[\Psi, A] = \rho E, \tag{7.13}$$

where E is a constant electric field in the y-direction. Setting E=0, equation (7.13) yields $\Psi = \Psi(A)$, which is the key assumption in the analysis of Tsinganos (1981). In this work we proceed with E≠0.

We are now in a position to treat the equation of motion (7.1), which we write as

$$\left(\frac{2M_a^2}{\beta c_s^2}\right)\rho(\mathbf{v}.\nabla)\mathbf{v} = -\nabla p + \left(\frac{2}{\beta}\right)\mathbf{j}\times\mathbf{B} - \left(\frac{2H}{\beta c_s^2}\right)\rho\hat{\mathbf{z}}, \qquad (7.14)$$

having used equation (7.12) to eliminate the density ρ. In keeping with Zweibel and Hundhausen (1982), we assume that the plasma pressure p takes the form

$$p = Q(x,z)\exp[-az], \qquad (7.15)$$

where $a = 2H/(\beta c_s^2)$ so that the equation of motion (7.14) becomes

$$\nabla Q + bQ(\mathbf{v}.\nabla)\mathbf{v} = -\left(\frac{2}{\beta}\right)\mathbf{j}\times\mathbf{B}\exp[-az],$$

and $b = 2M_a^2/(\beta c_s^2)$. Putting a=0 removes the gravitational term, while b=0, reduces the equations to the magnetostatic case. On substituting for **B** and **j** from (7.7) and (7.8) the above equation becomes

$$\nabla Q + bQ(\mathbf{v}.\nabla)\mathbf{v} = -\left(\frac{2j}{\beta}\right)\exp[-az]\nabla A. \qquad (7.16)$$

Putting b=0 in equation (7.16) gives the static case considered by Zweibel and Hundhausen.

To proceed further with b≠0, multiply equation (7.16) by a function F=F(x,z), and choose F such that

$$F\nabla Q + bQF(\mathbf{v}.\nabla)\mathbf{v} = \nabla(FQ) = \nabla G. \qquad (7.17)$$

For condition (7.17) to be satisfied, we make the identification

$$\frac{\nabla F}{F} = b(\mathbf{v}.\nabla)\mathbf{v}, \qquad (7.18)$$

and thus equation (7.16) may be rewritten in the form

$$\nabla G = -\left(\frac{2j}{\beta}\right)F\exp[-az]\nabla A. \qquad (7.19)$$

Along any fieldline we know that A= constant, and so for (7.19) to be satisfied, we also need G= constant along a fieldline. Defining a function S by

$$S \equiv \left(\frac{2j}{\beta}\right)F\exp[-az], \qquad (7.20)$$

and taking the curl of equation (7.19) we deduce the result,

$$\nabla S \times \nabla A = \mathbf{0}, \tag{7.21}$$

whence we have that ∇S is everywhere parallel to ∇A. Hence A(x,z), G(x,z) and S(x,z) have gradients everywhere parallel.

Following Zweibel and Hundhausen, next define an orthogonal coordinate system with ξ measuring distance along the level curves of A, and χ measuring distance transverse to the level curves of A. It then follows that A,G and S may be written as functions of χ only, namely $A=A(\chi)$, $G=G(\chi)$, $S=S(\chi)$, from which it may be shown that

$$G(x,z) = G(A(x,z)) ,$$

and

$$\frac{2j}{\beta} F\exp[-az] = \frac{2}{\beta} f(A),$$

where f is an arbitary function of A. On substituting the last result into equation (7.8) we obtain

$$\nabla^2 A + \frac{f(A)}{F} \exp[-az] = 0 . \tag{7.22}$$

In the limit $M_a = 0$, equation (7.18) gives F = constant, (which we take to be unity), and so equation (7.22) reduces to the result obtained by Zweibel and Hundhausen.

From equation (7.19), the function G is given by

$$G(A) = G_0 + \int^{A} f(U)dU , \tag{7.23}$$

where G_0 is a constant.

In order to solve (7.22) we are required to specify f(A), and determine the actual functional form of F, before solving for A. To find F, it is necessary to return to equation (7.18) and note that in component form we have

$$\frac{\partial}{\partial x}(\ln F) = b\left\{v_x \frac{\partial v_x}{\partial x} + v_z \frac{\partial v_x}{\partial z}\right\}, \tag{7.24}$$

and

$$\frac{\partial}{\partial z}(\ln F) = b\left\{v_x \frac{\partial v_z}{\partial x} + v_z \frac{\partial v_z}{\partial z}\right\}. \tag{7.25}$$

As noted above, when b=0, F=constant is the solution of equations (7.24) and (7.25). For b≠0, we proceed by adding (7.24) and (7.25) and substituting for **v** from (7.9), and so obtain the equation

$$\frac{\partial}{\partial x}(\ln F) + \frac{\partial}{\partial z}(\ln F) = \frac{b}{\rho}\left\{\frac{\partial \Psi}{\partial z}\,\frac{\partial}{\partial x}\left\{\frac{1}{\rho}\left(\frac{\partial \Psi}{\partial z} - \frac{\partial \Psi}{\partial x}\right)\right\}\right\} - \frac{b}{\rho}\left\{\frac{\partial \Psi}{\partial x}\,\frac{\partial}{\partial z}\left\{\frac{1}{\rho}\left(\frac{\partial \Psi}{\partial z} - \frac{\partial \Psi}{\partial x}\right)\right\}\right\}. \qquad (7.26)$$

A class of exact solutions may be determined by setting

$$\frac{\partial}{\partial x}(\ln F) + \frac{\partial}{\partial z}(\ln F) = beE, \qquad (7.27)$$

where E is the constant electric field appearing in (7.13), and 'e' is a constant scaling factor. The characteristics of the partial differential equation (7.27) are

$$x - z = \text{constant},$$

and

$$\ln F - eb\,\frac{E(a_1 x + a_2 z)}{a_1 + a_2} = \text{constant},$$

for constants a_1 and a_2, so that the general solution is

$$F = \exp[f_1(u)]\exp\left[-eb\,\frac{E(a_1 x + a_2 z)}{a_1 + a_2}\right], \qquad (7.28)$$

where we take

$$u = b(x - z)$$

and f_1 is some function with $f_1(0) = 0$, so that F=1 when b=0. Clearly we could generate other solutions by choosing 'e' to be some general, but specified, function of x and z.

For simplicity consider the case when

$$f_1(u) = u,$$

so that

$$F(x,z) = \exp\left\{b\left\{\left(1 - \frac{ea_1E}{a_1+a_2}\right)x - \left(1 + \frac{ea_2E}{a_1+a_2}\right)z\right\}\right\},$$

and equation (7.22) becomes

$$\nabla^2 A + f(A)\exp[-\lambda(x,z)] = 0, \qquad (7.29)$$

where

$$\lambda(x,z) = b\left(1 - \frac{ea_1E}{a_1+a_2}\right)x + \left\{a - b\left(1 + \frac{ea_2E}{a_1+a_2}\right)\right\}z \,. \qquad (7.30)$$

Before we consider solutions to equation (7.29), we must consider the right-hand side of equation (7.26). Noting that the induction equation (7.13) may be expressed as

$$\frac{1}{\rho}\left\{\frac{\partial A}{\partial z}\frac{\partial \Psi}{\partial x} - \frac{\partial A}{\partial x}\frac{\partial \Psi}{\partial z}\right\} = E \,, \qquad (7.31)$$

equation (7.26) becomes

$$\frac{\partial \Psi}{\partial z}\frac{\partial}{\partial x}\left\{\frac{1}{\rho}\left(\frac{\partial \Psi}{\partial z} - \frac{\partial \Psi}{\partial x}\right)+eA\right\} - \frac{\partial \Psi}{\partial x}\frac{\partial}{\partial z}\left\{\frac{1}{\rho}\left(\frac{\partial \Psi}{\partial z} - \frac{\partial \Psi}{\partial x}\right)+eA\right\} = 0, \qquad (7.32)$$

which has the general solution

$$\frac{1}{\rho}\left(\frac{\partial \Psi}{\partial z} - \frac{\partial \Psi}{\partial x}\right) + eA = h(\Psi) \,, \qquad (7.33)$$

where h is an arbitary function of the streamfunction Ψ. Eliminating ρ from (7.33) using (7.31) we obtain

$$\frac{\partial \Psi}{\partial x}\left\{2E - e\frac{\partial A^2}{\partial z} + 2h(\Psi)\frac{\partial A}{\partial z}\right\} - \frac{\partial \Psi}{\partial z}\left\{2E - e\frac{\partial A^2}{\partial x} + 2h(\Psi)\frac{\partial A}{\partial x}\right\} = 0 \,. \qquad (7.34)$$

The object now is to solve equation (7.34) for Ψ as a function of A,x and z. In general this is a formidable task, and here we will examine only one simple case.

When $h=h_0$, a constant, one can show that the solution of equation (7.34) is

$$\Psi = \Psi\left(2E(x+z) - eA^2 + 2h_0A\right) \,. \qquad (7.35)$$

This has the interesting property that the streamlines are not parallel to the fieldlines when $E\neq0$, so that the plasma flow drags the fieldlines along with the flow. When E=0 the flow of plasma is along the fieldlines.

Let us summarise the proceedure for finding solutions. Firstly, choose the arbitary function f to have a suitable form in equation (7.29), and then solve for A. Once f is chosen, G may be calculated from equation (7.23), and so Q is found from

$$Q = \frac{G}{F} \,.$$

Hence, the plasma pressure p is

$$p = Q\exp[-az],$$

and the density

$$\rho = \frac{p}{c_s^2}. \tag{7.36}$$

Finally, having solved for A, the magnetic field components are deduced from (7.7). For the velocity components, we use (7.35),(7.36) and (7.9). In the following sections we present solutions for particular choices of F.

7.3 Separable Solutions

With the choice

$$f(A) = \alpha A, \tag{7.37}$$

equation (7.29) becomes

$$\nabla^2 A + \alpha\exp[-\lambda(x,z)]A = 0, \tag{7.38}$$

and

$$G = G_0 + \alpha A^2. \tag{7.39}$$

After defining the variables

$$\eta = rx+sz \;\; ; \;\; \zeta = sx-rz \tag{7.40}$$

where

$$r = b\left(1 - \frac{ea_1E}{a_1+a_2}\right)$$

and

$$s = \left\{a - b\left(1 + \frac{ea_2E}{a_1+a_2}\right)\right\},$$

we find that equation (7.38) becomes

$$\frac{\partial^2 A}{\partial\eta^2} + \frac{\partial^2 A}{\partial\zeta^2} + \Omega^2 e^{\eta} A = 0, \tag{7.41}$$

where

$$\Omega^2 = \frac{\alpha}{r^2+s^2}. \tag{7.42}$$

We look for solutions to equation (7.41) of the form

$$A = Z(\eta)X(\zeta),$$

and so obtain the ordinary differential equations

$$X'' + \nu^2 X = 0, \tag{7.43}$$

and

$$Z'' + (\Omega^2 e^{\eta} - \nu^2)Z = 0, \tag{7.44}$$

where ν^2 is a separation constant. Clearly equation (7.43) has the solution

$$X(\eta) = d\cos(\nu\zeta+\theta),$$

for some arbitary constants d and θ. Making the substitution

$$\omega = \exp\left[\frac{1}{2}\eta\right],$$

equation (7.44) becomes

$$\omega^2 Z'' + \omega Z' + [4\Omega^2\omega^2 - 4\nu^2]Z = 0, \tag{7.45}$$

where a dash now denotes differentiation with respect to ω. The solutions of equation (7.45) are clearly Bessel functions, and are given by

$$Z(\eta) = J_{2\nu}\left(2\Omega e^{\eta/2}\right), \text{ if } \alpha > 0,$$

and

$$Z(\eta) = I_{2\nu}\left(2|\Omega|e^{\eta/2}\right), \text{ if } \alpha < 0,$$

which we represent collectively by

$$Z(\eta) = \Sigma_{2\nu}(2|\Omega|e^{\eta/2}).$$

Thus, the solution of equation (7.41) is

$$A = d\cos(\nu\zeta+\theta)\,\Sigma_{2\nu}(2|\Omega|e^{\eta/2}). \tag{7.46}$$

Note that in the limit $b\to 0$, the solutions reduce to the magnetostatic case considered by Zweibel and Hundhausen.

7.4 Non-linear Separable Solutions

With the prescription

$$f(A) = \alpha A^m,$$

equation (7.29) may be written

$$\frac{\partial^2 A}{\partial \eta^2} + \frac{\partial^2 A}{\partial \zeta^2} + \Omega^2 e^{\eta} A^m = 0, \tag{7.47}$$

where the symbols are as defined in the previous section. Looking for separable solutions of the form

$$A = X(\zeta)Z(\eta),$$

equation (7.47) becomes

$$\frac{X''}{X} + \frac{Z''}{Z} + \Omega^2 e^{\eta} X^{m-1} Z^{m-1} = 0 . \qquad (7.48)$$

Choosing

$$Z(\eta) = \exp\left[- \frac{\eta}{m-1}\right],$$

equation (7.48) becomes the ordinary non-linear differential equation

$$X'' + \Omega^2 X^m + \frac{X}{(m-1)^2} = 0, \qquad (7.49)$$

for which we require $m \neq 1$. Consider the case when $m = -3$, then since

$$X'' = \frac{d}{dX}(X')^2,$$

equation (7.49) may be integrated to give

$$(X')^2 = 2\Omega^2 + 4kX^2 - \frac{X^4}{16}, \qquad (7.50)$$

for some constant k. Integrating again gives

$$\zeta + t = \int^{X} \frac{dV}{\sqrt{2\Omega^2 + 4kV^2 - \frac{V^4}{16}}} \qquad (7.51)$$

for some constant t. Analogous solutions have been found in the magnetostatic case by Melville et al (1984).

7.5 Non-Separable, Non-linear Solutions

Finally, make the prescription

$$f(A) = \alpha \exp[-2A],$$

so that equation (7.29) may be written in the form

$$\frac{\partial^2 A}{\partial \eta^2} + \frac{\partial^2 A}{\partial \zeta^2} + \Omega^2 e^{\eta} e^{-2A} = 0. \qquad (7.52)$$

Defining the transformation

$$A = T + \frac{1}{2}\eta ,$$

equation (7.52) becomes

$$\frac{\partial^2 T}{\partial \eta^2} + \frac{\partial^2 T}{\partial \zeta^2} + \Omega^2 e^{-2T} = 0 , \qquad (5.53)$$

the solution of which has been discussed for the case of force-free magnetic fields by Low (1977), and for more general magnetostatic equilibrium by Melville et al (1983).

7.6 Summary

In the preceeding sections we have sought to illustrate how a class of exact solutions to the steady MHD equations may be generated, which have a constant electric field in the ignorable direction. These solutions may be applicable to the problem of emerging flux and magnetic reconnection. The electric field can be 'switched-off', and in this case the flow will be along the fieldlines. Such solutions may model siphon flow along arcades and other magnetic structures. The purpose of this chapter is to present a method of finding particular classes of exact solutions; the properties and applications of the solutions is to be studied in the future.

Chapter 8

8.1 Summary

A brief summary of the work presented in chapters two to seven is now given.

In part A, we showed how the corona can be modelled by extended standing disturbances, using a linear theory. The inclusion of inertial effects distorts the isobars, and the flow and magnetic field varies with altitude in a way that depends upon the basic flow (v_0) relative to the cusp speed (c_T), the sound speed (c_s) and the Alfven speed (v_A). The classification of the type of disturbances depends upon the flow speed in the basic state and upon the magnetic field and plasma pressure imposed at the coronal base.

In a cylindrical geometry, we saw that the symmetric solutions are qualitatively similar to those found in a cartesian geometry. Quantitatively, the disturbance is stronger in the central region of the cylinder and weaker at the edges, compared with the cartesian case. In addition, pressure gradients are found to be smaller in the cylindrical geometry compared with the cartesian geometry. Asymmetric solutions may also be found, which depend upon all three spatial variables

By including gravitational stratification in chapter four, we saw that a wider variety of possible magnetic topologies is possible. Previously, the fieldlines were either converging (for plumes) or diverging (for coronal holes or voids). When gravity is added, these two cases are supplemented by a diverging field that converges as we rise in the atmosphere (and vice-versa). This is reminiscent of the overlying magnetic field of a coronal streamer. In addition, there is an increase in the maxima of the plasma and magnetic pressure, a decrease in the curvature of the fieldlines. Also, the type of disturbance occurring in the plasma is now a function of altitude.

Although such simple modelling may not answer many detailed questions , this approach is enlightening on how the 'building blocks' of the corona behave.

In the second part of the thesis, we showed how the method given by Tsinganos (1981) for finding exact solutions may be used to find classes of solutions which may be relevant to the solar atmosphere. In a cartesian geometry, a class of solutions was presented which models subsonic flow in magnetic arcades. For symmetric arcades, the basic result is that the presence of a flow causes the arcade to rise in comparison with the static case. Increasing the flow speed will eventually cause the arcade to erupt. Solutions for non-symmetric arcades can be constructed which could model siphon flow in magnetic arcades.

In a cylindrical geometry, solutions can be found which model a sunspot field. The flow along the fieldlines could model Evershed flow, though for more realistic modelling the inclusion of gravitational effects is needed. Solutions with open fields could model coronal holes and plumes, whereas the partially open field solutions may model flows in X-ray bright points and their overlying plumes, together with the structure at coronal hole boundaries.

In chapter seven we presented a method of finding exact solutions when a constant electric field is present in the ignorable direction. In addition we showed how various classes could be determined.

8.2 Suggestions For Future Work

The approach followed in the first part of the thesis may prove useful in determining the basic contribution of various effects. For example, it would be useful to see the effect of viscosity on the plasma interactions, and how a more realistic energy equation, say by adding heat conduction, could alter the basic solutions.

Clearly, to model the corona more realistically, the analysis could be performed in a spherical geometry. This leads to a very messy set of equations, and it is the author's contention that it is easier to find exact solutions than to follow this approach!

As we sought to illustrate, the method of Tsinganos for finding exact solutions lends itself to numerous extensions. Including gravity and allowing supersonic flow would clearly be useful. Also, it is desirable to find solutions in a spherical geometry, which would be applicable to the solar corona. The properties of the solutions presented in chapter seven requires to be investigated, and the possibility of extending the method to find further classes of solutions considered. However, the most important task ahead is to compare the models with observations and make them more realistic.

Appendix

We here note the definition, and some of the elementary properties of the Jacobian of two differentiable functions.

By definition, the Jacobian of the functions f(x,z) anf g(x,z) is

$$[f,g] \equiv \frac{\partial f}{\partial x}\frac{\partial g}{\partial z} - \frac{\partial f}{\partial z}\frac{\partial g}{\partial x}. \qquad \text{(A1)}$$

From the definition (A1), the following relations follow,

$$[f,g] = -[g,f], \qquad \text{(A2)}$$

$$[f,g] = 0 \Rightarrow f=f(g), \qquad \text{(A3)}$$

$$[f,g+G] = [f,g] + [f,G], \qquad \text{(A4)}$$

$$[f,gG] = [f,g]G + g[f,G]. \qquad \text{(A5)}$$

References

Altschuler,M.D and Newkirk,G.: 1969, *Solar Phys.* **9**, 131

Altschuler,M.D, Trotter,D.E., Orrall,F.Q.: 1972, *Solar Phys.* **26**, 354

Bohlin,J.D.: 1969, Ph.D Thesis, Dept. of Astro.- Geophys., Univ. of Colorardo, Boulder.

Bohlin,J.D.: 1977, *Solar Phys.* **51**, 377

Bruzek,A and Durrant, C.J.: 1977, *Illustrated Glossary for Solar and Solar Terrestial Physics,* D Reidel, Boston.

Cargill,P.J and Priest,E.R.: 1980, *Solar Phys.* **65**, 251

Cargill,P.J and Priest,E.R.: 1982, *Geophys.Astrophys. Fluid Dyn.*, **20**, 227

Degenhart,D.: 1989, *Astron.Ap.*, **222**, 297

de Ville,A and Priest,E.R.: 1989a, *Ap.J.*, **340**, 579

de Ville,A and Priest,E.R.: 1989b, *Ap.J.*, **347**, 1167

de Ville,A and Priest,E.R.: 1990, *Ap.J.*, **359**,

de Ville,A and Priest,E.R.: 1990a, *Solar Phys.*, (submitted)

de Ville,A and Priest,E.R.: 1990b, *Geo.Astrophys.Fluid.Dyn.* (submitted)

de Ville,A and Priest,E.R.: 1990c, *Geo.Astrophys.Fluid.Dyn.* (submitted)

Hundhausen,A.J.: 1972, *Coronal Expansion and Solar Wind*, Springer-Verlag, New York.

Kopp,R.A and Holzer,T.E.: 1976, *Solar Phys.* **49**, 43

Lothian,R.M and Hood,A.W.: 1989, *Solar Phys.*, **122**, 227

Low,B.C and Tsinganos,K.: 1986, *Ap.J.*, **302**, 163

Melville,J.P., Hood,A.W. and Priest,E.R.: 1983, *Solar Phys.*, **87**, 301

Melville,J.P., Hood,A.W. and Priest,E.R.: 1984, *Solar Phys.*, **92**, 15

Meyer,F and Schmidt,H.U.: 1968, *Z.Angew.Math.Mech.*, **48**, 218

Montesinos,B and Thomas,J.H.: 1989, *Ap.J.*, **337**, 977

Moore,R and Rabin,D.: 1985,*'Sunspots,' Ann.Rev.Astron.Astrophys.* **23**,239

Pneuman,G.W.: 1966, *Ap.J.*, **145**, 242

Pneuman,G.W. and Kopp,R.A.: 1971, *Solar Phys.*, **18**, 258

Pneuman,G.W.: 1972, *Ap.J.*, **171**, 793

Pneuman,G.W. and Orrall,F.Q.: 1986, *Physics of the Sun* (ed) P.A. Sturrock, Vol II pp71-114

Priest,E.R.: 1984, *Solar Magnetohydrodynamics*, D. Reidel, Dordrecht.

Priest,E.R.: 1988, *Ap.J.*, **329**, 1009

Roberts,B.: 1985, in *Solar System Magnetic Fields*, (ed) E.R Priest (Dordrecht, Reidel)

Steinolfson,R.S.: 1982, *Aston.Ap.*, **115**, 39

Thomas,J.H.: 1988, *Ap.J.*, **333**, 407

Tsinganos,K.: 1981, *Ap.J.*, **245**, 764

Tsinganos,K.: 1982, *Ap.J.*, **252**, 775

Wilcox,J.M.: 1968, *Space.Sci.Rev.*, **8**, 258

Wu,S.T., Wang,S., Dryer,M., Poland,A.L., Sime,D.G., Wolfson,C.J., Orwig,L.E., Maxwell,A.: 1983, *Solar Phys.*, **85**, 351

Zweibel,E.G. and Hundhausen,A.J.: 1982, *Solar Phys.*, **76**, 261